

City Research Online

City St George's, University of London

Citation: Hewish, T. R. (1975). Enhanced conduction in N-hexane subjected to low electric stress : on-line study of controlled photo-currents: thesis presented for the degree of PhD to TCU Dept of Electrical & Electronic Engineering, 1975. (Unpublished Doctoral thesis, The City University)

This is the accepted version of the paper.

This version of the publication may differ from the final published version. To cite this item please consult the publisher's version.

Permanent repository link: https://openaccess.city.ac.uk/id/eprint/38114/

Copyright and Reuse: Copyright and Moral Rights remain with the author(s) and/or copyright holders. Copies of full items can be used for personal research or study, educational, or not-for-profit purposes without prior permission or charge, unless otherwise indicated, provided that the authors, title and full bibliographic details are credited, a hyperlink and/or URL is given for the original metadata page and the content is not changed in any way. For full details of reuse please refer to City Research Online policy.

City Research Online: http://openaccess.city.ac.uk/ publications@citystgeorges.ac.uk

ENHANCED CONDUCTION IN N-HEXANE SUBJECTED TO LOW ELECTRIC STRESS: ON-LINE STUDY OF CONTROLLED PHOTO-CURRENTS

T.R. HEWISH

Thesis presented for the degree of
Doctor of Philosophy
of the City University, London

1975

ABSTRACT

The photo-injection of electrons from thin metal films into a liquid insulant, subjected to an electric stress, is an established method of enhancing the natural conduction current. The interpretation and analysis of the waveshape of the current transient produced by this injection leads to a clearer understanding of the mechanism of charge transport.

This work introduced some new techniques to this field of study. Two grids were incorporated in the test cell containing the liquid. One grid shuttered the charge carriers, which were injected into a vapour gap to improve photo-emission, the second defined the drift field in the liquid. A grid shutter combined with back-illumination of the photo-cathode obviates the effects of bulk ionisation but it introduces its own distortion of the wave-shapes in the form of spreading on the current response to a pulse stimulus.

Instrumentation techniques and signal processing methods, in the form of digital correlation and cumulative averaging, were applied to the problems of measuring small signals in a noisy environment. On-line analytical programs were produced to interpret the results in terms of the criteria for electrohydrodynamic stability in the liquid.

A differential light-sensitive amplifier was constructed which enabled correlation to be established between the current and e.h.d. convection by measuring changes of light intensity, not detectable by the human eye, in a schlieren image of the drift field. Impure hexane has been found to be electrohydrodynamically unstable at low fields in accordance with recent theories. Purified hexane was stable over the range of low-stress which was applied, but displayed instability when charge was injected even at currents as low as 1 pA and an electric stress of 150 V cm^{-1}.

CONTENTS

		Page
	Abstract	i
	Contents	ii
1.	Introduction	1
	1.1 Background to the thesis	2
	1.2 The aim of the thesis	3
2.	Review of Published Work	6
	2.1 Preliminary	7
	2.2 Photo-injection of charge as a method of enhancing conduction	7
	2.2.1 Introduction	7
	2.2.2 The work of Le Blanc, Morant, Chong and Inuishi, Swan and Terlecki; 1959-1962.	8
	2.2.3 Photo-injection using X-rays (Secker, Lewis and Gray)	11
	2.2.4 The determination of impulse response (Buttle and Brignell)	11
	2.2.5 The work of Pugh, Bloor and Rahman	14
	2.2.6 High-mobility charge carriers in liquid insulants	16
	2.2.7 The work of Evison (1975)	18
	2.2.8 Summary of photo-injection results	20
	2.3 The effects of e.h.d. convection	21
	2.3.1 Introduction	21
	2.3.2 E.h.d. convection in non-polar liquids	21
	2.3.3 E.h.d. convection in polar liquids	24
	2.4 Significant results from other work	29
	2.4.1 The effects of using grid electrodes	29
	2.4.2 Delayed injection of negative charge carriers	33
3.	Problems in the measurement of charge transit times	34
	3.1 Introduction	35
	3.2 Noise	35
	3.3 Non-stationarity	37
	3.4 Non-linearity	39
	3.5 Instability	39
	3.6 The 'Long-tail' effect	40
4.	Theoretical background to the experimental work	43
	4.1 Preliminary	44
	4.2 The analysis of pico-ammeter circuits	44
	4.3 Signal Processing	48
	4.3.1 Sampling	48
	4.3.1.1 Introduction	48
	4.3.1.2 The sampling theorem	50
	4.3.2 Cumulative averaging	53

Page

4.3.3 Correlation 55
4.3.3.1 Introduction 55
4.3.3.2 The correlation functions 55
4.3.3.3 The impulse response of a system 57
4.3.3.4 The psuedo random binary sequence (prbs) 57
4.3.4 Deconvolution 59
4.4 Charge Mobility 61
4.4.1 Introduction 61
4.4.2 Diffusion 63
4.4.3 Distortion of the field by a grid 64
4.4.4 Space charge 67
4.4.4.1 Introduction 67
4.4.4.2 The occurrence of space charge 67
4.4.4.3 Transient s.c.l. currents in solids 68
4.4.4.4 The computer simulation of Evison (1975) 70
4.4.4.5 The charge-transit time in a non-uniform field 74
4.4.5 Liquid motion 76
4.4.5.1 Introduction 76
4.4.5.2 E.h.d. mobility 76
4.4.6 Electron trapping 78
4.5 E.H.D. stability 79
4.5.1 Preliminary 79
4.5.2 The work of Atten and Moreau, and Schneider and Watson; 1969;1972 79
4.5.2.1 Introduction 79
4.5.2.2 The stability theory of Atten and Moreau 80
4.5.3 E.h.d. stability during transient injection 83
4.6 Computer studies of e.h.d. stability 84
4.6.1 Preliminary 84
4.6.2 The effects of parameter values upon the critical voltage and current 85

5. Experimental method and apparatus 89

5.1 Experimental techniques for the study of conduction in n-hexane 90
5.1.1 Introduction 90
5.1.2 Preparation of the sample 90
5.1.3 Enhanced conduction in n-hexane at low fields 95
5.1.4 Measurement of electric current 100
5.1.5 Observation of liquid motion 102
5.2 Preparation of the liquid sample 105
5.2.1 Introduction 105
5.2.2 The purification system 105
5.3 The test cells 108
5.3.1 Introduction 108
5.3.2 The modified Buttle-cell 109
5.3.3 Factors influencing the design of a tetrode test cell 109

Page

5.3.4 Design of the tetrode cell 111
5.3.5 Preparation of the photo-cathodes 113
5.4 The stimulation and measurement of current transients 115
5.4.1 Introduction 115
5.4.2 Circuits for the stimulation of current transients 118
5.4.2.1 Circuit A. For use with mechanical shuttering of u.v. irradiation (step stimulus) 118
5.4.2.2 Circuit B. For electronic shuttering and a step stimulus 118
5.4.2.3 Circuit C. For electronic shuttering and pulse stimulus 119
5.4.2.4 Circuit D. Electronic shuttering with a p.r.b.s. signal as the stimulus 120
5.4.3 Current measuring apparatus 121
5.5 Apparatus for observing and recording liquid motion
5.5.1 Introduction 123
5.5.2 The schlieren system 125
5.5.3 The light-sensitive amplifier 126
5.6 Use of the on-line computer 128

6. Experimental Results 131

6.1 Preliminary 132
6.2 The results of tests on the purity of n-hexane 132
6.2.1 Water content 132
6.2.2 Gas liquid chromatography 134
6.2.3 U.V. spectrophotometry 134
6.2.4 Resistivity measurements 136
6.3 Microscopic examination of photo-emitters 136
6.4 Some characteristics of the modified Buttle cell and the tetrode cell 138
6.4.1 The modified Buttle cell 138
6.4.2 The tetrode cell 139
6.5 Results of the cumulative average process 139
6.6 Results of the cross-correlation method 141
6.6.1 Introduction 141
6.6.2 Results with air and hexane in the drift gap 142
6.6.3 Results with hexane only in the drift gap 142
6.7 Results from varying the experimental conditions 147
6.7.1 Introduction 147
6.7.2 Step-stimulus results 147
6.7.3 Pulse stimulus: results from varying drift gap field 147
6.7.4 Pulse stimulus: results with liquid covering the photocathode 152
6.7.5 Pulse stimulus: results from varying the pulse width 153
6.7.6 Pulse stimulus: results from reducing the intensity of the u.v. irradiation 153
6.7.7 The effects of argon above the hexane 153
6.7.8 The effects of filtering the u.v. irradiation 158
6.8 Simultaneous current transient and liquid motion observations 159

Page

6.8.1 Visual observation of liquid motion 159
6.8.2 Effect of drift gap stress on the disturbance signal 159
6.8.3 Disturbance velocity 161
6.8.4 Reducing charge injection 162
6.8.5 Both photo-diodes in light region of schlieren image 162
6.8.6 Disturbance signals in hexane of low resistivity 165

7. Concluding Discussion 167

7.1 Preliminary 168
7.2 Distortion of current transients 168
7.2.1 Introduction 168
7.2.2 The effects of space charge 169
7.2.3 The effects of grids 171
7.2.4 Other ionic charge carriers 172
7.2.5 Summary: distortion of transients 174
7.3 E.h.d. convection 176
7.3.1 Introduction 176
7.3.2 Studies of e.h.d. stability 177
7.3.3 Deductions from e.h.d. studies 179
7.4 General remarks 180
7.4.1 Photo-injection 180
7.4.2 Signal processing 181
7.4.3 Trapping model of charge transit 182
7.5 Conclusion 184
7.6 Suggestions for further work 186

8. Acknowledgements 187

9. References 188

10. Appendices 194

10.1 Journal of Physics paper: 'Experimental consequences of the E.H.D. stability criterion for dielectric liquids'. 195
10.2 Dublin Conference paper: 'On-line measurement of charge mobility'. 201
10.3 IEE York conference paper: 'The use of digital computers in measurement'. 206
10.4 Delft conference paper: 'Photo-injection into n-hexane'. 212
10.5 FM1600B computer programs. 217
10.5.1 Atten and Moreau stability criteria 218
10.5.2 Cumulative Averaging 218
10.5.3 Digital correlation 219
10.6 An analysis of the charge transit time in a space-charge distorted field in a uniform parallel-plate system 220

Chapter 1

Introduction

1. Introduction

1.1 Background to this thesis

The study of the conduction and breakdown processes in liquid dielectrics has occupied research workers for many years. The knowledge of this subject is still incomplete and although more progress has been made in recent years, the similar processes in gases and solids are more fully understood. The technological importance of these liquids as electrical insulants has been increased recently by the need to conserve the resources of energy available to mankind. Liquid dielectrics are now being used in rather different circumstances as number indicators, where the transmittive and reflective properties of liquid nematic crystals are utilised.

The study of the conduction properties of a liquid insulant presents many problems. Under conditions of high electrical stress the pre-breakdown and infra-breakdown phenomena involve a study of small time-intervals for time-lag observations or of the short pulses of charge which occur near breakdown. If the applied electrical stress is low then the currents are very small.

The measurement of these small quantities involves the experimentalist in the problems of noise and non-stationarity, and the work in this laboratory has been directed towards methods of overcoming these and other measurement problems. The philosophy on which the work has been based is the application of instrumentation to ensure consistency and accuracy of measurement and, more recently, for the purposes of processing the signals measured to evaluate statistical properties.

1.2 The purpose of this thesis

Much of the previous work in this laboratory has been concerned with the study and behaviour of liquid insulants when subjected to high electric stress.

The measurement and distributions of formative time-lags (Brignell, 1964; Beddow, 1968; Metzmacher, 1969) and the determination of statistical properties of the pulses of charge which occur near breakdown (Rhodes, 1971), involved making a large number of measurements and subsequently computing statistics. The concept of automatic measurement developed during this work, and this was followed by the desire to record, store, and compute from, these measurements in one automatic system.

During this time Buttle (1969) had investigated the problems of the unipolar injection of charge-carriers into the liquid subjected to low electric stress, and the method of digital correlation to obtain the impulse response of the liquid using a computer in an on-line mode. His investigations showed the need for further research towards an understanding of the basic-charge-transit mechanism, and into the uses of signal processing to overcome some of the problems of small current measurement which were mentioned in section 1.1.

The work in this thesis had several parallel intents apart from the overall object of advancing the state of knowledge of the conduction processes in liquid dielectrics. Firstly, the use of grids in a test cell to control charge injection and define fields was to be investigated. This method of control appears attractive, but as this work shows it creates some problems. Secondly, the application of some of the techniques of signal processing for the retrieval of small signals from a noisy environment was also to be examined. Finally, an investigation to see if the e.h.d. stability

1.2

predictions of Atten and Moreau equate with experimental observations was also to be made.

Choice of liquid

The chemical chosen for the work was n-hexane because, apart from its excellent properties as an insulant, so many experiments have been carried out using this hydrocarbon as the test liquid that it is possible to make comparitive studies with the results and conclusions of other workers. While the study of free-electrons in pure liquids is of great scientific interest, there is no suggestion yet of any application and therefore less pure liquids are of more technological importance. For example, there is the possibility of e.h.d. aiding cooling by convection, and charge-transport in liquid (c f. e.h.t. generators). Ultra high purity also puts severe constraints on the design of test cells since the very low pressures necessary to obtain this degree of purity restrict the movement of electrodes within the cell in order to vary experimental conditions.

Enhancement of Conduction

The conduction of n-hexane at low and medium electric stress is governed by the natural conductivity of the hexane which has been shown to be due to the presence of impurity ions. If these are removed, by applying a clearing field or by purification, the residual current is very small. Electrical conduction in high-fields involves emission of electrons from the cathode but the behaviour of the electrons after their injection is not fully understood. Thus, if electrons can be injected into low electric fields their behaviour can be studied more easily since the resultant current transients are present for a longer time, and collision ionization should not occur. The photo-injection method

1.2

using u.v. irradiation was chosen for this purpose since it gives a more uniform injected-charge density than the other methods that were available for non-polar liquids.

Arrangement of the thesis

In chapter 2, the results of published work having particular relevance to this thesis are reviewed, mainly photo-injection and e.h.d. convection studies.

Chapter 3 contains an examination of the problems in the measurement of charge-transit times and the theoretical background to the experimental work is presented in chapter 4.

In chapter 5, the techniques available for the study of conduction are examined and the methods and apparatus used by the author are described.

Chapter 6 contains the experimental results of tests on the liquid together with results of the signal processing techniques and the simultaneous recording of current transients and disturbances in the liquid.

The concluding discussions, together with the conclusions and suggestions for further work, are presented in chapter 7.

Chapter 2

Review of published work

2.1 Preliminary

Publications on the subject of conduction in liquid insulants are many and diverse. Fortunately, much of the earlier work has been the subject of books or review articles, e.g. Sharbaugh and Watson, 1962; Swan, 1962; Adamczewski, 1969; etc., and a recent publication (Hummell and Schmidt, 1974) surveyed thoroughly ionisation of dielectric liquids by high-energy radiation. Thus, from work already adequately reviewed, only the results which are most relevant to this project will be examined in this chapter.

There are two main sections covering, the work in which photo-injection was the charge enhancement process, and the work on e.h.d. convection. There are some results which could be in either classification but are in the former since this is surveyed first. The emphasis is on low-field conduction processes (< 10 kV/cm) in the non-polar liquid, n-hexane, but some results with polar liquids are included in the section on e.h.d. convection in view of the work in Grenoble.

2.2 Photo-injection of charge as a method of enhancing conduction

2.2.1 Introduction

This method of enhancing conduction has given reasonably consistent results for the mobility values of the resultant ionic charge carriers and 'free' electrons in liquid hydrocarbons. It has the advantage that a well-defined layer of negative charge carriers having a reasonably uniform density can be readily injected into a non-polar liquid, which is not possible with other methods, such as ionization of the liquid with high-energy radiation or high-field razor-edge injectors. In order to compare the published results, a table of mobility values etc. is included in section 2.2.8.

2.2.2 The work of Le Blanc, Morant, Chong and Inuishi, Swan, and Terlecki; 1959-1962.

Le Blanc (1959) was the first to apply the technique of photo-injection, previously used in gases, to a study of the mobility of charge carriers in hydrocarbons. Figure 2.1 shows the current transient obtained when a 50 ms pulse of u.v. light was directed

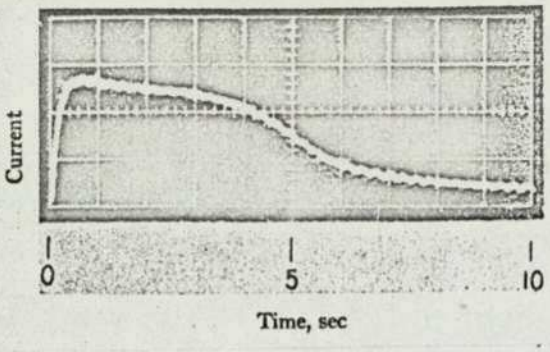


Figure 2.1 Current response to a 50 ms pulse of u.v. light on the photo-cathode (after Le Blanc).

through n-hexane on to an aluminium cathode. The magnitude of the current is stated to be about 10^{-12} A and the slow decay of the trailing edge of the pulse is a common feature of such transients. The variation of mobility values did not obey Walden's rule, which states that for ions in solution, the product of ionic mobility and solvent viscosity is independent of temperature. Le Blanc deduced from this rule that the charge carriers could not be ionic or due to electrons permanently attached to molecules. He suggested that the trapping hypothesis of Crowe (1956) was applicable (see section 4.4.6) and that the conduction resulted from an electron 'hopping' process. The point of inflexion on the trailing edge of the transients was assumed to occur at the mean transit time.

Morant (1960) was mainly concerned with the photo-injection process (figure 2.2) and confirmed that the photo-electric threshold

2.2.2

for an aluminium cathode corresponds to a work function of 4.1 eV for emission either into n-hexane or into a vacuum. Using a similar method of measurement, his value for mobility was about a third that obtained by Le Blanc. However, the liquid used by Morant was carefully purified and degassed at low pressure, thus there should have been no bulk ionisation present, which may account for the lower mobility.

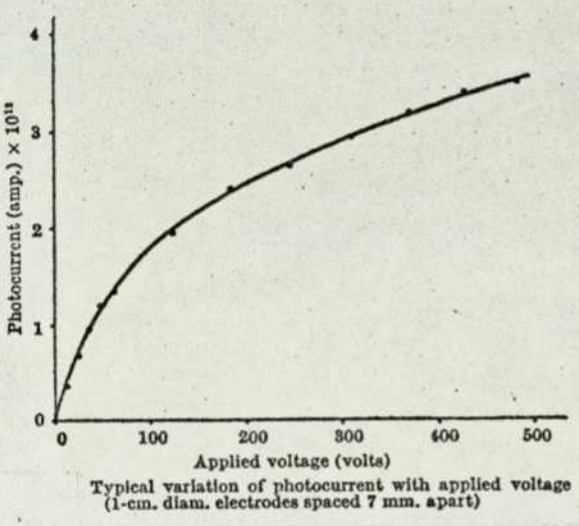


Figure 2.2

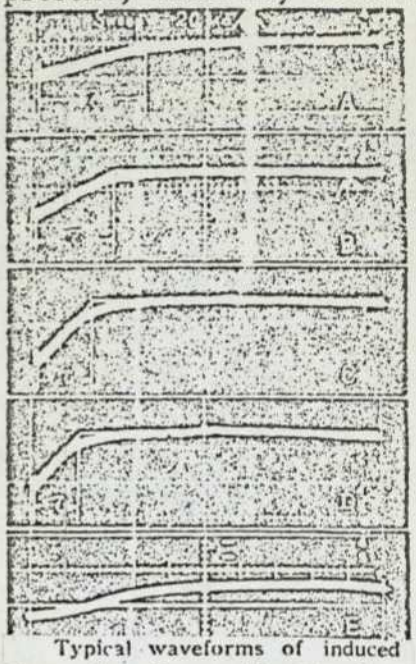


Figure 2.3

Typical waveforms of induced charges in *n*-Hexane (A ~ D) and *n*-Hexane with 1% Ethyl alcohol (E). Gap distance 0.1mm. Field Strength A: 0.15 MV/cm. B: 0.20 MV/cm. C: 0.275 MV/cm. and D: 0.385 MV/cm.

Photo-injection results of Morant, figure 2.2, and Chong and Inuishi, figure 2.3.

Chong and Inuishi (1960) used a similar purification process for the n-hexane as Le Blanc and a similar method of photo-injection except that the cathode was magnesium and the u.v. source was applied as 60 μs pulses. To overcome noise, the transient currents were integrated (figure 2.3) and it can be seen that the transients deviate from the ideal, being curved where there should be an abrupt change in slope at the transit time. The peak currents and the stress are much larger and e.h.d. convection is quite possible, although Chong and Inuishi claim field independence of mobility up to 500 kV cm^{-1}. They found that the addition of 1% ethyl alcohol to

the n-hexane halved the mobility value.

Terlecki (1962) made similar high stress measurements to Chong and Inuishi and came to the same conclusion, that mobility was independent of stress for the range 0-200 kV cm^{-1}. Terlecki used a step-function of u.v. radiation which caused distortion of the current transient for long transit times, in which cases he used the decay time, after the u.v. was switched off, for his measurements. E.h.d. convection is a possible reason for the distortion under these injection conditions.

Swan (1961) introduced the technique of injecting electrons from the surface of a thin evaporated metal film deposited on a quartz window, by the incidence of u.v. light through the quartz and onto the back of the film. As the film acts as a filter to the radiation, the possibility of bulk ionization of the liquid is appreciably reduced. Figure 2.4 curve A shows the variation of photocurrent for low fields (< 1 kV cm^{-1}) and curve B the variation for fields up to 40 kV cm^{-1}. Swan observed slow time variations in the currents when the illumination was switched on or off.

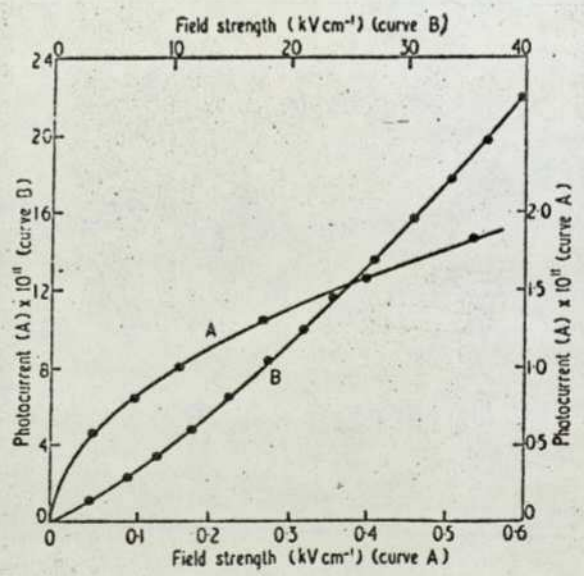


Photo-injected current in *n*-hexane (Swan 1961).

Figure 2.4. Results of back-illumination of a photo-cathode A: for low fields (< 1 kV cm^{-1}) and B: for fields up to 40 kV cm^{-1} (after Swan)

2.2.3 Photo-injection using X-rays (Secker, Lewis and Gray)

These workers used a cell devised by Secker (1965) in which a thin layer of ionization was generated by collimating a X-ray beam so that it strikes an aluminum foil electrode at a glancing angle (2^{o}) outside the liquid. Photo-electrons and some primary radiation generated a thin ion layer of about 0.1 mm thickness. Currents of the order of 10^{-10} A were induced in the n-hexane for a drift gap of 1.34 cm and applied voltages of 300 V to 5 kV. Secker and Lewis (1965) subsequently made mobility measurements of charge carriers of both polarities, see figure 2.5, which were later repeated by Gray (1967), who found that introducing air to the system caused an insignificant change in the transit times. The results have a wide spread which is probably due to the ionization resulting from primary X-ray irradiation, and this is supported by the presence of positive and negative polarity carriers. Secker and Lewis (1965) suggested that liquid motion was present and that the magnitude of this and the time for it to reach a steady value were related to the power input to the cell, because the mobility values increased as the X-ray beam intensified.

2.2.4 The determination of impulse response (Buttle and Brignell)

This work immediately preceeded that of the author in this laboratory and introduced several new approaches to the problems of mobility measurement. The concepts of signal processing were applied to the problem of small current measurement in the presence of noise and digital correlation was used to determine the impulse response of the system (Buttle and Brignell, 1968; Buttle 1969). A vapour gap was introduced above the n-hexane to enhance photo-emission and it was proposed that a grid electrode could be used to control injection into the liquid and to define the drift field

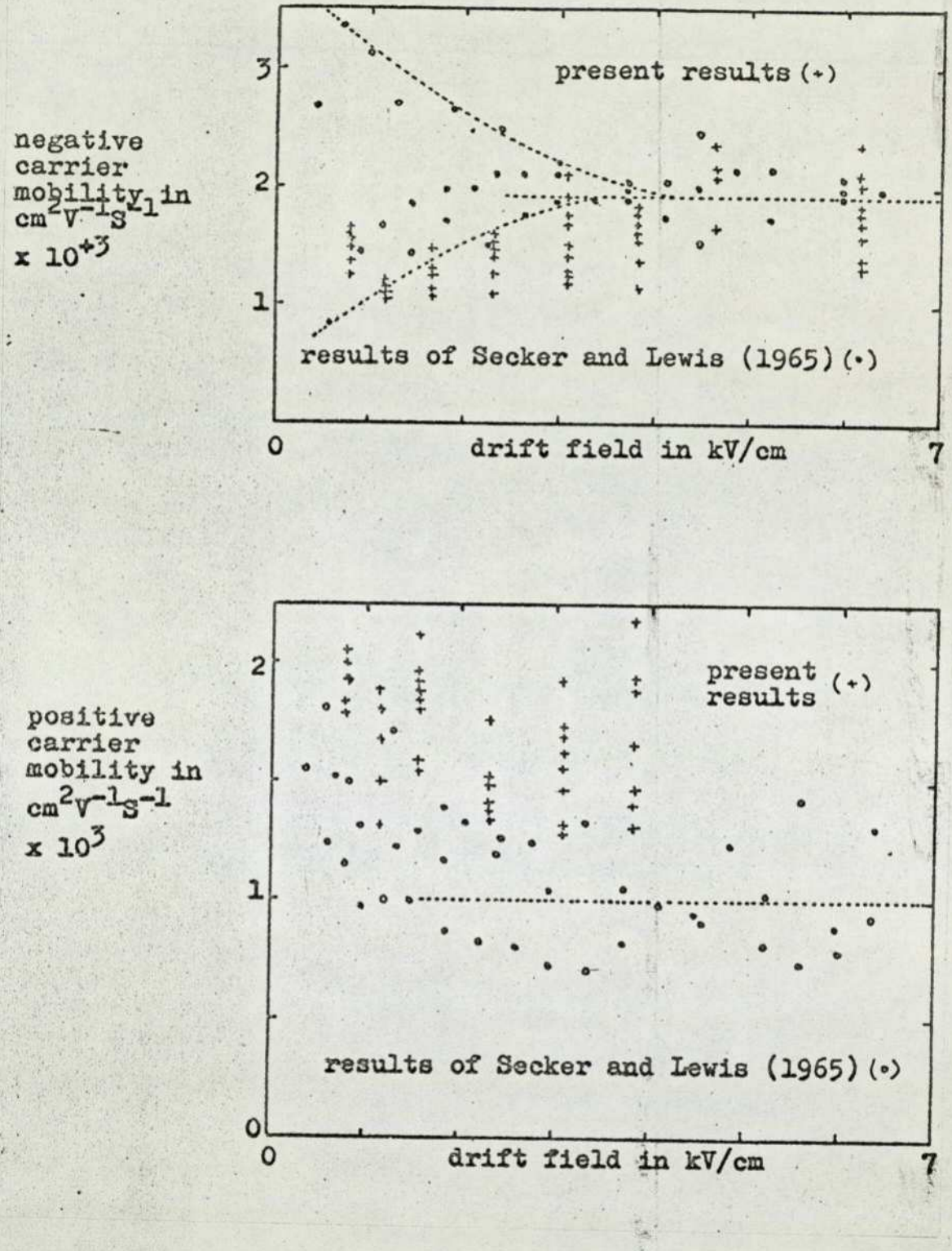
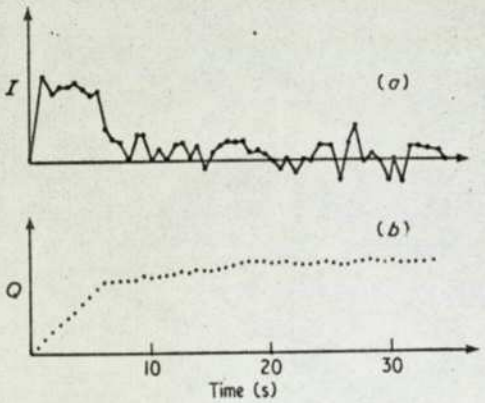


Figure 2.5 A comparison of the photo-injection mobility results of Gray ('present results') using an X-ray triode cell and those of Secker and Lewis (1965) who used a X-ray diode cell (after Gray).

(Buttle and Brignell, 1969). Similar mobility values were obtained with and without the vapour gap and it was concluded that the transit time through the vapour gap and any space charge effects in the vapour could be neglected. Figure 2.6, (after Brignell and Buttle, 1971), shows the estimated current transient to an impulse stimulus in a sample of n-hexane using the process of digital correlation (see section 4.3.3), together with the corresponding charge transient obtained by integration of the current waveform.



(*a*) A typical reconstructed current transient obtained with 400 V across a 1 cm gap.
(*b*) The corresponding charge transient obtained by integration.

Figure 2.6 The results of the digital correlation technique using a 63 bits p.r.b.s. stimulus (after Brignell and Buttle)

Brignell and Buttle also showed that no variation of mobility with input power occurred over the range 10^{-11} to 10^{-8} W (see figure 2.7) and concluded that the presence of e.h.d. convection was unlikely with low-power photo-injections. Some evidence was also obtained for the presence of a second negative charge carrier with a mobility about a third that of the main carrier.

The effect of a vapour gap is shown in fig. 2.8, where the initial spike close to the origin is due to the higher velocity of the carriers in the drift gap. The fall in current was explained as possibly being due to electrons rebounding from the liquid surface, but a more likely cause is an accumulation of space-charge at the surface.

2.2.4

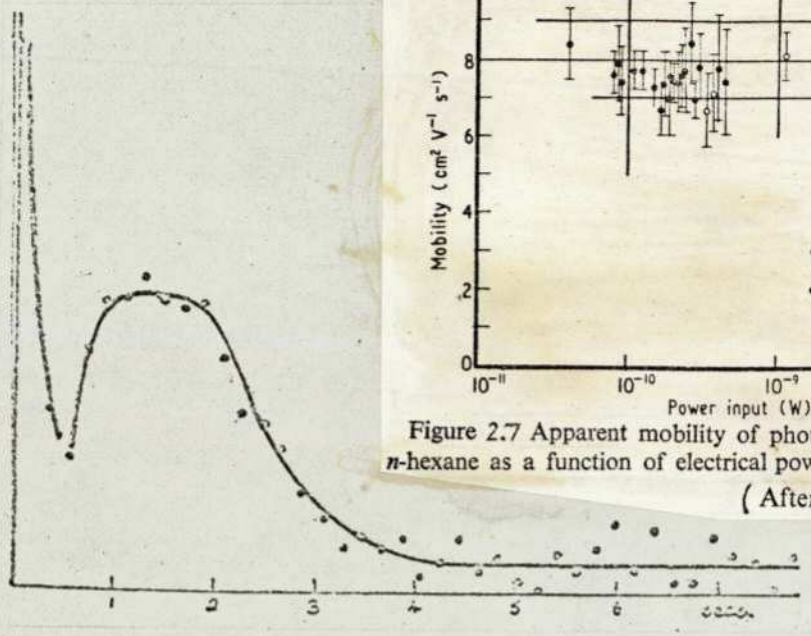


Figure 2.8 Impulse response of a test cell with an interelectrode gap of 11.5 mm of which 6.5 mm is occupied by n-hexane and the remainder by vapour. 500 volts was applied to the cell (after Buttle).

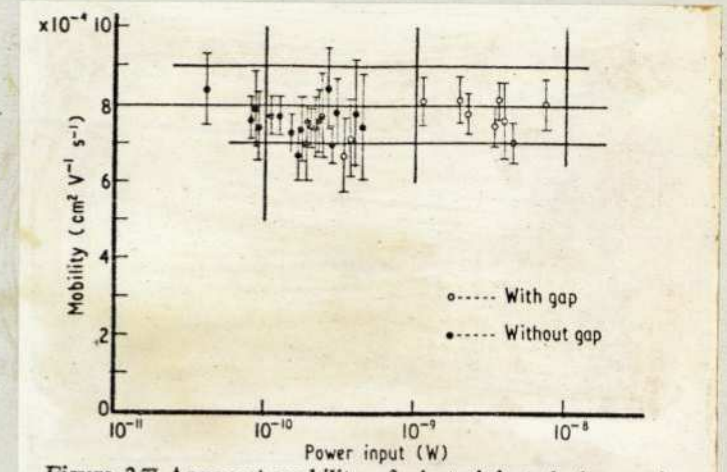


Figure 2.7 Apparent mobility of photo-injected charges in *n*-hexane as a function of electrical power input to the test-cell. (After *Brignell and Buttle*)

Buttle thought the 'long-tail' on his current transients could be the result of diffusion and non-linearity of the electric field in the outer regions of the gap. He developed a computer model of the charge transport process and tested this by simulating the s.c.l. current transients discussed by Many and Rakavy (1962). He also simulated the charge injection used in the digital correlation method and obtained the results in figure 2.9.

2.2.5 The work of Pugh, Bloor and Rahman

This group of workers at the University of Durham extended the photo-injection studies of Morant using purified n-hexane as the test liquid. Pugh (1968) irradiated the photocathode obliquely through the liquid and made a thorough examination of the photo-emission process, examining particularly thin film photo-emitters of aluminium, magnesium and gold. He observed a decay in the photo-emission with time, which was retarded if the photocathodes were stored under vacuum before they could be used in the test cell.

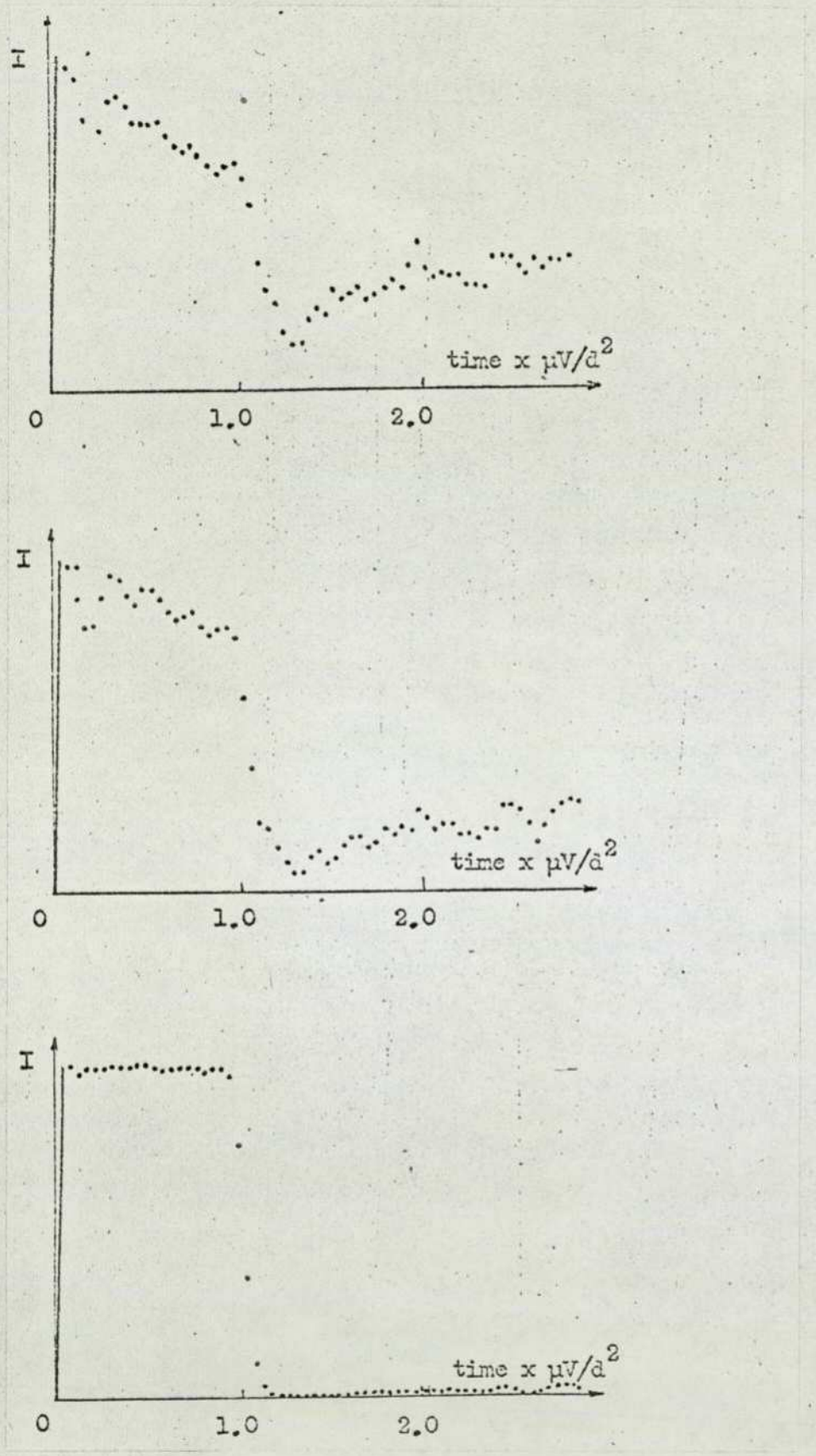


Figure 2.9 Impulse response of a computer simulation of the charge-transport process under s.c.p. conditions. The charge-injected in each case was proportional to the stress at the injection electrode. The top trace shows the greatest charge injection, the bottom the least (after Buttle).

2.2.5

The emission from gold was considerably less than the other two materials for the same field stress, presumably because of its higher work-function, and the decay of emission with aluminium and magnesium was thought to be due to oxidation.

Bloor (1970) measured negative charge mobilities in both highly purified degassed hexane and gassy hexane, and concluded that the mobility ($\simeq 10^{-7}$ m^2 V^{-1} s^{-1}) does not change after degassing and is also independent of field up to 140 kV cm^{-1}. He also concluded that dissolved oxygen reduces the photo-current but not the shape of the transient response to pulsed-charge injection. Rahman (1970) measured current transients arising from the injection of pulse and step-injected photo-charge into n-hexane. The occurrence of currents when the cell potentials were reversed in polarity suggests emission from the solid metal electrode due to u.v. radiation passing through the liquid. The mobility of the positive carriers was slightly greater than that of the negative carriers.

2.2.6 High-mobility charge carriers in liquid insulants

Minday, Schmidt and Davis (1969, 1971) reported high-mobility negative charge carriers in very pure n-hexane with mobilities about 100 times the slow carriers. Figure 2.10 shows the transients obtained by these workers using a pulsed u.v. light source and a vacuum deposited barium film. The overshoot in trace (b) is thought to be due to e.h.d. convection in less pure hexane where negative ions are the major carriers.

2.2.6

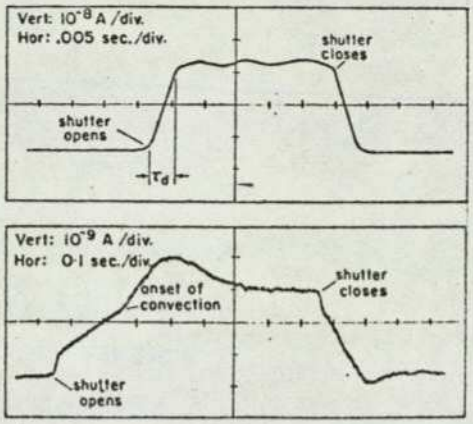


Figure 2.10 Current transients in n-hexane in response to pulse photo-injection (after Minday et al) (a) ultra pure (b) less pure

Figure 2.11 shows the drift velocities of fast charge carriers as a function of electric field for other very pure hydrocarbons (Minday et al, 1971) and argon (Miller et al, 1968) and for negative ions in n-hexane (Le Blanc, 1959). Measurements in a triode cell with photo-charge injection into the liquid demonstrated that only electrons could be drawn from the liquid into vapour above. Introduction of water vapour or oxygen as impurities into n-hexane, pure enough to inhibit electronic carriers, slowly produced ionic carriers as the impurity diffused into the hexane, until after two hours no electronic carriers could be measured.

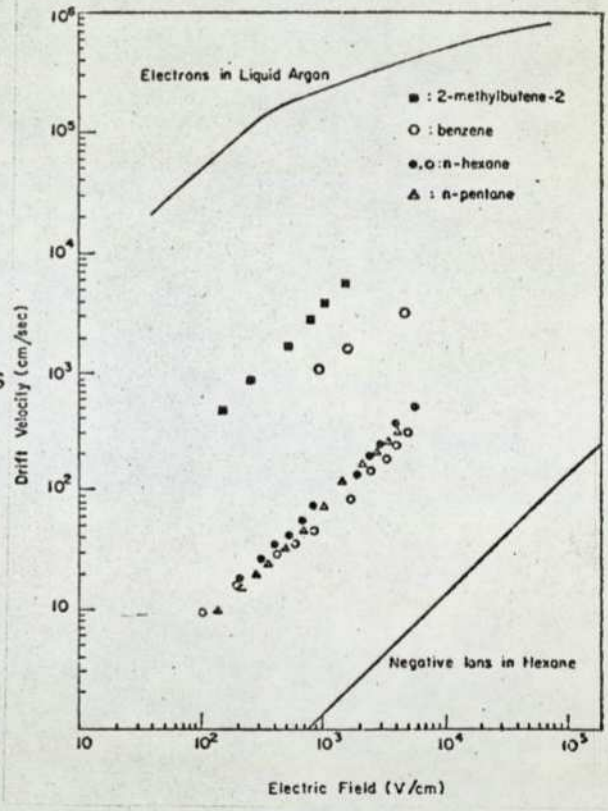


Figure 2.11 Drift velocity versus field for fast charge carriers in hydrocarbons and liquid argon and negative ions in n-hexane (after Minday et al).

2.2.6

The mobility of the ionic carriers ($\simeq 10^{-7}$ m^2 V^{-1} s^{-1}) was the same for both impurities, and the value of the electronic carrier mobility was also unaffected by the impurity. Conrad and Silverman (1969) and Schmidt and Allen (1970) also, independently, detected fast negative charge carriers following X-irradiation of highly purified n-hexane and other hydrocarbons. Their mobility values for n-hexane are similar to that obtained by Minday, Schmidt and Davis for the fast carrier.

2.2.7 The work of Evison (1975)

A co-worker in this laboratory, Evison, has recently investigated the modelling of charge injection following the earlier work of Buttle (see section 2.2.4). He also made photo-injection studies of enhanced conduction in n-hexane using a simple diode cell and plotted the results on normalised scales of current (with reference to a s.c.l. value) and time. Both pulse and step-stimuli were used for a series of transit current measurements in which the liquid sample, applied field, u.v. intensity and the polarity of the electrodes were variable parameters. He concluded that the 'long-tail' which was present on the transients was not due to bulk-ionisation effects (see figure 2.12), but to the presence of different types of charge carriers with a range of mobility values. He also found a marked similarity between the behaviour of charge carriers in liquid and solid insulants which supports the concept of 'trapping' as the conduction mechanism. An increasing slope on some of the transients currents from a step-injection of charge was considered to be due to e.h.d. convection.

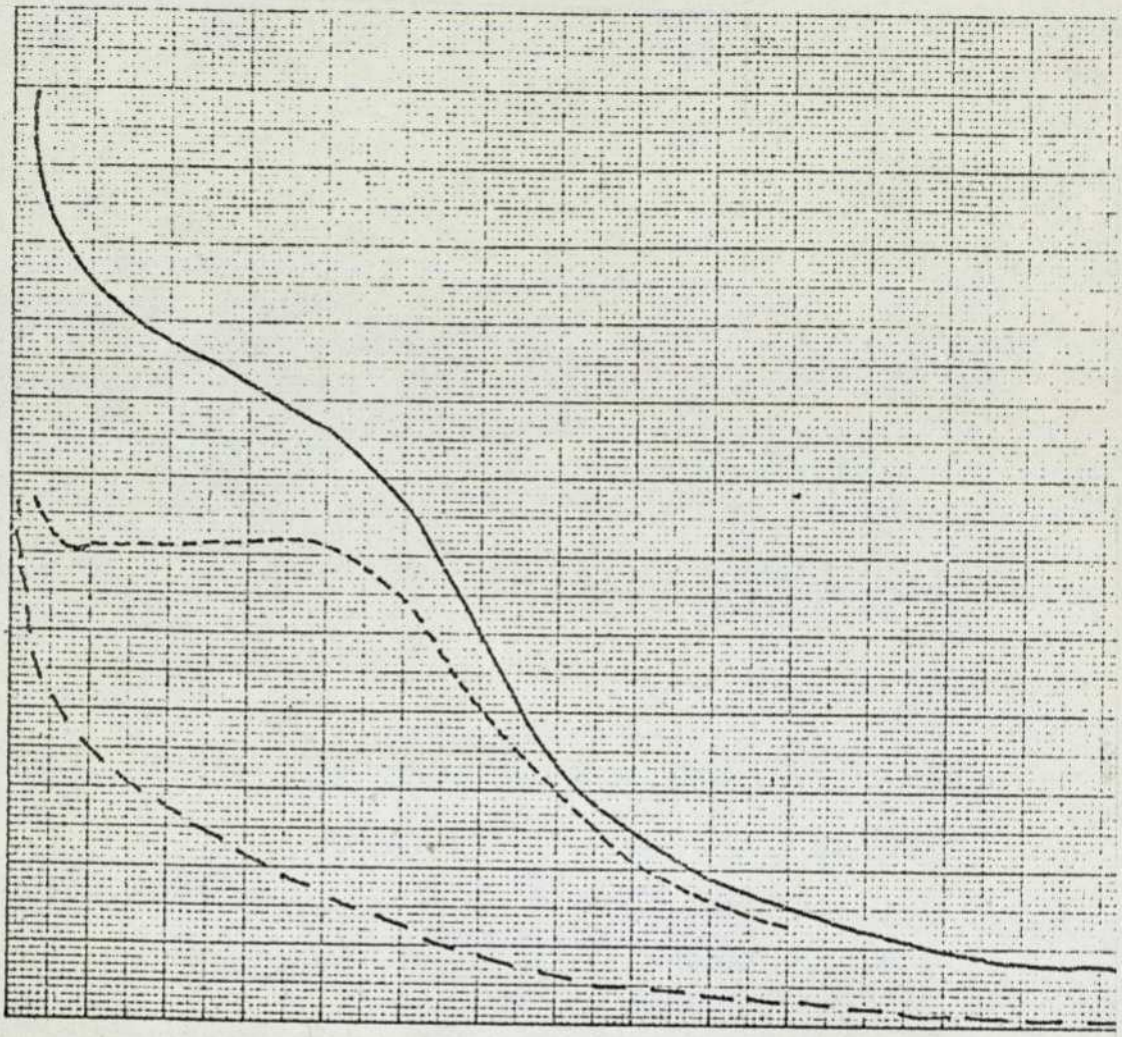


Figure 2.12 The elimination of bulk ionisation from transients (after Evison)

(a) normal polarity on electrodes ———

(b) reverse polarity on electrodes — —

(c) difference of (a) and (b) ------

2.2.8 Summary of photo-injection results

In table 2.1, the results of the various experiments where photo-injection was employed to enhance conduction are summarized.

TABLE 2.1

Author	Mobility ($\times 10^8$ m^2 V^{-1} s^{-1})	Activation Energy (eV)	Max. E $kVcm^{-1}$	Max. J A cm^{-2}	Resistivity (Ω cm)
Le Blanc (1959)	14 ± 1	0.14 ± 0.02	2	≃2	10^{16} - 10^{17}
Morant (1960)	≃ 5		1	≃ 4	10^{16} - 10^{17}
Chong & Inuishi (1960)	10	0.16	500		
	4.5 (1% C_2H_5OH)				
Terlecki (1962)	10		100		10^{19}
Swan (1961)	8		40	≃ 4	> 10^{18}
Secker, Lewis (1965) & Gray (1967)	μ_- = 10 → 30		5		
	μ_+ = 10 → 20				
Buttle (1969)	μ_{1-} = 7.5 ± 1		1	≃ 10	
	μ_{2-} = 2.5 ± 0.6				
Pugh (1968)	6		3	≃ 15	
Bloor (1970)	10		140		
Rahman (1970)	μ_- = 6.5		2.2	≃ 2	
	μ_+ = 8				
Minday et al (1971)	$\mu_{1\text{-SLOW}}$ ≃ 8	0.14	≃ 1		
	$\mu_{2\text{-FAST}}$ ≃ 700	0.18		≃ 10^4	10^{19}

2.3 The effects of EHD Convection

2.3.1 Introduction

This section includes results which have been influenced by e.h.d. convection but which were not examined in section 2.2, as well as those in which the study of motion in the liquid was the main concern. Ostroumov (1954) was the first person to present a system of basic equations to account for both the electronic and hydrodynamic phenomena in liquid motion, and in a series of experiments (Ostroumov, 1956) he demonstrated e.h.d. convection in polar liqiuds, observing the disturbance with a schlieren type optical system. This survey is confined to e.h.d. convection in low electric fields and although the emphasis is on non-polar liquids, some of the work in polar liquids which is very relevant, will also be reviewed.

2.3.2 E.h.d. convection in non-polar liquids

Gray and Lewis (1965) were first to point out the effects of liquid motion on measurements of ion mobility in non-polar liquids in general and n-hexane in particular. They concluded from their observations of the motion of a dye blob (see figure 2.13) in a low field ($\simeq$ 1 1kV/cm) that the ion and liquid velocities for the negative carrier were equal. They were able to detect liquid motion for an electrical power input of 10^{-7}W. For the positive carrier (the liquid was ionized by a beta-particle source on one electrode) the ion velocity was about twice that of the liquid. Smith and Calderwood (1968) also observed e.h.d. convection in hexane using the dye blob method and figure 2.14 shows their results for a peak stress of 250 V cm^{-1}. Schlieren observations of the motion were possible at steady fields above 2.5 kV cm^{-1}, or when the gap voltage was altered at lower fields, indicating the presence of ionic carriers

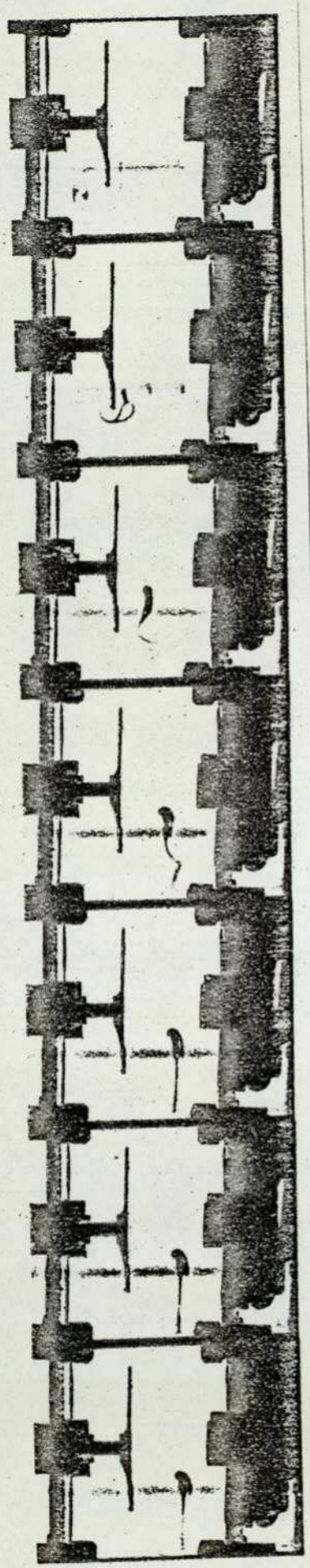


Figure 2.13 (after Gray and Lews)

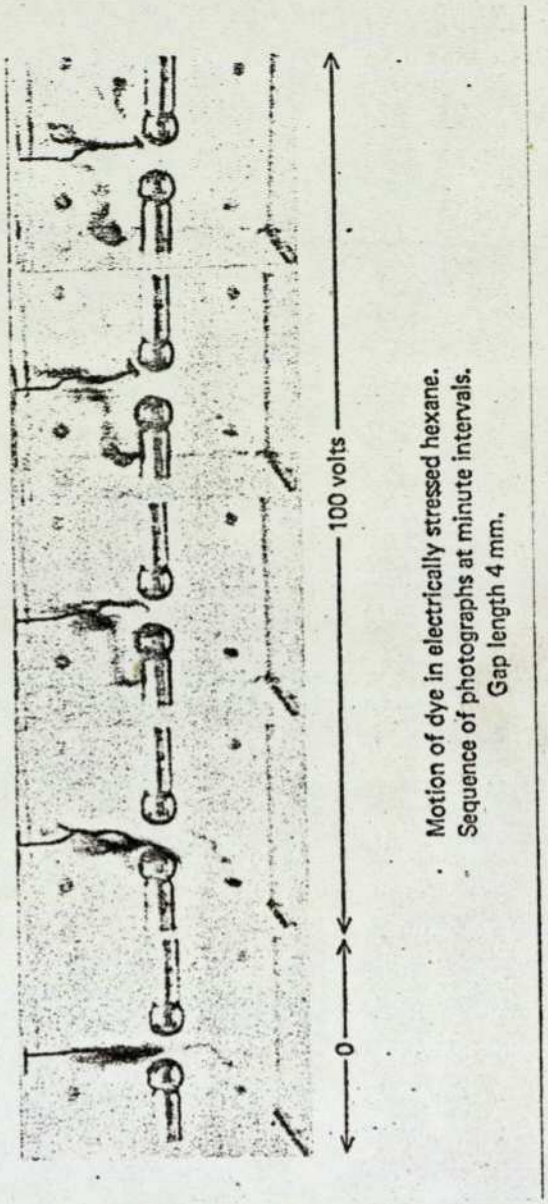


Figure 2.14 (after Smith and Calderwood)

Dye blob motion in electrically stressed n-hexane.

2.3.2

in the liquid under low-stress conditions. Coe, Hughes and Secker (1966) increased the injection and hence the liquid motion by using field-emitting razor-edge cathodes and Essex and Secker (1968) found a wide range of 'apparent' mobilities for n-hexane, when they varied the potential of the field-emitters but maintained the drift field stress constant. Extrapolating these results to the potential at which field emission commenced they proposed that the 'true' mobility was 2.7×10^{-8} m^2 V^{-1} s^{-1} (see figure 2.15). This is lower than the results obtained from the photo-injection studies (see table 2.1, section 2.2.8).

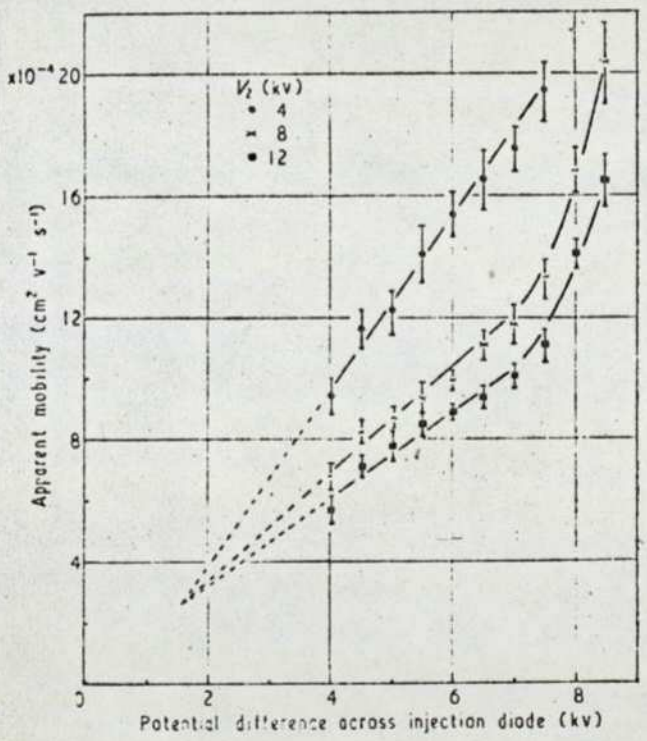


Figure 2.15 Variation of apparent mobility with p.d. across the injection diode. Each point represents the mean of at least 50 readings; mean deviations are indicated. (after Essex and Secker).

Gray and Lewis (1969) using a double-grid cell and a beta-source on the emitter to ionize the hexane, found that the apparent mobility of carriers in the drift-gap between the grids varied inversely as the field, which was thought to be due to 'liquid

2.3.2

motion saturation' at high fields. Figure 2.16 shows the variation of mobility with current. By extrapolating to zero current, Gray and Lewis suggested the true mobility for negative charge carriers was less than 2×10^{-8} m^2 V^{-1} s^{-1}.

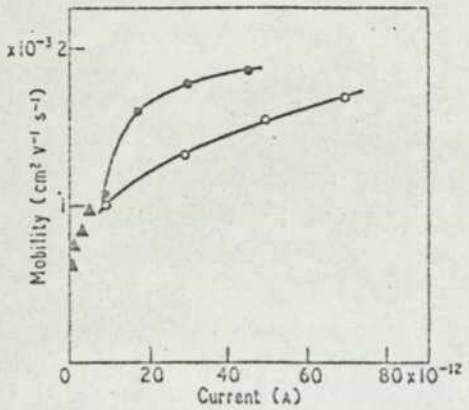


Figure 2.16 Apparent mobility versus current in drift field of 1 kV cm^{-1} for various experimental conditions (after Gray and Lewis).

Taylor (1972) also used razor-edge injectors in test cells of different hydrodynamic impedance and observed liquid motion by using Schlieren and laser-doppler anemonetry methods. He concluded there were two negative charge carriers present and estimated the true mobilities to be about 2×10^{-8} and 7.8×10^{-8} m^2 V^{-1} s^{-1}.

Thomas (1972) found that e.h.d. convection in a purified sample of n-hexane commenced at a stress of $\approx$ 18 kV cm^{-1}. This critical voltage agreed with the theoretical value which he derived, assuming a 'roll-cell' model for the e.h.d. convection.

2.3.3 E.h.d. convection in polar liquids

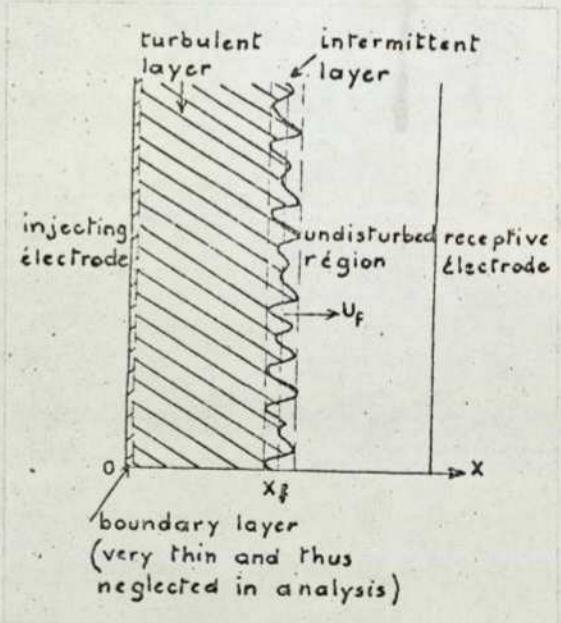
Atten and Gosse (1969) found that the mobility of positive ions injected from a permselective membrane into nitrobenzene was about ten times the true mobility. This was thought to be due to bulk liquid motion and led to the extensive study of e.h.d. convection by Atten, Gosse and their colleagues in Grenoble. At the

2.3.3

Lancaster conference, Hopfinger, Gosse and Atten (1970) and Filippini, Gosse, Lacroix and Tobazeon (1970) reported on studies of the e.h.d. phenomena using a schlieren system. Injection of positive ions into a polar liquid between parallel-plate electrodes resulted in e.h.d. convection (see figure 2.17(a), which was described in terms of the model structure in figure 2.17(b). A time lag between voltage application to the drift gap and the beginning of liquid motion was found to be proportional to the viscosity of the liquid and inversely proportional to the square of the mean electric stress in the liquid. The hydrodynamic mobility, μ_h, defined as average velocity/mean electric field was measured for the liquids. It was observed that the time-delay (before motion commences) is followed by a turbulence formation period, then the 'first transient', during which the turbulent region



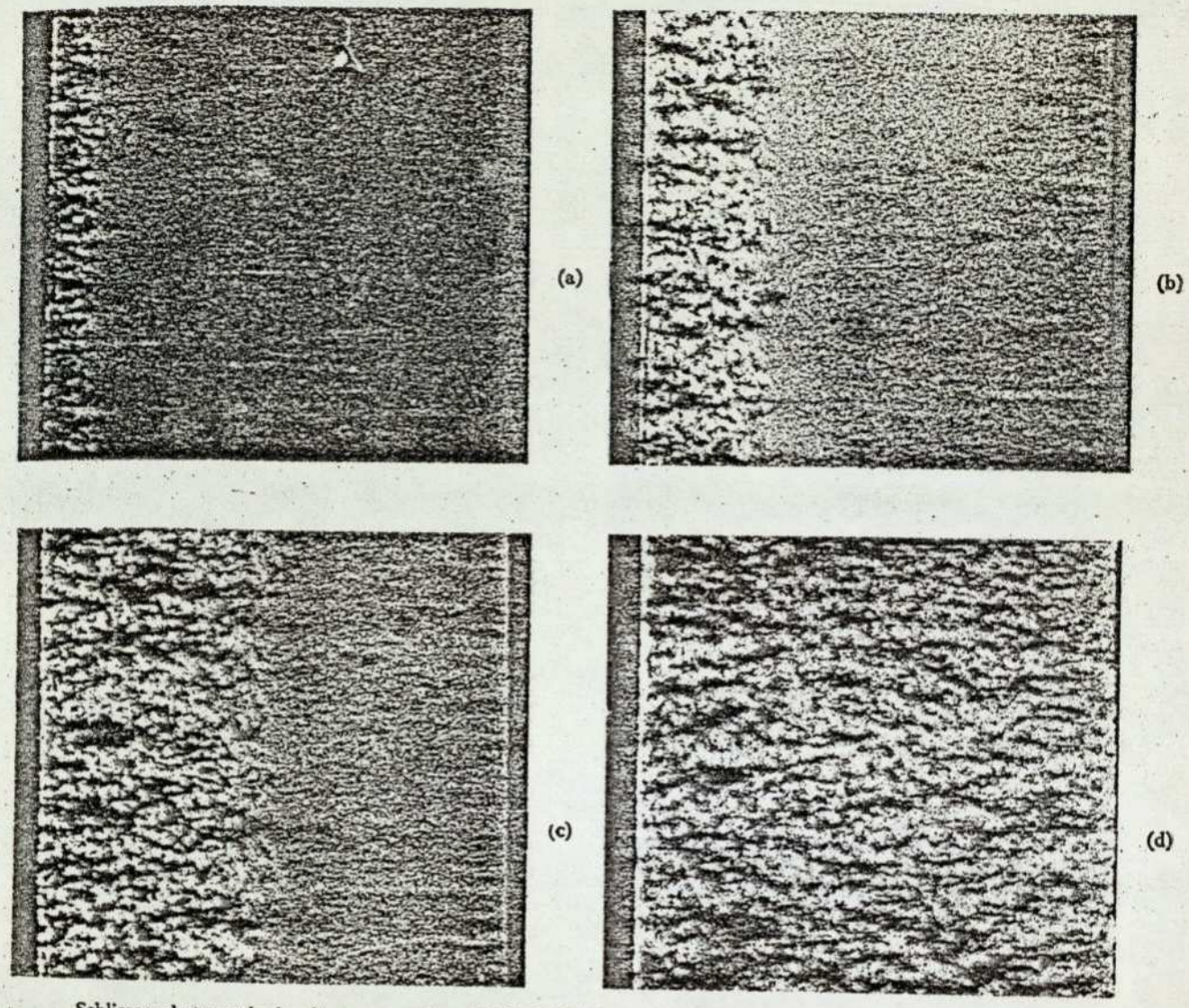
(a)



(b)

Figure 2.17 (a) E.h.d. convection from positive ion injection into a polar liquid (after Filippini et al).

(b) A model structure of the advancing convection (after Hopfinger et al).



Schlieren photographs in nitrobenzene, $V_a = 18$ kV, $L = 0.56$ cm; (a) 0.95 msec, (b) 1.9 msec, (c) 2.9 msec, (d) steady state.

Figure 2.18 E.h.d. instability in nitrobenzene following a step-injection of positive charge carriers (after Hopfinger and Gosse).

2.3.3

invades the liquid from the injector to the collector. During the 'second transient' period, the boundary layer at the collector was thought to control the current, and finally a steady-state condition was reached. Filippini, Lacroix and Tobazeon (1970) derived relationships between dimensionless parameters representative of the transit time and the critical voltage, for the four transient cases of current and voltage, step and ramp injection of positive charge-carriers. These relationships were then used to detect the onset of e.h.d. instability in nitrobenzene injected with protons. From the experimental results they obtained values for the critical voltages as follows:-

For current step injection: $V_c = 6 - 16$ V

For current ramp injection: $V_c = 7 - 20$ V

For voltage ramp injection: $V_c = 7 - 13$ V

For voltage step injection: $V_c = 2 - 5$ V,

whereas the theoretical criterion of Atten and Moreau for steady-state injection ($16\mu\eta/\varepsilon$) gives a critical voltage of 21 V for the same liquid. In an extension of this work, Hopfinger and Gosse (1971) reported schlieren observations (see figure 2.18) which strongly supported the assumption that if the applied voltage is sufficiently high, the 'self-generated' motion is turbulent shortly after the field is applied. Also the electric field distribution, as measured by the Kerr-optic effect, and the steady state of turbulence is uniform, implying uniform charge distribution, whereas when the liquid is motionless the charge density varies inversely as the square root of the distance from the injector.

Watson, Schneider and Till (1970) studied electro-convective effects in thin dielectric films of methyl phenyl siloxane Dow

2.3.3

Corning 703 using an electron beam as the injecting mechanism into a free surface, and a second beam to determine the surface potential. The transition from s.c.l. currents to convection-enhanced conduction is signified in figure 2.19 as the injection is increased, by the emergence of a well-defined peak in the surface potential versus time curves. Above the theoretical critical voltage, a cellular-convection motion of the liquid occurred corresponding to the transition from s.c.l. to convection-enhanced conduction.

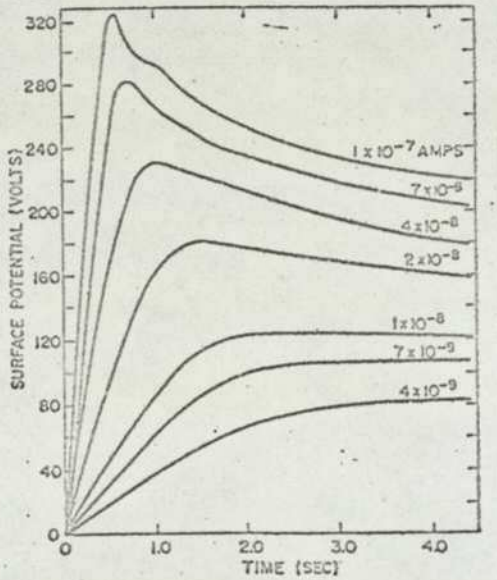


Figure 2.19 Typical charging characteristics for a sample of Dow Corning 703, with charging current as a parameter (after Watson et al).

Lacroix and Tobazeon (1972) measured the apparent mobility ($d^2/\tau V$) for Aroclor 1500, which is about six time more viscous than nitrobenzene and has a lower relative permittivity ($\varepsilon_r = 6.4$), by applying a step voltage and observing the current. The results are shown in figure 2.20 as apparent mobility versus voltage, whence the critical voltage is clearly seen to be ≈ 120 V. The upper trace, N_e, is a dimensionless form of the current, where the reference is the current that would flow if there was no e.h.d. convection.

2.3.3

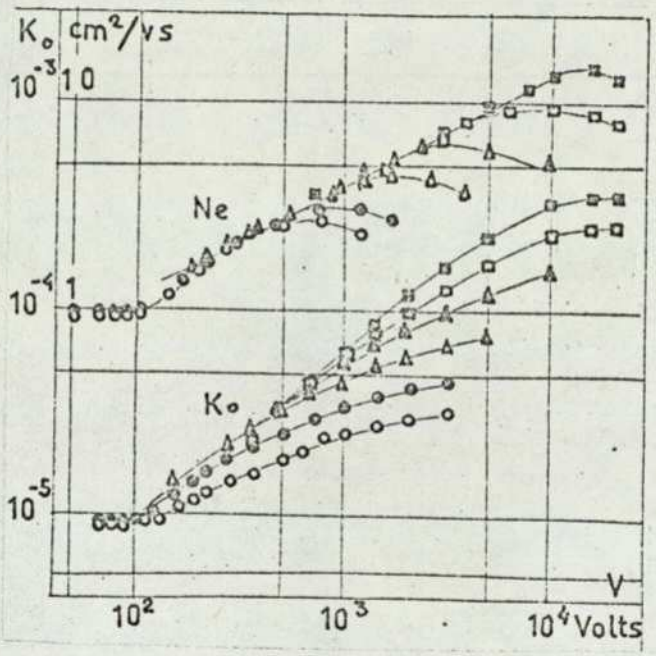


Figure 2.20 Lower trace: apparent mobility versus voltage
Upper trace: variation of the number Ne with voltage.
Both for Aroclor 1500. (After Lacroix and Tobazeon).

As the viscosity was reduced to 40% of its value at 20°C, by raising the temperature, the critical voltage remained ≈ 120 V. This value of V_c was 3 to 4 times smaller than that given by the stability criterion for steady-state conduction. The apparent mobility was found to vary approximately as $\varepsilon V/\eta$ up to a stress of 10 kV cm^{-1}, after which it became non-linear, due to a reduced q_o at the injector. When the voltage V was slightly greater than V_c, cellular convection was observed but if V was increased further the cellular structure was gradually replaced by turbulence. The strong dependence of the apparent mobility upon voltage, see figure 2.20, was not observed in the less viscous nitrobenzene (Filippini, Lacroix, Tobazeon; 1970).

2.4 Significant results from other work

2.4.1 The effects of using grid electrodes

Dey and Lewis (1968) constructed a triode cell for their experiments on ion mobility in liquid argon. The grid, with an

2.4.1

appropriate bias, controlled the injection into the drift field of ions of either polarity, which were produced by α-particle ionization of the liquid close to an electrode. The shapes of the transients (see figure 2.22) are distorted from the ideal waveforms

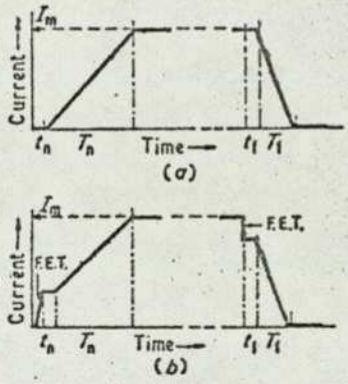


Figure 2.21 Ideal collector current transients caused by switching the emitter field in argon with a grid (a) ions only (b) free electrons + ions

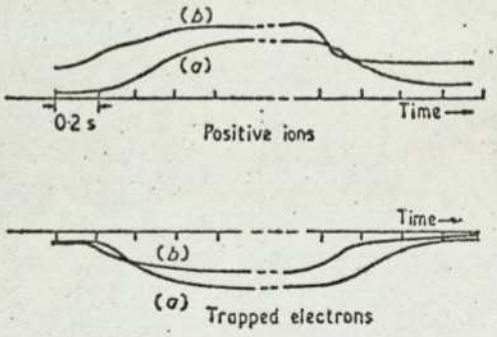


Figure 2.22 Ion transients in normal argon for a drift field of 1 kV cm^{-1}, without (a) and with (b) space charge distortion.

Both figures after Dey and Lewis.

in figure 2.21. Dey and Lewis suggested this was due to diffusion from the grid region and that, for high levels of injection, space charges disturb the drift field (figure 2.22b). Liquid motion resulting from ion movement was considered to cause the 'off' transient to be faster and more consistent than the 'on' transient. Similar effects were observed by Gray and Lewis (1968) using a double-grid cell and the same type of injection mechanism as Dey and Lewis.

When injection is by high-field razor-edge emitters, grids are used to define the drift field (Taylor, 1972). Figure 2.24 shows some of the waveforms observed for negative charge carriers in n-hexane using the experimental arrangement in Figure 2.23. The drift voltage is equivalent to a mean stress of 1.6 kV cm^{-1} in the

2.4.1

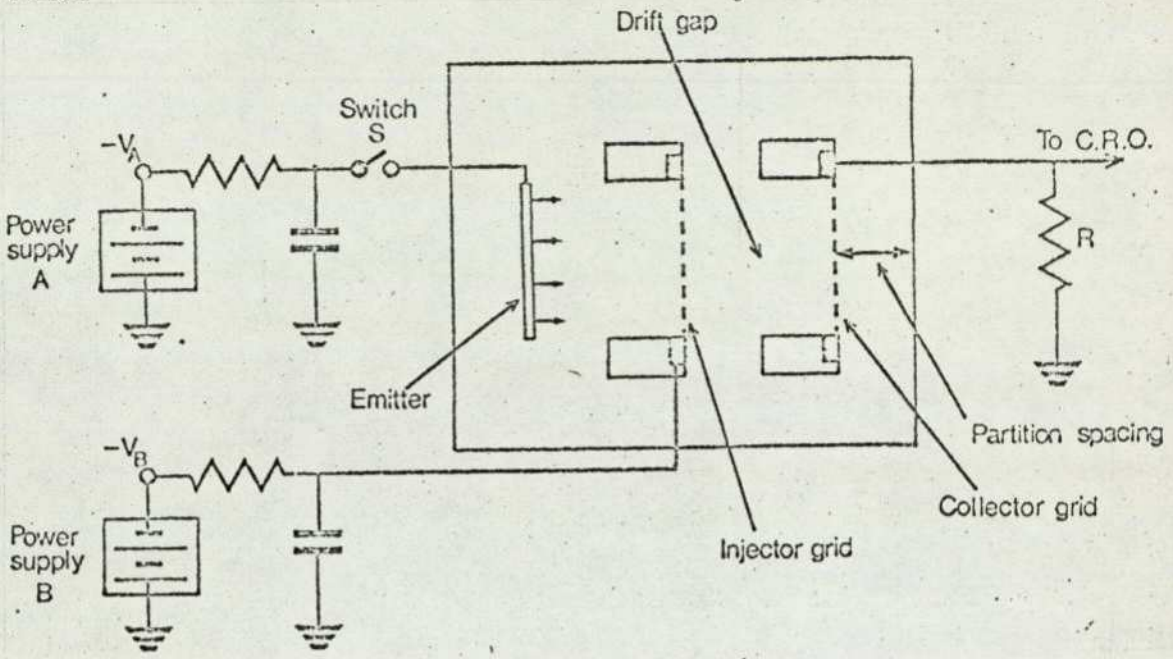


Figure 2.23 Experimental arrangement for the measurement of apparent mobility (after Taylor).

drift gap, and the injection voltage (V_A - V_B) is varied from 7.5 kV in trace (a) to 12 kV in (d) of figure 2.24. The apparent mobilities of the negative charge carriers were determined from the second maxima on the traces, though the first peak was considered to be evidence for the presence of a second negative carrier. An extrapolation of the apparent mobilities was made to determine the true mobility, by estimating the mobility value when injection just ceases, after Essex and Secker (1968), see section 2.3.2.

Minday, Schmidt and Davis (1971) used a double grid cell for their experiments in highly purified n-hexane. When water vapour or oxygen was allowed to diffuse into the liquid the current transients due to ionic carriers (figure 2.10) showed distortion, which was thought to be due to e.h.d. convection. This is probably true but the cause of the convection is more likely to be space-charge in the grid interstices (see section 4.4.3).

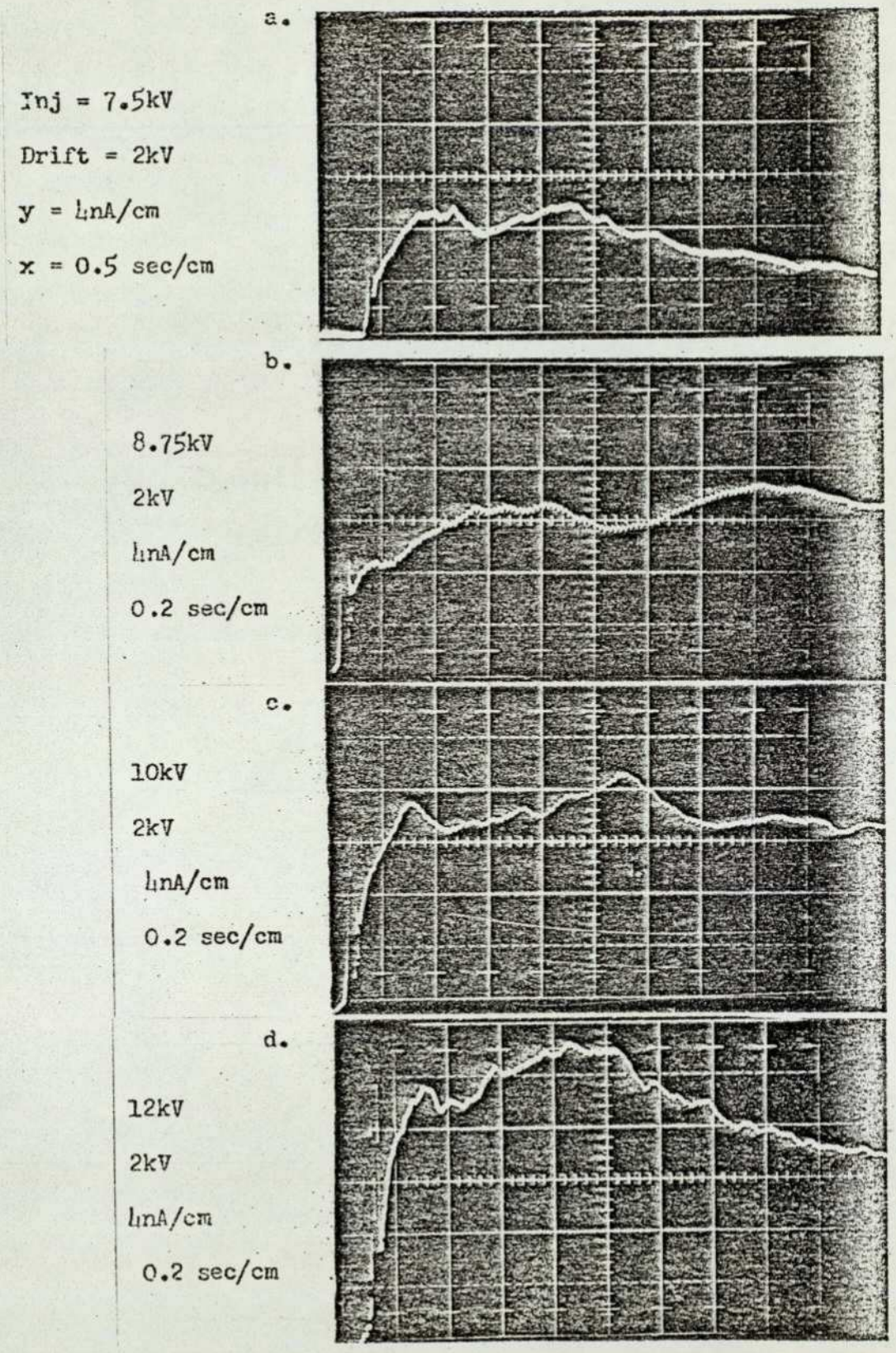


Figure 2.24 Current transients for negative charge carrier injection using razor-edge emitters (after Taylor).

2.4.2 Delayed injection of negative charge carriers

Felici and Sauviat (1972), reporting the use of electrodialytic varnishes as ion injectors into polar liquids, found a delay of tens of seconds when basic polymers were used to inject negative ions. In this case the electrons required for negative ion injection originate from the polymer itself not the aluminium or stainless steel discs upon which the varnish is applied to a thickness of 20 to 30 μm. After prolonged use, depolymerization ensues and the varnish layer breaks up.

Chapter 3

Problems in the measurement of charge transit times

3.1 Introduction

In this chapter and the next, frequent reference will be made to a book ('Laboratory on-line computing', Intertext, London; Brignell & Rhodes, 1975) which contains a thorough account of the methods of on-line computer-aided measurement developed in the laboratories in which the present work was done, some of which were realized by the present author. The existence of this book makes it unnecessary to burden this thesis with any but the more strictly relevant details, and it will be taken as the starting point for much of what follows.

The measurement of charge transit times in liquid dielectrics subjected to low electric stress and unipolar charge injection presents certain problems to the experimentalist. The velocity of the charge carriers, whether they are ions or molecular clusters, is very low, and thus the amount of current to be measured is limited to the order of pico-amperes. With currents of this magnitude the noise content is likely to cause difficulties in measurement. Non-stationarity in the background or quiescent current, non-linearity due to space-charge effects, and electro-hydrodynamic instability in the liquid are other problems which can arise. A feature of the current transients to pulse stimuli measured by many previous workers (see Chapter 2) is the slow decay or 'long tail' effect, which presents a further interpretive problem in the measurement of transit times.

The chapter examines these problems and discusses some ways of tackling them.

3.2 Noise

In telecommunications noise is defined as 'any unwanted signal', a definition which is equally applicable to the measurement

3.2

of small currents in liquid dielectrics.

The noise associated with a current transient has many sources both inside and outside the test cell, e.g., thermal agitation, the charge injection process, the measuring system (section 5.1.4), etc. Even after all reasonable means have been adopted to minimize noise, the current signal may remain obscured. One approach to the problem is to filter out the noise and this is often done using a low-pass filter. This may be a satisfactory solution if the charge transit time is known approximately and no further information is required from the current signal. However, it has the obvious disadvantage of eliminating any possibility of observing phenomena having a fundamental frequency above the cut-off frequency of the filter.

An alternative line of approach to the problem is possible if the noise is 'random'. Random noise has the important property of being uncorrelated, i.e. the cross-correlation of the noise signal $n(t)$ with another signal $s(t)$ is zero, i.e. the average $\overline{n(t).s(t)}$ is zero, where $s(t)$ is any signal other than $n(t)$. Infinite bandwidth is required to obtain complete uncorrelation and in practice it is not possible to completely eliminate random noise.

If a number of current responses to identical stimuli are averaged together, the random noise content is reduced by the averaging process. Provided the appropriate weighting is applied to each new response as it is included in the average, this can be a cumulative process. However, care must be taken to ensure that during this averaging process a significant amount of non-random noise, e.g. from quantization of samples of the response, is not added to the result.

3.3 Non-stationarity

The cumulative average process would appear to be an ideal solution to the problem of noise reduction and is certainly a powerful method. However the method of applying a direct pulse of charge to the liquid can give rise to non-stationary current signals. A stationary signal is defined as one for which the process statistics are independent of time. Thus if samples were taken of the current response to a pulse stimulus and the auto-correlation function, for example, was calculated, then repeating the process on the current responses to successive stimuli and obtaining identical auto-correlation functions would indicate stationarity (see also section 4.3).

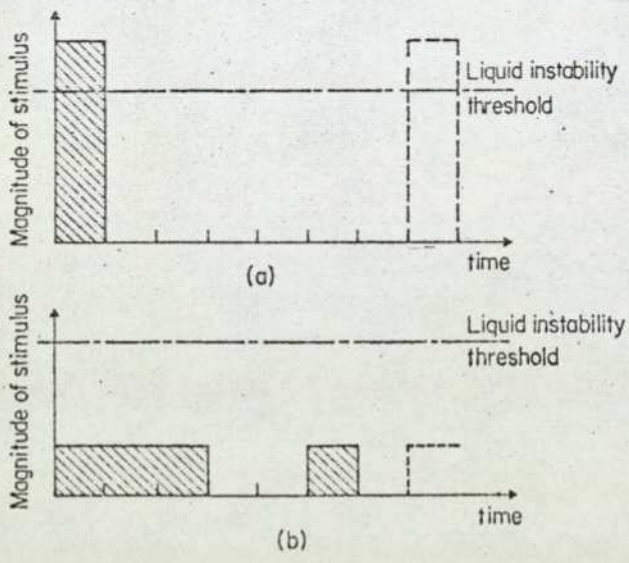
Several factors may cause non-stationarity during cumulative averaging. The pulse stimulus may cause an instability in the liquid which is still present to a small degree when the next stimulus is applied. This can generally be avoided by having a sufficiently long time interval between stimuli. Small variations in the voltages applied to the cell electrodes could cause changes in the standing or quiescent current particularly if one of the electrodes is used to control charge injection. Spontaneous changes in surface conditions at the electrodes, changes in ambient temperature and bulk ionisation could also vary the quiescent current and give rise to non-stationarity.

The effects of non-stationarity on the results of cumulative averaging are not necessarily catastropic. For example, a small change in the quiescent current level during averaging may not be sufficient to obscure the emerging current transient or prevent a meaningful measurement of transit time. However it is important that the experimentalist is aware of the pitfalls into which non-

3.3

stationarity can lead him.

Thus, the cumulative average process can give rise to non-stationarity if the pulse stimulus causes instability in the liquid, see figure 3.1a. However, if the stimulus is spread over the period of the transient in the form of a psuedo-random binary sequence (PRBS) and the impulse response retrieved by cross-correlation, see section 4.3.3, then non-stationarity due to instability may be avoided. Figure 3.1 illustrates this point by comparing the areas under the stimulus-time curve for a pulse and 7-bits PRBS stimulus. Much longer PRBS stimuli are used in practice, for example 1023 bits, to give more detail in the cross correlation result and also because as a stimulus it is stationary in so far as its fluctuations are faster than the variations in the current response (Brignell & Rhodes, 1975).



The area under the stimulus/time curve can be spread out more uniformly by utilizing a pseudorandom binary sequence, thus avoiding such hazards as instability, yet the impulse response can be retrieved by cross-correlation; (a) single pulse stimulus; (b) 7 bit PRBS stimulus.

Figure 3.1 A comparison between a single pulse stimulus and a p.r.b.s. stimulus (after Brignell and Rhodes).

3.4 Non-Linearity

Linearity, like stationarity, is an ideal concept which in practice can only occur within certain limits. For a system to be mathematically linear it must be both additive and homogeneous. In this work the system comprises the stimulus, the test cell containing the liquid, the measuring circuits and the signal processors, thus non-linearity could be present in any of these components. For example, the stimulus can cause non-linear charge injection and the charge injected can give rise to space charge limitation which results in a non-linear response. The current measuring circuit, if carefully constructed, should be approximately linear over the chosen range of operation and the digital signal processors are linear within the limits of quantization.

The PRBS stimulus method depends on the liquid responding in a linear manner, which is improbable if significant space-charge accumulates during the stimulation. Cumulative averaging is not so dependent on linearity, provided the liquid is stable and the electric field distribution within the cell is the same at the instant each identical stimulus is applied.

3.5 Instability

Liquid motion caused by instability imparts an additional component of velocity to the liquid which can be considered as a source of noise, non-stationarity and non-linearity in the measurement of charge transit times. If the transit time is defined as that of the charge moving relative to the liquid then the instability contributes an unwanted component to the current signal, i.e. noise. However, it is more probable that the measurement of the liquid motion contribution to the transit time is a crucial part of the investigations. Instability can give rise to non-stationarity if

3.5

the liquid is still in an unstable condition when the next stimulus is applied. Non-linearity is always present if instability occurs since there is no linear relationship between current response and applied stimulus in these circumstances.

In addition to these problems, the presence of liquid motion effects the charge transit time as measured from the current transient. The velocity of the charge relative to the liquid is less than the velocity relative to the electrodes if the liquid is moving in the direction of the injected charge. Thus it is important to establish whether instability is present and to what extent it contributes to the measured transit time. The theoretical analyses to establish criteria for the onset of e.h.d. instability are examined in section 4.5, and the experimental methods for determining the presence and extent of liquid motion are discussed in section 5.1.5.

3.6 The 'long-tail' effect

This characteristic of the small current transient, see figure 2.1, causes problems in the measurement of charge transit times and has been ascribed variously to instability, field distortion caused by space charge, liquid motion, etc.

Referring to figure 3.2, there are obvious difficulties in measuring the transit time in the responses to both step and pulse stimuli. Unfortunately, in many cases the method of measurement is not clearly stated and unless an actual transient plus the relevant data are available it cannot be determined. On the typical response to a step stimulus the transit time may be chosen between X and Y depending upon the explanations given for the distortion of the waveshape from the ideal. Similarly from the typical response

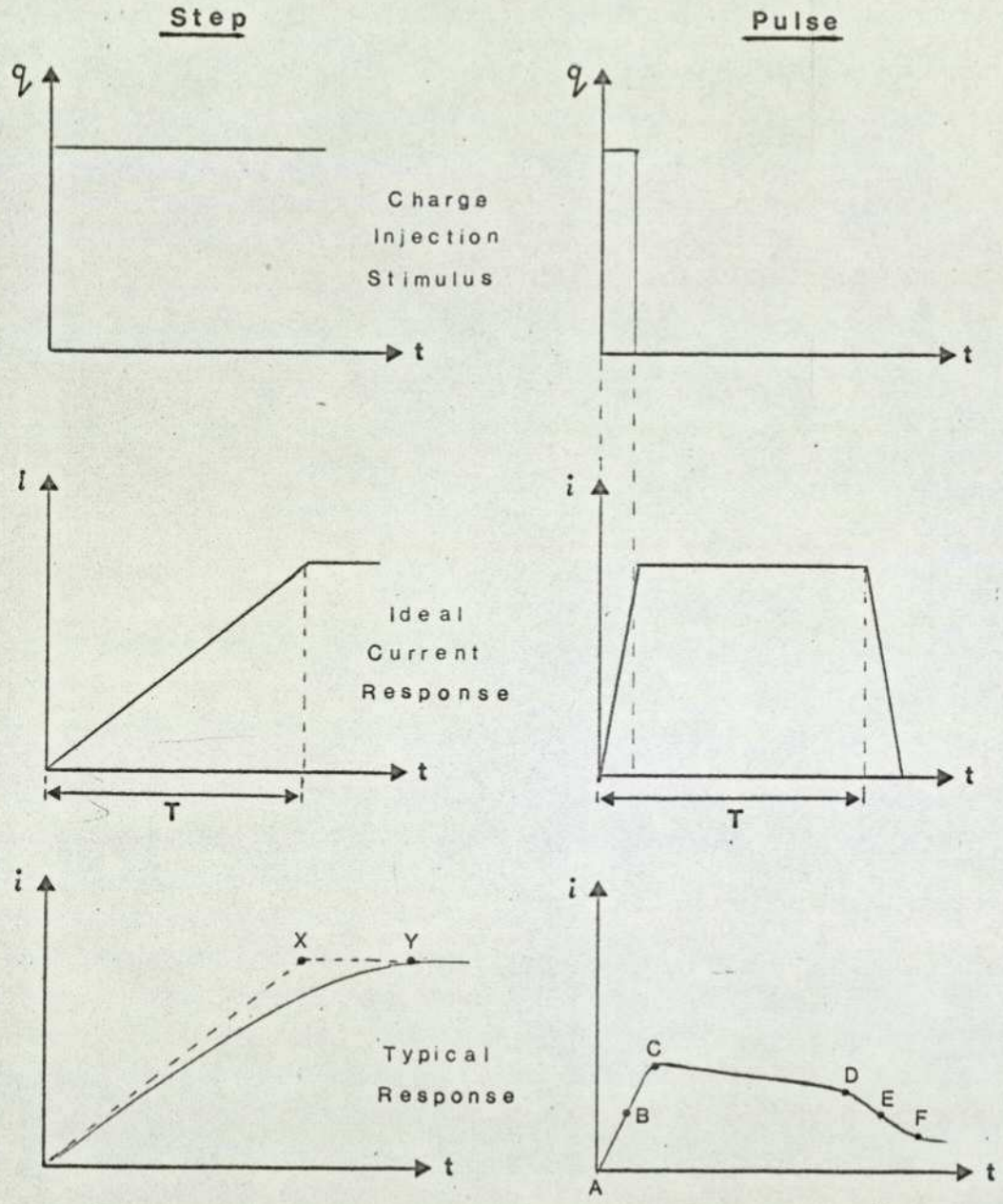


Figure 3·2 Ideal and typical current signals in response to step and pulse stimuli.

3.6

to the pulse stimulus, AD, BE or CF may be chosen as the transit time, in this case with justification since they are all about equal but this is not always so. When the transients differ in shape from these examples the problem is more difficult, particularly if the presence of bulk ionisation or charge carriers of differing mobilities is suspected (see Chapter 2).

Chapter 4

Theoretical background to the experimental work

4.1 Preliminary

The theoretical background of this work ranges from electric circuits to fluid dynamics and includes probability, sequential logic, and charge mobility. It is obviously impractible and unnecessary to examine each of these in the same depth, so more attention is given to those which are directly related to the experimental observations or to the measuring system. The first two sections concern parts of the system, that is the electrometer amplifier and the signal processing methods whereas the remaining three sections give the theoretical background to conduction in liquid dielectrics.

4.2 An analysis of pico-ammeter circuits

The term 'picoammeter' is used to describe an instrument containing a high-gain electrometer amplifier which will give an output voltage proportional to an input current of the order of picoamperes. The design of a picoammeter involves a compromise between sensitivity noise and 'rise-time', which is defined as the time taken t_R, for the output of an amplifier to change from 10% to 90% of its final value, in response to a step input signal. This is controlled by the relative magnitudes of resistance and capacitance in the measuring apparatus, especially the capacitance, since the value of resistance is determined by the sensitivity.

Figure 4.1 depicts the simplified circuit of a pico-ammeter in which C_1 is the total capacitance between input and output, and C_2 is the capacitance between input and ground, including the input capacitance of the amplifier. The voltage gain K of the electrometer amplifier is very large, typically 10^5, and the input bias current may be assumed negligible compared with i_1. Thus e_1 is approximately zero and, for the steady-state conditions, $e_o \simeq i_1 R_1$.

4.2

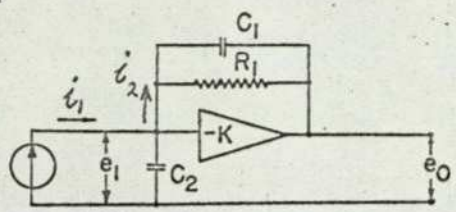


Figure 4.1 Simplified circuit of the picoammeter (after Presley).

To determine the transient response, the transfer function $H(s)$ of the system can be determined in terms of the Laplace operator, where

$$H(s) = e_o(s)/i_1(s).$$

The analysis which follows is given in more detail than would normally be warranted, because an erroneous result has been presented in the literature (Presley, 1966).

Referring to figure 4.1,

$$e_o = - Ke_1,$$

$$i_2 = i_1 - e_1.sC_2,$$

and $$e_1 - e_o = i_2.R_1(1 + sR_1C_1)^{-1}.$$

Hence

$$- e_o/K - e_o = R_1(i_1 + e_o.sC_2/K)(1 + sR_1C_1)^{-1}$$

and $$e_o \{\frac{K+1}{K} + sR_1C_2[K(1 + sR_1C_1)]^{-1}\} = - i_1R_1(1 + sR_1C_1)^{-1},$$

which re-arranged gives

4.2

$$e_o/i_1 = - R_1(1 + 1/K)^{-1}\{1 + sR_1[C_1 + C_2/(1 + K)]\}^{-1} \quad (4.2)$$

Provided K is large $C_2(1 + K)^{-1}$ is much less than C_1, and therefore

$$H(s) \simeq - R_1(1 + sR_1C_1)^{-1} \quad (4.3)$$

Thus the time constant of the output of the picoammeter for a step input current is equal to the product R_1C_1. R_1 is the resistance of the feedback resistor and C_1 is mainly due to its self-capacitance. Praglin and Nichols (1960) have shown that, if the components C_3 and R_3 are added to the feedback path as in figure 4.2 and R_3C_3 is made equal to R_1C_1, the new time constant is

$$R_1(C_1 + C_2)(1 + K)^{-1} \quad (4.4)$$

Equation 4.4 implies that the time constant and hence the rise-time would be negligible if K was sufficiently large, but as previously stated, the circuits in figures 4.1 and 4.2 are simplifications and for high value resistors the effect of distributed capacitance to ground should also be included. If this is done the resistance and capacitance would be infinitely distributed as in a transmission line.

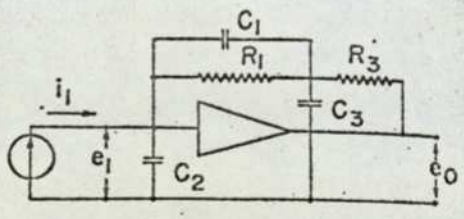


Figure 4.2 Modified picoammeter circuit using a lag network in the feedback path to compensate for the effect of R_1C_1 (after Presley).

4.2

A gross approximation to this is shown in figure 4.3 where the resistance is split into two equal parts and the capacitance to ground is represented by C_4.

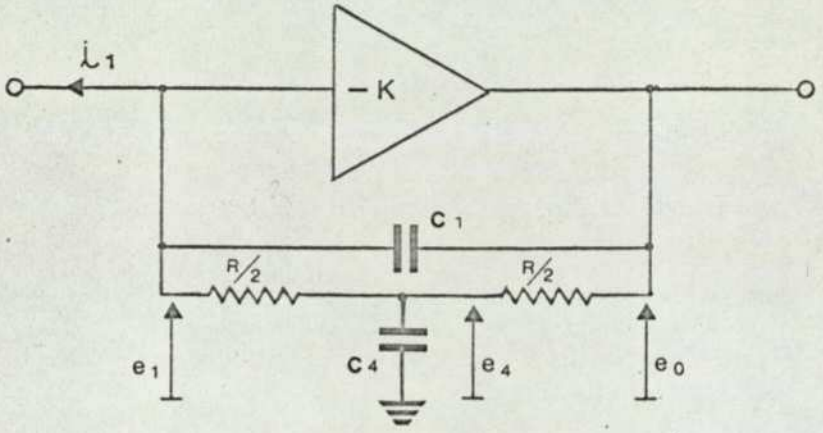


Figure 4·3 An approximate equivalent circuit for distributed capacitance to earth across R.

Assuming, as in the previous analysis, that the amplifier input bias current is negligible compared with i_1, then

$$i_1 = (e_o - e_1)sC_1 + 2(e_4 - e_1)/R,$$

$$e_4 sC_4 + 2(e_4 - e_1)/R - 2(e_o - e_4)/R = 0,$$

and $$e_1 = - e_o/K.$$

Eliminating e_4 and e_1 and re-arranging gives

$$i_1 = e_o\{sC_1(1 + K)/K + 4(K - 1)\left[KR(4 + sRC_4)\right]^{-1}\}$$

If K is large, $e_o \simeq i_1\{sC_1 + 4\left[R(4 + sRC_4)\right]^{-1}\}^{-1}$

$$\simeq i_1 R(1 + sRC_4/4)(1 + sRC_1 + s^2R^2C_1C_4/4)^{-1}$$

since $H(s) = e_o(s)/i_1(s)$

$$H(s) \simeq \frac{R(1 + sRC_4/4)}{1 + sRC_1 + s^2R^2C_1C_4/4} \qquad (4.5)$$

4.2

Solving for s in the denominator, gives for the poles

$$s = 2[- RC_1 \pm (R^2C_1^2 - R^2C_1C_4)^{\frac{1}{2}}](R^2C_1C_4)^{-1} \qquad (4.6)$$

Examining equation 4.6, it can be seen that s has two real negative roots if C_1 exceeds C_4, or a single negative root if C_1 is equal to C_4, corresponding to the overdamped and critically damped conditions for the circuit. However if C_4 is greater than C_1, s is complex indicating a damped oscillatory response from the circuit to a step input of current.

This analysis of a simplification of the true circuit illustrates the possible effect of the distributed capacitance to earth of the feedback resistor upon the response of the picoammeter. It is essential for optimum performance that the response should be checked before a series of measurements is made.

4.3 Signal Processing

4.3.1 Sampling

4.3.1.1 Introduction

In order to process the current signals in an on-line digital computer, it is necessary that they are converted to digital signals. This necessitates sampling the current signal at discrete intervals and converting each sample to a binary signal which is representative of the magnitude of the sample. The result of the processing which follows is very dependent upon the validity and accuracy of the sampling and digitization.

Both of these operations introduce noise as is illustrated in figure 4.4 (after Brignell and Rhodes, 1975). The sampled form $f_2(t)$ of the original source signal $f_1(t)$ is represented by a series of discrete points coincident with $f_1(t)$ at the sampling instances. Normally the amplitude of the samples are held constant while they

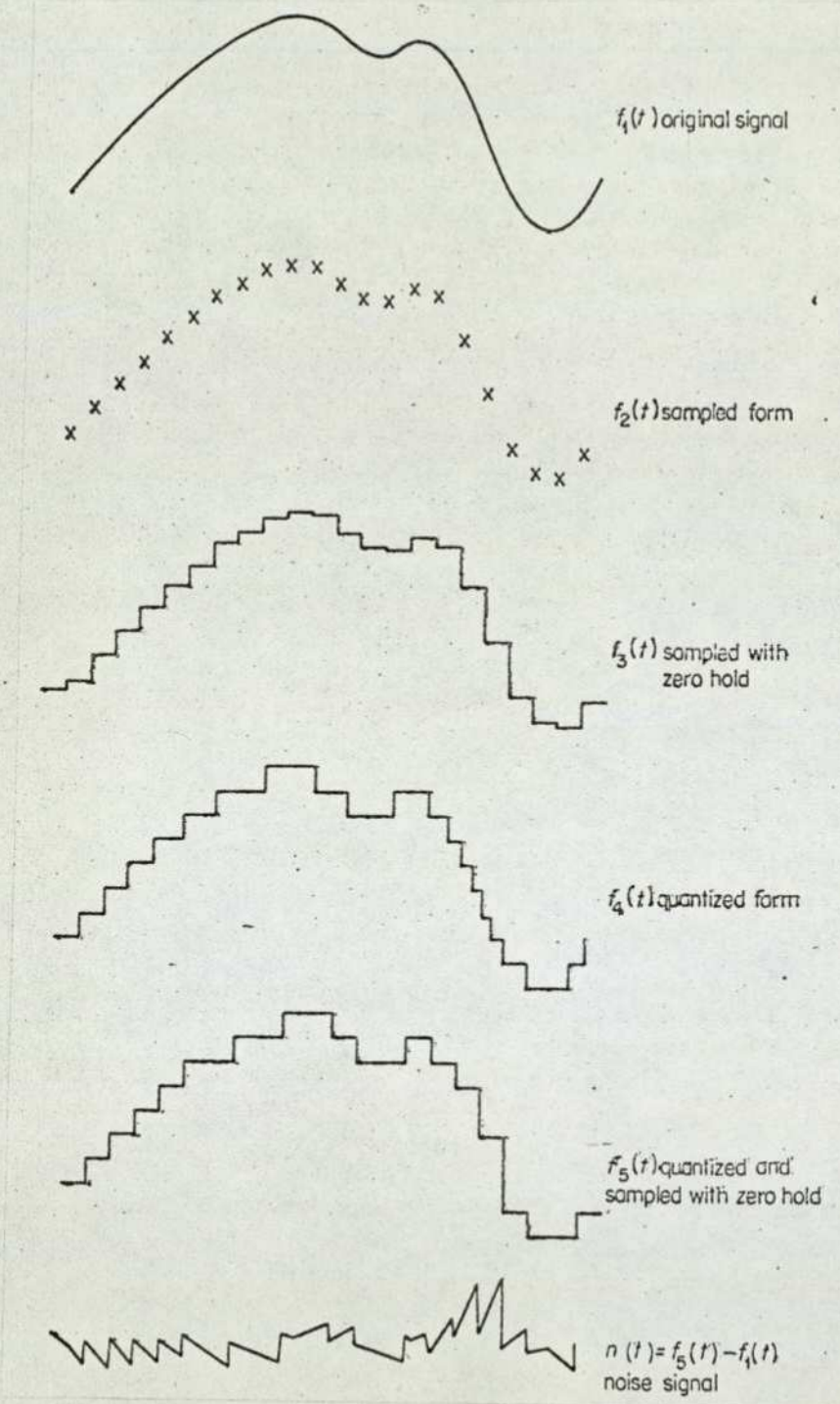


Figure 4.4 A continuous signal and its discrete forms (after Brignell and Rhodes).

4.3.1.1

are digitized or quantized. This is termed 'sampling with zero order hold' and is represented by $f_3(t)$, which can be regarded as comprising the original signal $f_1(t)$ plus a noise signal. The digitization by an analogue-to-digital converter introduces more noise as a result of quantization error, that is no increment of a sample smaller than that represented by the least significant bit can be accommodated. Since the conversion operation takes a finite time the final form $f_5(t)$ is delayed with reference to $f_4(t)$, and $n(t)$ represents the total noise introduced by both sampling and quantization. Figure 4.4 is obviously an exaggeration and the noise can be minimized by reducing the quantization error and increasing the sampling rate. However, it can be seen that $n(t)$ covers a wide spectrum of frequencies and in most analyses of digital processes it is assumed to be uncorrelated, i.e. white noise. This assumption is normally valid unless the digital process causes significant amplification of part of the spectrum, in which case the noise may predominate in the result.

4.3.1.2 Sampling Theorem

The sampling functions, see figure 4.5, for unit sampling period $\sqcup\!\sqcup(t)$ or $\alpha(t)$ (Bracewell, 1965, Helm, 1959) are given by

$$\sqcup\!\sqcup(t) = \frac{d\alpha(t)}{dt} = \sum_{n=-\infty}^{n=+\infty} \delta(t - n); \quad n = \ldots -2, -1, 0, +1, +2 \ldots$$

$$; \quad \alpha(0) = 0, \qquad (4.7)$$

where δ is the unit impulse function.

4.3.1.2

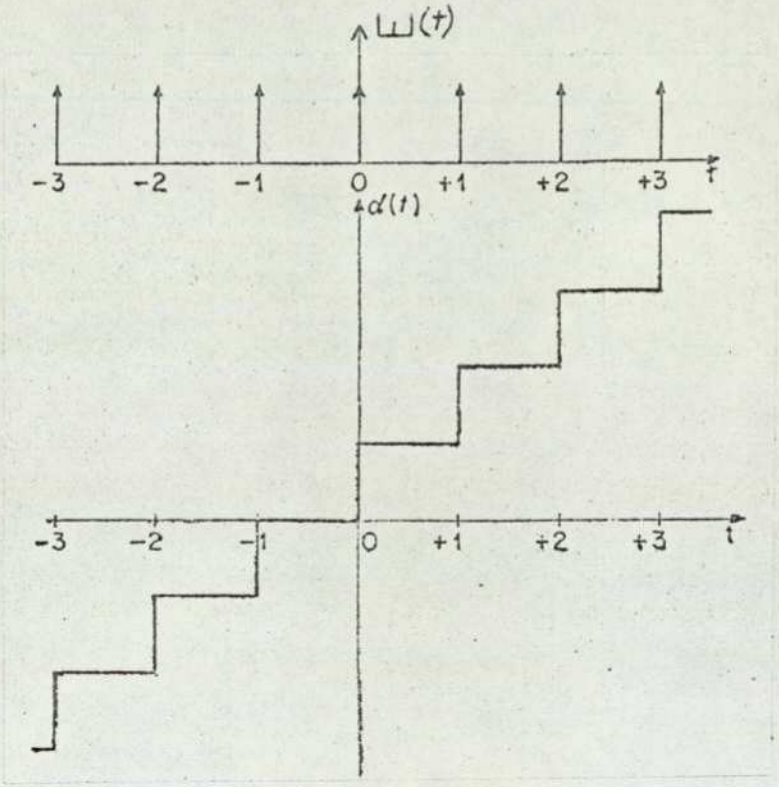


Figure 4.5 The sampling functions ⊔⊔(t) and α(t) (after Brignell and Rhodes)

A signal $x(t)$ sampled at intervals T can be represented by the product $x(t)$⊔⊔(t/T), a form which only has meaning within an integral. Thus, the Laplace transformation $X(s)$ is given by

$$X(s) = \int_{-\infty}^{+\infty} x(t) \text{⊔⊔}(t/T) \exp(-st)\,dt$$

$$= \int_{-\infty}^{+\infty} x(t) \exp(-st)\, d\alpha(t/T) \qquad (4.8)$$

The Stieltjes integral, equation 4.8, reduces to

$$X(s) = \sum_{-\infty}^{+\infty} x(nT) \exp(-snT) \qquad (4.9)$$

using the sampling property of δ as expressed by equation 4.7. Substituting $z = \exp(sT)$ gives

$$X(z) = \sum_{-\infty}^{+\infty} x(nT) z^{-n}$$

The z-transform of the impulse response of a causal system is given by

4.3.1.2

$$H(z) = \sum_{n=0}^{n=+\infty} h(nT)z^{-n}$$

So the z-transformation is carried out by simply setting the coefficient of z^{-r} equal to the rth sample ordinate of the signal or response function. Figure 4.6 shows the implications of this transformation, i.e. the mapping between the z and s domains.

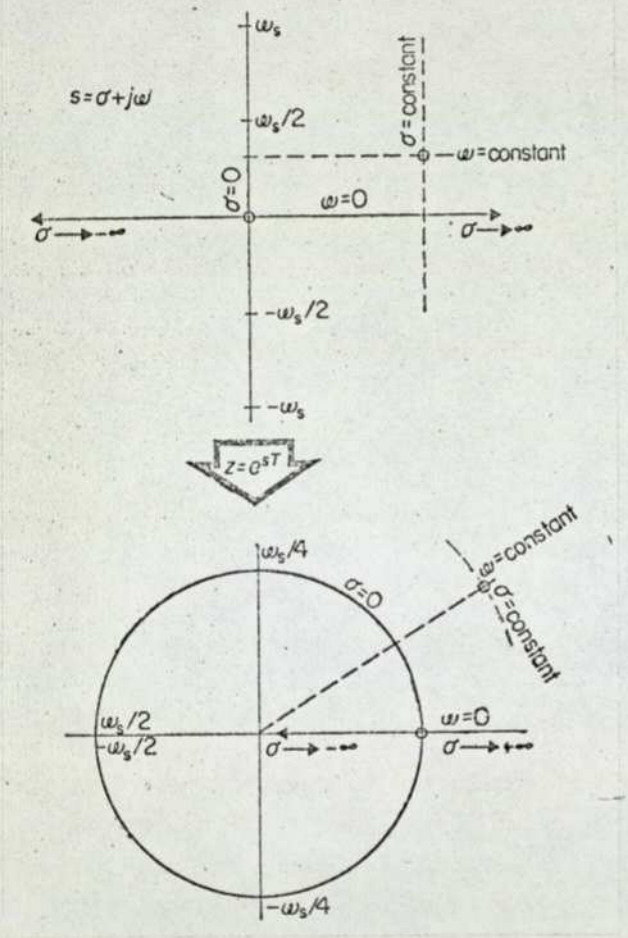


Figure 4.6
The z transform mapping
(after Brignell and Rhodes).

The sampling frequency $\omega_s = 2\pi/T$ is the time interval between samples and ω is expressed in the s domain as a fraction of ω_s. In the z domain the ω axis is mapped into the unit circle, the mapping for s to z being many-to-one. This mapping is unique only if all $\omega < \omega_s/2$. Any $\omega > \omega_s/2$ has an indiscernible alias in the range $0 < \omega < \omega_s/2$. This is a statement of the sampling theorem, that is, the sampling frequency must be at least twice the maximum

4.3.1.2

frequency present in the signal to prevent aliasing (Beauchamp, 1973).

4.3.2 Cumulative averaging

This method of signal processing, described briefly in section 3.2, produces an average of i signals each of m samples after the ith signal, x_i, but before the $(i + 1)$th signal. An advantage of this method is that the average $(\bar{x})_i$ is available after each signal and only 2 m samples need be stored, whereas to obtain the average of n signals by direct calculation, it would be necessary to store $m.n$ samples before computation by the equation

$$(\bar{x})_n = \frac{1}{n}\sum_{j=1}^{n} x_j \quad . \tag{4.10}$$

The relationship between $(\bar{x})_i$ and $(\bar{x})_{i-1}$ can be obtained from equation 4.10, thus

$$(\bar{x})_i = \frac{1}{i}\sum_{j}^{i} x_j = \frac{1}{i}\left(x_i + \sum_{j=1}^{i-1} x_j\right)$$

and hence $(\bar{x})_i = \{x_i + [i - 1](\bar{x})_{i-1}\}/i.$ (4.11)

Examination of this equation (4.11), which represents the cumulative average process, shows that the procedure necessary to compute the rth sample of $(\bar{x})_i$ is

(a) Multiply the rth sample of $(\bar{x})_{i-1}$ by $(i - 1)$,

(b) Add the rth sample of x_i to the result of (a),

(c) Divide the result of (b) by i.

This method of computation gives a more accurate result than would be obtained by dividing before adding. This is because the digital representation of the samples is limited by the quantization to a maximum of ten bits, in this work. A description of the computer

4.3.2

programs written by the author to cumulatively average signals and display the results is included in the appendix (section 10.5.2).

4.3.3 Correlation

4.3.3.1 Introduction

The sampled form of the current is a sequence of values at discrete time intervals, and signals of this type are examples of a discrete stochastic process. These signals have certain probablistic properties which depend upon their source and also upon the conditions at the time they were obtained. The fundamental theory of probability has been dealt with rigorously by Papoulis (1965) and only the probability functions directly related to this work will be examined. This section is concerned specifically with the cross correlation of a response signal with its stimulus to obtain the impulse response of the stimulated system. For this purpose, the stimulus must have certain properties which are defined in terms of its autocorrelation function.

4.3.3.2 The correlation functions

Correlation is essentially an averaging process, thus if we define the average or mean value of x as $\varepsilon\{t\}$, then autocorrelation is defined by the equation

$$R_{xx}(t_1, t_2) = \varepsilon\{x(t_1).x(t_2)\} \tag{4.12}$$

The implications of using the ensemble average $\varepsilon\{x\}$ instead of the time average $\bar{x}$ are fully discussed by Brignell and Rhodes (1975). The ensemble average of a function $g(x)$ of x is defined in terms of the distribution $F(x)$ as

$$\varepsilon\{g(x)\} = \int_{-\infty}^{+\infty} g(x)\, dF(x) \tag{4.13}$$

where $F(x) = \text{Prob}\{x(t) \leqslant x\}$

The distribution $F(x)$ can be thought of as the fraction of time for which $x(t)$, the instantaneous signal amplitude, is less than x, the argument of $F(x)$.

4.3.3.2

Equation 4.13 can be expressed in discrete form as

$$\varepsilon\{g(x)\} = \sum_{\text{all } k} g(x_k)\ P_k \qquad (4.14)$$

where P_k is the jump in $F(x)$ at x_k, i.e. the probability of $\{x(t) = x_k\}$.

The time average of $g(x)$ can be defined as

$$\overline{g(x)} = \underset{T\to\infty}{\text{Lt}} \left\{ \frac{1}{2T} \int_{-T}^{+T} g|x(t)|dt \right\}$$

and in practice with stationary signals it is permissible to make the ergodic assumption that $\overline{g(x)} = \varepsilon\{g(x)\}$.

A stationary signal has been defined (section 3.3) as one for which the statistics, e.g. auto-correlation, are independent of time. Thus, if $\tau = t_1 - t_2$, auto-correlation can be defined for stationary signals, as

$$R_{xx}(\tau) = \varepsilon\{x(t + \tau).x(t)\}$$

or

$$R_{xx}(\tau) = \underset{T\to\infty}{\text{Lim}} \frac{1}{2T} \int_{-T}^{+T} x(t + \tau).x(t).dt \qquad (4.15)$$

Similarly the cross-correlation of two stationary signals $x(t)$ and $y(t)$ can be defined as

$$R_{xy}(\tau) = \varepsilon\{x(t - \tau).y(t)\} = \varepsilon\{x(t).y(t - \tau)\}$$

and

$$R_{yx}(\tau) = \varepsilon\{x(t - \tau).y(t)\} \qquad (4.16)$$

In this work the signals, once acquired, comprise a set of samples, and these correlations are more usefully expressed in a discrete form, stationarity being assumed henceforth. Thus the auto-correlation of a sequence (x_i) of N samples can be determined from

$$R_{xx}(k) = \frac{1}{N-k} \sum_{i=1}^{N-k} x_{i+k}.x_i \qquad (4.17)$$

4.3.3.2

and the cross-correlation of sequences x_i and y_i, each of N samples from

$$R_{xy}(k) = \frac{1}{N-k} \sum_{i=1}^{N-k} x_i y_{i-k} \quad . \tag{4.18}$$

4.3.3.3 The impulse response of a system

The output $y(t)$ of a causal linear system is related to the input $x(t)$ by the operation of convolution (Papoulis, 1965), which is defined by the equation

$$y(t) = \int_{-\infty}^{\infty} x(t - \lambda).h(\lambda).d\lambda = x(t) * h(t) \tag{4.19}$$

* is the symbol for convolution and $h(t)$ is the response of the system to a unit impulse.

Substituting equation 4.19 in 4.16, gives

$$R_{yx}(\tau) = \varepsilon\{x(t - \tau). \int_{-\infty}^{\infty} x(t - \lambda).h(\lambda).d\lambda\}$$

$$R_{yx}(\tau) = \int_{-\infty}^{+\infty} \overline{x(t).x(t + \tau - \lambda)}.h(\lambda).d\lambda$$

$$= R_{xx}(\tau) * h(\tau) \tag{4.20}$$

If we chose as the input a signal $x(t)$ whose auto-correlation function $R_{xx}(\tau)$ is equal to an impulse $\delta(\tau)$, then equation 4.20 becomes

$$R_{yx}(\tau) = \delta(\tau) * h(t) = h(t), \tag{4.21}$$

since from (4.19), $y(t) = h(t)$ if $x(t)$ is an unit impulse.

4.3.3.4 The pseudo random binary sequence (prbs)

One signal with an auto-correlation equal to $\delta(t)$ is white noise, but it this were used the computation necessary to determine the cross-correlation $R_{xy}(\tau)$ would be difficult and excessive because the bandwidth and integration time would be theoretically finite. Fortunately the prbs signal has an auto-correlation which

4.3.3.4

is almost an impulse and is therefore commonly used in place of white noise. The advantage of the prbs signal is that it has only two levels, which can be recorded by the computer as the logic levels '0' and '1', together with the corresponding sample of the response $y(t)$. For a prbs sequence $\{x_i\}$ the autocorrelation can be redefined from equation 4.17, as

$$R_{xx}(k) = \frac{1}{L} \sum_{i=1}^{L} x_{i+k} \cdot x_i$$

and since $x_{i+L} = x_i$, it is periodic with period L.

A prbs can be generated using a shift register with feedback applied to the first stage, through modulo-two gates (see figure 4.7(a) and (b)).

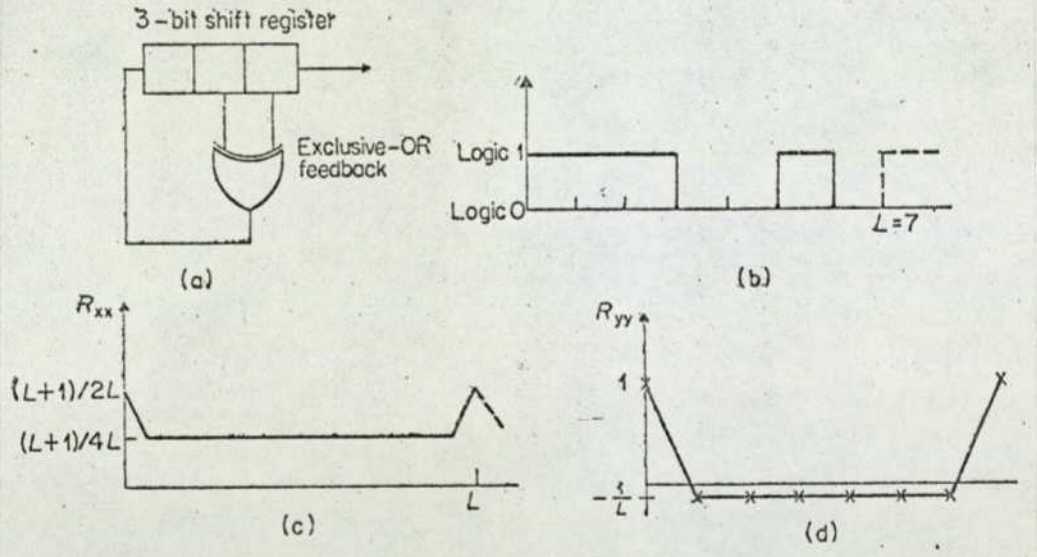


Figure 4.7(a) 3-stage p.r.b.s. generator; (b) the output sequence; (c) the autocorrelation function; (d) autocorrelation of the modified sequence (after Brignell and Rhodes).

The design of these sequence generators is well known (Davies, 1966) and one was constructed for this work by Pinckard (1972) under the supervision of the author.

Figure 4.7(c) shows the autocorrelation $R_{xx}(k)$ obtained by joining up the points of the discrete autocorrelation.

4.3.3.4

The values of $R_{xx}(k)$ are

$$R_{xx}(k) = \frac{L+1}{2L}; \quad k = nL; \quad n = 0, 1, 2, 3, \ldots\ldots$$

$$R_{xx}(k) = \frac{L+1}{4L}; \quad k \neq nL.$$

It is possible to obtain the ideal unit spike at the origin and zero elsewhere by a linear transformation but the approximate transformation, $y = 2x - 1$, which has computational advantages is normally used. Thus when the sequence state, x, is + 1, the new state y is also + 1, but when x is 0, y is - 1.

This transforms the auto-correlation to

$$R_{yy}(k) = 1; \quad k = nL$$

and $$R_{yy}(k) = -1/L; \quad k \neq nL$$

as in figure 4.7(d) for the 7 bit sequence.

The -1/L offset is usually negligible, e.g. for 1023 bit sequence it represents less than 0.1% of the impulse amplitude, but it can be eliminated during display by plotting $(LR_{yy} + 1)/(L + 1)$ instead of R_{yy}.

The discrete cross-correlations, which joined up form the impulse response of the system, are computed by the equation

$$R_{xy}(k) = \frac{1}{L} \sum_{i=1}^{L} x_i \cdot y_{i-k}, \qquad (4.22)$$

where x_i represents the + 1 and - 1 values of the prbs, and y_{i-k} is the sequence of digitized samples of the system response to the prbs stimulus. A description of the programs which were written to perform this computation is in section 10.5.3 of the appendix.

4.3.4 Deconvolution

Convolution, as defined by equation 4.19 is an operation in the

4.3.4

time domain, which when transformed to the z-domain becomes an operation involving the multiplication of polynomials and is expressed as

$$Y(z) = X(z).H(z) \qquad (4.23)$$

where the z transforms are defined as

$$H(z) = \sum_{t=-\infty}^{\infty} h(t).z^{t}, \qquad \text{etc.}$$

If the measuring instrument in a system, for example the picoammeter which follows the test cell in this work, has a characteristic response, then the true signal from the source is corrupted by being convolved with that response. With continuous signals the deconvolution to obtain the true response of the source involves the difficult problem of solving an equation containing integrals in the time domain or function division in the frequency domain. However, deconvolution in the z domain involves the relatively easy task of dividing polynomials. Thus if the impulse response of the picoammeter, and the picoammeter plus test cell are $H_p(z)$ and $H(z)$ respectively, then.

$$H(z) = H_p(z).H_c(z) \quad \text{(Convolution)}$$

and $$H_c(z) = H(z)/H_p(z) \quad \text{(Deconvolution)}$$

where $H_c(z)$ = the ideal response of the test cell.

A further step is to extend $H_p(z)$ to include the empty test cell as well as the picoammeter, then $H_c(z)$ would be the impulse response of the liquid sample alone. The computation and validity of these operations is at present being investigated in the laboratory (K.J. Pocknell, private communication), together with the technique of adaptive modelling (Brignell and Rhodes, 1975; Beck, 1968).

4.4 Charge mobility

4.4.1 Introduction

If an externally applied field is imposed on a liquid dielectric between two plane electrodes then a current will flow due to the movement of ions in the liquid under the influence of that field. The term 'ion' will be used for convenience although the charge carrier could be a polaron, or a molecular cluster carrying an electronic charge. The current density at a point in the liquid can be expressed in terms of the field as follows (Hummell and Schmidt, 1974).

The field E at any point in the liquid is related to the current density resulting from the movement of the ions by

$$j_1 = eE(n_+\mu_+ + n_-\mu_-) \qquad (4.24)$$

where e is the electronic charge, 1.602×10^{-19} C, μ_+ and μ_- are the mobilities and n_+, n_- the local densities of the ions. Diffusion of ions will also give rise to a current density if there are ion density gradients present, given by

$$j_2 = -e(D_+ \text{ grad } n_+ - D_- \text{ grad } n_-) \qquad (4.25)$$

where D_+ and D_- are the diffusion gradients. The sum of the current densities due to the field and diffusion is the conduction current density

$$j_c = j_1 + j_2.$$

If there are more than one species of negative and/or positive charge carrier then there would be additional terms in equations 4.24 and 4.25.

The electric field E is determined by the externally applied voltage and the geometry of the electrodes only if the density of the positive and negative ions is the same everywhere in the liquid.

4.4.1

When n_- is not equal to n_+, as in the case of unipolar charge injection, the local field strength will be affected by the space-charge density, according to Poisson's equation

$$\text{div } E = \frac{e(n_+ - n_-)}{\varepsilon_o \varepsilon_r}$$

where $\varepsilon_o = 8.85 \times 10^{-12}$ C.V^{-1}m^{-1} and ε_r is the relative dielectric constant. The measurement of the mobility of unipolar injected negative charge carriers by the 'time-of-flight' method depends on the validity of an expression derived from equation 4.24. If we neglect the contribution of both the positive charge carriers and diffusion to the current density, we have

$$j = eE\, n_-\, \mu_-$$

But, $j = e\, n_-\, v$

where v is the velocity of the ions.

thus

$$v = E.\mu_- \qquad (4.26)$$

If the ions can be assumed to drift a distance d in a homogeneous field E, equal to V/d, then v is constant and it follows from equation 4.26 that the time to traverse the distance d is

$$t_d = \frac{d}{E\,\mu_-} = \frac{d^2}{V.\mu} \qquad (4.27)$$

A further examination of the possible effects of these assumptions and approximations upon the determination of mobility by the time-of-flight method is made in the following section.

4.4.2 Diffusion

The order of magnitude of the effect of diffusion upon the charge distribution following unipolar injection can be determined by considering the diffusion which occurs in time t in the direction of movement of the charge.

The diffusion distances may reasonably be assumed to exhibit a Gaussian distribution (Einstein), for which the standard deviation x is $(Dt)^{\frac{1}{2}}$. Expressing this as a fraction of the gap width d gives a measure of the effect of diffusion on the charge front during the transit time T, thus

$$x/d = (D t)^{\frac{1}{2}} d^{-1} \qquad (4.28)$$

A measurement of the diffusion constant D_- for negative ions in n-hexane, by Gazda (1963), yielded the result

$$D_- = (2.75 \pm 0.22) \times 10^{-9} \text{ m}^2 \text{ s}^{-1}$$

An independent determination of the negative ion mobility μ by Gzowski (1962) on a sample of n-hexane from the same source, produced the result

$$\mu_- = (9.5 \pm 0.5) \times 10^{-8} \text{ m}^2 \text{ V}^{-1} \text{ s}^{-1}$$

since $\mu_-/D_- = 34.5 \text{ V}^{-1}$, these results are in reasonable agreement with the Nernst-Einstein law, i.e.

$$\mu/D = e/kT \ (\simeq 39.0 \text{ V}^{-1} \text{ at } 25^{\circ} \text{ C})$$

Assuming the approximate expression for transit time

$$t = d^2/\mu V$$

The value of x/d (equation 4.28) for V = 500 V, d = 1 cm, and μ_- and D_- as stated above, is 7.6×10^{-3} i.e. less than 1%.

Belmont (1973) has examined the effects of diffusion upon an injected pulse of charge. He concluded that using the standard deviation, $x = (Dt)^{\frac{1}{2}}$, as an estimate of the width of the distribution, there would be a little over half the total charge

4.4.2

within the limits $\pm x$, and to enclose 99% of the charge the limits should be extended to $\pm 3.6\ (Dt)^{\frac{1}{2}}$. As the charge approaches the collecting electrode the distribution will no longer be Gaussian and assuming a worst case of total uncertainty in the distribution, the spreading as a fraction of d would be $7.2\ (Dt)^{\frac{1}{2}}$ i.e. about 5.5%, assuming the same values for D, μ, V and t as before.

4.4.3 Distortion of the field by a grid

The presence of grids in the test cell to control injection and define the field in the drift gap, distorts the electric field in such a way as to weaken the field in the interstitial regions of the grid.

An enlargment of the grid mesh which was used for most of this work is shown in figure 4.8. The one-dimensional field and equipotential distributions in figure 4.9 illustrate the distortion caused by single grid wires for the cases of zero and small positive potentials at the grid, with reference to the cathode, in a parallel plate system. With a mesh grid, and more positive grid voltages, the distributions will differ but similar distortions will occur. The 'edge-effects' depicted in figure 4.9(a) are minimized in the test cell by using a guard ring around the anode.

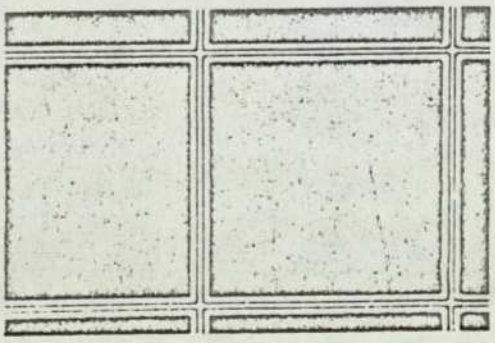
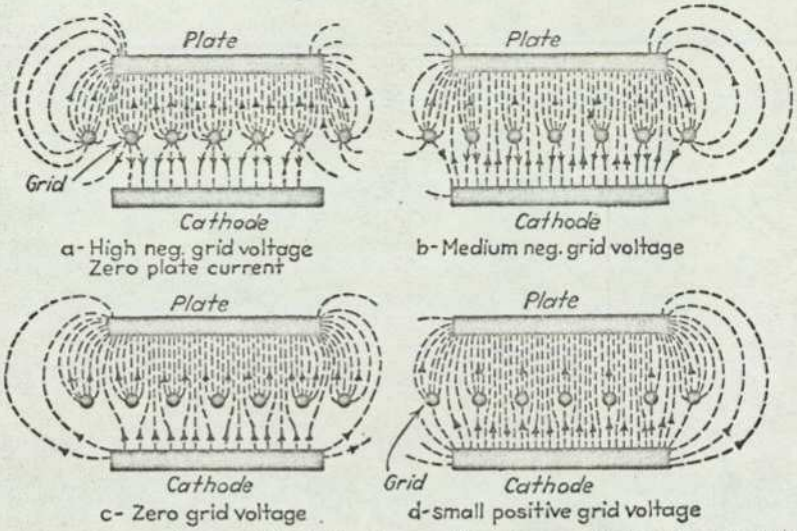


Figure 4.8 A photomicrograph of the grid mesh, magnification x 260. (Courtesy of E.M.I. Electronics Ltd.)



Approximate field distribution resulting from applied voltages in a triode with plane parallel electrodes for fixed positive plate voltage and four values of grid voltage. Arrows indicate the direction of the force on an electron.

Figure 4.9(a) One-dimensional field distribution (after Reich).

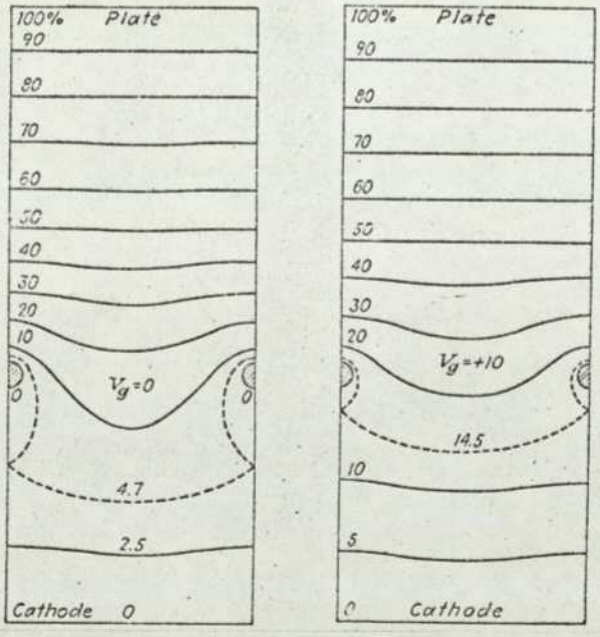


Figure 4.9(b) Equipotential contours in the plane electrode triode: (i) grid at zero potential; (ii) grid positive (after Spangenberg).

4.4.3

In such a region of reduced effective applied field, the amount of space charge required for limiting to occur is also greatly reduced. As can be seen in the appendix (section 10.2), this was a factor which was somewhat underestimated by the author and his predecessors (Buttle and Brignell, 1969) in proposing grid control as a solution of some of the experimental problems.

In a vacuum tube, this field effect at a grid would have an indiscernible effect on a pulse of electrons since there electrons travel under ballistic laws and conserve their momentum through the field-free space. However, for the low-mobility ions in liquid dielectrics the situation is very different, particularly when the maximum field is about 1 kV cm^{-1}, in this case space-charge limitation is the important factor. As a pulse of negative charge moves through an electric field, the latter is modified by the field due to the charge density ρ and permittivity ε in accordance with Poisson's equation

$$\nabla E = \frac{\rho}{\varepsilon}$$

This modification can reduce the field to a very low value or even zero locally, especially if the applied field was already weak. There will also be a build-up of the moving charge as it passes through a local region of weak field which, in turn, will lead to a further diminuition of the local field in accordance with Poisson's equation, with the increased possibility of an occurrence of space charge limitation. If this does happen then the flow of charge from the space charge limited region is controlled by the diffusion process which, combined with a weakened electric field, will cause a spreading of the pulse of charge.

For fields less than 1 kV cm^{-1} the spreading of the pulse will be greater, and this does not include a consideration of the

4.4.3

possibility of a similar spreading occurring as the pulse is gated through the control grid. However, this latter effect would be considerably less than at the field grid when photo-injection is into an air/hexane vapour gap (Hewish & Brignell, 1972), due to the higher mobility of ions in the vapour phase.

4.4.4 Space-charge

4.4.4.1 Introduction

Since space-charge effects are considered to be an important contributory factor to the distortion of current transients, this section has been extended to include an examination of the analyses by others of this problem. Some of these analyses relate to charge injection into solids in which the space charge effects are very similar to those in liquid insulants. Also, an examination is included of the computer modelling of this problem by a colleague (Evison, 1975), and an analysis by Brignell of the effect of space-charge on the charge transit time.

4.4.4.2 The occurrence of space-charge

An accumulation of space charge is most likely to occur at the surface of the charge-injecting electrode, i.e. the photo-cathode, and this is more probable when the control grid is being used to gate pulses of charge into the drift gap. With this method of controlled injection there are periods of tens of seconds, when the control grid is biased negatively with reference to the cathode, during which space-charge can accumulate. Under these conditions, the accumulated space-charge will be sufficient to inhibit photo-injection until the grid is gated positive.

The one-dimensional solution of Poisson's law is

$$\frac{dE}{dx} = -\frac{\rho}{\epsilon} \qquad (4.29)$$

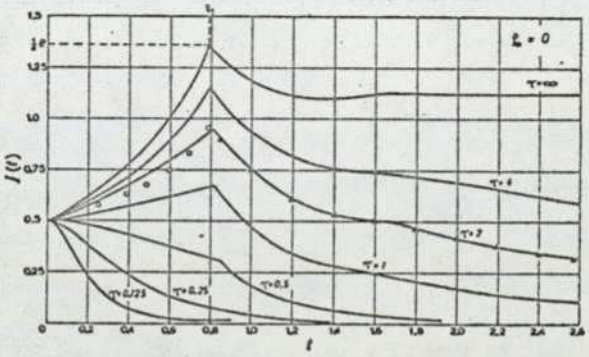
4.4.4.2

Thus, the field acting on the front edge of a pulse of charge, as it is gated from the space charge region through the grid, will be greater than on the remainder, thus causing the pulse to spread. This is not the same situation as that in which continuous space-charge limited current flows, since as soon as the grid is gated positive the accumulation of space charge is depleted and s.c.l. conditions no longer exist.

A similar effect could occur at the field grid as the charge enters the region of non-uniform electric field (see section 4.3.3). In the weaker field at the centre of the grid interstices, bunching and accumulation of charge would occur as the velocity decreases, which could result in the formation of space charge regions. These would cause further spreading of the pulse.

4.4.4.3 Transient s.c.l. currents in solids

Many and Rakavy (1962) considered step-injected space-charge limited currents in insulating and conducting crystals. Their results (figure 4.10) were derived from Poisson's equation and a



The time dependence of the SCLC density for insulating crystals characterized by various trapping times, and $\theta_0 = 0$.

Figure 4.10 Theoretical transient s.c.l. currents in solids (after Many and Rakavy).

system of equations relating the free and trapped carriers. The upper curve represents the case of no trapping, that is the trapping time τ is infinite, and as the time before trapping occurs

4.4.4.3

decreases, so does the value of the peak current. The variables are non-dimensional so that on the curves the transit time t and the trapping time τ are normalised to the transit time in the absence of space charge, $d^2/\mu V$, and the current density to $\varepsilon\mu\ V^2/d^3$ so that the space charge limited current density

$$J_{scl} = 1.125\ \varepsilon\mu\ V^2/d^3$$

is represented by $j(t) = 1.125$.

Papadakis (1967) analyses the case of pulsed-charge injection into solids and obtained similar results (figure 4.11) in terms of the parameter $\beta = E_o/e_o$, where E_o is the field in the absence of space charge and e_o is the change in field strength across the injected

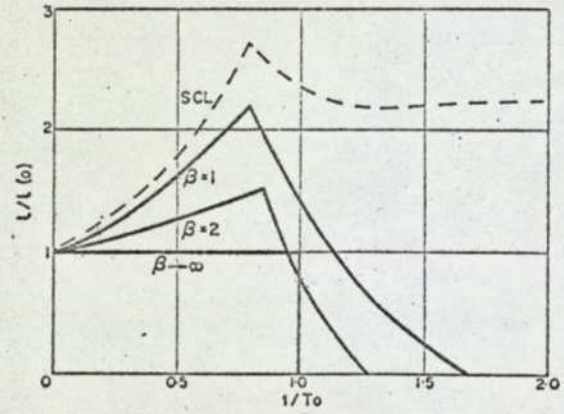


Figure 4.11 The time dependance of the transient current in the absence of deep trapping (after Papakis).

charge layer at $t = 0$. As $\beta \to \infty$, the current tends to a rectangular wave shape, but as $\beta \to 1$ (maximum distortion of the field) the peak of the current approaches and exceeds the steady-state s.c.l. value. The term 'space-charge perturbed' is used to describe currents which are subject to the influence of space charge, i.e. they are close to the s.c.l. condtion. Mort and Scher (1971) show the transition from the injection of small pulses of charge to a step (figure 4.12) by extending the results of

4.4.4.3

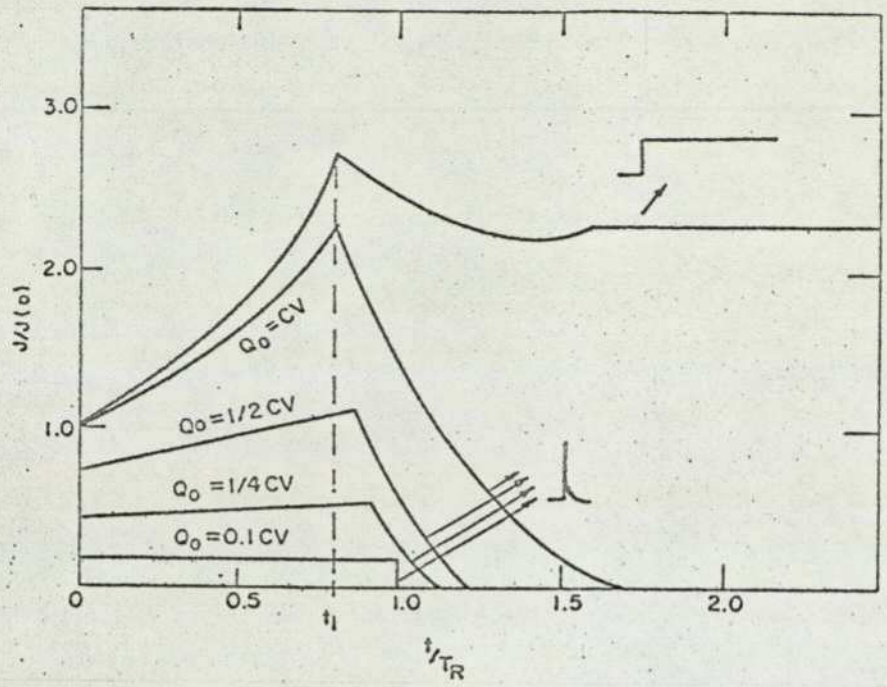


Figure 4.12 Idealized current response to pulse injection of varying amounts of charge. The upper trace represents the full s.c.l. current which requires step-function injection (after Mort and Scher).

Papadakis. Their parameter Q_o was in terms of CV, which is defined as the maximum charge which can be injected under pulse conditions.

Hartman and Lipari (1973) applied numerical techniques to obtain the field distribution and the current transient for various rates of charge injection based on an expression for the charge injected Q at time t in terms of the total charge injection A and a constant τ, which determines the rate of injection, as follows:

$$Q = A[1 - \exp(-t/\tau)]$$

Figure 4.13 shows the results for a high injection rate $\beta = 40$ and an intermediate injection rate $\beta = 3$. The parameter B is a measure of the quantity of charge injected in the pulse relative to the s.c.l. value when $\beta = 1$.

4.4.4.4 The computer simulation of Evison (1975)

The basis of this method is to quantise the dielectric into a number of cells in series and to allocate a quantity of charge to

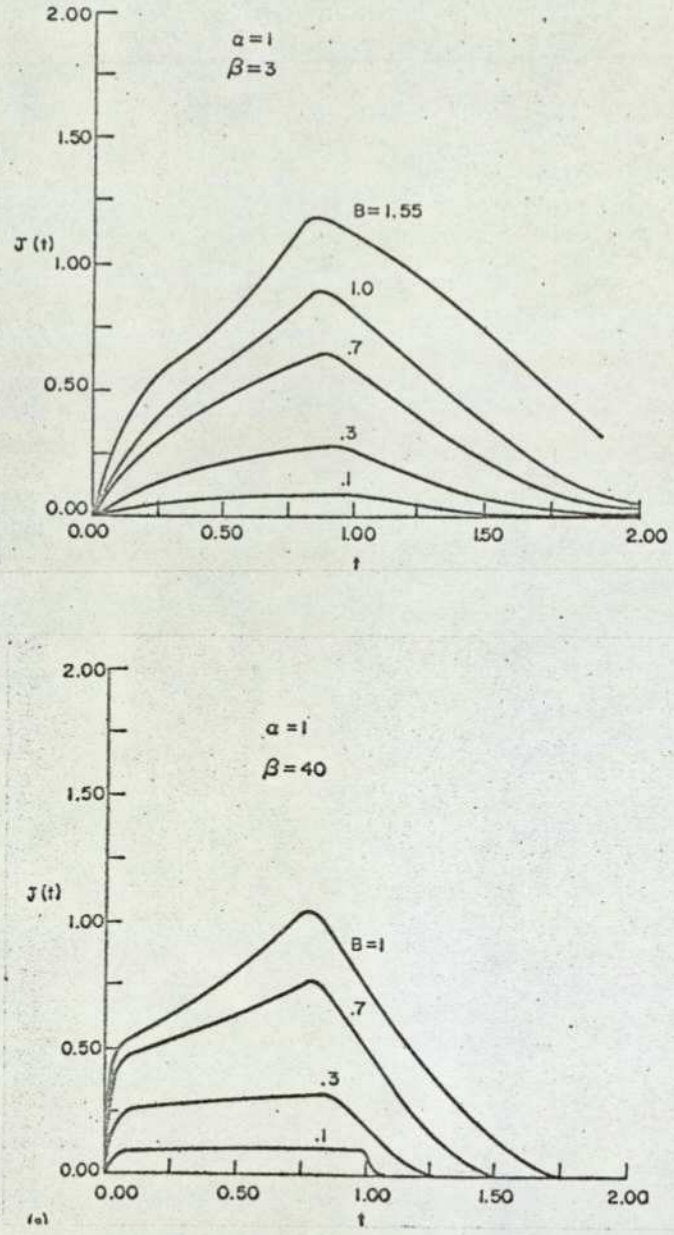


Figure 4.13 Time dependance of the theoretical transient current from the application of numerical techniques (after Hartmann & Lipari).

Upper Trace: The value B = 1.55 corresponds to a s.c.l. condition There is no blocking layer ($\alpha = 1$) and the rate of injection is intermediate ($\beta = 3$).

Lower Trace: The rate of charge-injection is very high ($\beta = 40$).

4.4.4.4

each cell. Using Poisson's law the stress distribution is calculated, also the movement of each packet of charge in the simulation time. This completes one cycle of the simulation, after which the charge and stress distributions and the instantaneous value of the current are available. The charge is then reallocated to the cells in accordance with the new distribution and a second cycle begins. The s.c.1. transient in fig. 4.14 was obtained by assuming initially zero charge, and then injecting sufficient charge into the first cell to bring the stress at the cathode to zero, before each cycle of computation. The stress and charge distributions for t = 0.65 T (figure 4.15) and for t = 0.8 T (figure 4.16) correspond to

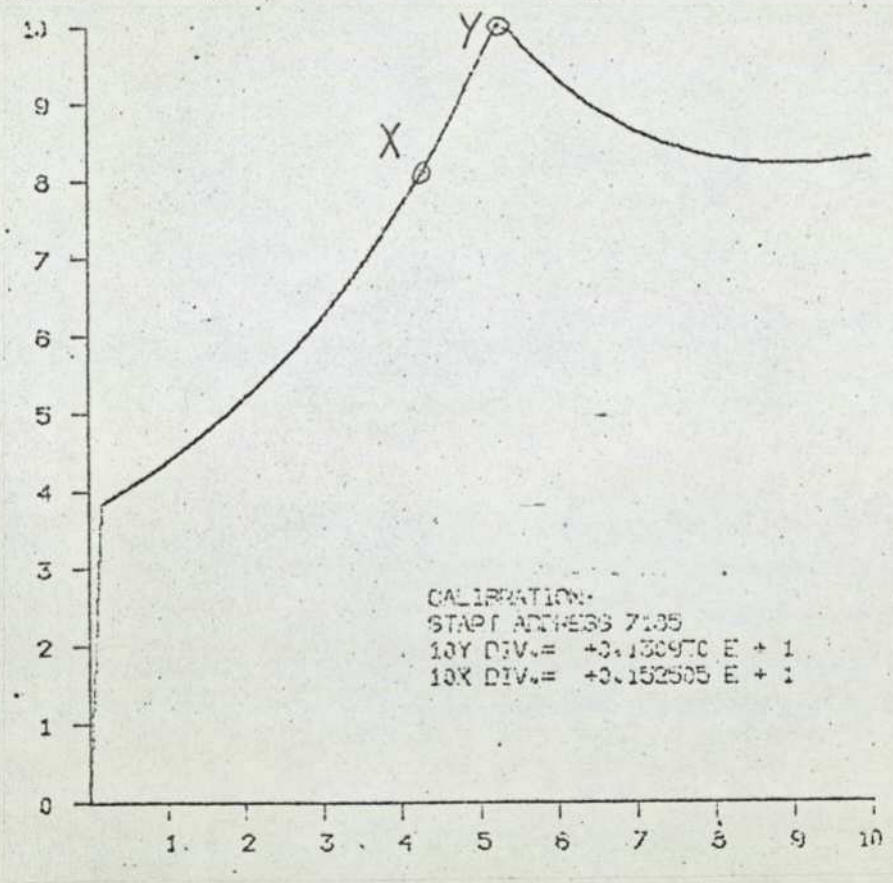


Figure 4.14 S.c.1. transients from a computer model of charge-transit (after Evison).

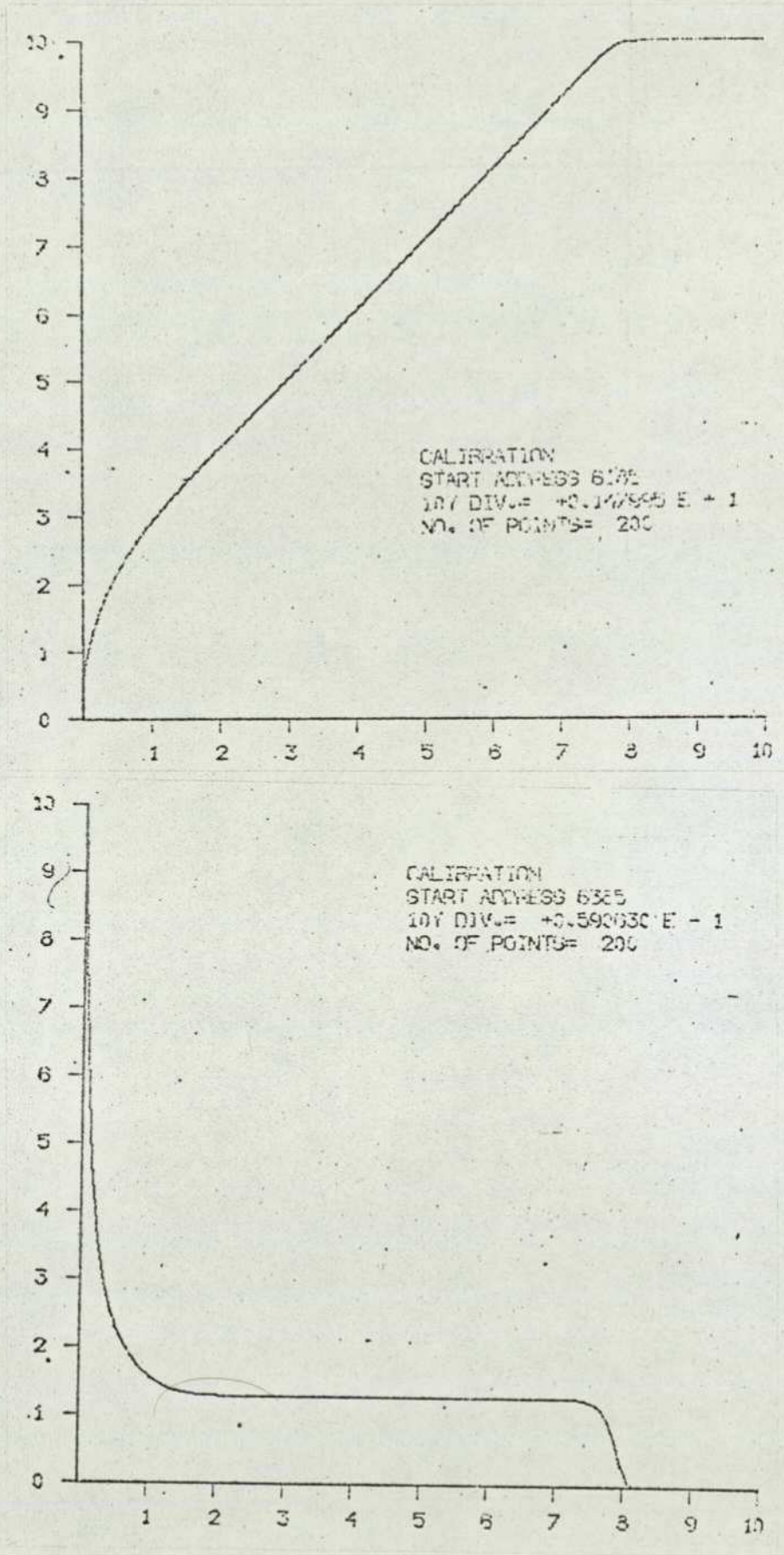


Figure 4.15 Simulated stress and charge distributions for t = 0.65 T during an s.c.l. transient (point X on figure 4.14) after Evison.

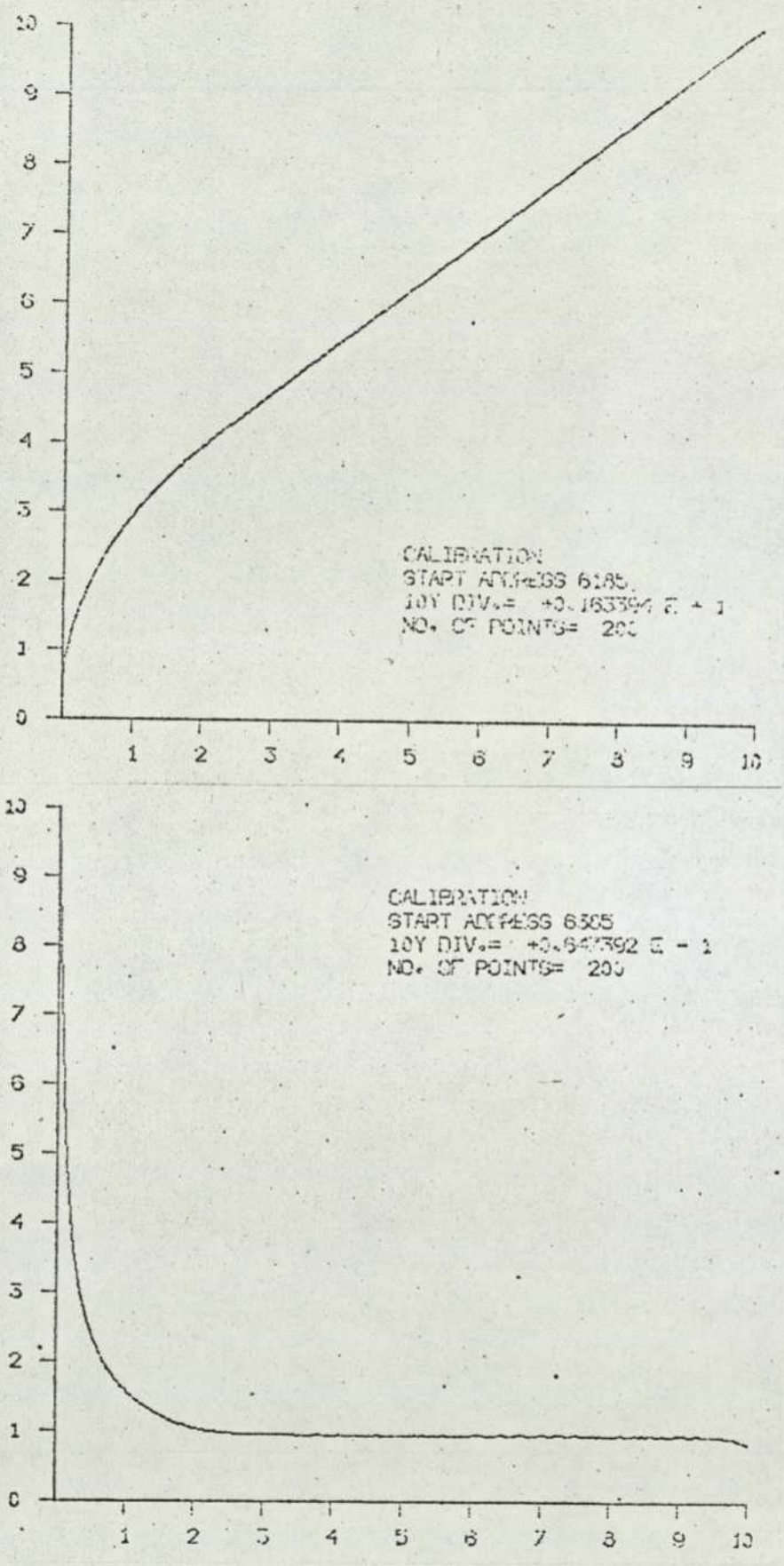


Figure 4.16 Simulated stress and charge distributions for t = 0.8 T during an s.c.1. transient (point Y on figure 4.14) after Evison.

4.4.4.4

X and Y respectively on the current curve.

This model can be used for pulse injection and for the injection of two charge carriers of different mobilities and of different signs if so desired. The analysis of currents resulting from charge injection into a non-uniform field can also be investigated by establishing a fixed charge distribution corresponding to that field before injection.

The model can also be used in an adaptive mode to determine the charge input required to produce a known transient. Figure 4.17 shows the current transient obtained from the model compared with a transient supplied by the author. In this case only the rate of charge injection and the value of mobility were adapted, whereas the initial stress distribution was, without doubt, non-uniform since injection was through a grid, also it is possible that more than one charge carrier was present. The effects of diffusion and e.h.d. instability are not included in the present computer model.

4.4.4.5 The charge transit time in a non-uniform field

An analysis (Brignell, private communication) of the charge transit time in a field, with a non-uniform stress due to the presence of space charge is included in the appendix (section 10.6). This analysis is one-dimensional and assumes a parallel plate electrode system with unipolar injection of charge, thus the field variations, which occur when injection is through a grid, are not considered.

The results of this analysis for a drift gap of width d and potential difference V_o show that V_o and the steady state value of the current density J_o can be expressed in terms of the s.c.l.

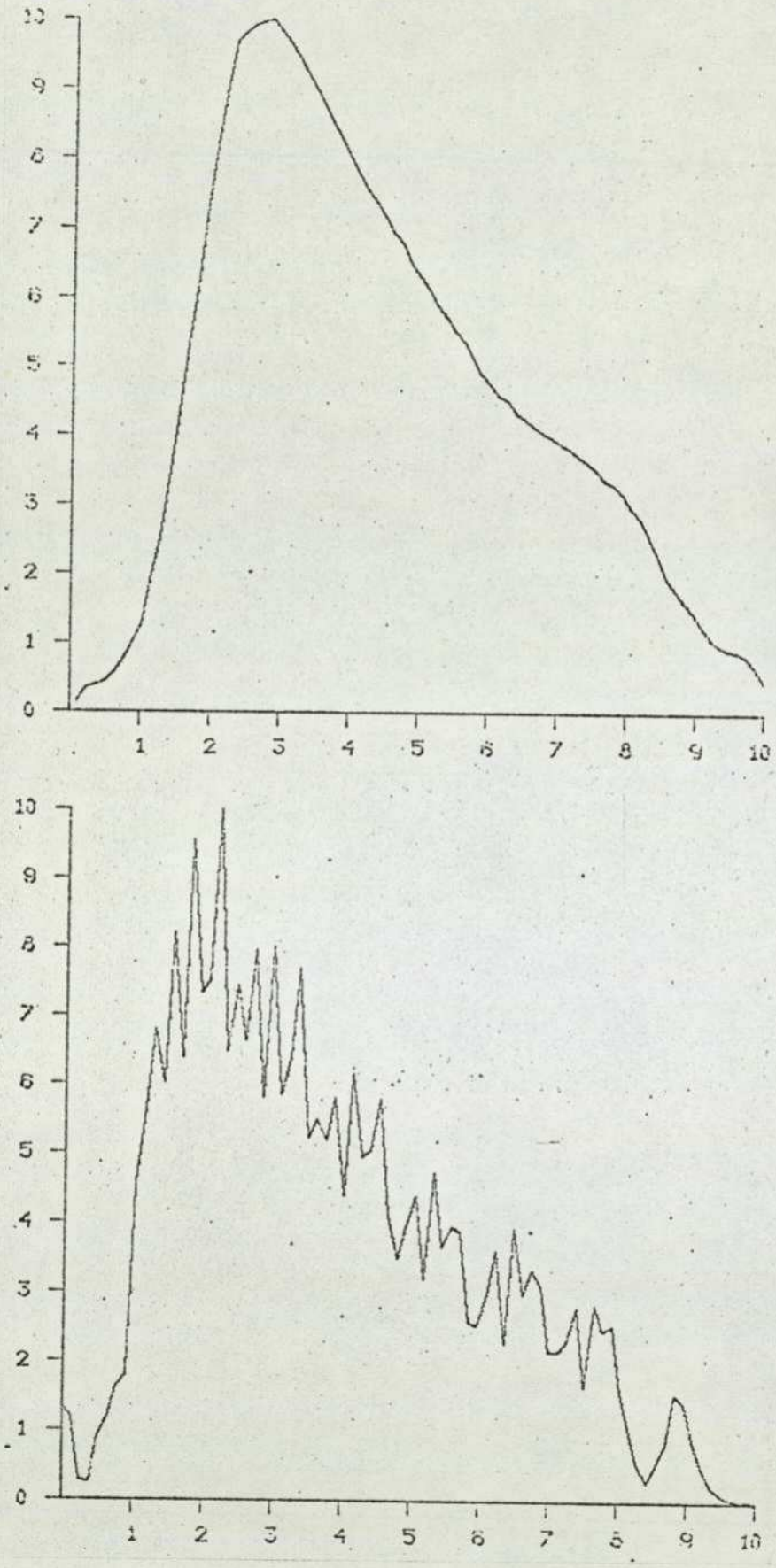


Figure 4.17 Result of Adaptive modelling to determine the charge input required to produce a known transient (top trace). The lower trace shows the response transient from the computer model (After Evison).

4.4.4.5

values and a non-dimensional constant R (equal to a/d where a is a constant), thus

$$V_o/V_{scl} = (1 + R)^{\frac{3}{2}} - R^{\frac{3}{2}} = (J_{scl}/J_o)^2$$

Similarly the transit time t can be expressed in terms of the s.c.l. value

$$t/t_{scl} = \{1 + R^{\frac{1}{2}}) - R^{\frac{1}{2}}\}\{(1 + R)^{\frac{3}{2}} - R^{\frac{3}{2}}\}$$

where $t_{scl} = 4d^2/3\ \mu\ V_o$.

The limiting values of t are t_{scl} (R = 0) for strong injection and $d^2/\mu\ V_o$ ($R \to \infty$) for very weak injection.

Hence, the transit time increases to a maximum of 1.33 times the value obtained by excluding the effects of space charge, as the space charge limited value is approached.

4.4.5 Liquid motion

4.4.5.1 Introduction

This section is restricted to theory concerning the effects of bulk liquid motion upon mobility measurements, whereas the theory of electro-hydrodynamic (e.h.d.) stability is examined in section 4.5.

It is probable that when space-charge limited currents flow either permanently or transiently, then measurements of ionic-mobility will be subject to variations as a result of e.h.d. convection. That is to say, the observed velocity of the ions will differ from the drift velocity, and a measurement of charge mobility by the 'time-of-flight' method will produce a result which is at variance with one measured in the absence of e.h.d. convection.

4.4.5.2 E.h.d. mobility

E.h.d. mobility μ_h is defined (Felici, 1971b) as the ratio of the 'mean' velocity v to the 'average' field $\bar{E}$. Thus, if the ions are carried along by the liquid, but their drift velocity, i.e. $\mu\bar{E}$

4.4.5.2

in the absence of e.h.d. convection, is small compared with v, then their 'apparent' mobility will equal μ_h. By equating, as an approximation, the drag caused by the shearing of the liquid to the average electric force on the space charge Felici (1971b) obtained expressions for the e.h.d. mobility, thus:

With strong injection; $\mu_h^2 \simeq \varepsilon/2p$

With weak injection: $\mu_h^2 \simeq qd/2pE$

and generally; $\mu_h^2 \simeq a\varepsilon/2p$, where $a = qd/\varepsilon E$.

In the above ε = permittivity, p = mass density, q = mean space charge density, and d = drift gap width.

Assuming a more definite model for the e.h.d. convection, that is a fluid streamer behaving like a Poiseuille flow in a pipe, Felici obtained a value for $\mu_h \simeq 0.14\ (\varepsilon/p)^{\frac{1}{2}}$ for strong injection and calculated values for various ions. Applying this expression to n-hexane gives

$$\mu_h \simeq 0.14(1.885 \times 8.85 \times 10^{-12}/0.652)^{\frac{1}{2}}$$

$$\simeq 7.082 \times 10^{-7}\ m^2\ V^{-1}\cdot s^{-1}$$

This value compares with values for unidentified negative ions in n-hexane of $7 \times 10^{-8}\ m^2\ V^{-1}\ s^{-1}$.

To test the formula for weak injection, an approximate mean value for q of 25×10^{-18} X m^{-3} was determined from one of the author's results where the mean field was 5×10^4 V m^{-1} in a drift gap of 1 cm. This gives a value for μ_h of $1.96 \times 10^{-11}\ m^2\ V^{-1}\ s^{-1}$ which suggests that e.h.d. convection should be negligible under these conditions.

4.4.5.2

One obvious objection to these calculations is the unknown nature of the ionic carriers in n-hexane, since the approximate expressions for μ_h assume them to be n-hexane ions.

4.4.6 Electron trapping

The model of a partly trapped, partly free electron is based on the assumption that an injected electron travels a distance l before it becomes attached to a molecule. After a finite time it escapes from the molecule and moves on before becoming trapped again. If the trap 'depth' is expressed as a potential difference U, then the mean time spent in a trap can be expressed as

$$A\exp(eU/kT)$$

where A is a constant with the dimensions of time.

In the presence of an electric field E, the effective trap 'depth' is reduced by aE, where a is the 'radius' of the trap ($a \ll 1$) thus the mean time spent in a trap is now

$$A\exp\{e(U - aE)/kT\}$$

and the mean time between traps is $l/\mu E$, where μ is the electron mobility. Thus, the effective mobility μ_e is given by

$$\mu_e = \frac{l}{E\{l/\mu E + A\exp[e(U - aE)/kT]}$$

$$= \frac{\mu}{1 + \mu EAl^{-1}\exp|e(U - aE)/kT|}$$

In practice, the '1' in the denominator can be neglected, giving

$$\mu_e = \frac{l}{EA}\exp\{-e(U - aE)/kT\}$$

Experimental values can be found for U and a by varying T and E independently, and measuring μ_e.

4.5 E.H.D. stability

4.5.1 Preliminary

The classical theory of elastic collisions between ideal spherical particles indicates, on a microscopic scale, that significant momentum exchange occurs between particles of similar size, for example ions and molecules. However, it does not explain the high velocities, several orders of magnitude greater than the ionic drift velocity, which can be induced in a dielectric liquid by an electric field. This phenomenon was known and correctly attributed to mechanical charge transport by Faraday (1838), but it is only in recent years that a more satisfactory theoretical treatment has emerged of the mechanism and the forces involved. This theory treats a dielectric liquid subjected to electric stress as an electro-hydrodynamic system, that is one in which hydrodynamic and electrostatic forces define the conditions existing within the system.

4.5.2 The work of Atten and Moreau, and Schneider and Watson: 1969-1972

4.5.2.1 Introduction

Similar criteria for the e.h.d. stability in a liquid insulant (subject to unipolar charge injection) were independently established by these workers for the space-charge-limited current case (Schneider and Watson; 1970) and for the general case (Atten and Moreau; 1969; 1970; 1972). Since this latter work treated the problem generally, the attentions of the author have been directed at this analysis. A recent contribution by Atten (1974) which included an examination of the possible reasons for the disagreement between the aforementioned theory and experiment, is discussed in section 4.5.3.

4.5.2.2 The stability theory of Atten and Moreau

Atten and Moreau (1972) have approached the problem of e.h.d. stability by the method of determining the reaction of the system, expressed as a set of electrical and hydrodynamic equations, to small perturbations. The method adopted, which involves linearising the equations and then applying very small perturbations, is commonly used in the study of hydrodynamic stability (Chandrasekhar, 1968).

The system is defined as an incompressible dielectric liquid of zero conductivity situated between two parallel-plane electrodes of infinite area. It is assumed that charge carriers of uniform density and of the same sign as one of the electrodes are injected into the liquid, and that the effects of diffusion can be ignored. In formulating the equations of the system, the magnetic effects of moving charge are neglected since they are negligible in comparison with the electrostatic forces. Variations in temperature are also neglected since any heat loss due to the Joule effect is considered to be minimal.

In order to obtain solutions from the four equations which were derived it was necessary to define three limiting electrical conditions, two of which are the potentials on the electrodes. The third condition involves a consideration of the magnitude of the electric charge density at the injecting electrode, and for convenience this was defined as q_o and assumed constant. In addition two conditions involving hydrodynamic considerations are imposed on the component w of the liquid velocity normal to the electrodes. Following the application of dimensional analysis to the four partial differential equations governing this electro-hydrodynamic system, three dimensionless numbers were obtained, as follows

4.5.2.2

$$C = \frac{q_o d^2}{\varepsilon V}; \quad R = \frac{\mu p V}{\eta}; \quad M = \frac{1}{\mu}\left(\frac{\varepsilon}{p}\right)^{\frac{1}{2}} \tag{4.32}$$

where; d = distance between the electrodes

V = p.d. across the electrodes

q_o = charge density at the injector surface

ε = permittivity of the liquid

η = viscosity of the liquid

p = mass density of the liquid

μ = mobility of the charge carriers.

C is a measure of the charge injected into the liquid. If $C \ll 1$ (weak injection), the electric field suffers little space-charge distortion, whereas if $C > 1$ (strong injection) there is considerable modification of the electric field by space-charge. R is representative of the speed of the ions in a uniform field and M represents the ratio of the e.h.d. mobility μ_h (see section 4.4.5.2) to the actual mobility of the ions μ.

If the reference velocity is chosen as η/pd, a further critical number T is obtained, which is given by

$$T = M^2 R = \varepsilon V/\mu\eta \tag{4.33}$$

This is analogous to the Rayleigh number in the Benard stability problem in hydrodynamics.

Using the perturbation method, with further analysis Atten and Moreau made the following deductions:

1. If C, that is the charge injection density, can be fixed independently of the other parameters, there is then a critical voltage V_c which determines the onset of instability.

4.5.2.2

2. For weak injection ($C \ll 1$), a critical number P, defined by

$$P = TC^2 = q_o^2 d^4/\mu\eta\varepsilon V, \qquad (4.34)$$

determines the boundary between stability and instability. This number relates the increase of electrical energy caused by the perturbation to the decrease of energy due to viscous forces. A critical value can be calculated for this number from the equilibrium energy state and is 220.76.

3. It is not possible for the perturbations to cause an oscillatory motion in the liquid under any conditions, only stationary cellular disturbances.

4. The variation of T_{crit}, the stability criterion, as a function of C for the four cases,

   I Injector and collector both solid planes,

   II Injector solid; collector a free surface,

   III Injector free; collector solid,

   IV Injector and collector both free surfaces,

   is as shown in figure 4.18 (after Atten and Moreau).

5. A determination of T_{crit} for case III produced the result 95.150, which is in close agreement with the approximate result of Schneider and Watson of 99.5 for similar conditions.

6. The results for T_{crit} in the other three cases were, Case I: 160.750; Case II: 134.255; Case IV: 76.358.

4.5.2.2

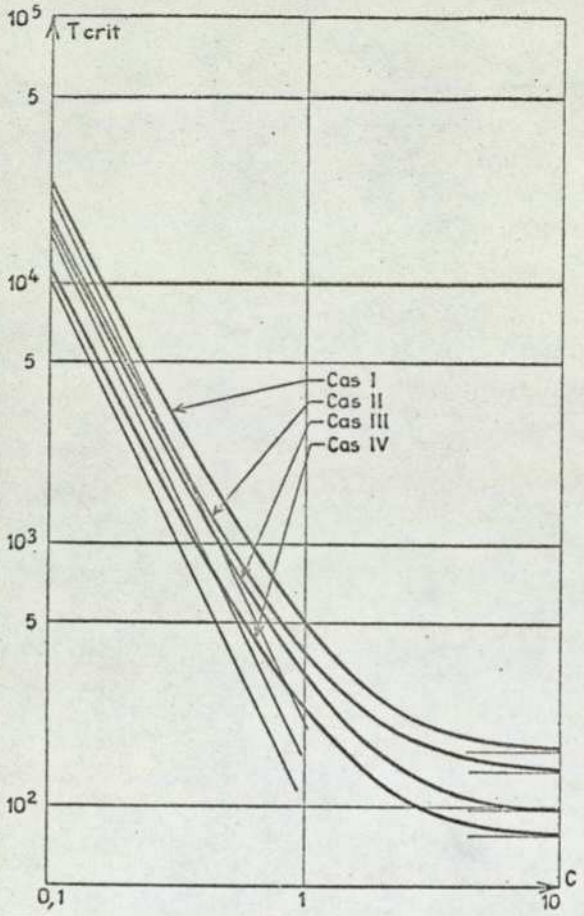


Figure 4.18 Variations of the stability criterion T_{CRIT} as a function of the parameter C for differing boundaries (see text). After Atten and Moreau.

4.5.3 E.h.d. stability during transient injection

The stability problem as analysed in the previous section assumed that the space-charge and electric field distributions in the liquid are stationary. Under the majority of experimental conditions this is not the case, and the values for the critical voltage, as determined experimentally, have been consistently lower than the theoretical values with the exception of the experimental verification by Watson, Schneider and Till (1970). Atten (1974) attempted to explain these discrepancies by analysing the case of space-charge limited constant current injection using the method of quasi-stationary approximation. The results of this analysis were

4.5.3

disappointing since they indicated that the amplification of the velocity disturbance is very low at the moment this disturbance becomes detectable in experimental observations. For a reasonable value of the amplification factor, the stability criterion T_{crit} would be about 3 times that derived theoretically for the steady state.

Atten concluded that the disagreements suggest the theoretical model is too idealized because it does not take into account all the injection effects.

4.6 Computer studies of e.h.d. stability

4.6.1 Preliminary

At the commencement of this work, the e.h.d. stability theory of Atten and Moreau attracted the attention of a colleague, Dr. J.E. Brignell, and the author, as a possible method of predicting the onset of e.h.d. convection during experiments. Since the results of the theory, the non-dimensional numbers, appear in terms of the space charge density at the injecting electrode, it was not possible to apply these directly to this task. Accordingly, an on-line computer program was developed to compute the critical numbers from the experimental values of current density, drift gap width, and applied voltage, and the liquid parameters of relative permittivity, viscosity and charge mobility.

The method of computation and some of the results have been described previously (Hewish and Brignell[2], 1972), and this publication forms section 10.1 of the appendix. Some further results are presented in this section.

4.6.2 The effects of parameter values upon the critical voltage and current

The stability curves (see fig. 2 of appendix 10.1) of the critical numbers A (=T) versus C and current density J versus applied voltage V are for constant values of charge mobility, liquid viscosity and permittivity, and drift gap width. The values of some of these parameters, in particular the liquid mobility, could be erroneous, in which case the boundaries of the stable region will be displaced. Each of these parameters will be considered and the effects of an error in their values assessed. The equations which are relevant are

$$A = T = \varepsilon V_{crit}/\mu\eta; \qquad C(\text{computed}) = q_o d^2/\varepsilon V;$$

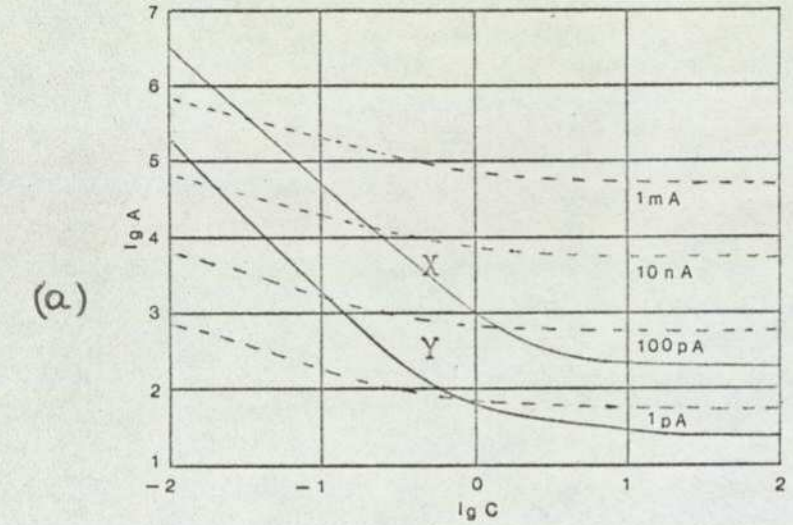
$$V_{crit} = 160.75\ \mu\eta/\varepsilon; \quad J_{crit} = 1.125\ (V_{crit})^2 \mu\varepsilon/d^3 \qquad (4.35)$$

Unless they are varied the values of the other parameters have been chosen as

$$d = 1 \text{ cm}; \quad \varepsilon_R = 1.885; \quad \mu = 7.5 \times 10^{-8}\ m^2\ V^{-1}\ s^{-1};$$

$$\eta = 3.26 \times 10^{-4}\ Kg\ m^{-1}\ s^{-1}.$$

Charge mobility. μ appears in each of the equations 4.35 except that for C. It is significant then because of the presence of V_{crit} ($= \mu\eta A/\varepsilon$), J_{crit} varies as μ^3. Figure 4.19 shows the A v C and J v V curves (logarithmic axes) for $\mu = 8 \times 10^{-8}$ and $2 \times 10^{-8}\ m^2\ V^{-1}\ s^{-1}$. From figure 4.19(a) it is evident, that for medium or weak injection, instability can occur at a lower value of C if the mobility is in fact lower than the measured value. For weak injection the critical value of C (for constant voltage) decreases proportionally as μ decreases. Figure 4.19(b) shows a similar increase in the region of instability as the mobility is decreased. These findings are not unexpected, since the



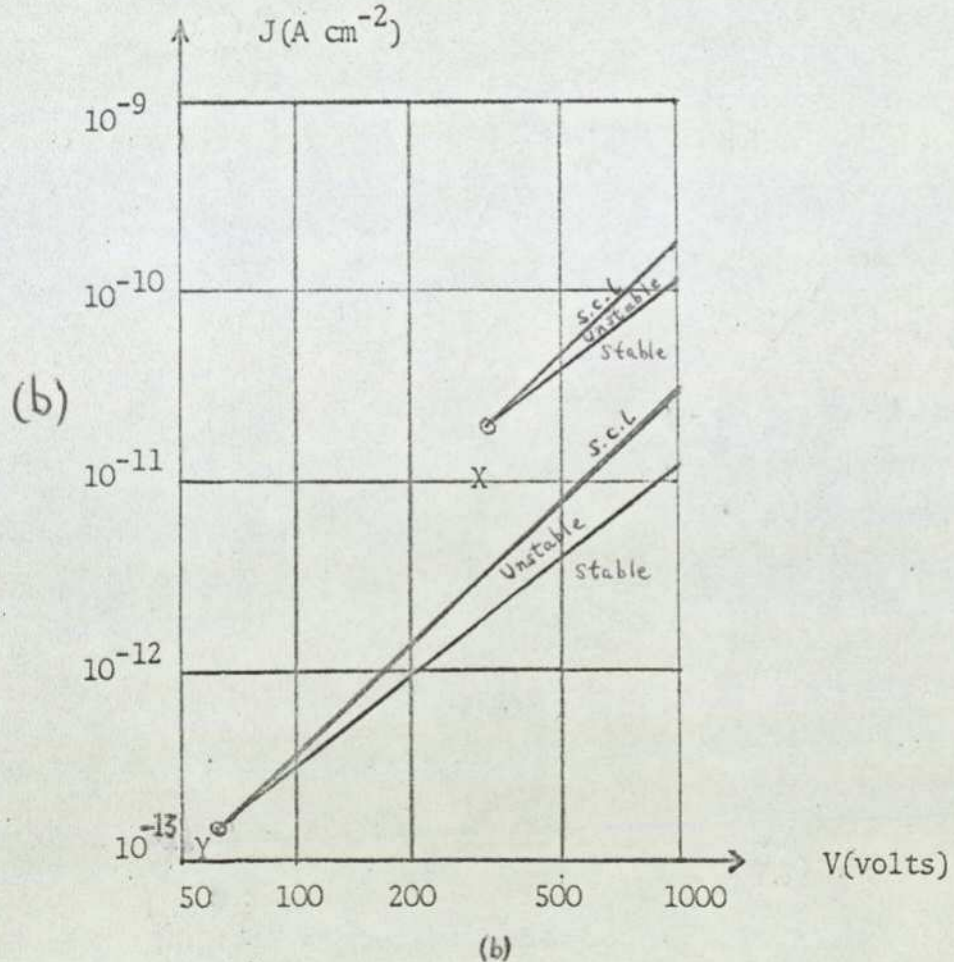


Figure 4.19 (a) A versus C and (b) J versus V curves for $\mu = 2 \times 10^{-8}$ (X) and 8×10^{-8} m^2 V^{-1} s^{-1} (Y) on logarithmic axes.

4.6.2

possibility of instability for weak injection depends upon P > 220.76 and P has μ in its denominator.

The locus of the critical values for e.h.d. convection are shown in figure 4.20, for two ranges of mobility values, 10^{-8} to 10^{-7} m^2 V^{-1} s^{-1} and 10^{-8} to 10^{-5} m^2 V^{-1} s^{-1}.

Viscosity. The critical current only varies as the square of the viscosity. Thus, changes in viscosity, resulting from temperature variations, have little effect on the critical values. Over the temperature range 25°C to 65°C the viscosity varies from 3.29×10^{-4} to 2.18×10^{-4} Kg m^{-1} s^{-1} (Landolt and Bornstein, 1951), the critical voltage from 252 V to 168 V, and the critical current from 7.7 to 3.45 pA.

Permittivity. Variations of permittivity cause the critical voltage and current to vary in inverse proportion. Thus, transient local (or general) increases in permittivity within the liquid could cause significant reductions in the critical conditions for e.h.d. convection.

Drift gap width

An error in measuring the width of the drift gap can affect the critical current significantly ($J_{crit} \propto d^{-3}$) but not the critical voltage as this is independent of gap width.

From these observations it can be concluded that, as mobility and viscosity are the liquid parameters which are most likely to be affected by experimental conditions, it is these which will have the maximum effect on the critical values of voltage and current for the onset of e.h.d. convection.

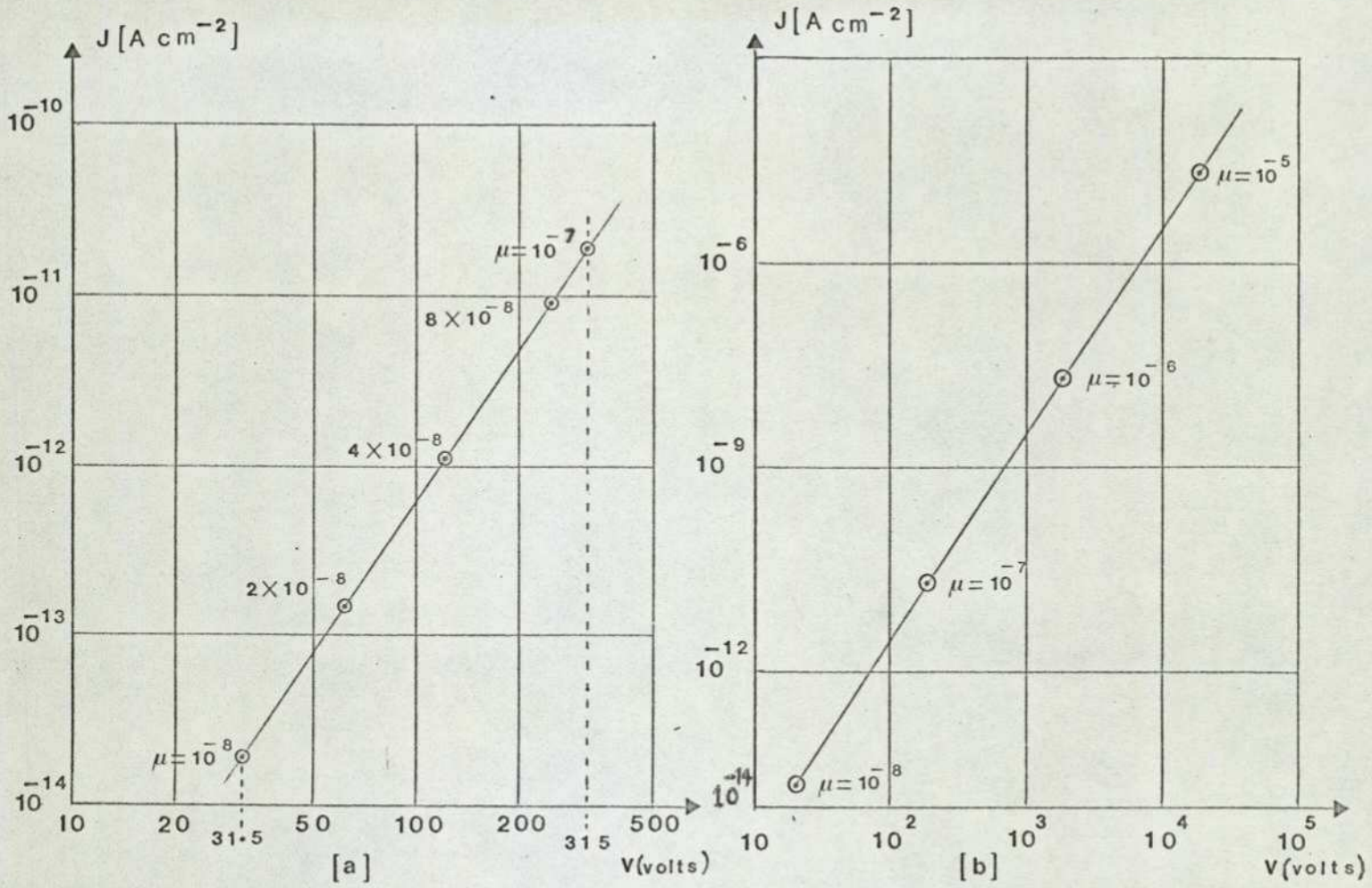


Figure 4·20. Loci of critical points for differing mobility values.
(Units of mobility are $m^2 V^{-1} s^{-1}$)

Chapter 5

Experimental method and apparatus

5.1 Experimental techniques for the study of conduction in n-hexane.

5.1.1 Introduction

The techniques which have been adopted by the many experimentalists in the study of electrical conduction in n-hexane are examined in four sections (5.1.2 to 5.1.5). Firstly the preparation of the sample of liquid, secondly the method employed to enhance conduction, thirdly the measurement of electric current (or charge), and finally the observation of motion in the liquid. Section 5.2 describes the methods used by the author to prepare the liquid samples and section 5.3 contains details of the test cells and the photocathodes. The circuits and apparatus for controlling charge injection and measuring current are described in section 5.4, and the methods used for observing and recording liquid motion are outlined in section 5.5. A description of the on-line computing facilities which were used in this work concludes this chapter.

5.1.2 Preparation of sample

The composition of the sample is probably the most variable factor in experiments with n-hexane, and the range of mobility values for the charge carriers which have appeared in the literature is an indication of the varying degree of purity as well as the differing experimental conditions (see chapter 2). The ideal initial condition is a pure sample to which pre-determined quantities of impurities could be added in order to effect comparitive measurements.

To detect free electrons in n-hexane (Minday, Schmidt, and Davis, 1969 and 1971), a high degree of purification is required and extreme care is necessary to remove traces of impurities, in particular the electron capturing materials, e.g. water and oxygen. The samples must be processed under ultra-high-vacuum conditions using vacuum deposited metal films and molecular sieves as

5.1.2

selective getters.

Morant (1960) found that photo-currents of any sort could be induced in n-hexane only if it was thoroughly degassed by a final distillation at a pressure of less than 10^{-5} torr to remove dissolved oxygen. His experiments were at low stress, less than 700 V cm^{-1} Nevertheless this conclusion appears to be at variance with that of Le Blanc (1959) who later communicated to Sharbaugh and Watson (1962) the opinion that, provided the partial pressure of oxygen in hexane was less than 100 torr, photo-currents greater than 10^{-12} A could be detected under low stress conditions.

Swan (1961) obtained similar photo-current characteristics to Morant and Le Blanc (see chapter 2) using a simple distillation system which allowed the liquid to be degassed at a pressure of about 10^{-3} torr. The 'back-illumination' method of photo-injection used by Swan is described in section 5.1.3.

Chromatographic analysis (Kahan and Morant, 1965; Kahan, 1964) of the 'special for spectroscopy' grade of hexane, used by Morant (1960), Swan (1961), and others, showed that a typical sample contained approximately 77% of n-hexane before treatment, see figure 5.1. However, the chromatogram, figure 5.2, of 99% pure hexane supplied by Koch-Light laboratories and used by many later experimenters indicates only two detectable hydrocarbon impurities i.e. 2,4 dimethyl pentane (0.07%) and 3-methyl pentane (0.034%).

In addition to a low isomer content, a further consideration is the transparency of the sample to ultra-violet radiation. Koch-Light hexane contains very small quantities of benzene (Pugh, 1968) and other unsaturated compounds (Rahman, 1970) which absorb strongly in the ultra-violet wavelengths used for photo-injection (2,000-

5.1.2

4,000 A°). The energies involved (6.2 - 3.1 eV) are sufficient to cause radicals to be formed some of which may be expected to react with impurity molecules, e.g. oxygen, to form other impurity com-

Identification of chromatograph peaks of figure .

1	*iso*-pentane	0·1%
2	*n*-pentane	1·6%
3	2 methyl pentane or 2,3 methyl butane, or both	3·8%
4	3 methyl pentane	5·1%
5	*n*-hexane	77·0%
6	2,4 dimethyl pentane	11·7%
7	methylcyclopentane	0·7%

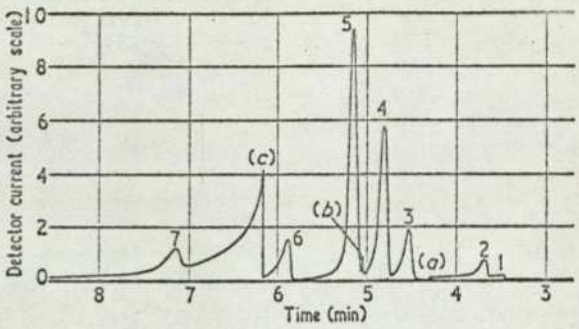
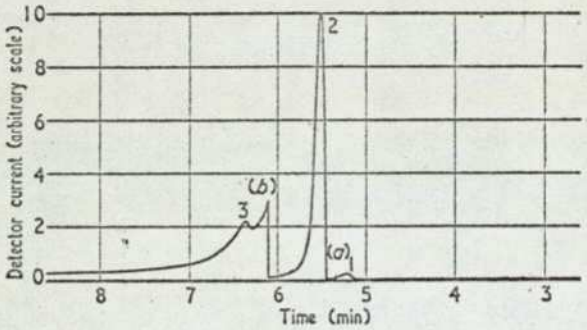


Figure 5.1 Typical chromatogram of hexane (special for spectroscopy grade). (The vertical sensitivity was reduced by 3.3 times at (a) and by a further ten times at (b). It was returned to the initial value at (c).) After Kahan and Morant.

pounds. Oxygen and many of the unsaturated hydrocarbon compounds have a significant electron affinity (Forster, 1964; 1967) with electron attachment energies of less than 1 eV and are known to form stable negative ions, a process which could contribute to the increase in conductivity of n-hexane exposed to photo-injection of electrons. The optical absorption of Koch-light n-hexane at u.v. wavelengths is considerably reduced by passing the hexane through a dry silica gel column (Potts 1952). Pugh (1968) measured the optical absorption of Koch-Light n-hexane before and after percolation through silica gel, which had been dried for several hours at 250°C under vacuum and then cooled in an atmosphere of pure argon. He also made absorption measurements on untreated samples of n-hexane from other suppliers including Hopkin and Williams 'spectrosol' grade and concluded that two percolations of the Koch-

5.1.2

Light hexane through activated silica gel produced a sample with the best transmission properties. However, using the same procedure, Rahman (1970) found that a second percolation through freshly activated silica gel caused no remarkable improvement in the u.v. transmission. Figure 5.3 shows Rahman's results together with



Chromatogram of 99% pure *n*-hexane. (The vertical sensitivity was reduced by 33 times between (*a*) and (*b*).)

Figure 5.2 Chromatogram of 99% Koch Light n-hexane, see text p. 91. After Kahan and Morant.

the transmittance curve (E) he obtained for untreated 'spectrosol' grade n-hexane.

Although silica-gel treatment removes most of the water from the sample as well as unsaturated hydrocarbons, further dehydration can be achieved if the liquid is passed through a molecular sieve. Pollard (1971) used a column of B.D.H. type 4A sieve material (sodium alumino-silicate) which has a nominal trap size of $4A^{o}$. This has no selective filtering action on hydrocarbons but it was found to remove 50% of the water remaining in the liquid, after it had percolated through a column of dried silica gel. Both silica gel and molecular sieve material can add solid particles to the liquid so the columns were fitted with sintered glass disc filters

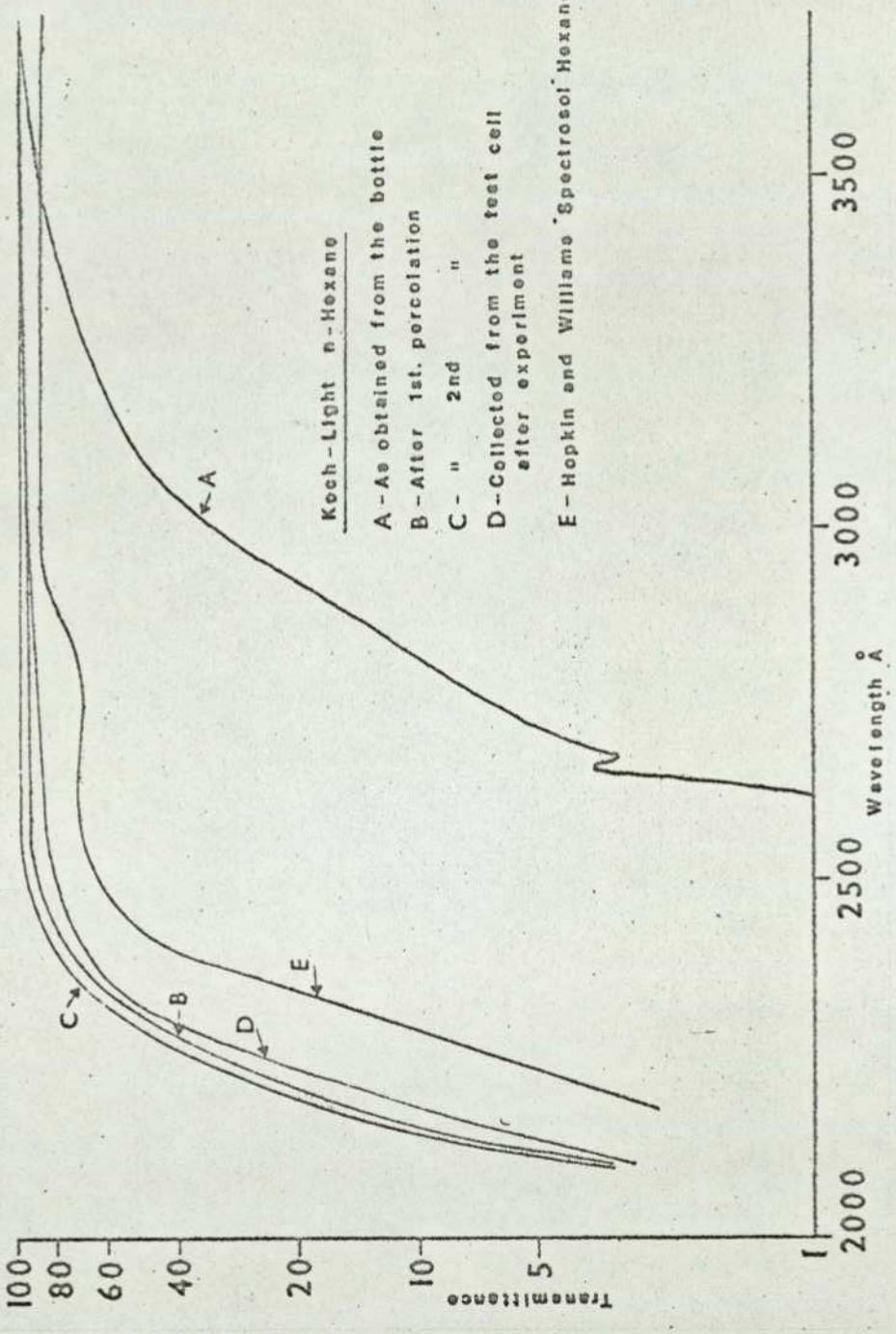


Figure 5.3 The optical obsorption of samples of n-hexane. Optical path length 10 cm., Reference cell air. (After Rahman).

5.1.2

(No. 4 porosity with a maximum pore diameter of 1 μm) to remove these. Rhodes (1971) removed smaller particles by further filtering through a cellulose nitrate membrane which had a maximum pore diameter of 0.1 μm.

For this work Koch-Light n-hexane, 99% purity, was pre-treated using columns of dried silica-gel and molecular sieve with a final filtering through a cellulose nitrate membrane. It was then vacuum distilled and degassed, using the 'Morant' method, at a pressure of approximately 10^{-6} torr before being introduced under vacuum to the test cell. This treatment is described in more detail in section 5.2.

5.1.3 Enhanced conduction in n-hexane at low fields

If we define a reasonable degree of purity by reference to a sample having a resistivity of 10^{18} Ω cm, a stress of 1 kV cm^{-1} would produce a conduction current density of 10^{-15} A cm^{-2}. Such currents are found to exhibit a high noise content. Thus transient current densities greater than this value are required for the behaviour of the injected carriers to be determinable. Several methods of producing an enhancement of the natural conduction current are in use, and these will be discussed briefly, except for the mode of photo-injection which, as it was adopted for this work, will be examined in more detail.

Ionization of a dielectric liquid by high energy particles or photons was first investigated by J.J. Thomson (1897) who found an increase in the electric conductivity of vaseline oil when it was irradiated by X-rays and P. Curie (1902) reported similar effects using radium as the energy source. Adamczewski (1969) surveyed ionization and conductivity in dielectric liquids and Hummel and

5.1.3

Schmidt (1974) reviewed more recent work, in particular, that concerned with the action of high-energy radiation on dielectric liquids especially hydrocarbons. Many experimentalists use short pulses of X-rays and ionize a layer of the liquid near one of the electrodes. Schmidt and Allen (1969, 1970), using this method, observed the rise and decay of the 'free'-electron current in eight saturated hydrocarbons including n-hexane. Their results were verified using a step function of X rays, in this case the initial rise of the ionization current is due to the electrons and not the less-mobile ions. Similar results were obtained by Conrad and Silverman (1969) who irradiated n-hexane with a 25 nS pulse of X-rays with a maximum photon energy of 2.5 MeV using the thin-layer technique. A nitrogen laser supplying 10 nS pulses of 3371 A^{o} light was used by Devins and Wei (1972) to generate 'fast' initial carriers in n-hexane lightly doped with tetramethyl phenyl diamine by bulk biphotonic ionization. Gray and Lewis (1969) used a triode cell, shown in fig. 5.4, in which the ions were generated in n-hexane by a collimated beam of X-rays in a thin layer close to one electrode and injected into the drift space by switching the potential on a grid. In the double grid cell (figure 5.5), also used by Gray and Lewis, a 150 mCi tritium β-particle source on the emitter ionizes liquid close to this electrode. This cell is of particular interest to the author since the grid arrangement is similar to that used in this work (see Section 5.3). Other high energy particles which have been used to ionize n-hexane include α, γ and neutron particles, but X-rays have the advantage that the resultant ionization can be localized more easily.

5.1.3

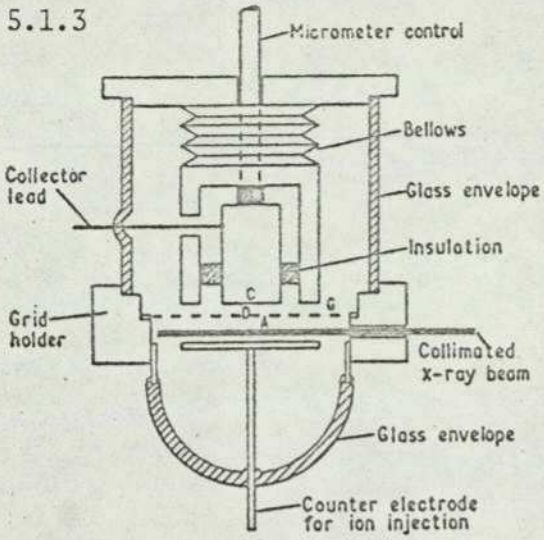


Figure 5.4 X-ray triode cell (after Gray and Lewis)

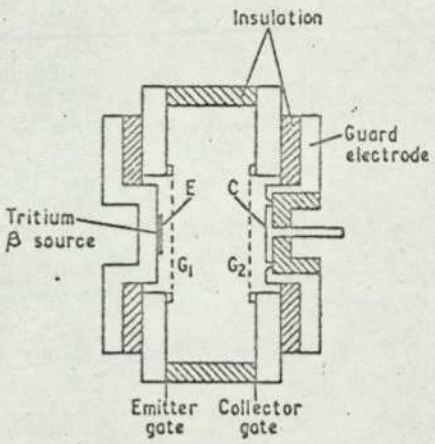


Figure 5.5 Double-grid cell (after Gray and Lewis)

In polar liquids an attractive method of charge carrier enhancement is the injection of known ions either using an electrodialytic membrane to inject H^+ or Cl^- ions (Briere and Gosse, 1968) or a conductive glass which injects Na^+ ions (Filippini et al, 1969). Possibly the latter method of injection could be employed in non-polar liquids, provided sufficiently high electric stress could be applied at the glass-liquid interface to facilitate injection of ions into the liquid. Grid control of the injected ions could then be employed to study conduction in a low drift-field region. Electrons injected from thin film Al-Al_2O_3-Au diodes into cyclohexane, benzene and liquid helium (Silver et al, 1967) and nitrobenzene (Bright et al, 1970) produce small transient currents, typically 2×10^{-12} A peak at a stress of 300 V cm^{-1} into cyclohexane (Silver et al, 1968). The author carried out a brief experimental study of such devices but found them too unreliable for the present project. Bright and his co-workers also used silicon carbide reverse junction diodes to inject electrons into nitrobenzene and measured peak currents of 3 μA per mm of exposed junction length with no visible deterioration in performance. Al-

5.1.3

though the source is non-planar the strong injection can be readily controlled by varying the diode junction current and the device would appear to be a possible injection source for non-polar liquids. Watson and Clancy (1965) described a scanning electron-beam source which injected a uniform charge pattern on the free surface of a dielectric liquid and using this method Watson (1965) observed, that for surface potentials above a certain critical value, the liquid becomes unstable and convection occurs. The analysis (Schneider and Watson, 1969) of this phenomenon is discussed in section 4.5.2.1.

High field emission from sharp-line metal surfaces, e.g. the edges of razor blades, into n-hexane (Coe et al, 1966) can be used to inject charge carriers of either polarity into a drift space. If the emitter is positive with reference to the collector electrode, electrons tunnel from the liquid molecules to the emitter and positive ions are injected, whereas with the polarities reversed, electrons are emitted from the metal and are rapidly trapped to form a negative charged ion or polarized molecular complex. Again, grids have been used to control the relatively large currents, typically 10^{-6} to 10^{-4} A, which result from an array of these injectors, and to define the drift field (Essex and Secker, 1968; Taylor, 1972), but the injection source remains non-uniform and non-planar. A more serious objection to these devices is the high-field ionization at the tips of the injectors which could generate differing species of charge carriers. Furthermore, they might be expected to be injectors of turbulence, even in a system which is nominally stable.

Emission of electrons into n-hexane by irradiating the

5.1.3

negative electrode or cathode with X-rays (Secker, 1965) is also accompanied by the generation of primary radiation products within the liquid, however, if lower-energy radiation, i.e. ultra violet, is used these bulk ionisation effects are considerably reduced. The earlier work of Le Blanc, 1959; Chong and Iniushi, 1960; Morant, 1960; Terlecki, 1962; etc., has often been reviewed and it is not proposed to describe their injection methods in detail. Each of them irradiated the cathode with a pulse or step of u.v. light through the liquid and Morant showed that bulk ionisation effects were reduced by filtering the radiation. Swan (1961) attempted to reduce the production of ions in the liquid through primary radiation by directing the U.V. light through a quartz window on the inside of which there was deposited a thin film of aluminium with a transmittance for visible light of about 50%. The anode was a stainless steel disc spaced about 0.4 mm from the aluminium-coated window, and by reversing the polarity it was found that the current injected with the metal-film as cathode was about 100 times that injected with the film as anode. This ratio remained the same when the cell was emptied of hexane and evacuated which suggested to Swan that some radiation passed through the metal film and released electrons from the stainless steel disc, but did not directly ionize the liquid. Buttle and Brignell (1969) adopted the 'back-illumination' method of photo-injection and also introduced a vapour gap between the liquid and the cathode to increase the rate of electron emission (see figure 5.6). They also proposed to add a grid at or below the liquid surface to provide a uniform drift gap as well as a means of electronic control of the emission. This proposal was taken up and extended in the

5.1.3

present work in which these functions are performed by two grids, see figure 5.7. The first B is located near the photo-cathode A, ensuring that the current response to an applied voltage pulse originates from the cathode-grid interelectrode gap. The second grid C is positioned at the liquid surface enabling the field applied to the sample to be accurately defined and through its screening effect ensuring that the current transient, I, results from charge movement in the liquid only.

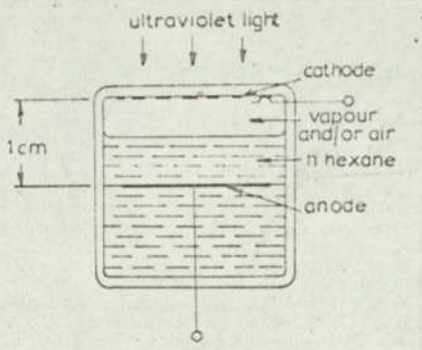


Figure 5.6 Photo emission in a vapour gap (after Buttle and Brignell).

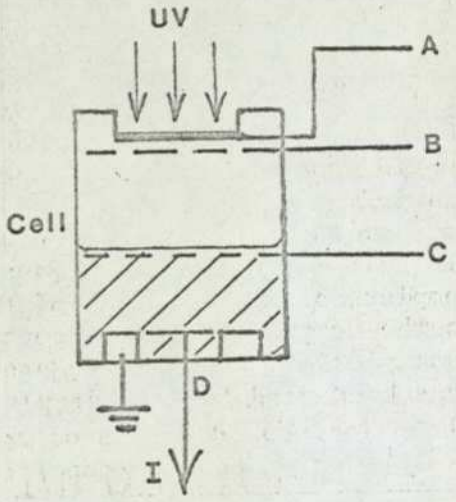


Figure 5.7 Grid control of photo-emission into a vapour gap.

5.1.4 Measurement of electric current

As a result of the advances in electronics in recent years, the measurement of small current and small quantities of electric charge can now be made using semiconductor electrometer amplifiers. These have particular advantages, not least those of low cost and their small size, which means that they can be positioned close to the signal source thus reducing the problems of

5.1.4

'pick-up' of electrical noise. Integration of current , i.e. charge measurement, has been employed to reduce noise, but interpretation of results is more difficult, and a feature of this work is the identification of small signals buried in noise (see chapter 4). For measurements in the required range of 1-100 pA, the high input impedance, low bias current and sensitivity-speed product of semiconductor electrometers compare favourably with the characteristics of electrometer-valve and other more expensive types of amplifiers.

Evison (1975) has examined the constraints governing the design of picoammeters which involve a compromise between sensitivity, noise and speed of response. In section 4,2, an analysis of picoammeter circuits showed the effects of capacitance upon the performance of these devices in particularly the speed of response to a pulse of input current. The distributed capacitance to ground along the high-value feedback resistor should also be included in the analysis which then becomes very difficult, although even a lumped circuit approximation demonstrates the possible complications. Presley (1966) describes a method of reducing this distributed capacitance by surround R_1 with a uniform electric field as shown in figure 5.8, if very short rise-times are required.

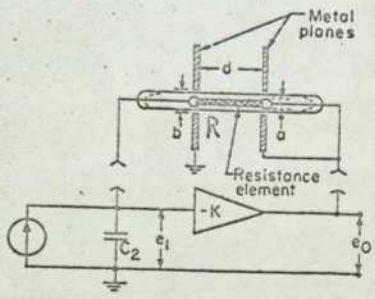


Figure 5.8 Reducing distributed capacitance by a uniform electric field around R (after Presley).

The important sources of noise in picoammeters are the resistor R_1, the amplifier, and external electrical noise including mains hum. In

5.1.4

practice the first two sources are minimised by a careful choice of these components and the major noise problem is the reduction of 'pick-up' of external noise, i.e. inductive or capacitive coupling between the input connections to the amplifier and sources of alternating voltage or current. The most common of these sources is the mains supply to other experimental equipment, lighting, etc., and this can only be reduced by careful screening of the amplifier and test cell and the avoidance of earth loops. The inductive coupling can be minimised by making the connection between the test cell and the picoammeter, of non-microphonic, screened, high impedance cable and as short as possible. The capacitive coupling is also minimised by using as short a connection as possible between the amplifier input and test cell. The connecting link should also have a low capacitance to ground.

5.1.5 Observation of liquid motion

The direct observation of liquid motion and the estimation of velocity in the case of low-conductivity non-polar liquids subjected to uniform unipolar injection and low electric stress has only been possible through the injection of a visible additive, e.g. Sudan Black dye (Gray and Lewis, 1965 and 1969). During his investigations of the mechanism of electrophoretic deposition, Brown (1964) studied the effects of applying a uniform d.c. field to various liquids, including hexane, by observing the movement of fine particles introduced into the liquid. He also used the 'dye-drop' method and a Schlieren system during his work.

Indirect observations avoid the addition of an impurity to the sample, but have led to conclusions which in retrospect must be

5.1.5

regarded as dubious. For example, Brignell and Buttle (1971) concluded that the absence of any dependance of apparent mobility of photo-injected charges on electrical power input implied inexistent effects of an electrohydrodynamic origin. Similarly Belmont (1973) concluded that no significant liquid motion effects were present in his results since the total-gap irradiation and larger ionisation methods produced similar mobility values with differing power inputs. However, the limits of error on the mobility values obtained by these workers are sufficiently wide to accommodate the presence of liquid motion (Hewish and Brignell, 1975).

The laser-Doppler optical probe used by Taylor (1972) to measure liquid velocity in n-hexane depends upon minute particles in the liquid scattering the light, which suffers a frequency shift proportional to one component of the particle velocity. An approximately Gaussian distribution of frequencies is obtained for laminar flow, but if turbulence is present considerable broadening of the frequency spectrum occurs and it is difficult to determine a meaningful velocity (Taylor and House, 1971). This difficulty can be alleviated using a photon-counting photomultiplier tube as the detector followed by a digital autocorrelator which produces an output containing the required spectrum of frequencies, provided the correlation delay time τ is correctly set (Abbis et al, 1974).

Schlieren observations (Holder and North, 1963) depend on the deflection of a light beam from its undisturbed path when it passes through a medium in which there is a component of the gradient of the refractive index normal to the beam. The refractive index will vary if the density varies as a consequence of temperature or pressure gradients. Ostroumov (1956), using a type of schlieren

5.1.5

apparatus, observed electrically induced motion in unpurified polar and non-polar liquids. This motion, superimposed upon thermal convection, was observed as the temperature gradients it induced in the liquid. Farazmand (1961) used a Toepler-Schlieren optical system to observe motion at breakdown stresses in n-hexane and Smith and Calderwood (1968) detected motion in 'spectrosol' hexane between spherical electrodes 4 mm apart at voltages greater than 2.5 kV using a similar system. Filippini et al (1969 and 1970) used a Toepler-Foucault schlieren method, shown in figure 5.9, to observe motion following unipolar injection into

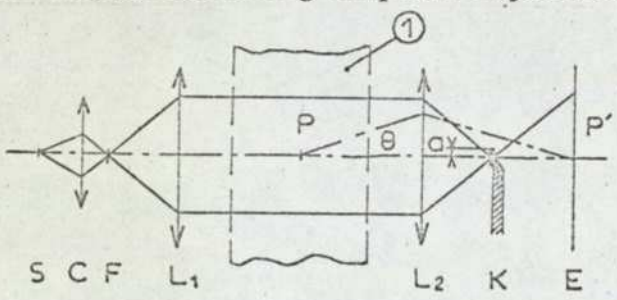


Figure 5.9 A Toepler-Foucault schlieren method (after Filippini et al)

nitrobenzene and aroclor between plane electrodes spaced a few mm apart, with applied voltages in the range 100 V - 2 kV. In these experiments the liquid motion was made visible by thermal gradients which pre-existed in the vicinity of the electrodes.

Taylor (1972) made schlieren observations of razor-blade injection into n-hexane using a laser as the light source, see figure 5.10, and Thomas (1972) found that thermal gradients of a few hundreths of a degree per cm were detectable using a helium-near laser and short focal-length lenses.

5.1.5

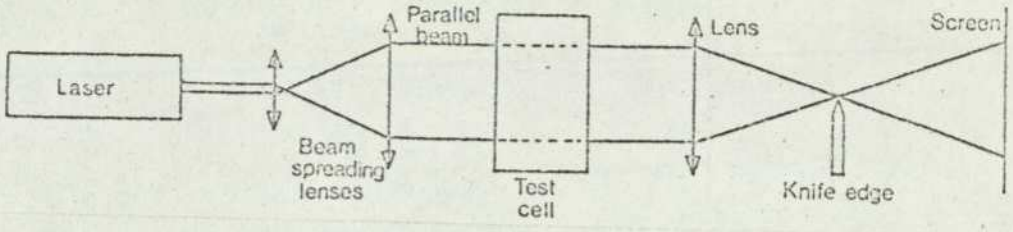


Figure 5.10 A laser schlieren arrangement (after Taylor).

The ultimate sensitivity in a conventional schlieren system is dependent upon the human eye, or photographic film, used to record the observations. This sensitivity can be increased by using photo-electric devices to detect the variations in light intensity at the screen, and these have the additional advantage of providing an electrical signal which can be recorded simultaneously with the current transient, (Hewish and Brignell, 1975).

5.2 Preparation of the liquid sample

5.2.1 Introduction

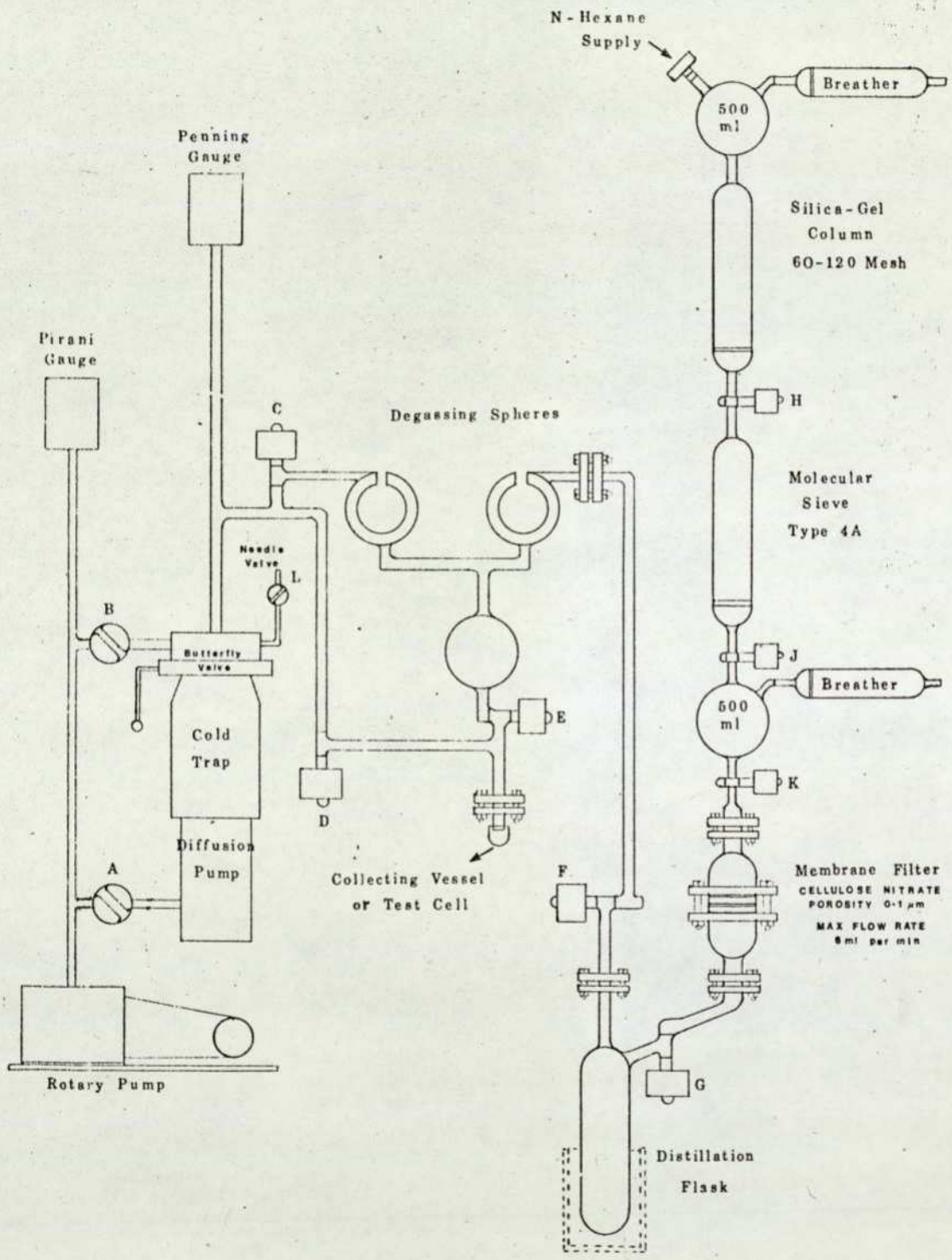
The purification process adopted has been described in principle by Pollard (1971) though some modifications have been incorporated. The purification plant is designed to remove from Koch Light 99% n-hexane the following impurities; unsaturated carbon compounds, isomers of n-hexane, water, gases and particles. Included in chapter 6 are the results of tests made on the liquid to assess the effectiveness of the purification.

5.2.2 The purification system

The process of purification is carried out in two stages within a plant, a photograph of which is shown in Fig. 5.12.

1st stage. Referring to the schematic diagram (Fig. 5.11), the n-hexane supply (99% Koch-Light) is admitted to a 500 ml flask

Figure 5.11 HEXANE PURIFICATION PLANT



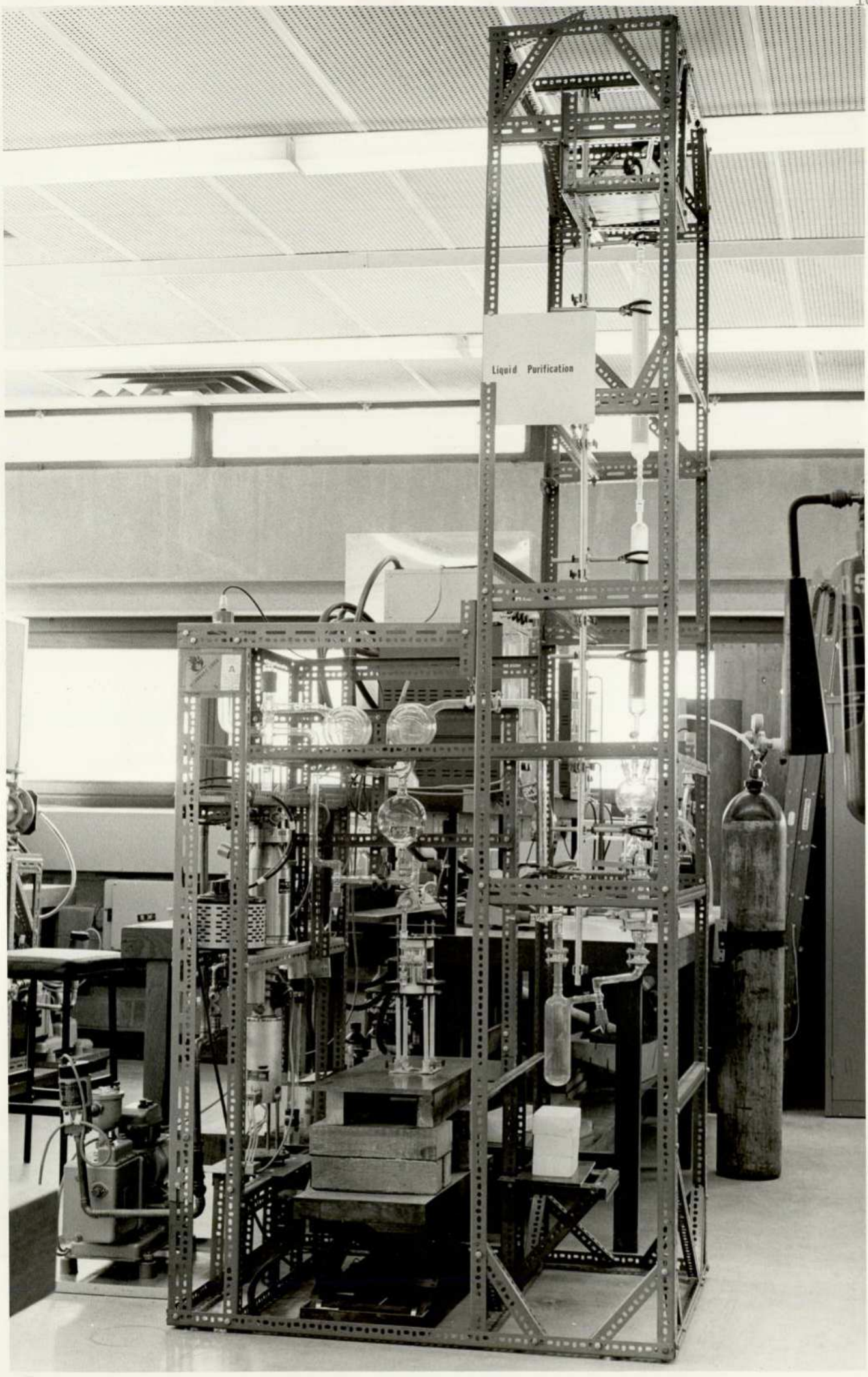


Figure 5.12 The Liquid Purification apparatus.

5.2.2

at the top of the silica-gel column, which is then closed to the atmosphere except for a dry breather tube containing self-indicating silica gel. The liquid then flows under gravity through the silica gel and molecular sieve columns which remove unsaturated hydrocarbons and water, and collects in the second 500 ml flask above valve K.

2nd stage. The distillation system as far as valve G is pumped to better than 10^{-6} Torr, then valve F is closed and the distillation flask cooled to approximately - 80° C by immersion in a mixture of methyl alcohol and liquid nitrogen. By careful control of valves K and G the liquid is slowly filtered through the cellulose nitrate membrane to remove particles of greater than 0.1 μm cross-section. Valve G is closed when sufficient filtrate has accumulated in the distallation flask and while there is still liquid above valve G. The degassing spheres are cooled with liquid nitrogen, valve F is slowly opened and the liquid distilled and degassed at a pressure of $< 10^{-5}$ Torr, solidifing on the spheres. The distallation rate can be controlled by varying the temperature of the distallation flask, and terminated by closing valves F and C in that order. The distillate collects above valve E as the liquid nitrogen in the degassing spheres evaporates and can be admitted to an evacuated test cell when required.

5.3 The test cells

5.3.1 Introduction

At the commencement of this work, some measurements were made with a glass test cell, constructed by Buttle (1969), containing a thin film aluminium cathode deposited on the inside of a quartz window and a stainless steel anode. It was decided to modify

5.3.1

this cell by introducing a grid electrode between the photoemitter and the anode to test the feasability of grid control of emission. Following further measurements a new cell was designed, which contained two grids and this was used for the remainder of the experimental work.

5.3.2 The modified Buttle-cell

The cell, as used by Buttle, consisted of two sections, the photo-cathode assembly, and the remainder of the cell which contained the anode and a pyrex-metal-pyrex graded seal which served as a guard ring. The sections were joined by a cone and socket joint, so the upper section, shown in figure 5.13a, could be removed to refresh the photo-cathode. During the modification, it was found necessary to lower the anode so as to position the stainless steel grid below the pyrex-metal-pyrex seal, in order that the tungsten connections could be sealed into the pyrex glass, see figure 5.13b. The new grid-anode spacing was made equal to the old cathode-anode gap of 1.2 cm.

5.3.3 Factors influencing the design of a tetrode test cell

Before considering the actual design, it is advisable to look at the materials which can be used in contact with hexane without significantly affecting its purity. P.t.f.e. has exceptional chemical resistance, there are no known solvents, and it is attacked at room temperature only by molten alkali metals and fluorine (Brydson, 1969). Its resistivity is greater than 10^{18} Ω cm, the breakdown strength is about 200 kV cm^{-1}, and the relative permittivity up to 1 MHz is 2.1. P.t.f.e. is not transparent however, so to observe the level and any movement of the liquid it was necessary that at least part of the walls of the cell should

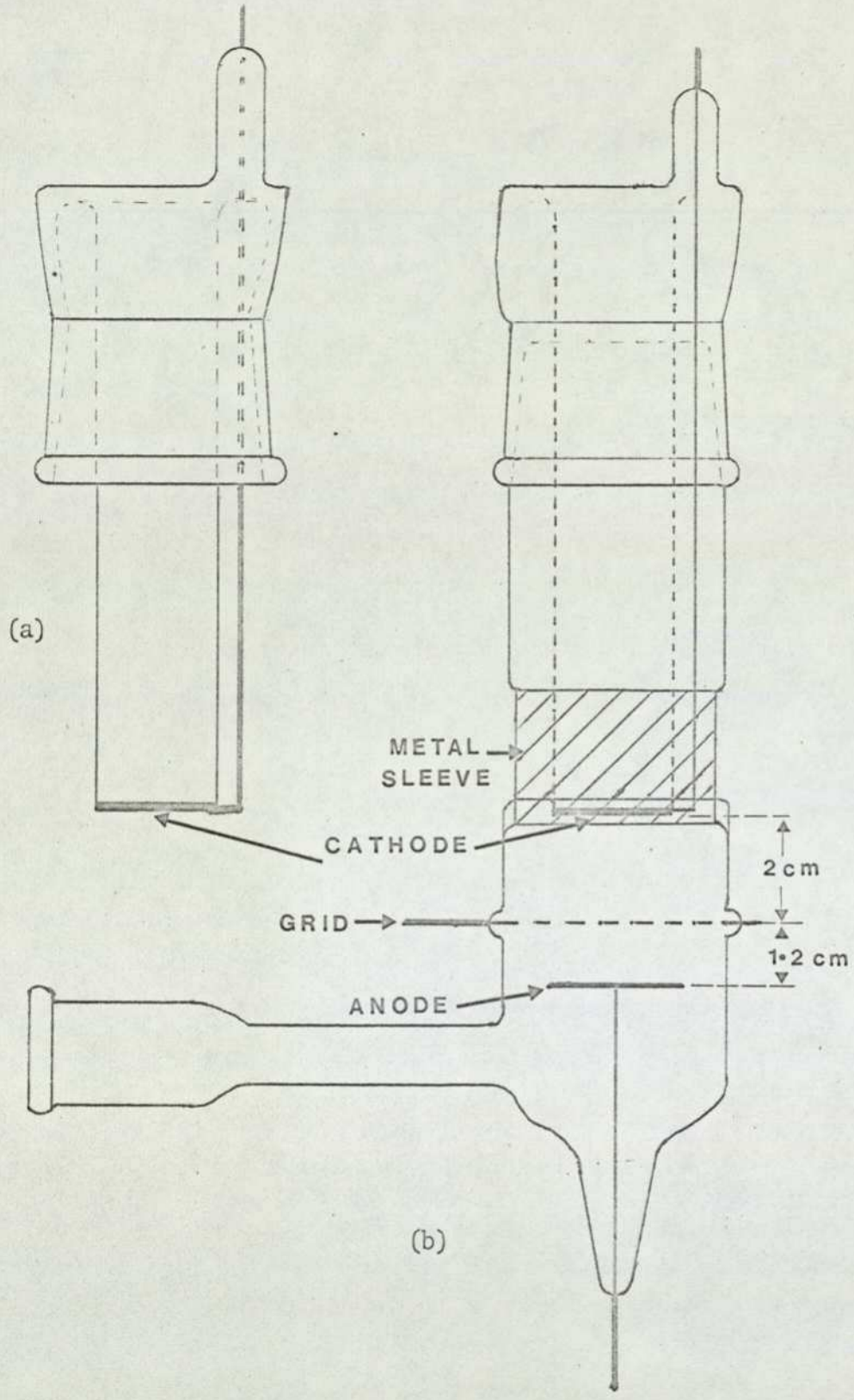


Figure 5.13 The modified Buttle-cell showing (a) upper section including photo-cathode, (b) the complete cell.

5.3.3

be of glass. Good quality stainless steel is one of the most inert metals and was used within the test cell except for the fine mesh of the grids, where the only suitable material available was nickel, electroplated onto a copper deposition.

The main requirements of the cell were that it should have four electrodes with facilities for altering the spacing between them and a provision for passing a beam of light through the drift-field gap. It was decided that 'back-illumination' photo-emission was the method of charge enhancement most suitable for this work and that the photo-cathode should be readily replaceable. It was also decided initially to fit the cell into a simple distillation system used by Buttle (1969), into which the purified hexane would be introduced under vacuum from a closed flask. Later this method was discarded, see chapter 6, and the cell was filled directly from the purification and distillation system described in section 5.2.

5.3.4 Design of the tetrode cell

The complete test cell, shown in cross-section in fig. 5.14, has an upper and a lower section of p.t.f.e. on which are mounted the electrode assemblies, separated by a pyrex-glass mid-section which forms the walls of the cell. This glass-section was formed from two, FG50, flat flange joints with the faces of the two flanges parallel. The lower face of the upper p.t.f.e. section and the upper face of the lower p.t.f.e. section were fitted with concentric 'O' rings to form a vacuum seal with the glass flanges when the whole assembly was clamped together by the 0 b.a. nuts and studs and the bakelite plates.

The upper electrode assembly contains a quartz disc on the lower face of which is deposited a thin-film aluminium photo-cathode,

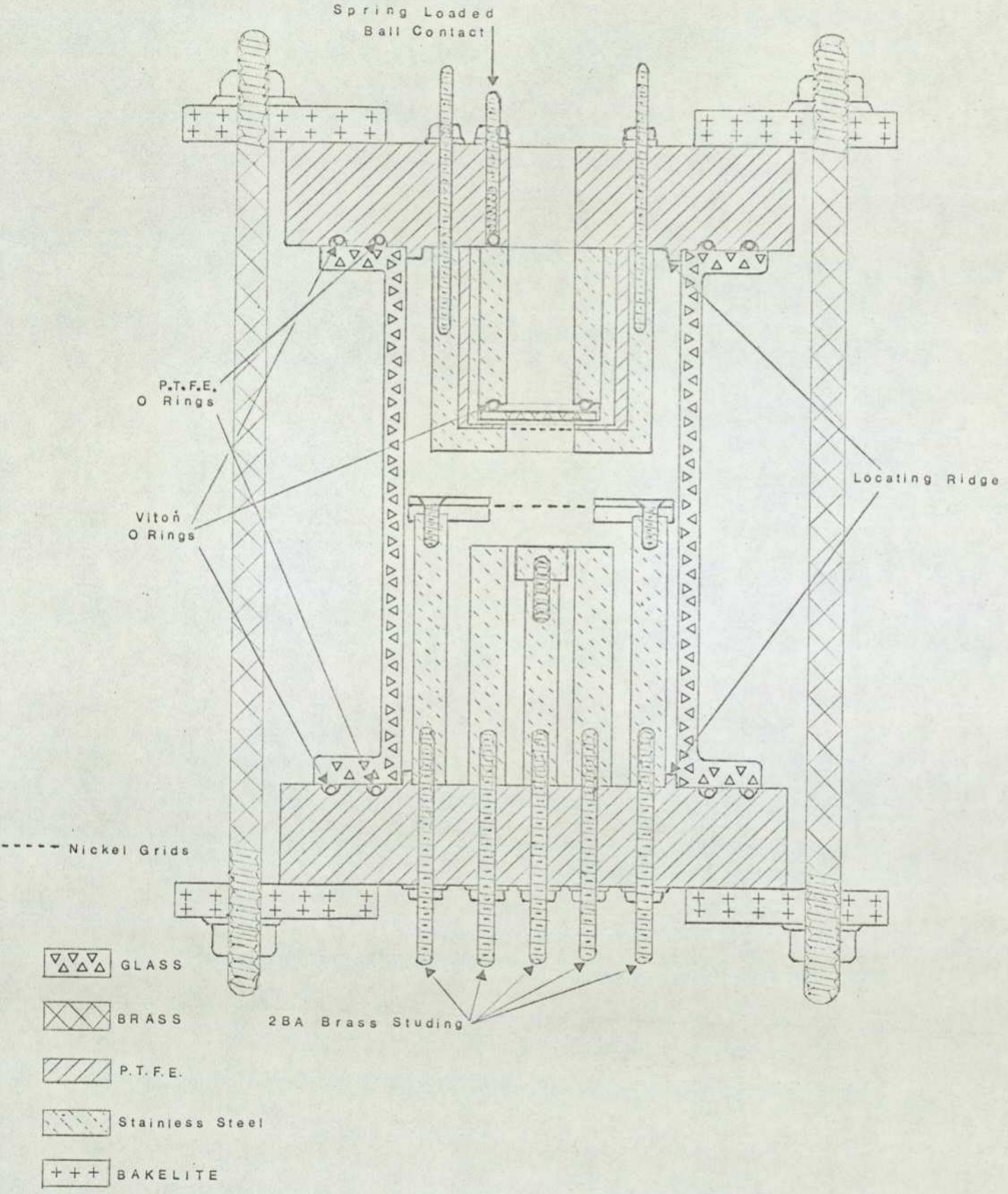


Figure 5.14 Cross-section of Tetrode Test cell.

5.3.4

see section 5.3.5. This is held in contact with the lip of a stainless steel cylinder by an 'O' ring, which also provides a vacuum seal and a second inner concentric cylinder, through which the u.v. light passes. The first grid, or control grid, is clamped in an outer concentric cylinder insulated from the others by a thin layer of p.t.f.e. This outer cylinder had a knife-edge machined at the top on its outer edge so that a vacuum seal was formed as it was pulled into the upper section of p.t.f.e. when the nuts on the studs were tightened.

On the lower section of p.t.f.e. is the second or field grid clamped in a stainless steel ring which is mounted on four pillars and a cylindrical guard ring surrounding the disc anode, of 1 cm^2 cross-section, mounted on a pillar. All these stainless steel components had machined knife-edges in contact with the p.t.f.e. to provide vacuum seals. The liquid could be introduced to and drained from the cell through a p.t.f.e. plug which could be clamped on to base of the lower p.t.f.e. section and which fitted into standard glassware.

The glass section, see figure 5.15 was fitted with a valve-controlled outlet to evacuate the cell and a pair of pyrex flats for schlieren observations.

5.3.5 Preparation of the photocathodes

Thin film aluminium photocathodes were found to give the most reliable emission characteristics and were used for this work. The quartz discs were cleaned and washed with deionized water then carefully dried before being fitted into a stainless steel substrate holder, which could accommodate four discs. The holder had a masking device which allowed a thicker outer ring of aluminium or

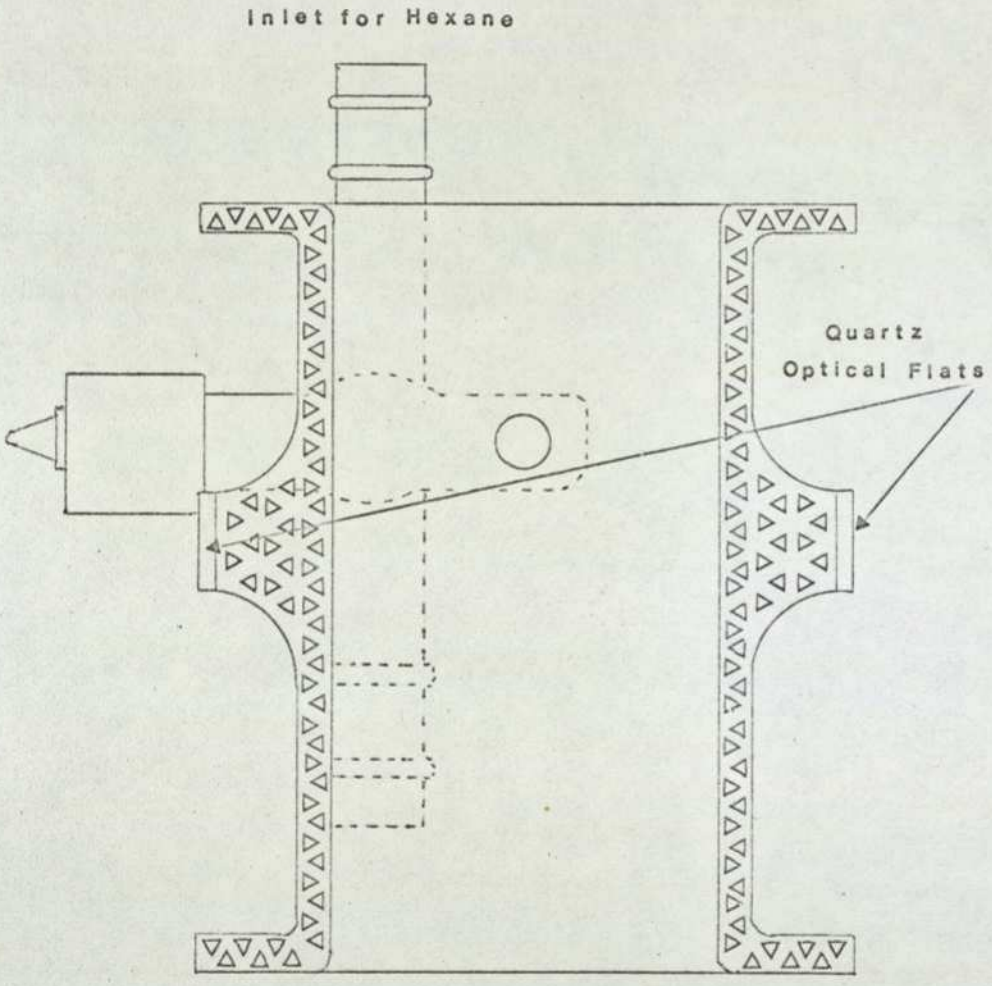


Figure 5.15 Glass-section of test cell showing schlieren windows and hexane inlet.

5.3.5

chromium to be deposited, to provide a stable electrical contact with the stainless steel cathode assembly in the cell. The second deposition, of approximately 150 A^{o} of aluminium, was made over the whole disc area. After cooling the discs were removed from the vacuum deposition plant and stored under vacuum to reduce oxidation until they could be fitted to the cell.

5.4 The stimulation and measurement of current transients

5.4.1 Introduction

An injection of negative charge carriers from the photo-cathode into the drift field gap gives rise to a current transient. This charge injection, which could be of step or pulse form, can be controlled by either mechanical shuttering of the UV light or 'electronic' shuttering i.e. changing the potential of the control grid, see figure 5.16. If mechanical shuttering of the irradiation is used then the control grid must be held about 20 V positive with respect to the photocathode, or alternatively, removed from the cell. For electronic shuttering, the photocathode is continuously irradiated and the control grid is held about 1 V negative with reference to the cathode in the 'cut-off' state. To inject negative charge carriers through the control grid, its potential must be made positive with reference to the cathode. The static tetrode characteristics of the cell are shown in section 10.2 (Hewish and Brignell, [1] 1972).

5.4.1

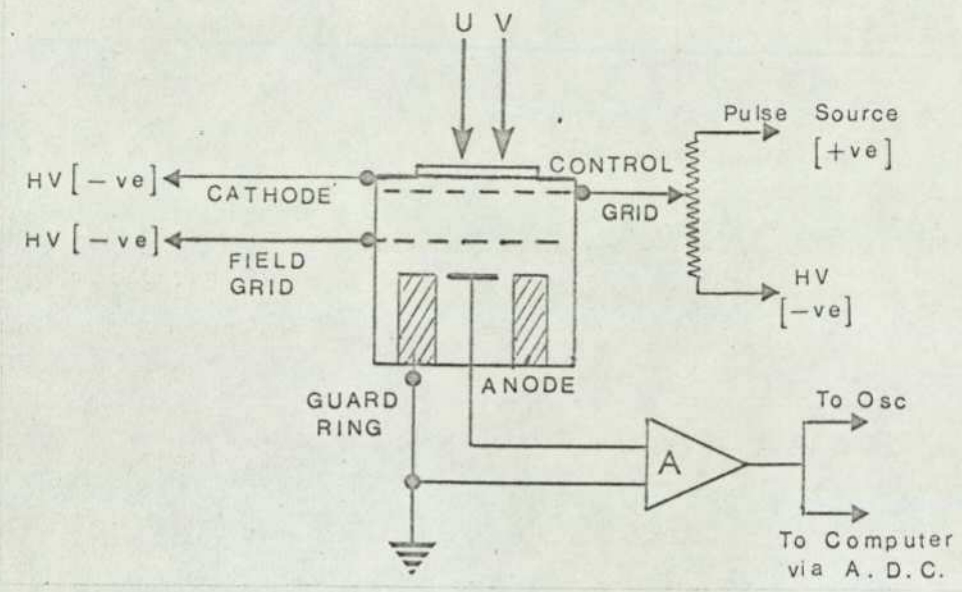


Figure 5.16 Diagram showing the electrical connections to the test cell.

The current transient only begins when the injected charge arrives at the field grid, thus there will be a delay between the shuttering stimulus and the start of the transient equal to the time taken for the charge to traverse the inter-grid space. This time-delay will depend upon several factors, some of which can be controlled by the experimentalist, e.g. the inter-grid electric field. It was considered advantageous, to enable results to be compared, for the time-scale of the transients to be directly related to the time of application of the stimulus.

A major part of this work was concerned with processing current transients in an on-line digital computer and the circuits described in the next section incorporate facilities for sampling the transients. This was done by an analogue to digital converter connected online to the digital computer which enabled sampling to

5.4.1

be completely computer-controlled, as in the cross-correlation experiments, or partly computer-controlled, with the final decision to take samples controlled by the potential or logic state of an EXT. SAMPLE line. Figure 5.17 illustrates the external control of the sampling process and the states of the two relevant control lines. Negative logic is employed, so + 4.5 V ≡ logic '0' and 0V ≡ '1'. Sampling can only occur while the EXT SAMPLE line is at logic '1', and during this time a sample is taken and transferred to the computer each time the EXT CONVERT line changes from logic '0' to '1'. For correct operation the voltage being sampled must lie between - 10 and + 10 V and the maximum rate of sampling must not exceed 35,000 samples/second. The number of samples of each transient which are required and the number of transients or blocks of samples to be recorded are part of the data supplied by the experimenter to the computer before each set of measurements. A simple calculation ensures that the EXT SAMPLE line is held in the logic '1' state long enough for the stated number of samples per transient to be transferred to the computer.

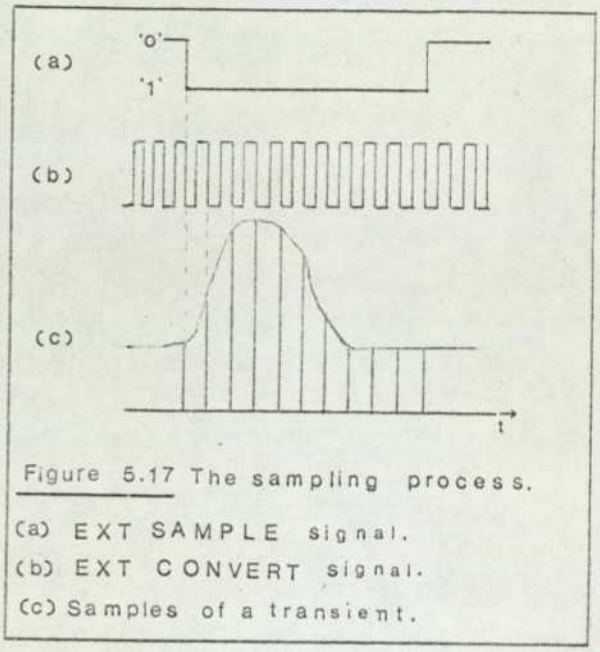


Figure 5.17 The sampling process.
(a) EXT SAMPLE signal.
(b) EXT CONVERT signal.
(c) Samples of a transient.

5.4.2 Circuits for the stimulation of current transients

5.4.2.1 Circuit A. For use with mechanical shuttering of u.v. irradiation (step stimulus)

In this case the opening of the mechanical shutter is detected by radiation falling on the OCP71 photo-transistor, in figure 5.18, which in turn causes its collector potential to rise. The next EXT CONVERT pulse changes the state of the JK bistable and of the EXT sample line which allows sampling to commence. The worst-case time variation between stimulus and sampling is one clock-pulse period, which typically, would be 10 mS. Sampling ceases when the shutter is closed.

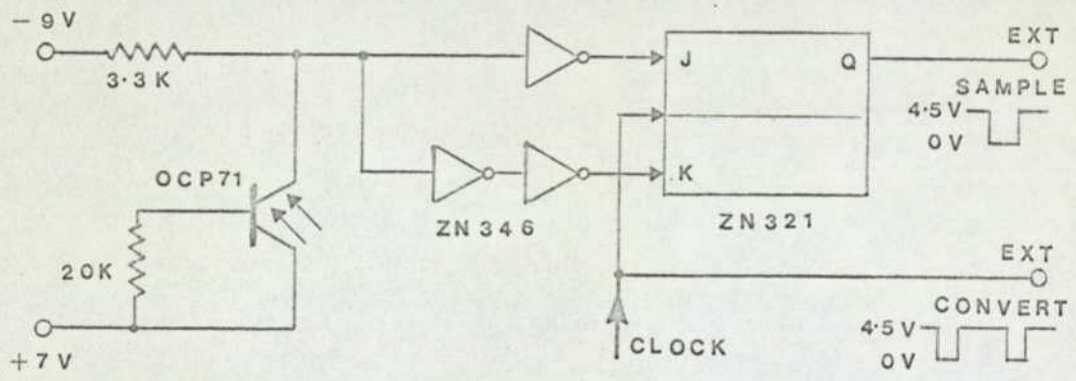


Figure 5·18 Sampling Control Circuit : Mechanical Shuttering.

5.4.2.2 Circuit B. For electronic shuttering and a step stimulus

The sequence of operations is initiated by moving the switch to position A, in figure 5.19, which causes the JK bistable to be set by the next EXT CONVERT pulse, thus changing the state of the EXT SAMPLE line and allowing sampling to commence. The change in potential of the EXT SAMPLE is amplified and inverted and fed to the control grid high resistance potential divider as a positive voltage step. The sampling and the voltage steps are terminated by returning the switch to position B. In this circuit there is no time variation, for successive transients, between the application of the

5.4.2.2

voltage step to the grid and the first sample of a transient.

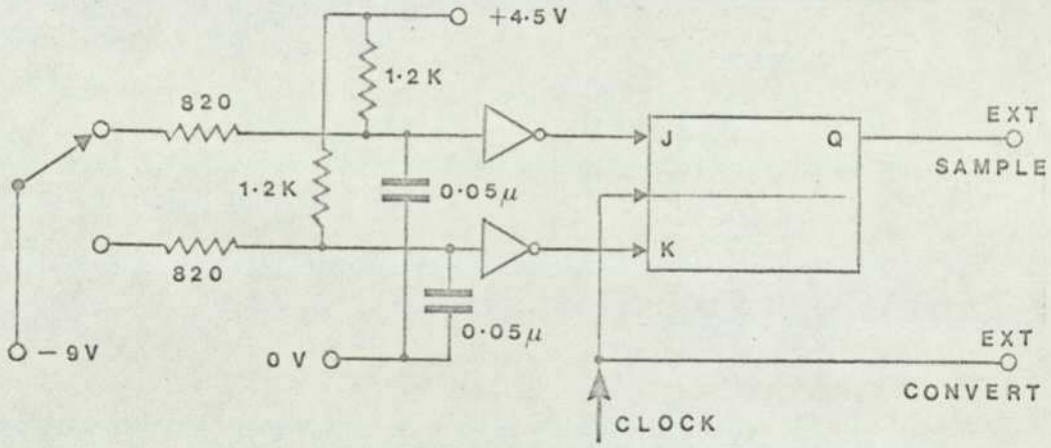


Figure 5·19 Sampling Control Circuit: Step Grid Stimulus.

5.4.2.3 Circuit C. For electronic shuttering and pulse stimulus

This circuit differs from A and B in that successive applications of the pulse stimulus, the sampling of a specified number of transient responses, and the transfer of the samples to the computer are completely automatic, once the process has been set in operation by a command to the computer. Referring to figure 5.20, a 'divide-by-2^N' counter, formed from three 'divide-by-16' digital integrated circuits in cascade, counts the EXT CONVERT pulses and gives an output which is used as the EXT SAMPLE signal. This output also triggers a pulse generator, the output pulse of which is amplified and inverted and applied through the resistor chain to the control grid. There is access to each 'divide-by-2' stage of the counter, thus N can range from one to twelve. In a typical experiment N may equal eleven in which case the frequency of the EXT CONVERT pulses would be 2048 times that of the EXT SAMPLE signal and the pulse stimulus. This means that for 1024 pulses the EXT SAMPLE signal would be in the logic '1' state and for the next 1024 pulses, in the logic '0' state. Thus

5.4.2.3

not more than 1024 samples can be requested, the remaining period of time being used to allow the current to resume a quiescent state before the automatic application of the next stimulus.

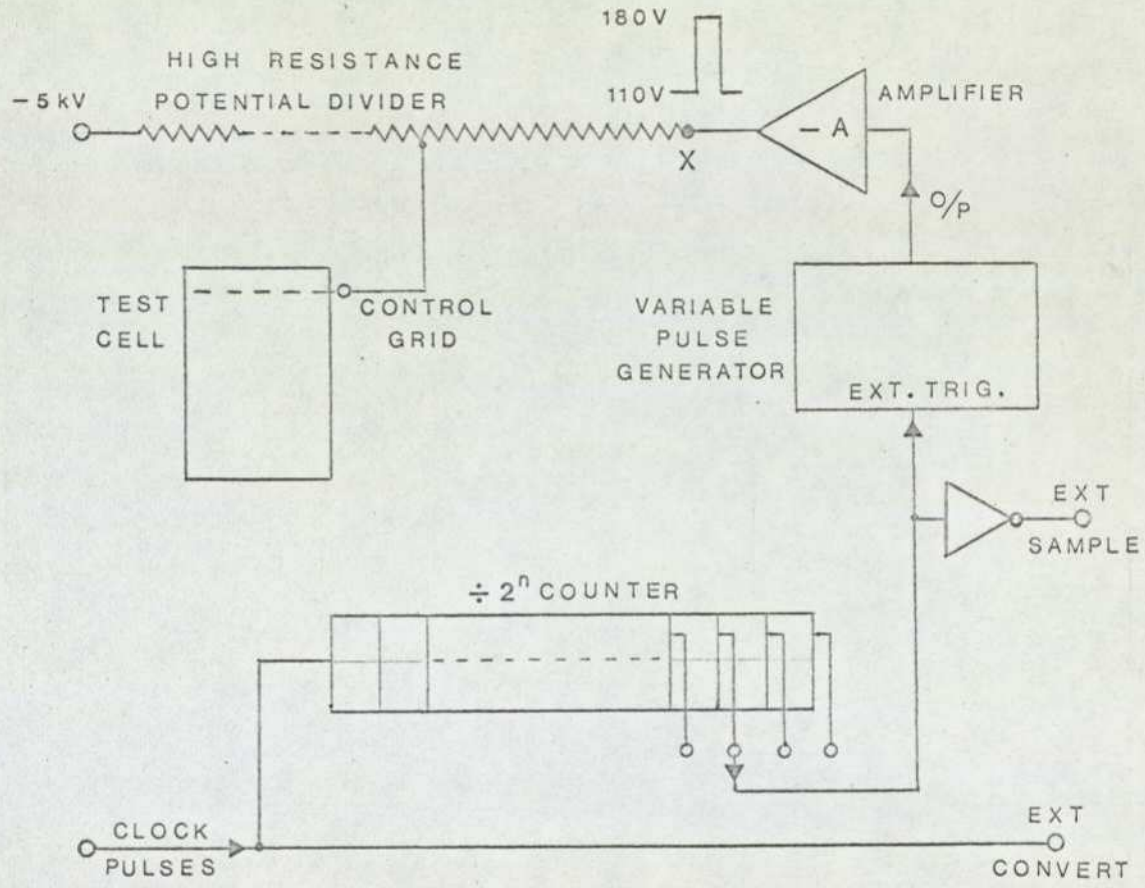


Figure.5.20. Circuit for producing pulse stimuli and control of cumulative average process.

5.4.2.4 Circuit D. Electronic shuttering with a p.r.b.s. signal as the stimulus

With this circuit, see figure 5.21, the psuedo-random binary sequence generator, see section 4.3.3, is driven by the EXT CONVERT pulses. The p.r.b.s. signal is amplified and fed via the resistor chain to the control grid as the stimulus. After the stimulus has been applied for a time equivalent to several sequences, the

5.4.2.4

commencement of sampling is initiated by a command from the computer and with each sample the corresponding state of the p.r.b.s. signal is transferred to the computer. Sampling ceases when the specified number of samples equal to the sequence length, have been transferred, and a program, see sections 4.3.3 and 10.5.3, derives the impulse response of the liquid sample from the transferred data.

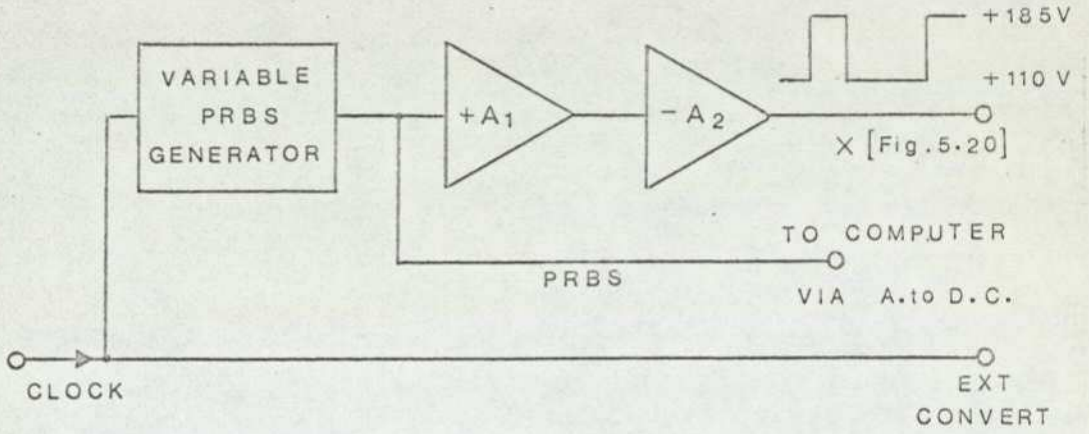


Figure. 5.21. PRBS stimulus generation and control circuit.

5.4.3 Current measuring apparatus

Some preliminary measurements were made with the apparatus used by Buttle (1969) which contained an Analog Devices Type 301 amplifier with a nominal 7 Hz bandwidth. This was considered too slow for the proposed measurements so a new current measuring circuit was designed, due consideration being given to the factors discussed in section 5.1.4. A COMTEC type MF1-2B solid-state electrometer amplifier, with a d.c. open loop gain of 10^5 and a unity gain transition frequency of 1 MHz, was selected for this circuit. The amplifier has a fully protected dual MOSFET input with an impedance of 10^{14} ohm and an input bias current of 10^{-14} A. The amplifier is fully encapsulated, has overall dimensions of 32 x 32 x 15 mm, and is mounted in a p.t.f.e. insulated base fitted

5.4.3

with a screening can. Figure 5.22 shows the final circuit for measuring currents up to 10 pA, i.e. with the feedback resistor R_1 equal to 10^{12} Ω. Since the effective capacitance in parallel with R_1 is unknown and distributed along the resistor, the values of the components of the compensating network R_3C_3 were first set at 1 MΩ and 0.23 μF (after Presley, 1966). However, when the circuit was tested by coupling a triangular wave voltage generator to the input through a small capacitor (after Praglin and Nichols, 1960) it was found necessary to reduce C_3 to 0.1 μF to obtain a satisfactory 'square' waveform at the output. This wave form had a rise time of 10 mS. If R_1 is changed to 10^{11} Ω, to measure currents up to 100 pA, then R_3 must be reduced to 0.1 MΩ and the rise time falls to about 1 mS. As indicated by the dotted line in figure 5.22, the

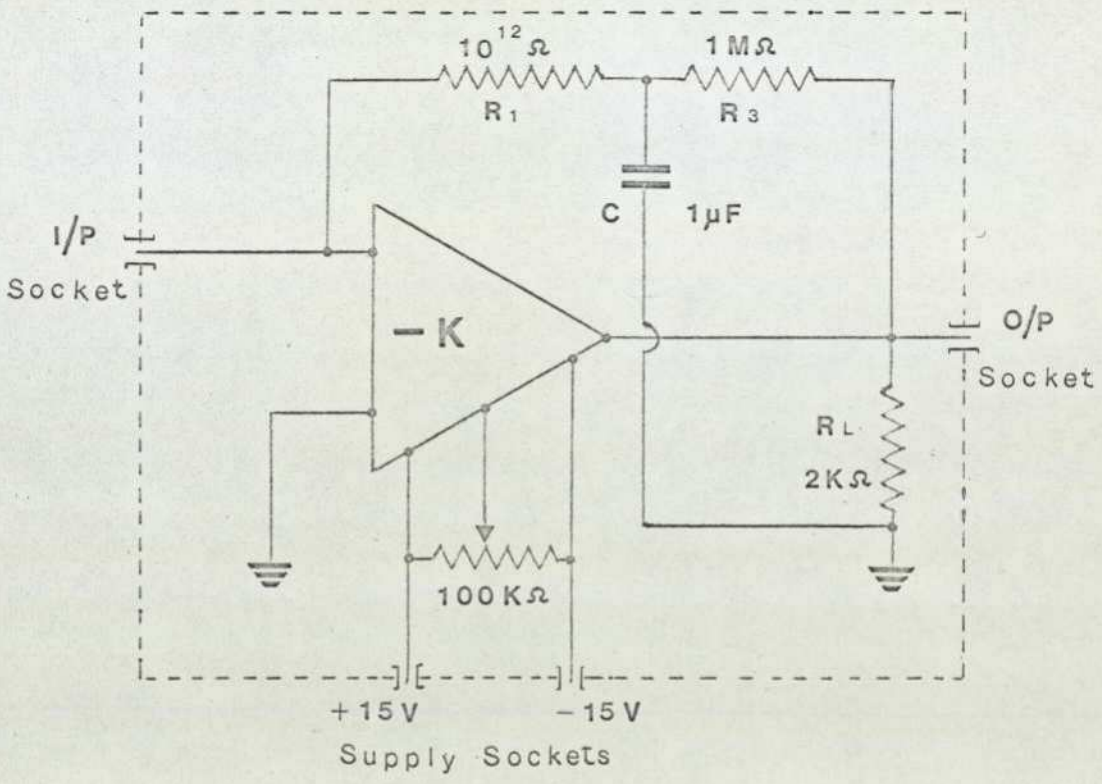


Figure 5.22 Circuit of pico-ammeter (for currents < 10 pA).

5.4.3

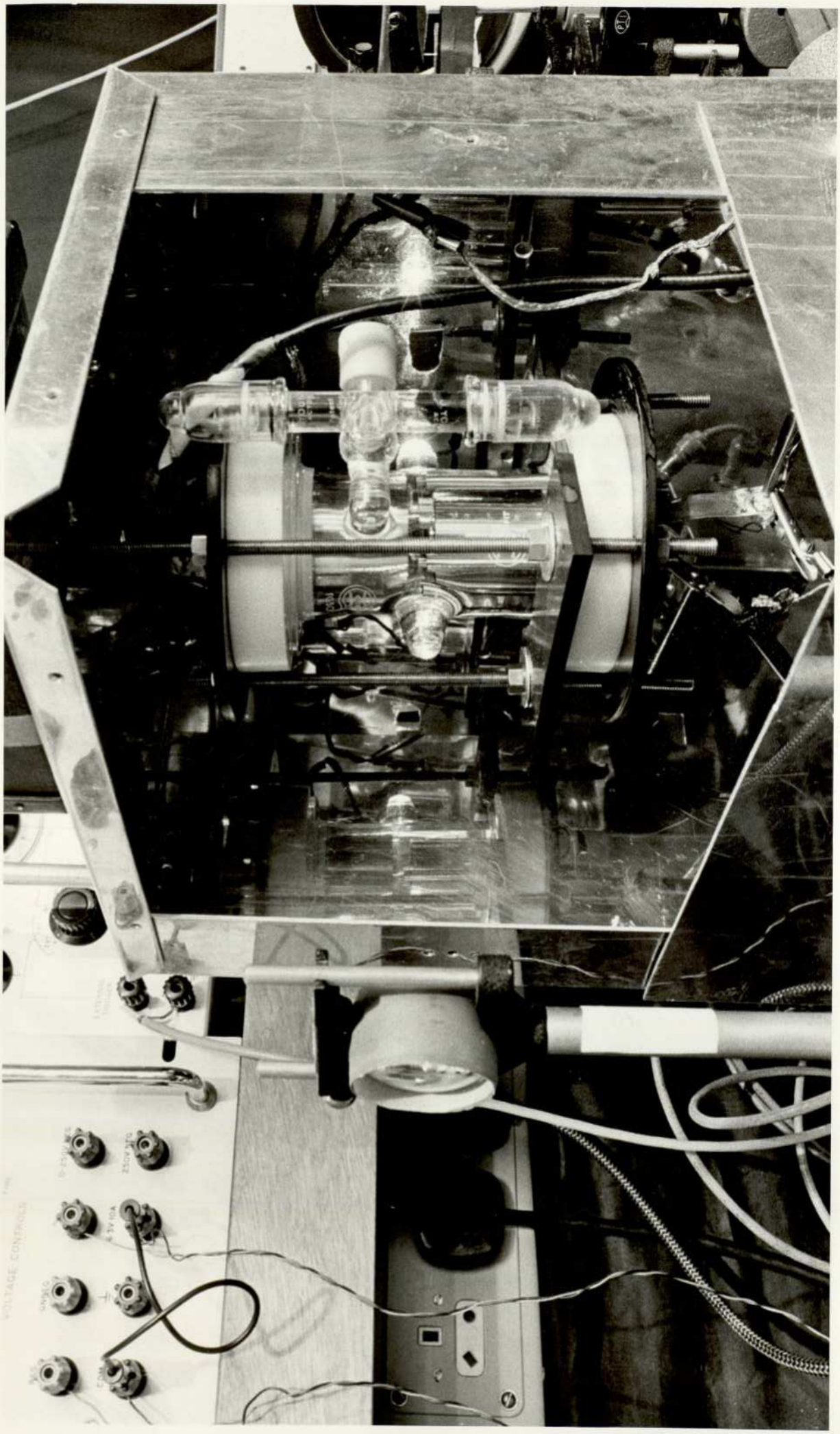
components were mounted in a small aluminium screening box which could be positioned close to the test cell, so that only a short screened cable was necessary to interconnect the input socket to the anode. The + 15 V and - 15 V supplies were fed into the amplifier through screened leads and sockets from the power supply designed and built by Buttle (1969). These supplies were virtually free of hum and were not a significant source of the noise in the amplifier output. The output was fed through a screened coaxial cable to the analogue to digital converter for sampling and to a storage oscilloscope. As both these devices had a high input impedance and the COMTEC amplifier is designed for a load of 2 KΩ, a resistor R_L of this value was included in the amplifier. Figure 5.23 shows the test cell with the grids removed during some schlieren observations. The upper section of the test cell enclosure has been removed for the photograph and the aluminium box containing the pico-ammeter can be seen in position below the test cell.

5.5 Apparatus for observing and recording liquid motion

5.5.1 Introduction

In section 5.15 the various methods available for observing liquid motion were examined. For this work it was decided that a low power laser schlieren system would give the best results; although at one stage a conventional light source using a projector bulb and condensor lenses was substituted to see if better results could be obtained. In fact this was not the case, and all the recorded observations were made with the laser system. The sensitivity of the human eye has definite limitations particularly in the observation of small disturbances on a poorly illuminated

Figure 5.23 The test cell



5.5.1

screen. To eliminate human frailty, in this respect at least, a light-sensitive amplifier was developed to detect very small disturbances of the schlieren image; this is described in section 5.5.3

5.5.2 The schlieren system

The experimental schlieren system, shown in figure 5.24 is mounted on optical benches positioned on opposite sides of the test cell enclosure. The light from the source S is focussed on to the knife edge E after passing through the lenses L_1, L_2 and the test

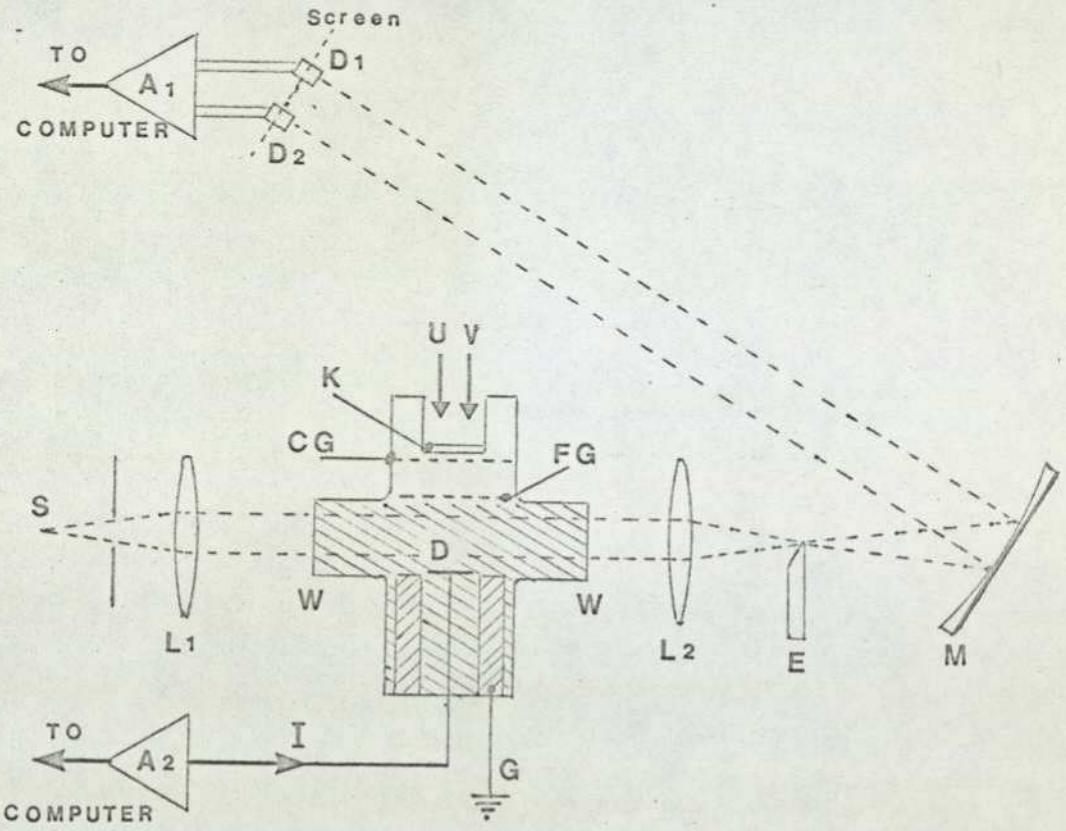


Figure 5.24 The experimental schlieren system, see text.

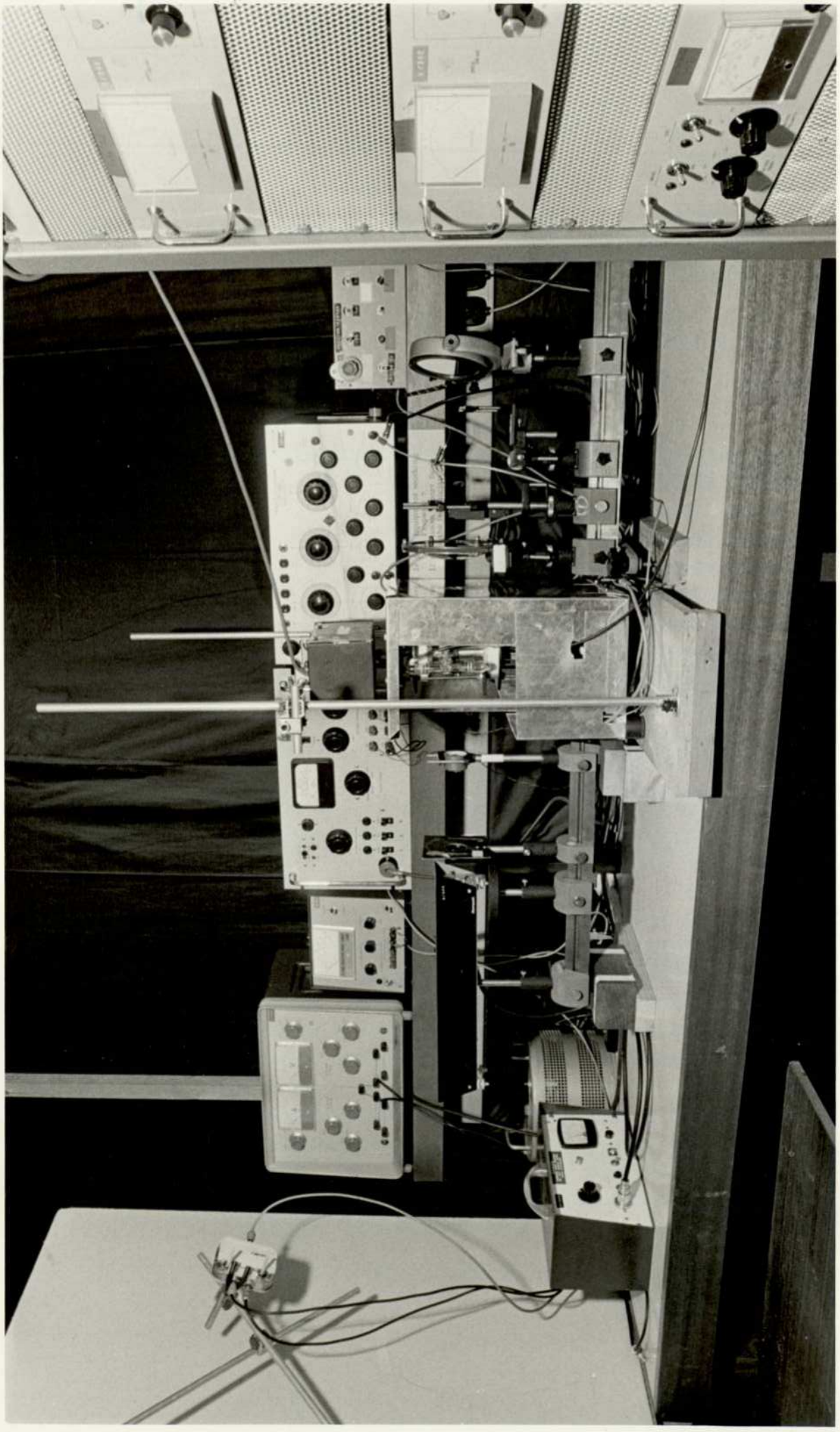
5.5.2

cell windows W. The schlieren image of a disturbance D within the test cell is focussed on a plane containing the light sensitive diodes D_1 and D_2. With the laser as the light source the stop T was closed to a pinhole and a focus of this was formed on the knife edge. In the photograph of figure 5.25 the laser is on the left and above it is the light sensitive amplifier supported on crossed aluminium rods in front of a screen. To the right of the test cell the schlieren mirror is visible and in the foreground are the power supplies for the u.v. deuterium lamp and the cell electrodes.

5.5.3 The light-sensitive amplifier

This was designed to respond to a change in the light falling on one pair of light-sensitive diodes positioned close to each other in the schlieren image. This differential effect will detect a schlieren disturbance but should produce no output if a change in overall intensity occurred, e.g. as a result of a change in the light output of the source. As the diodes used were not matched, some output would occur in the later case but it would be less than that from a disturbance in the cell. The circuit, shown in figure 5.26, has a high gain amplifier with FET inputs giving a very high input impedance operating as a differential amplifier. The potentials of the amplifier inputs can be balanced using the coarse and fine potentiometers for the existing light intensities falling on the diodes. Any differential disturbance of these intensities appears as a change in the amplifier output voltage which is sampled and fed to the computer with the current transient.

Figure 5.25 Schlieren apparatus



5.5.3

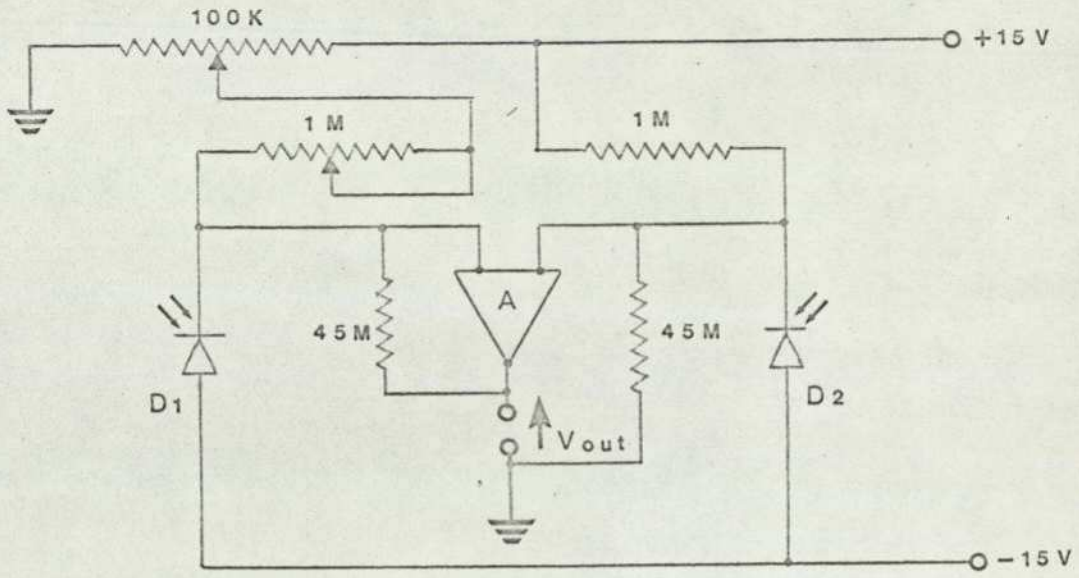


Figure. 5.26. Circuit of light sensitive amplifier.

5.6 Use of the on-line computer

The measurement problem, which is discussed in detail in Chapter 3, is typical of one which benefits from the introduction of an on-line computer (Brignell and Rhodes, 1975). The problem exhibits such complications as low amplitude signals, a low signal to noise ratio, non-stationarity, non-linearity, etc.

The on-line computer which was chosen for this work is a Ferranti FM1600B. Although it was designed with military applications in mind it has many features which make it suitable for use in the laboratory (Rhodes, 1971), e.g. up to 22 peripherals can be linked to the computer and serviced on a priority basis. The FIXPAC computer language is peculiar to this machine and can incorporate three addresses in one instruction which makes it more powerful than most small computer languages. Programs were developed for this work by the author, to operate the following computer peripherals; the analogue to digital converter, the digital incremental plotter and the visual display unit. In

5.6

figure 5.27, the current signal from the test cell is amplified, fed as a voltage to the analogue to digital converter and transferred to the computer as a block of digitized samples for processing. With cumulative averaging the result is viewed on the visual display unit before the next transfer of samples from the converter. A copy of the result can be obtained on the digital plotter when required. In this work there was sufficient time to view the result between block transfers. If this had not been the case, there would have been a loss of information on the display but the higher priority of the converter peripheral would have ensured correct transfers and processing until the maximum sampling rate of the converter, about 35000 samples per second, was reached. A faster rate of sampling and transfer is now available with the acquisition of a transient recorder (Buffam & Brignell, 1975) and disc store.

Suites of programs have also been written to determine the theoretical limits of e.h.d. stability and perform the operations of cumulative averaging and cross correlation (see Appendix, section 10.5).

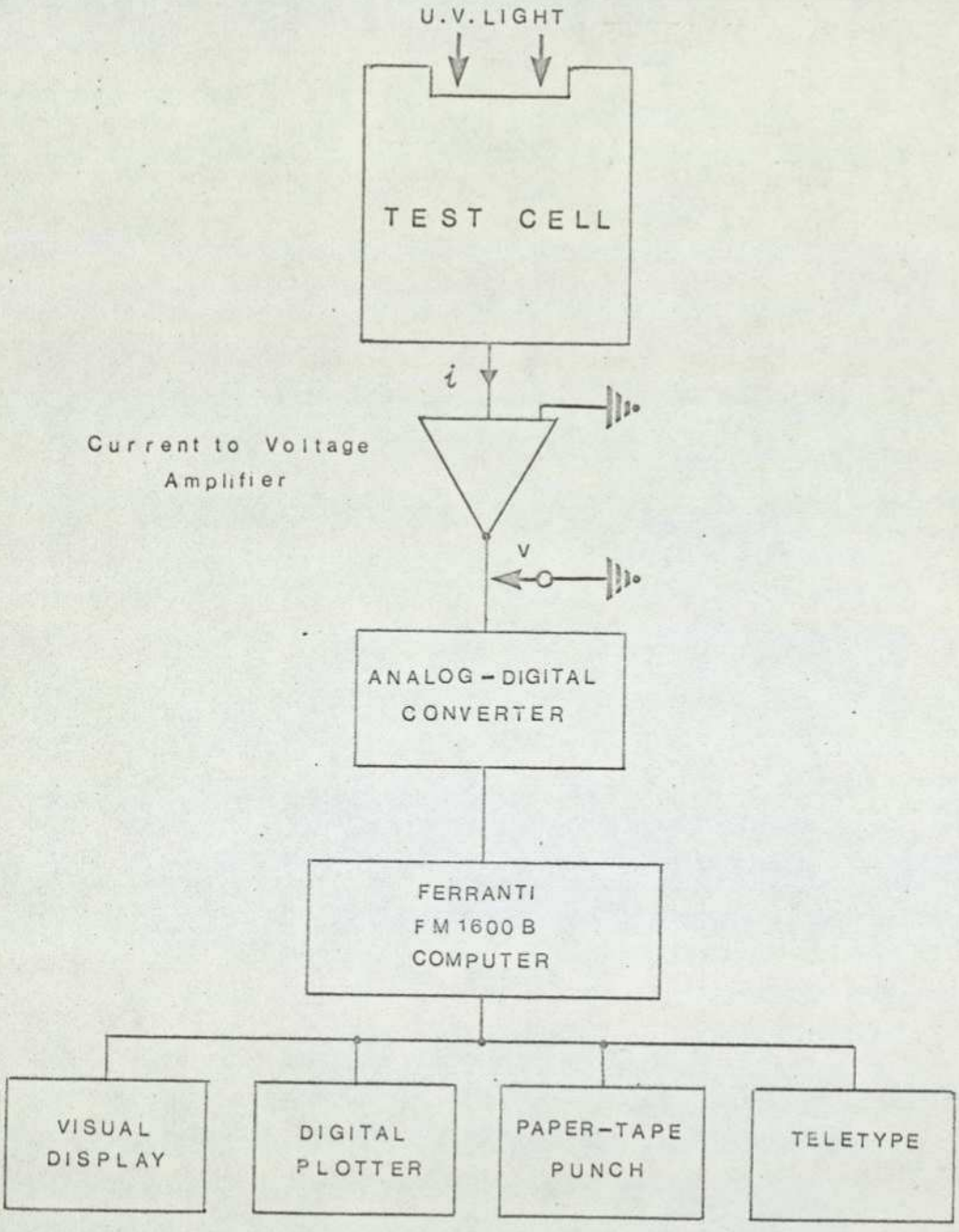


Figure 5.27 The links between the FM1600B, some of its peripheral equipment and the test cell.

Chapter 6

Experimental Results

6. Experimental Results

6.1 Preliminary

The results of the experimental work will be presented in sections which reflect the several aspects of the investigations. With the exception of section 6.2, 6.3 and 6.4, all have a common theme, i.e. the recording of current transients in the tetrode test cell and the determination of carrier mobility from time of flight measurements. In section 6.5, the results of cumulatively-averaging a number of noisy transients are presented, and this technique appears also in section 6.7 where the results of varying the configurations and potentials of the test cell electrodes are presented. Section 6.6 is devoted to a comparison between results obtained by the cross-correlation method and cumulative-averaging technique. Finally, section 6.8 contains the results of simultaneous current transient measurements and schlieren observations recorded by the light-sensitive amplifier.

6.2 The results of tests on the purity of n-hexane

6.2.1 Water Content

The water content of the n-hexane, after treatment and distillation in the apparatus described in section 5.2, was measured with a Panametrics Model 100 hygrometer. The probe was permanently sealed into a measuring cell which could be fitted to the distillation apparatus and evacuated. A quantity of the distilled hexane was then introduced under vacuum and the measurement made. The water content of freshly distilled hexane was consistently less than 1 part per million by volume, compared with 250 p.p.m. for a freshly-opened bottle of Koch-Light 99% n-hexane.

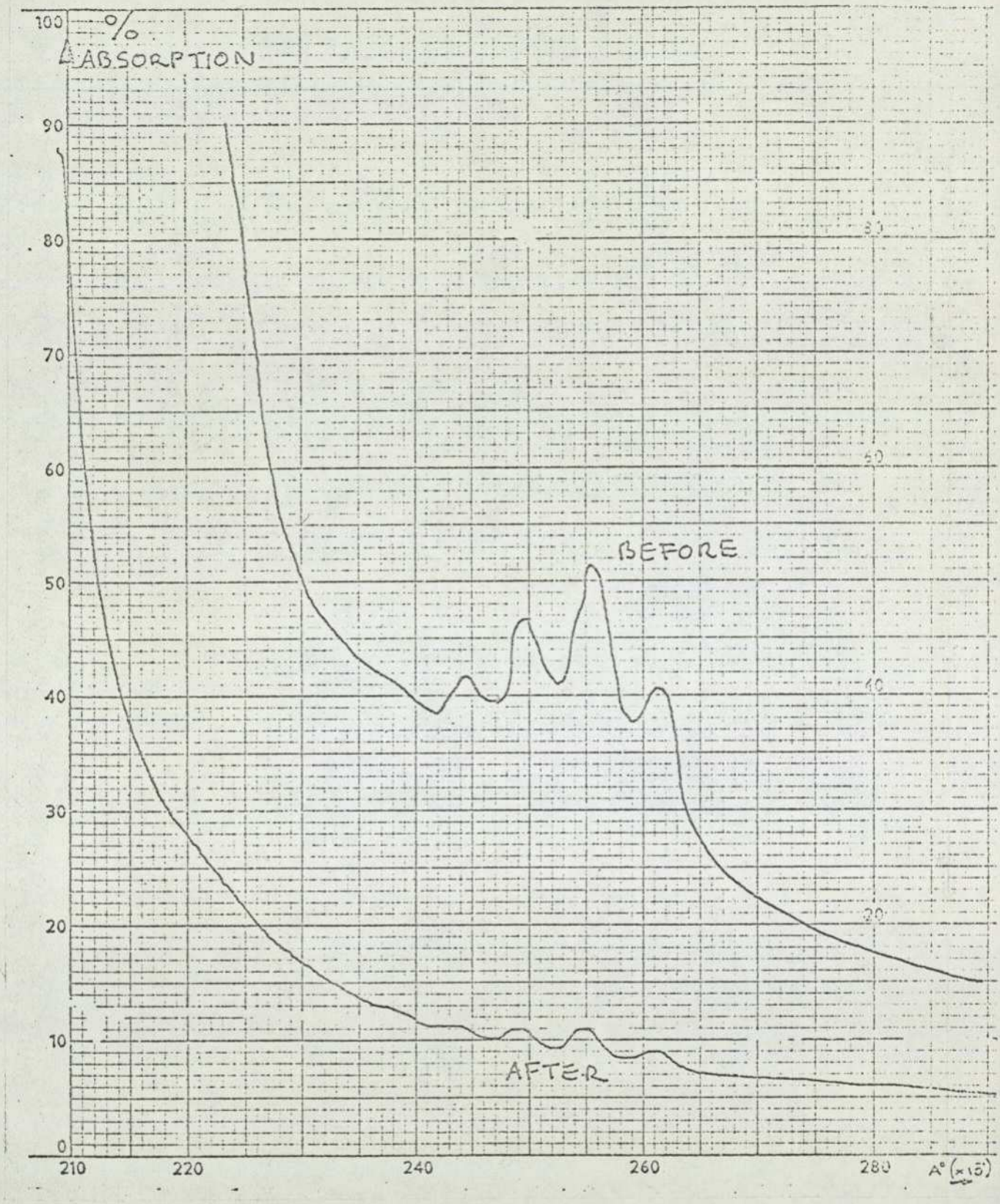


Figure 6.1 Absorption versus Wavelength for n-hexane before and after purification, see text. (After Evison).

6.2.2 Gas Liquid Chromatography

Analyses of four samples of Koch Light 99% n-hexane at various states of treatment and usage, by gas-liquid chromatography on a Pye 104 gas chromatograph were obtained. The four samples were as follows:

A. From a freshly opened bottle of n-hexane.

B. After an initial simple vacuum distillation process.

C. Treated and distilled in the apparatus described in Section 5.2

D. Treated and distilled hexane after being used for photo-injection experiments in the test cell.

The impurity that was identified in each case was a small quantity of benzene, less than 0.1% in sample A. The benzene contents of samples B and C were 45% and 10% of that of sample A respectively, and other unidentified impurities were reduced in similar proportions. In sample D, the benzene content had increased, compared with C, to 30% of that in sample A, indicating that u.v. irradiation increases the proportion of unsaturated hydrocarbons in n-hexane.

6.2.3 U.V. Spectrophotometry

The results obtained by Evison (1975), see figure 6.1, show the u.v. absorption of the liquid before and after treatment in the same purification plant, see section 5.2. Similar measurements, made by the author, using a Perkin-Elmer type 402 u.v.-visible spectrophotometer revealed the necessity of re-activating the silica gel column in this purification plant regularly. The graphs, in figure 6.2, show more absorption of u.v. after treatment than before, and this was found to be due to the state of the silica-gel column which showed considerable yellowish discolouration due to

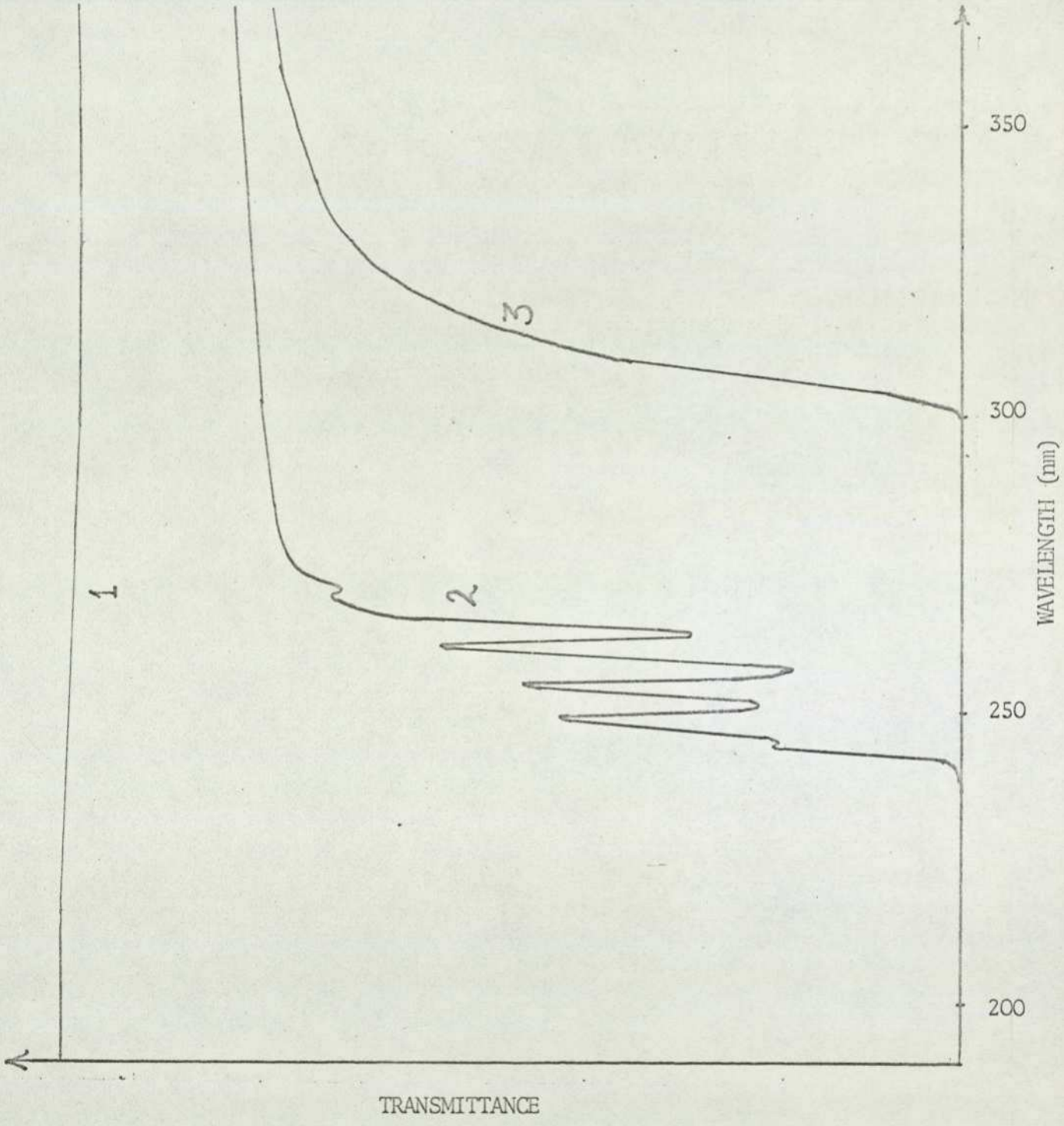


Figure 6.2 Transmittance versus Wavelength, showing the effect of deterioration in the silica gel columns of purification plant.

Trace 1: Air (reference); 2: Hexane Before Treatment;
3: Hexane after 'treatment'.

6.2.3

the presence of unsaturated hydrocarbons. This sample of poorly-treated hexane also had a poor resistivity and was totally unsuitable for photo-injection studies.

6.2.4 Resistivity measurements

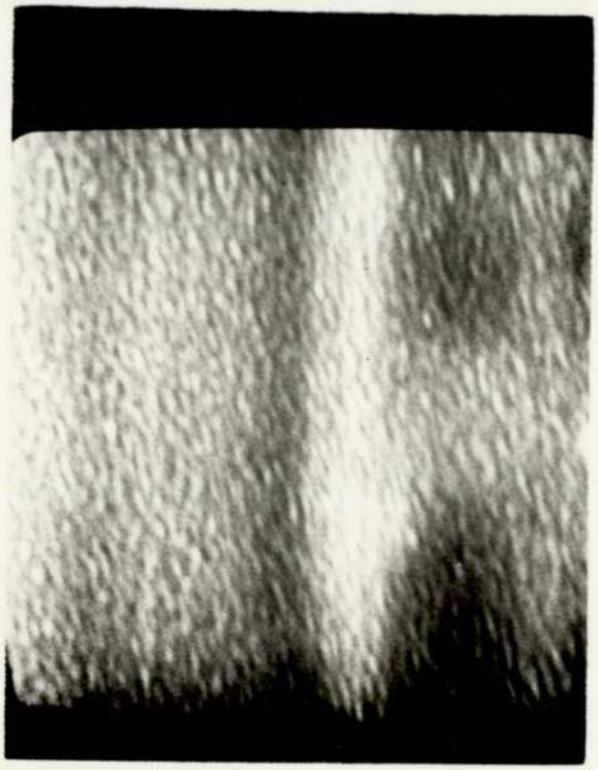
No direct method of measuring the resistivity of the samples was available in the laboratory, but it was possible to obtain an indication of the magnitude of the resistivity when the sample was in the test cell. The dimensions of the anode and the drift field gap were 1 cm^2 and 1 cm respectively for the majority of the measurements, and the resistivity was determined by measuring the change in current for a change in drift gap voltage. The sensitivity was unfortunately limited (by the maximum safe voltage which could be applied) to a maximum resistivity of about 10^{16} Ω, but this was a useful indication of the state of the liquid.

6.3 Microscopic examination of photo-emitters

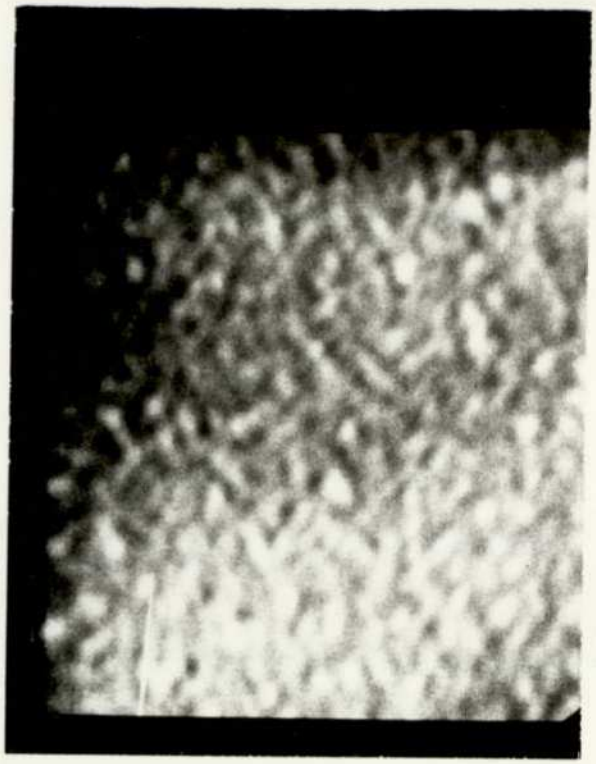
With an air/hexane-vapour gap in the test cell, the amplitude of transient currents measured under similar experimental conditions decreased to zero over a period of days. When the hexane was removed and the cell evacuated the current was much smaller than was obtained with a new photocathode in vacuum, thus it was concluded that the photocathode had deteriorated in the air-vapour atmosphere.

An examination of the surfaces of two of the photo-emitters using a scanning electron microscope was made by Dr. P.E. Secker (private communication), and the results are shown in figure 6.3.

The aluminium thin film surfaces were deposited at the same time, but B was subsequently used as a photocathode in an air/hexane -vapour atmosphere until the measured current decreased to



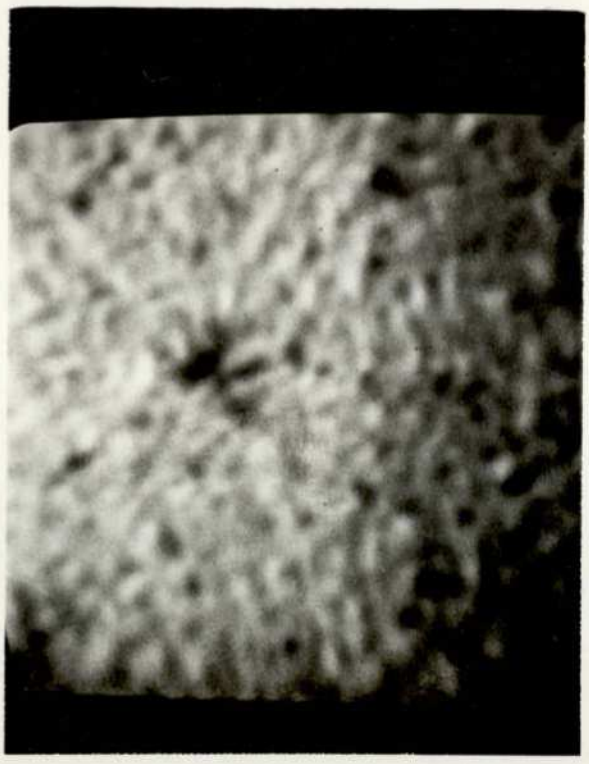
A: Magnification
x 22,000



A: Magnification
x 50,000



B: Magnification
x 22,000



B: Magnification
x 50,000

Figure 6.3. Micrographs of surfaces of new (A) and used (B) Al photo-emitters.

6.3

negligible proportions. Apart from the discontinuties there seems to be little doubt that the surface of emitter B is covered with a partially insulating layer. The workers at the University College of North Wales have found evidence of a similar phenomenon. It is thought that photo-ionization of the air-hexane vapour leads to polymerization on the emitter surface so that an insulating polymer coating forms which inhibits electron emission.

6.4 Some characteristics of the modified Buttle cell and the tetrode cell

6.4.1 The modified Buttle cell

Tests were carried out with a partial vacuum in the cell, see section 5.5.2, to examine the problems of grid-control of photo-emission. These tests showed that the grid-cathode spacing (12 mm) was too large for a satisfactory mutual conductance, since to change the anode current from zero to maximum required a 200 V increase in the grid potential. Also the current was very noisy and this was found to be due to two main causes. Firstly, the poor screening of the test cell from radiated noise particularly from the Hanovia mercury vapour lamp. This lamp also produced a fluctuating output and was replaced by a deuterium light source (Ealing Optics LPS 201) for the remainder of the work. Secondly, the electrical connection to the aluminium film of the photo-cathode was by a springy nickel 'cat's whisker' contact which had a tendency to be intermittent.

Attempts to measure transient currents, with n-hexane below and a vapour gap above the grid, were unsuccessful due to deterioration of the photo-cathode and excessive noise. A fracture of the glass around the grid occurred as the cell was being dismantled to renew the photoemitter causing irreparable damage.

6.4.1

As a decision had already been made to design and build an improved cell with an additional electrode, see section 5.3.4, the Buttle cell was not reconstructed.

6.4.2 The tetrode cell

The results of the measurements made to determine the characteristics of this cell are in section 10.2 (Hewish and Brignell,[1] 1972). An important feature of these characteristics is the approximately linear increase in anode current which occurs as the control grid potential is raised from zero to about + 20 V with reference to the cathode. Thus, when the quiescent current is just zero, the application of a positive voltage step pulse of this magnitude to the control grid, injects charge and gives rise to a current transient. This is the method of charge injection used to obtain the results in the following sections, unless another method is specifically mentioned.

6.5 Results of the cumulative-average process

The theory of the process of cumulative-averaging and the computer programs which have been developed are described in section 4.3.2. This method of reducing the noise content of current transients was used for a large number of the measurements and was particularly valuable where the peak currents were less than 1 pA, as a result of a low drift field stress or reduced emission from the photocathode.

The results of cumulatively-averaging an increasing number of transients, n, are shown in figure 6.4. Each current transient is similar in appearance to the first result (n = 1) and is the response to a second pulse of negative charge injected through the control grid (see figure 5.18). The capacitive breakthrough of

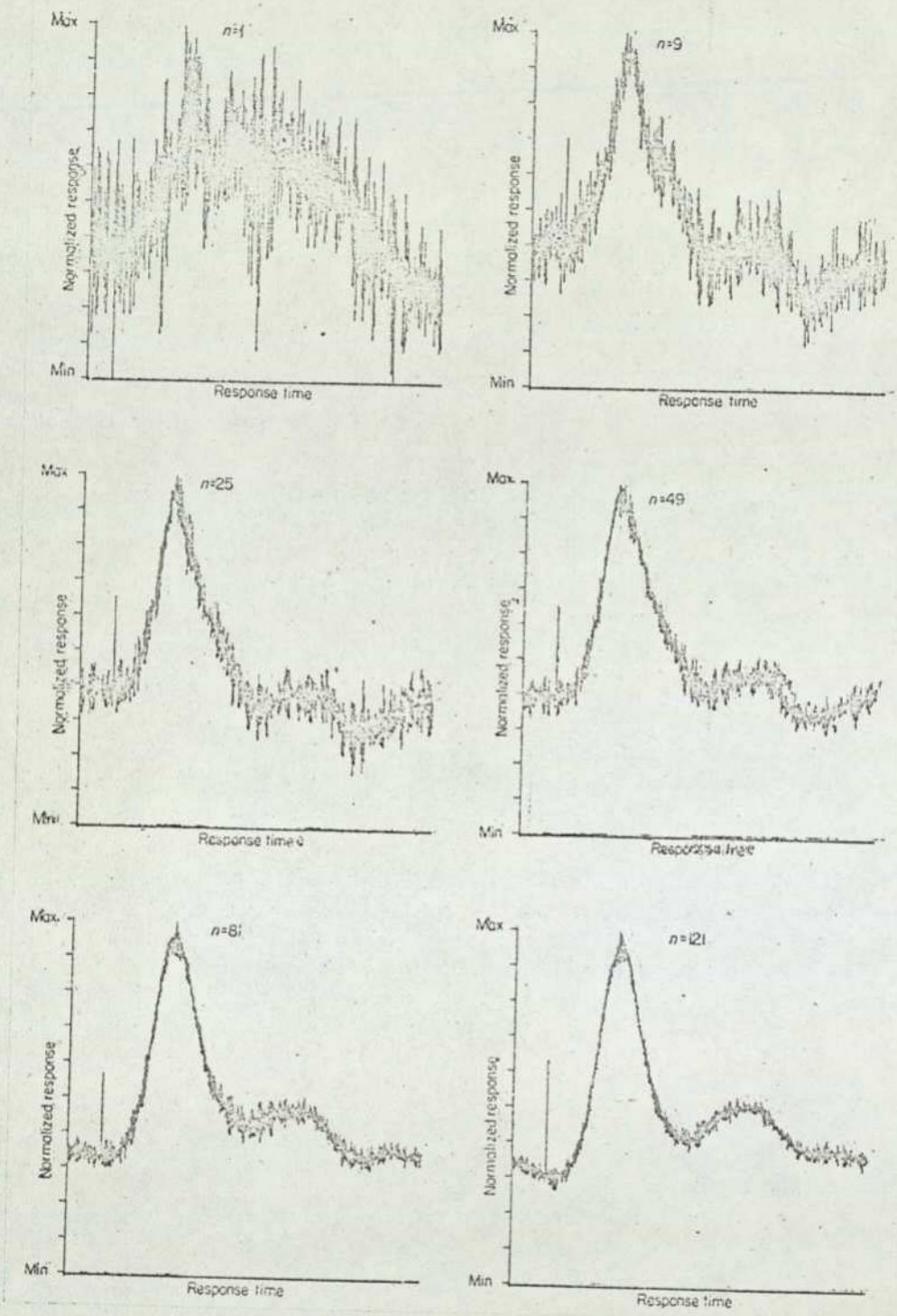


Figure 6.4 The results of cumulatively-averaging an increasing number of transients responses to identical pulse stimuli. By Hewish, from Brignell and Rhodes, 1975.

6.5

the control grid voltage pulse appears on each result as a negative spike at the origin and a positive spike after 2 seconds. The drift field stress was 500 V cm^{-1}, the response time scale is 20 seconds and the time interval between transients was 40 seconds. The two peaks which emerged during the averaging correspond to mobilities of about 10^{-7} and 3×10^{-8} m^2 V^{-1} s^{-1}.

In each result the calibration of the vertical axis is normalized to the difference between the maximum and minimum sample in the averaged result. Thus, this difference is 1.4 pA for n = 1 but it has fallen to 0.4 pA for n = 121 as a result of the averaging process. The maximum and minimum values, the number of samples per transient and the value of n are printed out with each result and successive results can be plotted to the same scale by making minor alterations to the computer program.

6.6 Results of the cross-correlation method

6.6.1 Introduction

In these results the stimulus applied to the control grid is a pseudo random binary sequence waveform, see section 4.3.5 in which the two voltage levels correspond to charge injection (logic '1') and no charge injection (logic '0'). The result of cross-correlating this binary sequence with samples of the current produced by this stimulus produces the response of the system, including the liquid, to an impulse. Section 6.5.2 compares the results obtained with air and with hexane in the cell and section 6.5.3 compares cross-correlation and cumulative-averaging under similar experimental conditions. Normalised values of the cross-correlation results are plotted on a time scale which depends on the sequence length and the clock rate.

6.6.2 Results with air and hexane in the drift gap

Figure 6.5 shows a cross-correlation result for the system with air in the test cell in place of hexane. A similar result was obtained with a partial vacuum in the cell, indicating that this curve represents the response of the system, without hexane, i.e. the cell and the current measuring circuit. Figure 6.6 shows the result with hexane in the cell to the level of the field grid and an air-vapour mixture above. The sequence length was 1023 bits and the clock rate was 100 pulses per second. The fluctuations which occur after the initial transient are thought to be due to non-linearities in the system, possibly because the 'logic 1' voltage level was set too high, causing the system to become non-linear (see section 3.4). Also, the initial pulse-shaped transient indicated a higher value of mobility than expected and this was found to be due to a small bubble of vapour trapped under the field grid which forms a high-mobility region in the drift gap. Figure 6.7 is a cumulatively-averaged result from 16 transients with a 100 ms voltage-pulse applied to the control grid forming the stimulus. The experimental conditions were in other respects identical to those for the cross-correlation result in figure 6.6 and a close similarity between the two can be observed.

6.6.3 Results with hexane only in the drift gap

The level of hexane was slightly above the field grid and no vapour bubbles were trapped in the drift gap for the results shown in figures 6.8, 6.9 and 6.10. The cross-correlation result in figure 6.8 is for an applied drift gap stress of 800 V cm^{-1} whereas the result in figure 6.7 is for a stress of 500 V cm^{-1}, but in each case the field grid-cathode p.d. was maintained at 500 V. In these results only the first 200 correlated results from a 1023 bit

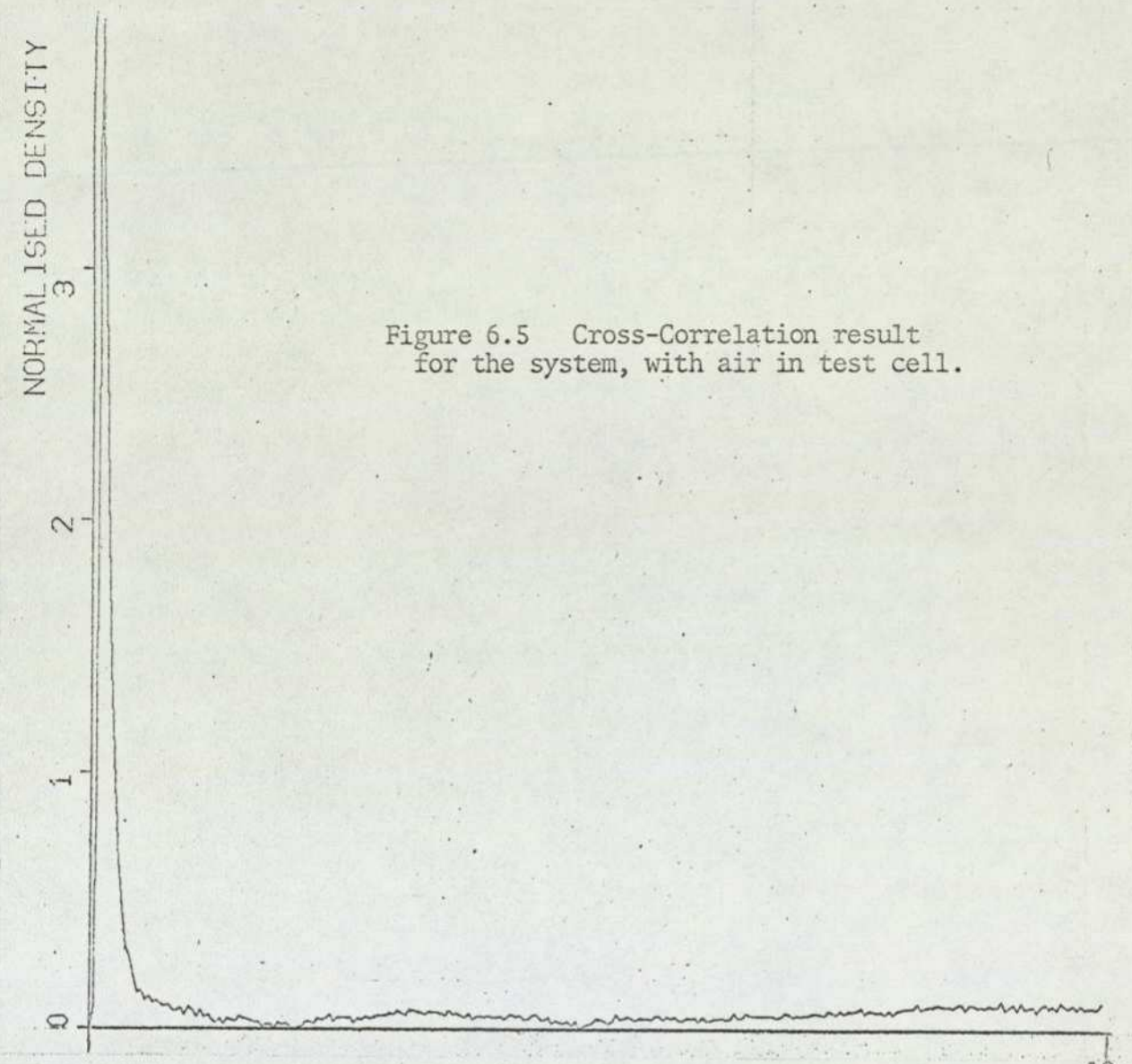


Figure 6.5 Cross-Correlation result for the system, with air in test cell.

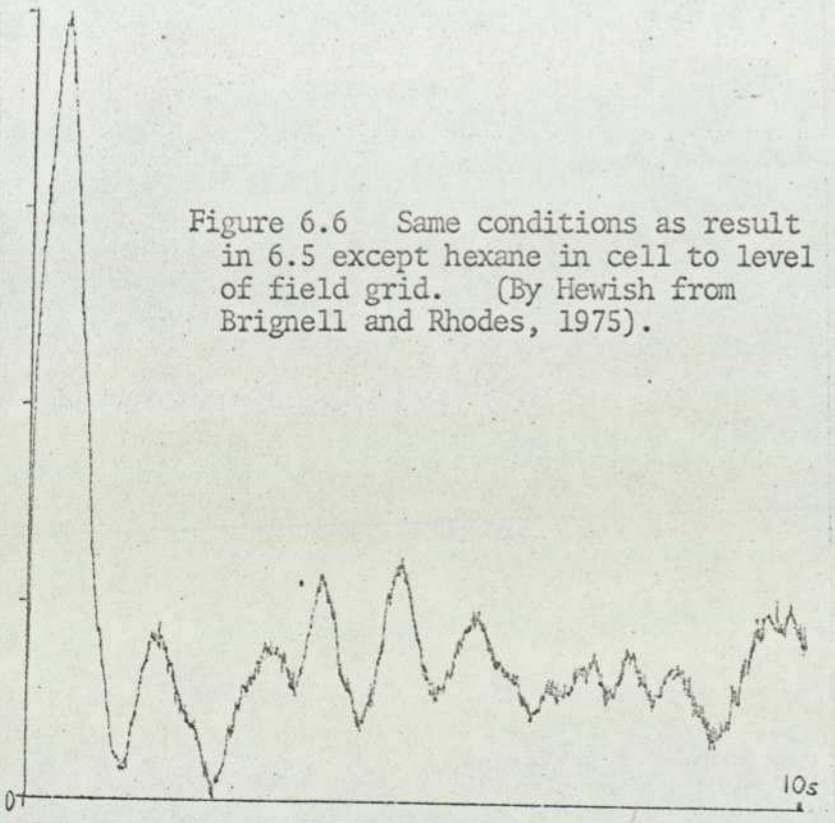


Figure 6.6 Same conditions as result in 6.5 except hexane in cell to level of field grid. (By Hewish from Brignell and Rhodes, 1975).

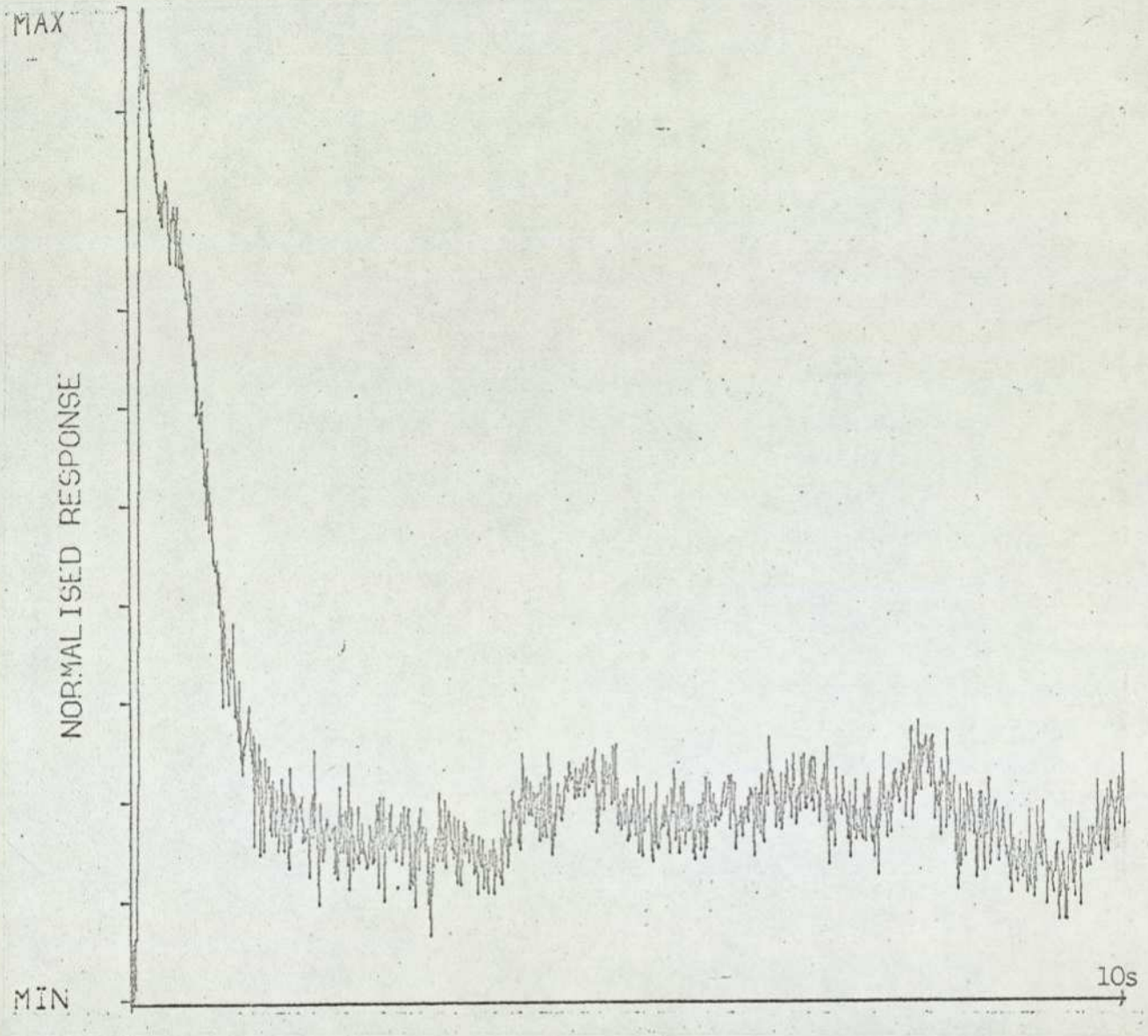


Figure 6.7 Cumulative-average result from 16 transients, to be compared with the digital correlation result in figure 6.6.

6.6.3

sequence have been plotted, corresponding to a time base of 20 seconds, since the remainder showed only minor fluctuations about the quiescent current level. It is apparent that there are larger currents and fluctuations in figure 6.9 which is contrary to expectations since the stress is lower. This is because of the difficulty in setting accurately the two voltage levels of the stimulus. If the lower level is set above the cut-off value, charge will be injected continuously through the control grid. If the higher level is greater than about 25 V above the cut-off value, because of an incorrectly set lower level or for some other reason, the injection process is non-linear and it is possible for a reduction to occur in the current when the voltage is increased further, as the control grid begins to act as a collector (Hewish and Brignell[1], 1972).

Figure 6.10 shows a cumulative-average result obtained from twenty transients which was obtained under similar experimental conditions to those prevailing when the results in figure 6.9 were acquired, except that the quiescent grid voltage level was set with more accuracy. The capacitive breakthrough spikes mark clearly the edges of the 500 mS pulse stimulus. Similar large spikes of opposite polarity can be clearly seen, close to the origin, in the cross-correlation results, figures 6.9 and 6.8. Their large size is because they were occurring at each change in the sequence and therefore contribute significantly to the cross-correlation. These spikes can be removed by very carful screening, see the results in figure 6.6, but they have some value as time-markers.

Time-of-flight measurements on these figures yield mobility values of about 7×10^{-8} m^2 V^{-1} s^{-1}.

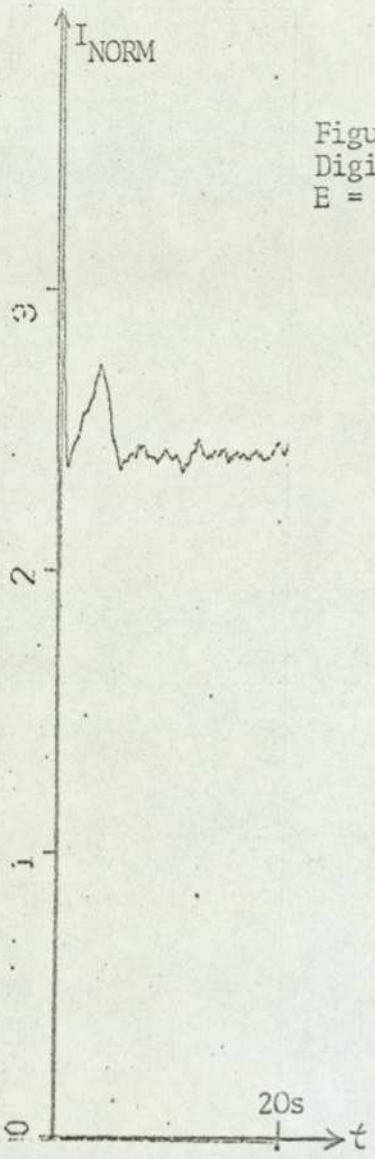


Figure 6.8
Digital Correlation
E = 800 V cm^{-1}

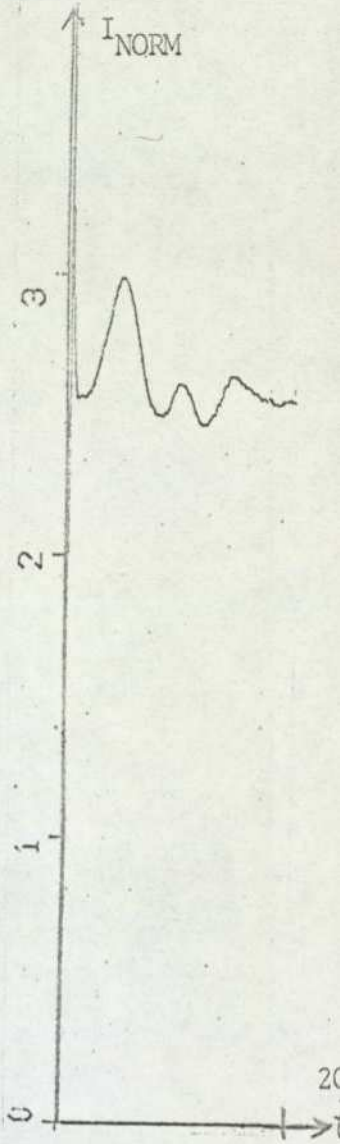


Figure 6.9
Digital Correlation E = 500 V cm^{-1}

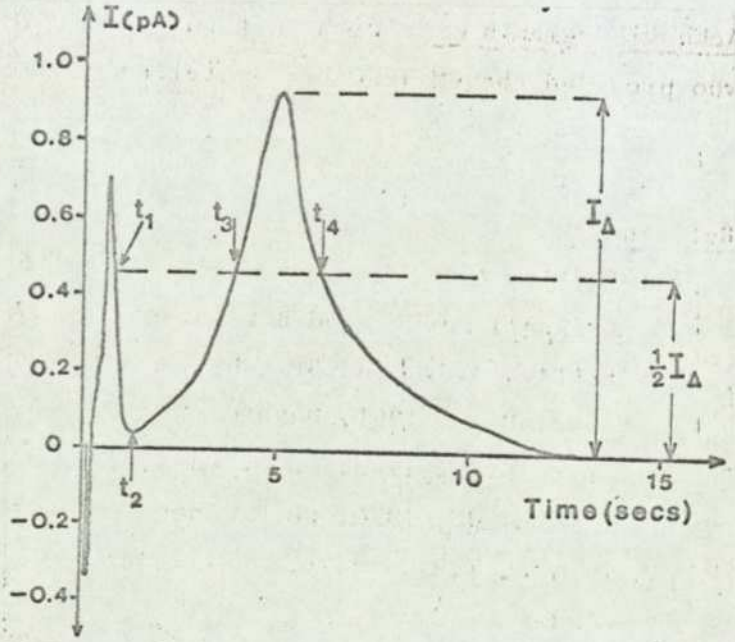


Figure 6.10 Cumulative-average result obtained under similar experimental conditions to the digital correlation results in figures 6.8 and 6.9.

6.7 Results from varying the experimental conditions

6.7.1 Introduction

This section contains, of necessity, a small selection from a large number of experimental results which were obtained as graphical output from the digital plotter of the on-line computer, and a smaller number photographed from the screen of a storage oscilloscope or traces on a pen recorder during the periods when the computer was unavailable. The sub-divisions have been chosen to emphasise different variables in the experimental conditions. Unless stated otherwise, the hexane was level with the field grid and an air-vapour gap existed in the remainder of the cell which contained the control grid and photocathode.

6.7.2 Step-stimulus results

The step-stimulus result in figure 6.11 is representative of those obtained when the u.v. light was suddenly applied to the photocathode with the control grid held positive with reference to the cathode. Similar results were obtained when the step-impulse was applied in the form of a positive voltage step to the control grid. The mobility value calculated on either edge of the transient in figure 6.11 is about 6.6×10^{-8} m^2 V^{-1} s^{-1}.

6.7.3 Pulse stimulus: results from varying the drift gap field

In figure 6.12 the effects upon the current transient of varying the drift gap field for a 200 ms pulse stimulus applied to the control grid are shown.

For these measurements the liquid sample was level with the field grid, above which there was a low pressure vapour gap. This is indicated on the transients by the minimal delay between the front edge of the transient and the first spike. This delay represents the short transit time of the charge carriers between

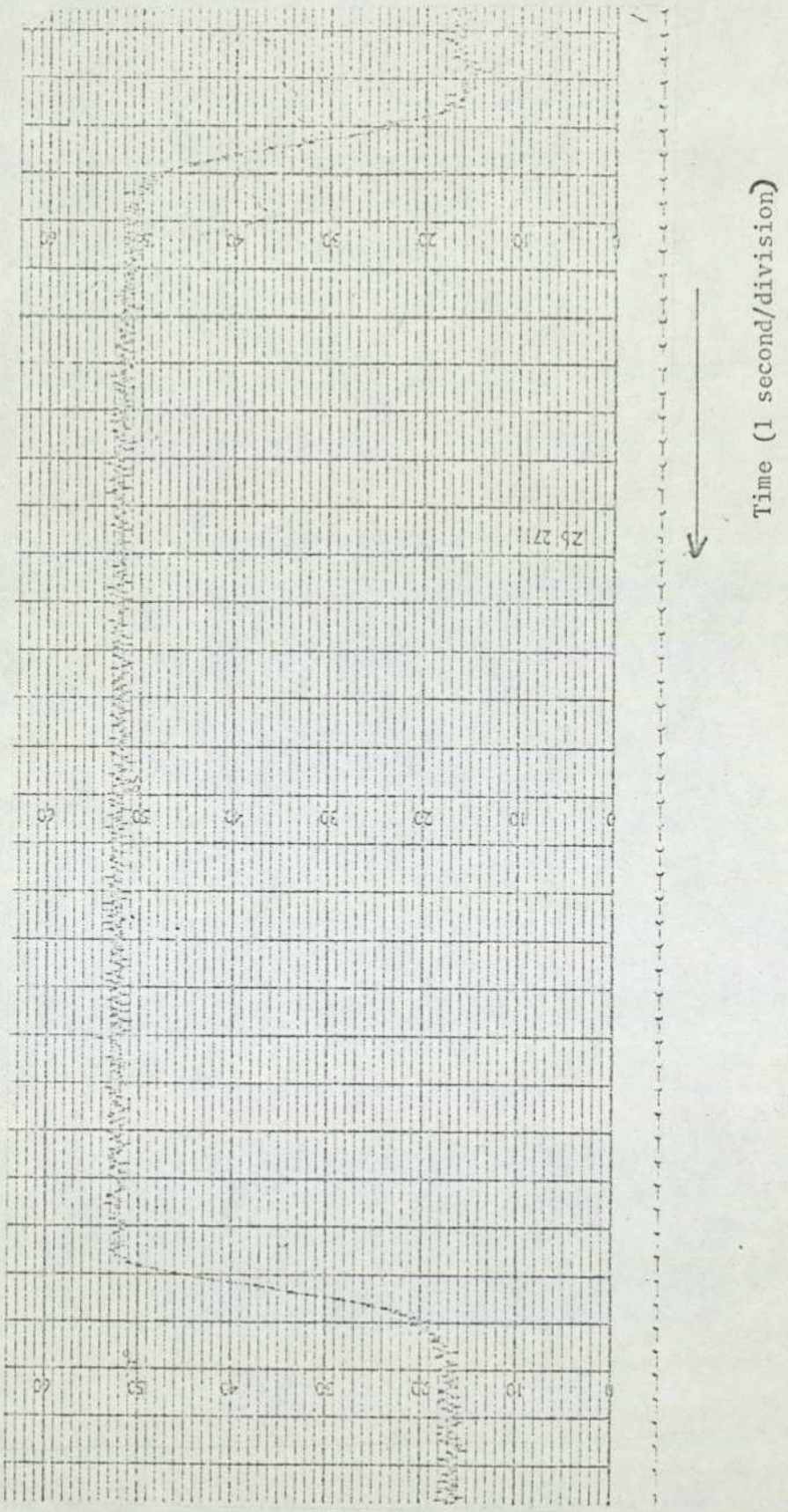


Figure 6.11 Transient response to a step-impulse

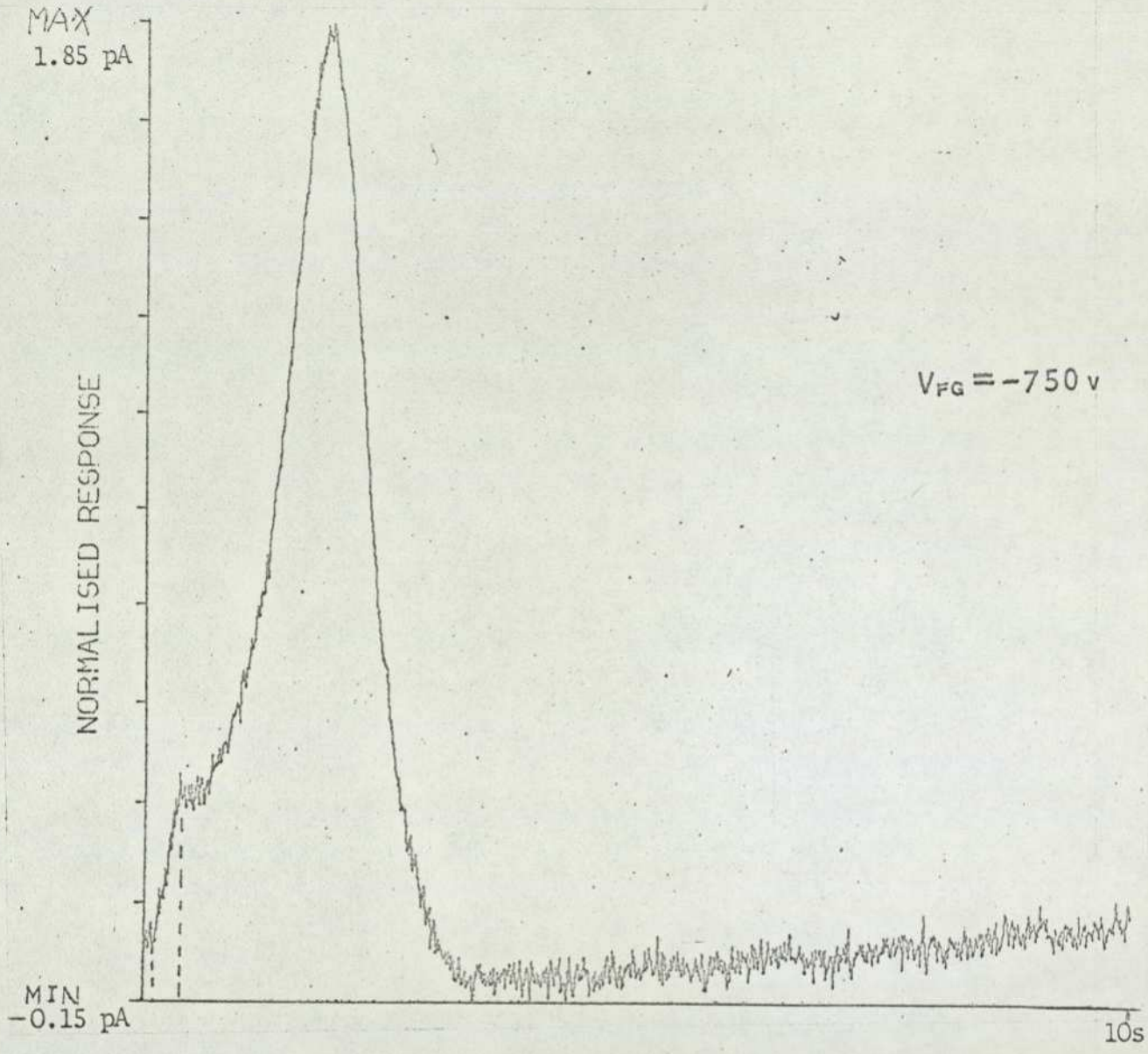


Figure 6.12(a) Cumulative-average result (5 transients) measured in identical conditions to 6.12(b) and (c), except V_{FG} = - 750 V.

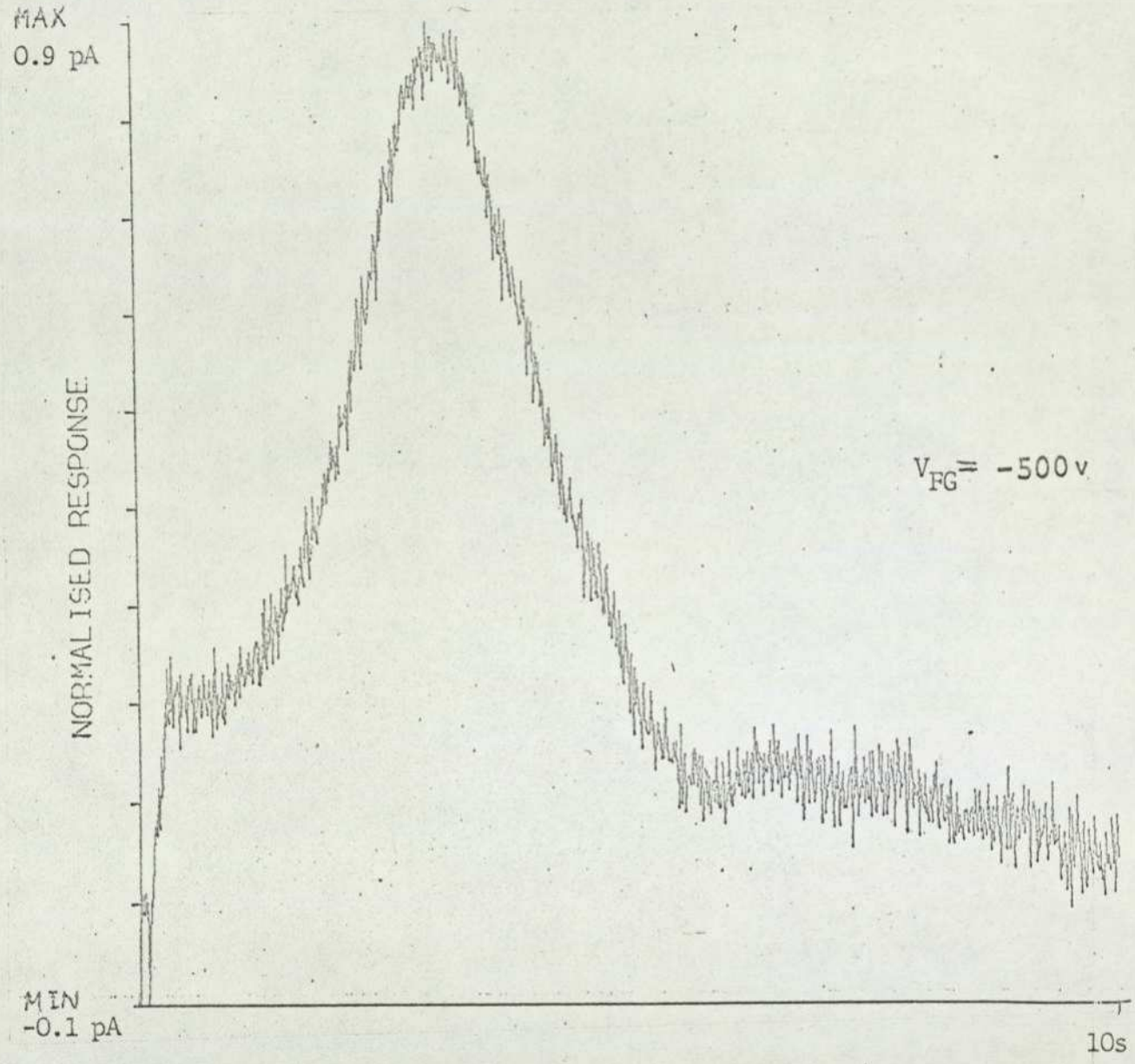


Figure 6.12(b) As for 6.12(a) except V_{FG} = - 500 V and 19 transients were averaged.

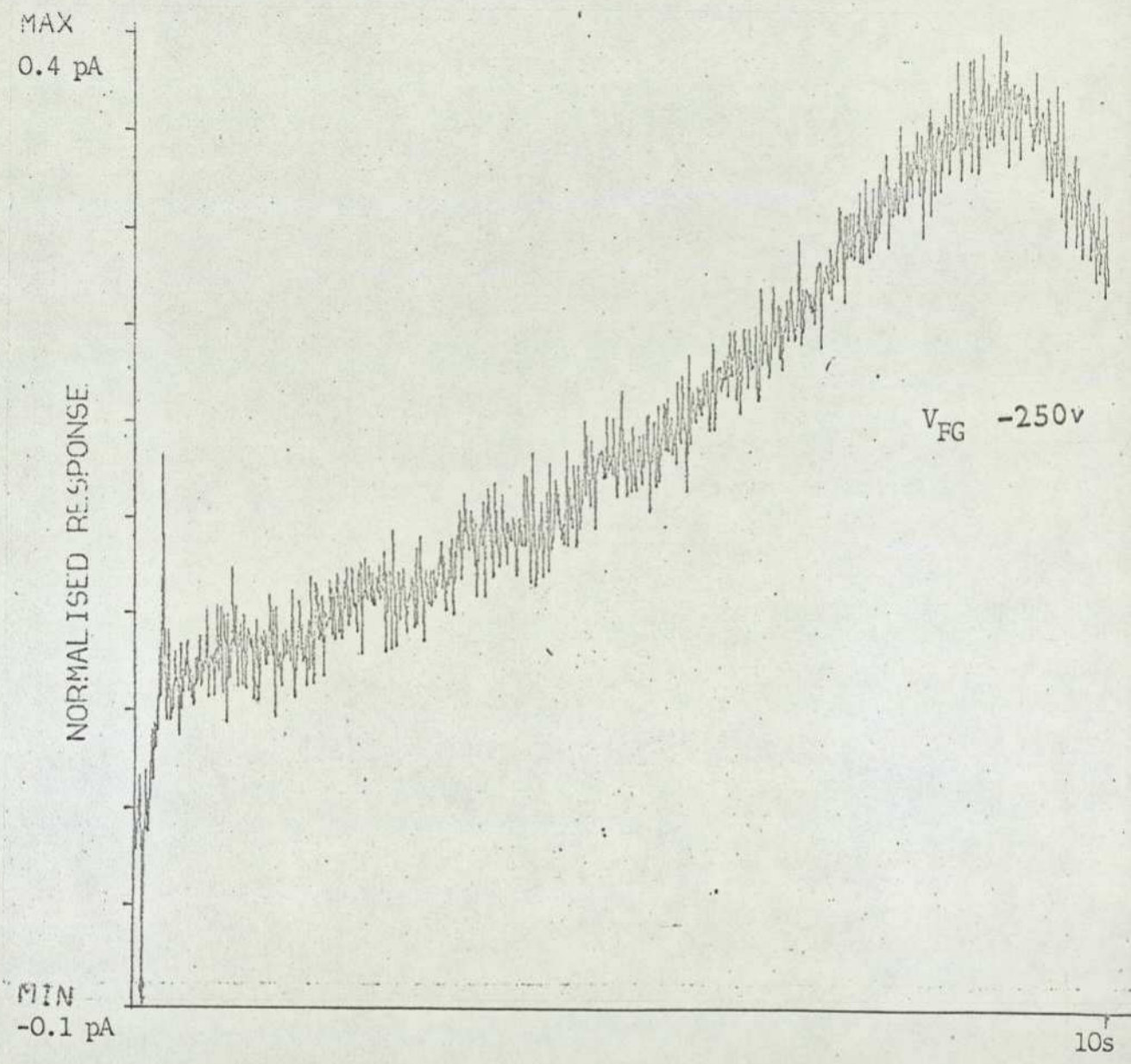


Figure 6.12(c). As for 6.12(a) and (b) except V_{FG} = - 250 V and 28 transients were averaged.

6.7.3

the two grids. The mobility values, calculated from the peak current in each case shows a progressive decrease with the applied field for 7.6×10^{-8} m^2 V^{-1} s^{-1} at 750 V cm^{-1} to 4.5×10^{-8} m^2 V^{-1} s^{-1} at 250 V cm^{-1}.

6.7.4 Pulse stimulus: results with liquid covering the photocathode.

In this case, figure 6.13, no vapour gap existed and photo-injection was directly into the hexane. The applied field from the cathode through the control grid to field grid was about 200 V cm^{-1} and that in the drift gap was 500 V cm^{-1}. The two peaks are thought to be due to field distortion due to space charge effects and are discussed more fully in chapter 7.

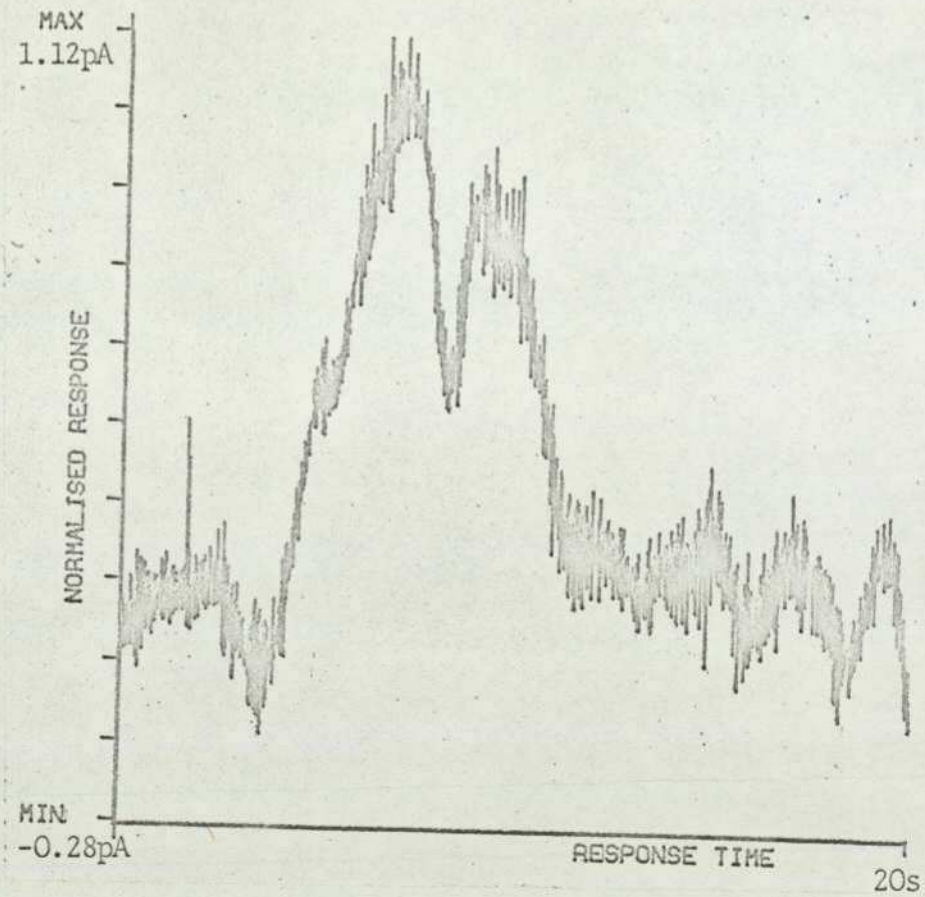


Figure 6.13 Cumulative-average result (15 transients) from photo-injection directly into n-hexane.

6.7.5 Pulse-stimulus: results from varying the pulse width

The effects of altering the pulse width of the voltage pulse applied to the control grid are shown in figure 6.14. There is less injected charge and hence the peak current is less when the pulse width is reduced but, also, a small plateau below the peak and before the tail of the current transient can be seen.

6.7.6 Pulse stimulus: results from reducing the intensity of the u.v. irradiation

Figure 6.15 shows the effect of reducing the intensity of the u.v. light falling on the photocathode and thus the charge which is injected. The current curve for the weak injection, obtained by averaging 100 transients, has a distinct plateau after the peak. A comparison can be made between these results and those of section 6.7.5. In both cases reduced charge injection produces a transient current with a peak followed by a plateau and a long tail. These observations are discussed in chapter 7.

6.7.7 The effects of argon above the hexane

Argon, nominally 99.999% pure, was introduced into the distillation system to atmospheric pressure, before the cell was filled with hexane to the level of the field grid. The transient currents recorded in response to a two second

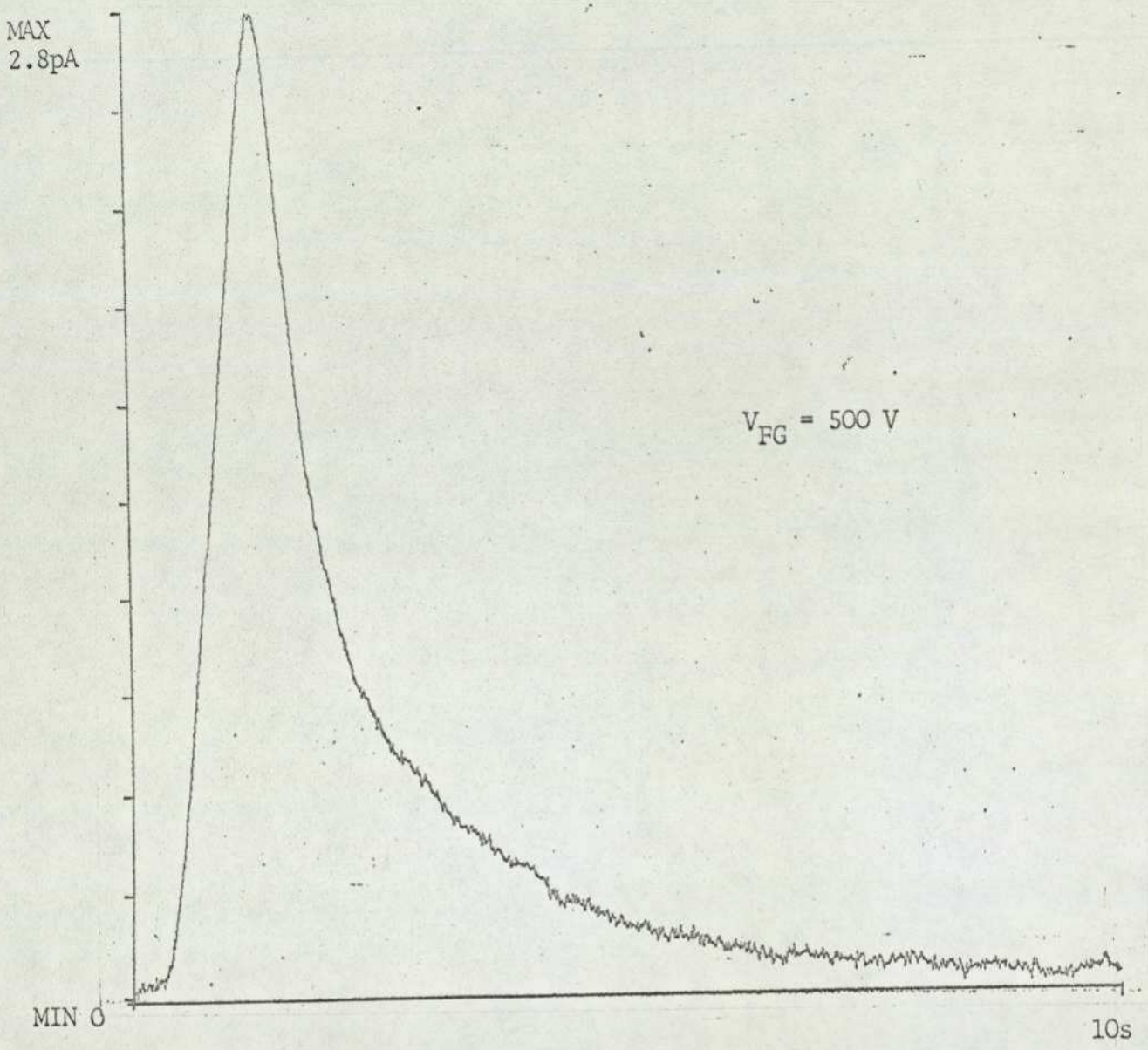


Figure 6.14(a) The pulse-stimulus was present for 0.5s in this cumulative-average result (4 transients) compare with 6.14(b) where the pulse stimulus was present for only 0.25s.

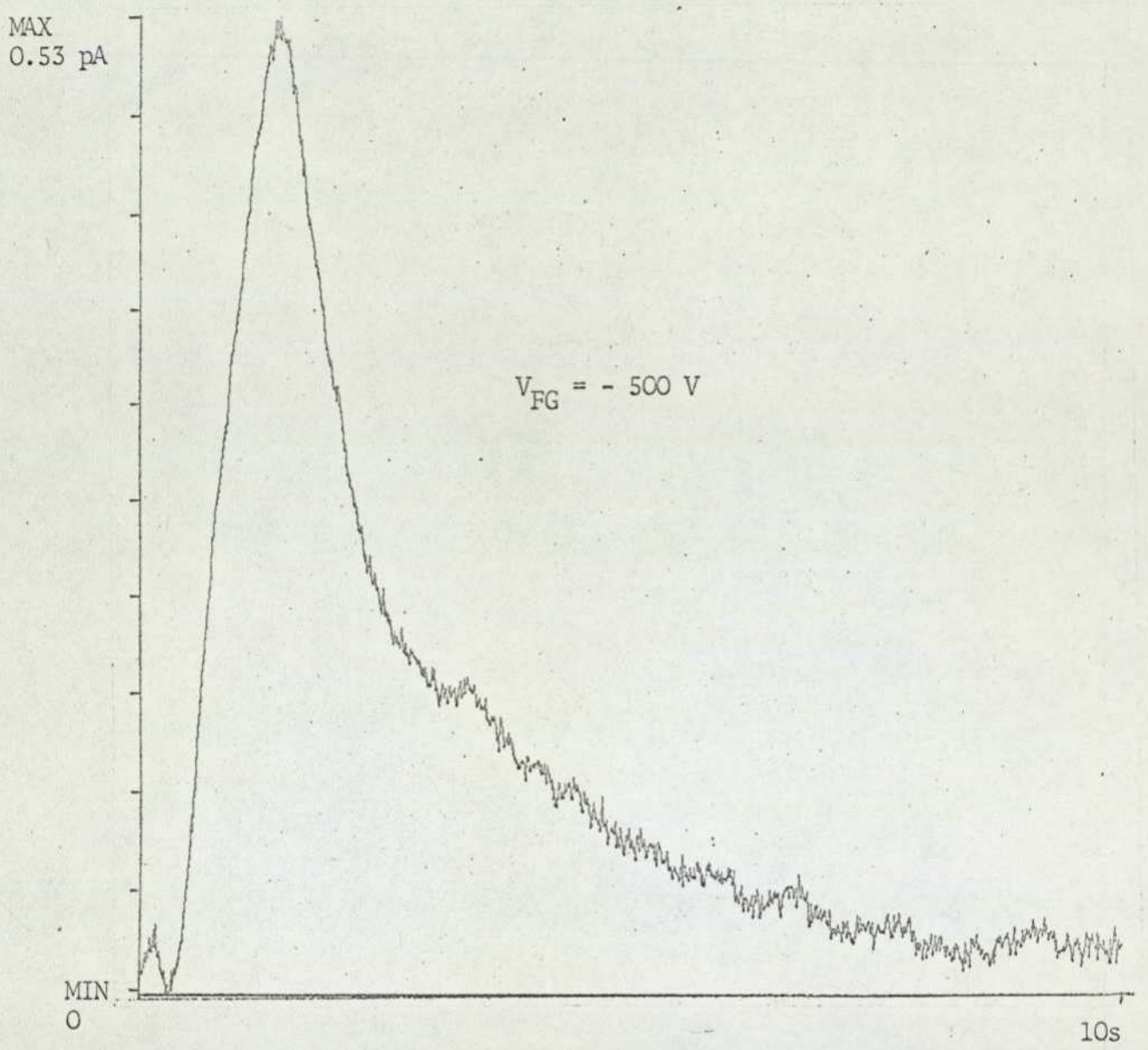


Figure 6.14(b) Cumulative average of 8 transients. The experimental conditions were the same as for 6.14(a) except the pulse width has been halved (0.25s).

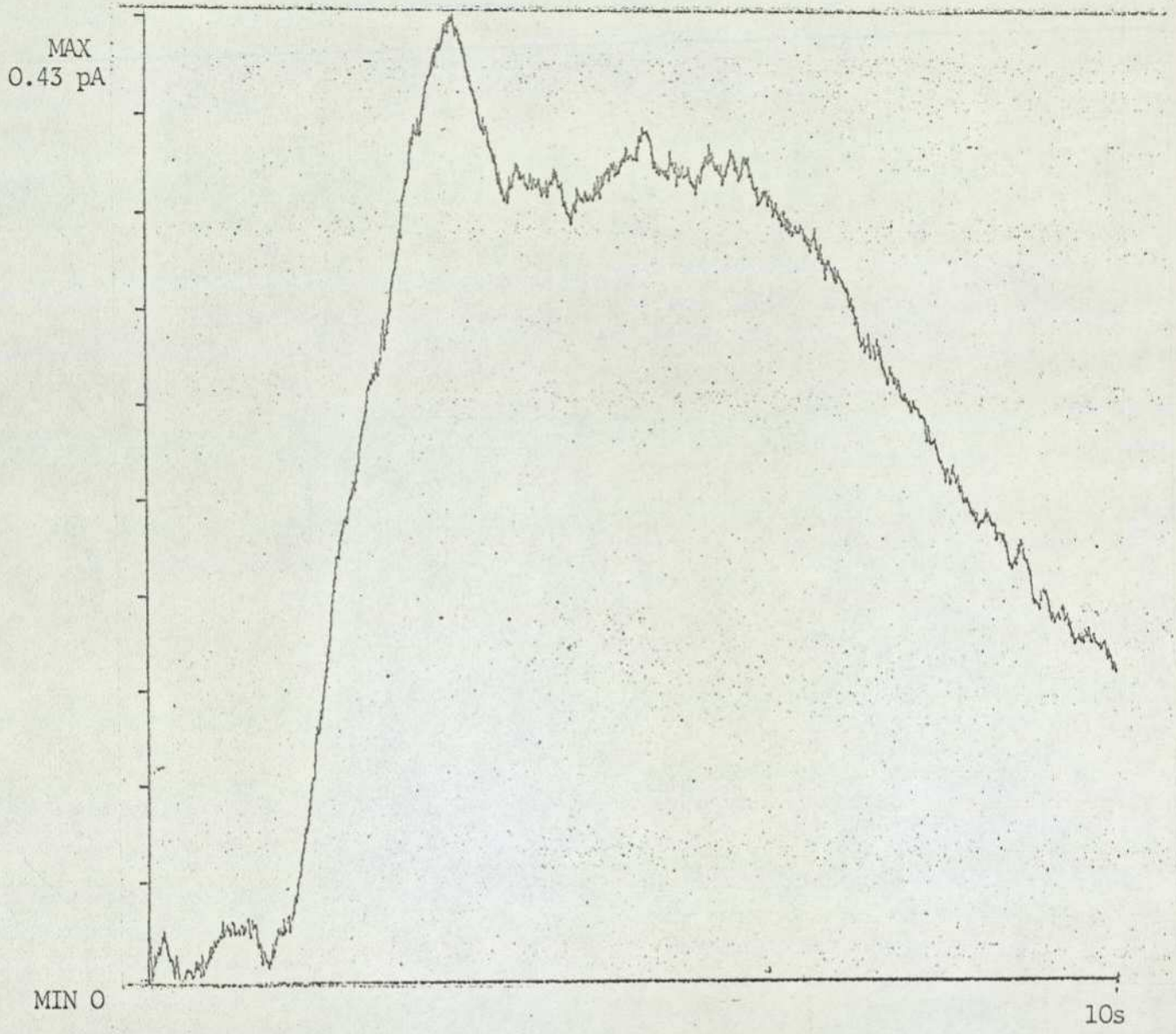


Figure 6.15(b) Cumulative average of 100 transients with identical experimental conditions to 6.15(a) except charge-injected reduced.

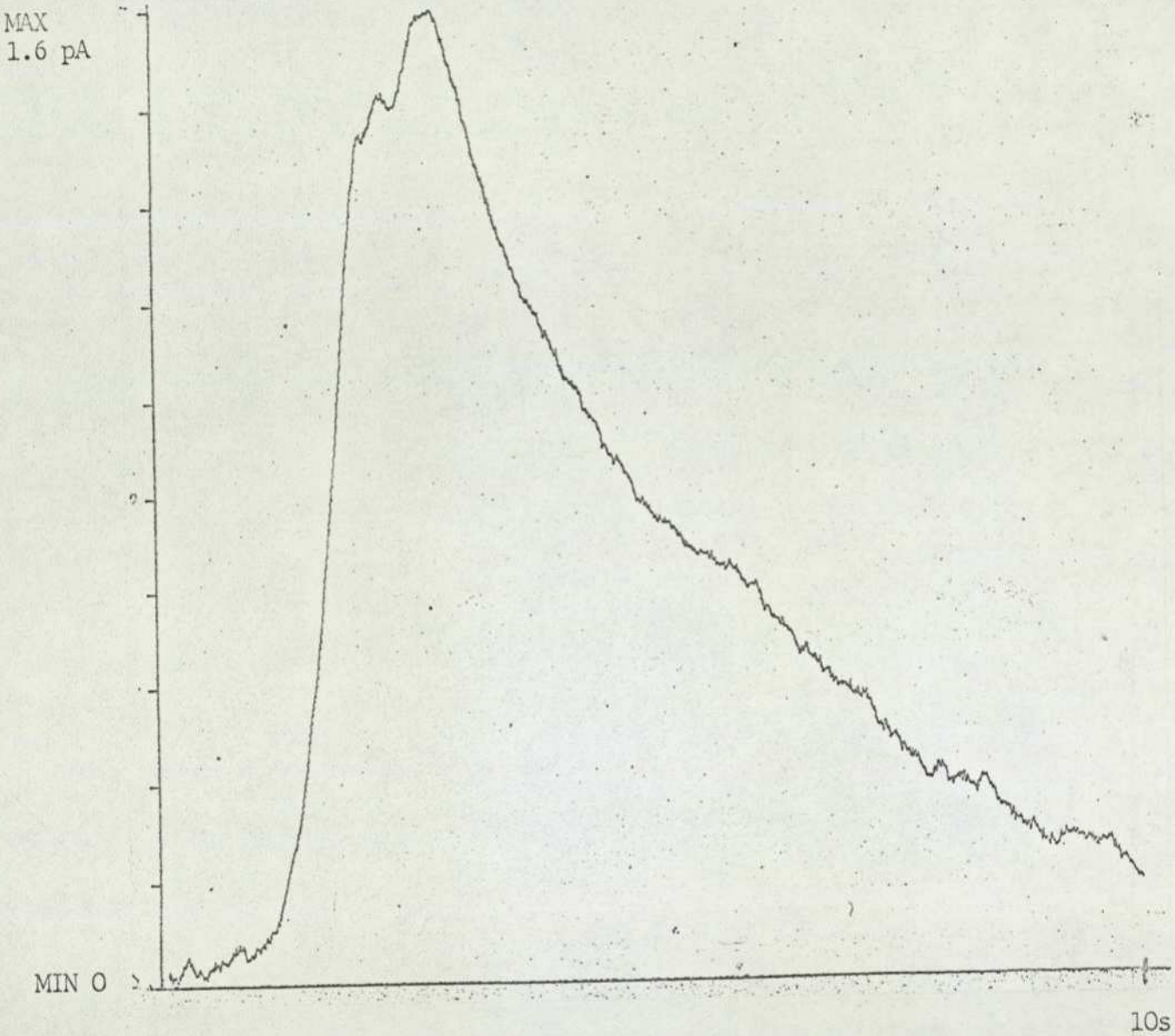


Figure 6.15(a) Cumulative average of 16 current response transients to a 0.5s pulse stimulus. Experimental conditions identical to 6.15(b) except for increased charge injection.

6.7.7

pulse stimulus were similar to those obtained with an air-vapour gap at atmospheric pressure and give mobilities of about 7×10^{-8} m^2 V^{-1} s^{-1}. However, the currents did not appear for several minutes after the photocathode was irradiated on some occasions. It was thought that the current might be flowing into the control grid, but this was found not to be the case. Further investigations, with argon only in the cell, and a step stimulus in the form of mechanical shuttering of the u.v., showed that the delay-time before the appearance of current was a function of the time between the step stimuli. This phenomena is thought to be due to surface effects at the photocathode, particularly as it was absent the first time the irradiation was applied at the start of the experiment (see chapter 7).

6.7.8 The effects of filtering the u.v. irradiation

When a OX7 2 mm ultra-violet filter, see figure 6.16, was introduced between the deuterium lamp and the photo-cathode the measured currents were reduced in amplitude but no significant change in the shape of the transients was detected.

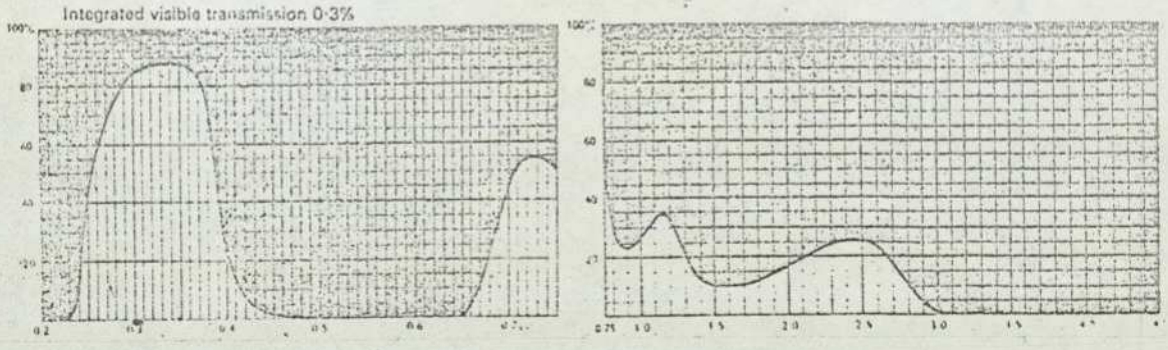


Figure 6.16 Transmittance versus wavelength (μm) for O x 7 ultra-violet filter, thickness 2 mm. (courtesy of Chance-Pilkington).

6.8 Simultaneous current transient and liquid motion observations

6.8.1 Visual observation of liquid motion

The presence of liquid motion was first detected when small disturbances of the schlieren image on a screen were observed as current responses to pulse stimuli were occurring. The applied stress to the drift gap was 1 kV cm^{-1} and the peak current was 6 pA. The disturbance appeared as a shimmer in the image but it was not possible to attribute more definite properties to it. Using the light sensitive amplifier, see section 5.5.3, a definite correlation is established between the current transient and any disturbance of the schlieren image.

6.8.2 Effect of drift gap stress on the disturbance signal

In figure 6.17, the current transient to a pulse stimuli and the signal from the light sensitive amplifier are plotted on a twin-channel pen recorder. Interchanging the positions of the diodes in the schlieren field causes an inversion of the light signal as expected, and maximum sensitivity was obtained by locating one of the diodes in the dark region of the image. Records of these measurements were also obtained by feeding the current and light signals into the two channels of a Biomation transient recorder (Buffam and Brignell, 1975), which sampled the signals and transferred the samples to the computer store. A graph from the computer digital plotter of the two signals appears in section 10.4 (Hewish and Brignell, 1975).

Examination of these results show there is a time interval between the peak of the current pulse and the peak of the disturbance signal, which represents the change in light intensity at the diode positioned approximately in the middle of the 1 cm drift gap. This time interval was found to decrease approximately

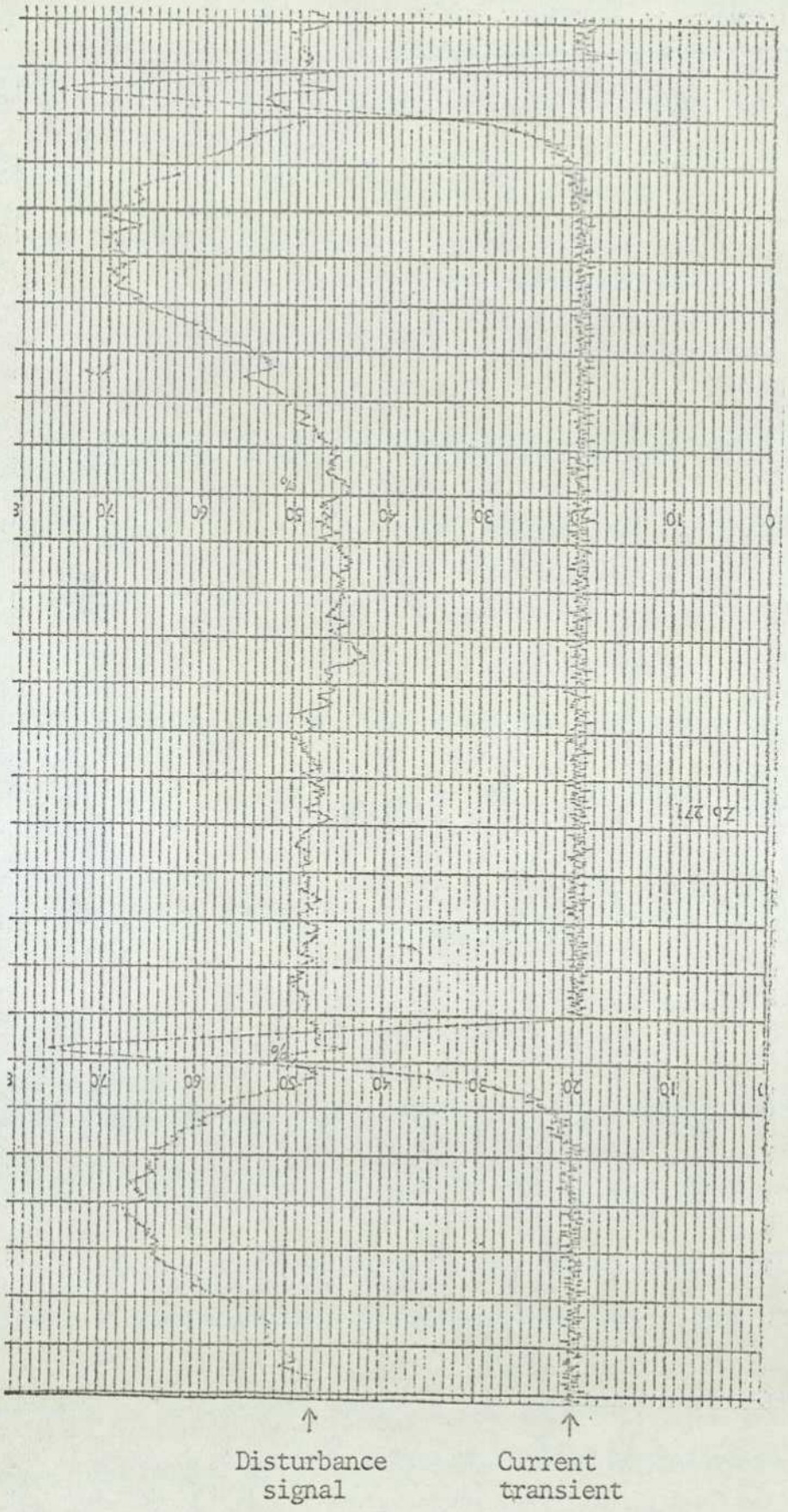


Figure 6.17 Current transient to a pulse stimuli and the disturbance signal from the differential light-sensitive amplifier.

6.8.2

as the square of the applied field over the limited stress range of 1 kV cm^{-1} to 250 V cm^{-1}, see figure 6.18. The minimum current and

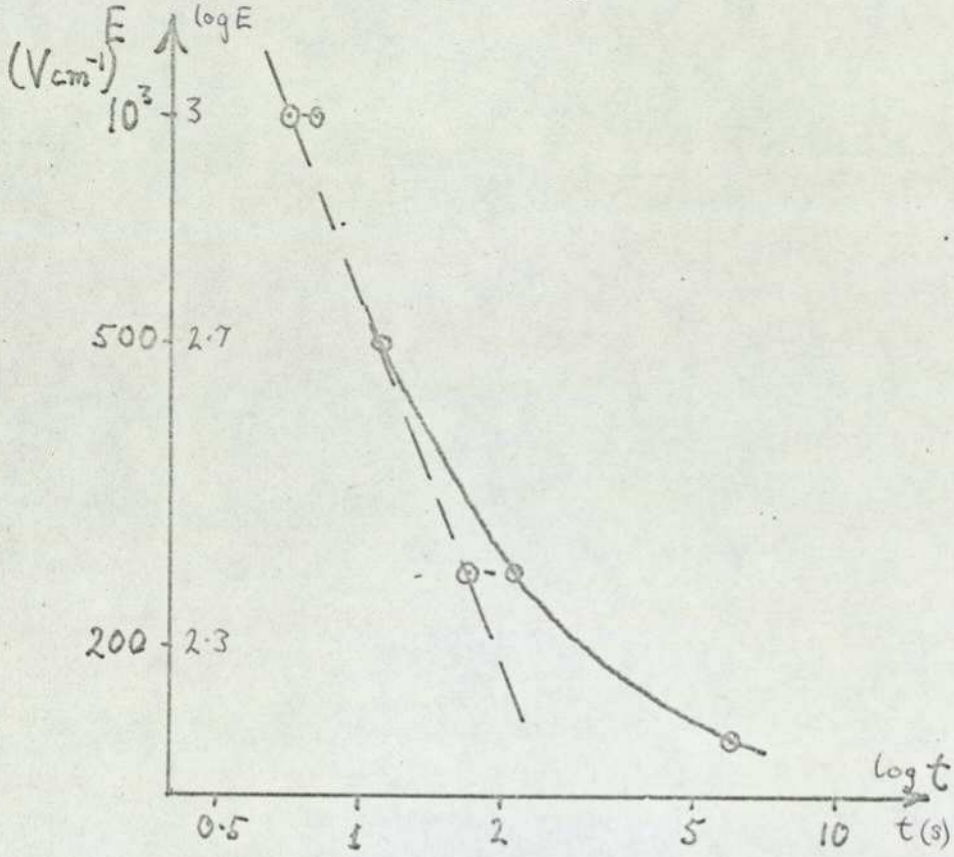


Figure 6.18 Log E versus log t where V = applied stress and t = time delay before disturbance reaches detecting diode in schlieren field.

field for which the disturbance could be detected was 1 pA at 150 V cm^{-1} under transient conditions of step and pulse charge injection, but this does not eliminate the possibility of undetected disturbances occurring in the liquid at lower values of current and field. Some of the disturbance signals, see figure 6.17, showed a small oscillation occurring before the major slow pulse which is thought to be due to a small transitory movement of the liquid before the main disturbance 'wave-front'.

6.8.3 Disturbance velocity

When the detecting diode was moved in the schlieren image towards the field grid the time interval between the current and

6.8.3

disturbance peaks decreased. This effect is detected from the signals produced by a step injection of charge (in figure 6.19), which also shows that the disturbance signal is maintained for the duration of the current transient and slowly decreases after the current has returned to zero. From these observations the velocity of the disturbance was found to be approximately 10^{-3} m s^{-1}, when the applied drift gap stress was 1 kV cm^{-1}. The velocity of the charge pulse was measured as about 6.5×10^{-3} m s^{-1} corresponding to an 'apparent' mobility of 6.5×10^{-4} m^2 V^{-1} s^{-1}. If 'true' mobility is defined as the mobility of the current relative to the liquid then this would 5.5×10^{-4} m^2 V^{-1} s^{-1}, i.e. about 15% less. It was not possible to determine the disturbance signal at the field grid as this was obscured in the image by the supporting metal ring, but from the observations at other positions the time interval between the peaks at the grid is thought to be less than 0.1 second.

6.8.4 Reduced charge injection

When the pulse width was reduced by 50% there were corresponding reductions in the amplitudes of the current and disturbance signals. However, no significant change occurred in the time interval between the peaks of the signals. A further reduction in pulse width reduced the signals to a level where it was not possible to positively identify the location of the peaks.

6.8.5 Both photo-diodes in light region of schlieren image

The previous observations of the disturbance signal were with one diode in darkness. If both diodes are in the drift gap region of the schlieren image, the signal is more symmetrical, see figure

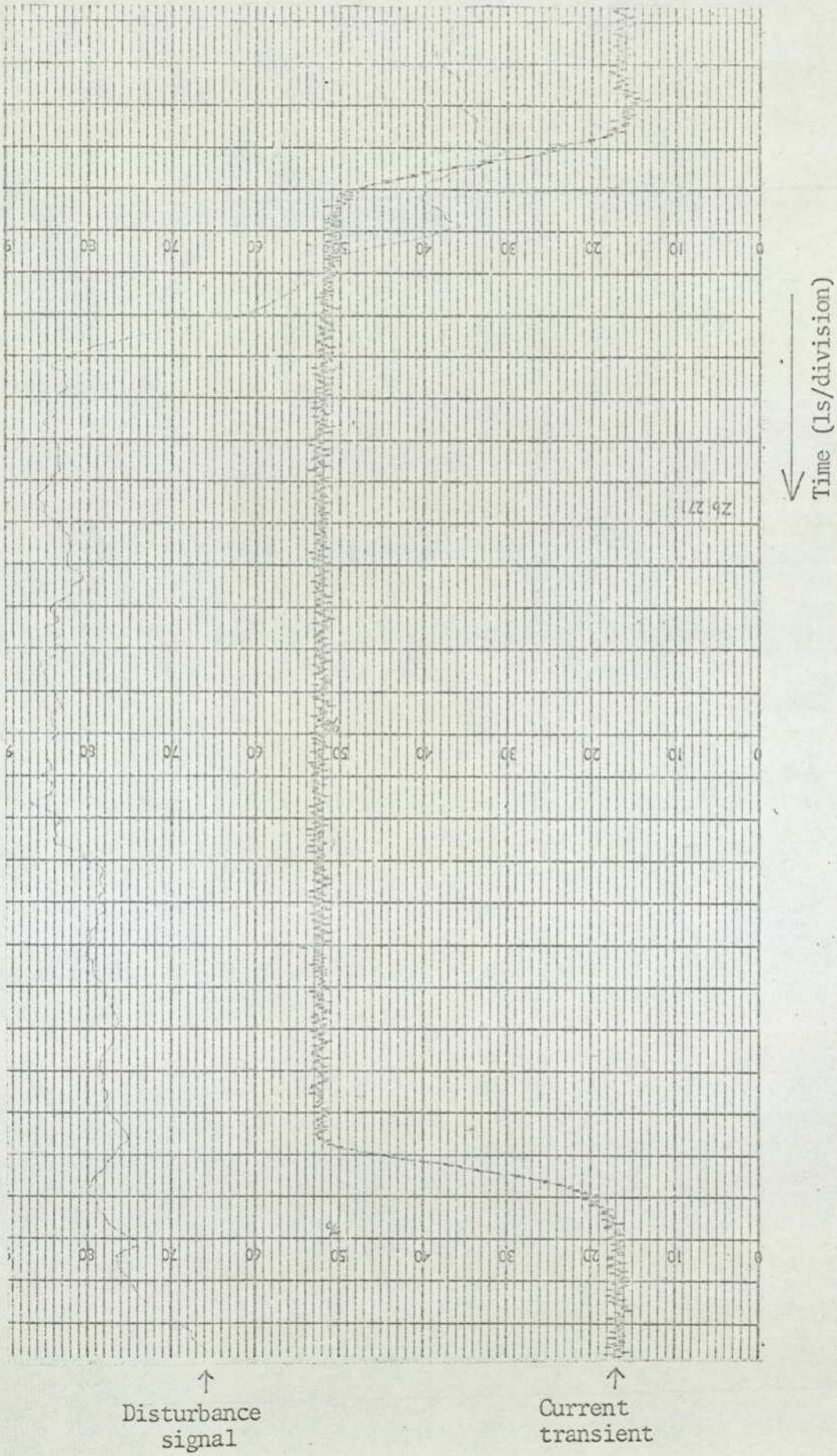


Figure 6.19 The current response to a step (or strictly a long pulse) - stimulus and the schlieren disturbance signal.

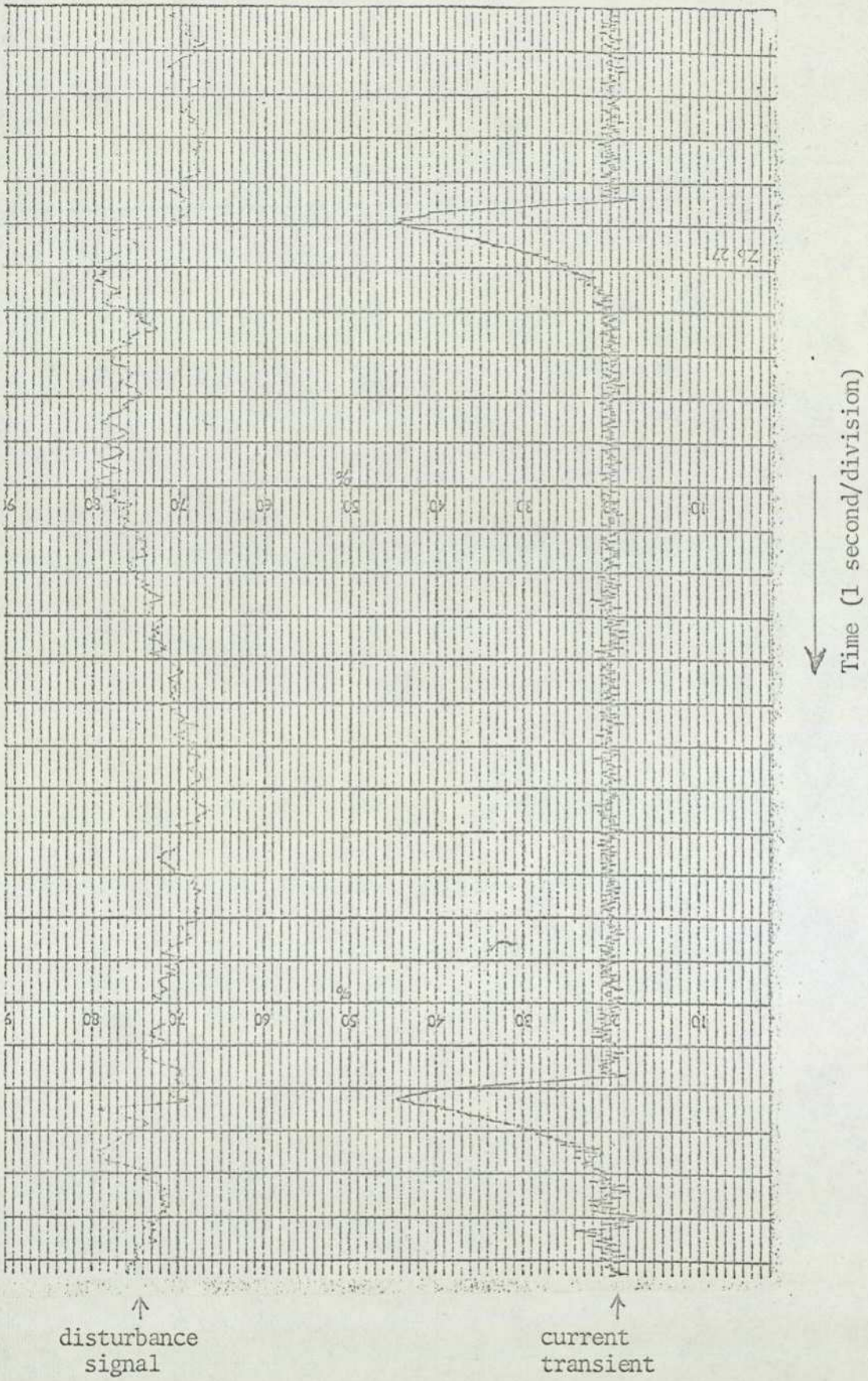


Figure 6.20 Showing the smaller disturbance signal when both diodes are in the light region of the schlieren field.

6.8.5

6.20, but the amplitude is reduced. Also interpretation of the signal is more difficult since some of the asymmetry is due to mismatch in the diodes' response to light and some is due to the ambient light intensity at each diode. The initial oscillation previously observed in figure 6.17, is more noticeable but the peak is of much lower amplitude.

6.8.6 Disturbance signals in hexane of low resistivity

The hexane used in the photo-injection experiments (sections 6.8.1 to 6.8.5) had a resistivity greater than 10^{16} ohm cm. Less pure hexane, containing a high proportion of unsaturated hydrocarbons and unsuitable for photo-injection studies, had a resistivity of 5×10^{14} ohm cm. This was used in the cell between two plane electrodes spaced approximately 14 mm apart. Upon the sudden application of an applied stress of 700 V cm^{-1} current and disturbance signals were recorded, see figure 6.21, and visual observation confirmed the presence of a general swirling of the liquid which slowly diminished as the current settled to a steady

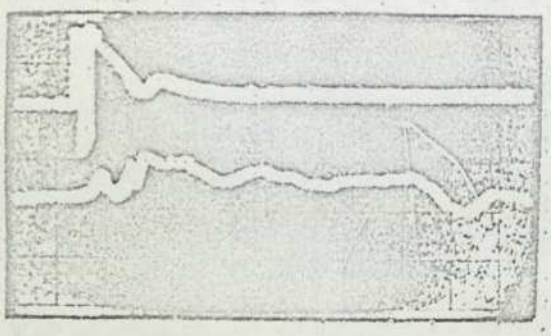


Figure 6.21 Oscilloscope traces of transient current (upper trace) and disturbance signal lower trace following sudden application of a stress of 700 V cm^{-1}.

Time Scale:- 5 seconds/division Upper trace amplitude:- 10 pA/division

value of about 2 pA. A disturbance was only detected, upon application of a stress of 350 V cm^{-1}, after the cell had been left undisturbed with zero applied field for several minutes, indicating that this liquid movement is related to the clearing action of an applied field upon ionic carriers present in the liquid. Similar tests with higher purity hexane (resistivity greater than 10^{16} ohm cm.) produced no detectable disturbances in the liquid when stresses up to 2 kV cm^{-1} were suddenly applied.

It is interesting to compare the disturbance which occurs in an 'impure' liquid subjected to a sudden electric stress (figure 6.21) with that occurring in a purer liquid of lower conductivity under stress and subjected to a step, or more precisely, a long pulse of unipolar charge injection (figure 6.19). The disturbance signal is more variable and more persistent when swirling movements of the liquid occur (figure 6.21) even after the current has declined to a steady value. With the unipolar charge injection the disturbance signal is not dissimilar in appearance to the current transient, except that the amplitude of the signal decreases slowly while the current flows and more rapidly after the current has returned to zero.

The implications of these observations are discussed more fully in the next chapter.

Chapter 7

Concluding Discussion

7.1 Preliminary

The work in this thesis will be discussed in the light of two major inter-related phenomena, which in the opinion of the author have dominated the experimental observations. One of these is the distortion observed on the current responses to charge-injection (section 7.2) and the other is e.h.d. convection (section 7.3). These discussions are followed by general remarks concerning other aspects of the work, the conclusions and some suggestions for further work.

7.2 Distortion of current transients

7.2.1 Introduction

Transient currents, measured in response to either a step or pulse stimulus, are distorted to varying degrees, depending upon the presence or absence of space charge and e.h.d. convection, the method of charge carrier enhancement and the geometry of the test cell. Further corruption to some degree is also introduced by the electronic system used to detect and amplify the current. The resultant waveshape of the transient, distorted from the ideal, see fig. 3.2 section 3.6, has then been used to explain, for example, the presence of a number of charge carriers, or to provide supporting evidence for a particular model of the conduction process. However, recent evidence indicates that many of these explanations and models were based on untenable premises or insufficient evidence. The current transients observed in this work also contain a significant amount of distortion, and while the author will offer explanations which seem plausible in the present state of knowledge, he recognises that future work may invalidate them.

7.2.2 The effects of space-charge

The leading-edge of a current response to a sudden step injection of charge can be distorted from the ideal ramp wave shape in a number of ways. These may be described in terms of the rate of change of the gradient di/dt and the amount of 'overshoot' at the top of the 'ramp'. For true space-charge limited injection, neglecting for the present the effects of e.h.d. convection, the gradient di/dt would increase as a result of distortion of the electric field by the space charge, in accordance with Poisson's law. This is shown clearly in the work of Many and Rakavy (1962) and others in solids (see section 4.4.4.3). Evison (1975) who studied a whole range of conditions by simulation, has referred to this work in his examination of the distortion on current transients and commented upon the marked similarity between current transients resulting from strong charge injection, as in the case of Taylor (1972), and the theoretical results of Many and Rakavy. Further distortion from e.h.d. convection would undoubtedly be present in Taylor's results (figure 2.24, section 2.4.1). Thus any transient that displays these features will most probably be subject to space-charge limitations or perturbations. For example, in this present work, curves resulting from pulse injection for different drift fields (figure 6.12, section 6.7.3) bear a strong resemblance to the theoretical curves of Mort and Scher (figure 4.12, section 4.4.4.3) for space-charge perturbed (s.c.p.) currents from pulse-injection of charge into solids.

Bulk ionisation, as a result of the u.v. irradiation penetrating the photo-emitter and ionising impurities within the

7.2.2

the liquid, gives rise to a decreasing gradient *di/dt* (Bloor, 1970). When it is combined with layer injection from the photo-emitter, considerable distortion of the current transients can occur (see figure 7.1), particularly as the transients do not normally show discrete changes of gradient, but become rounded. If the possibility of more than one carrier is considered, then interpretation is even more difficult, if not impossible (Evison, 1975). Although the use of a control grid normally obviates the effects within the drift space of bulk ionisation, which is represented by a stationary quescent current, it may contribute to space charge near the control grid. However, this is not thought to be as significant a factor in the results of this work as was injected space charge. Figure 6.15 (section 6.7.6) again demonstrates this, since, with the reduction of the injected charge, the ideal 'ramp and plateau' shape of a non-s.c.p. transient begins to emerge. This effect would have been more marked if a higher stress had been applied to the drift space, so increasing the charge velocity and resultant current. The overshoot on this and other transients is a feature of s.c.l. and s.c.p. currents. However, if an abrupt increase in the slope

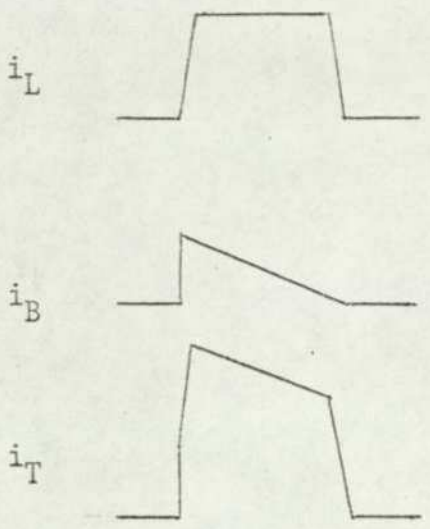


Figure 7.1 The effect of bulk ionisation (ideal currents).
i_L is current due to charge-layer injection only.
i_B is current due to bulk ionisation only.
i_T is the sum of i_L and i_B.

7.2.2

occurs near the overshoot this may indicate that e.h.d. convection has commenced, see figure 2.10 in section 2.2.6. Minday, Schmidt and Davis (1971) state that the apparent mobility is high on the trailing edge of this transient because an established faster convective flow remained, until all the ions were collected. They also suggest that the small overshoot on the trailing edge might be due to space charge. If e.h.d. convection is occuring, this overshoot could be caused by the motion of ions relative to the drift field near the collector. As the end of the charge layer reaches the collector, the net current, resulting from the convective motion of ions in an electric field weakened by space charge, could be negative and appear as an overshoot. If this explanation is correct then these 'overshoots' would be a common feature of current transients in which e.h.d. convection occurred.

There is some evidence of 'overshoots' in the work of the present author, e.g. figure 6.12b, but the currents are several orders of magnitude smaller than those of Minday et al. This is true of all previous measurements of currents due to ionic carriers resulting from photo-injection. In earlier work, these effects were often masked by the limited bandwidth of the electrometer amplifier, whereas with the modern picoammeter care is necessary that similar artefacts are not imposed upon the current transient, e.g. by an impedance mismatch.

7.2.3 The effects of grids

Minday, Schmidt and Davis (1971) used four grids to obtain high-speed electronic control of 'free' charge carriers in ultra-pure n-hexane, but used mechanical shuttering of the u.v. irradiation for their observations of ionic carriers. When the electronic shuttering for electron mobility measurements was used a constant

7.2.3

background of convective flow was established. Minday et al do not give more information about this fluid motion which was most likely caused by space charge accumulating in the grid regions (see section 4.4.3), but its presence in an ultra-pure liquid with a resistivity of $\simeq 10^{19}$ ohm cm is significant. Since the momentum exchange between electrons and liquid molecules would be too small to induce e.h.d. convection, it must be due to ionic charge-carriers. Even if the movement of these ions contributed only 5% towards the 'free-carrier' current, 5×10^{-10} A say, this could be sufficient to cause convection if the current is space charge perturbed. It would have been interesting to see results from slower electronic shuttering in this work of Minday, Schmidt and Davis, particularly in the case where the ionic carriers were predominant.

7.2.4 Other ionic charge-carriers

The other work reviewed which used grids to control injection of ionic carriers from non-uniform sources use either high field razor-edge injectors or high-energy ionization methods. In these cases the current waveforms exhibit considerable distortion and the mobilities which are derived, often by an extrapolation process, are about one third or less of the value for ionic carriers obtained in photo-injection test cells. S.c.l. conditions undoubtably exist at the injectors and at the grids in these systems, but this fact does not account for the lower mobility. It appears that this can only be due to a different type of charge-carrier. In the photo-injection studies there is strong evidence that the ionic charge carrier in n-hexane is an oxygen ion, particular after the work of Minday, Schmidt and Davis, whereas although charge-carriers of a mobility $\simeq 10^{-3}$ m^2 V^{-1} s^{-1} are occasionally detected (Taylor, 1972), they are normally

7.2.4

obscured by slower carriers. It is possible that these are hexane ions since the energies involved, greater than about 37 eV, are sufficient for ionisation to occur (Mathieu, Blanc, Patau, 1968). In the present work, however, with grids in a cell, the distortion can be difficult to interpret; the current transient in figure 6.13 section 6.7.4 is a typical example. This shows severe distortion when compared with other results in chapter 6, however in this case, photo-injection was directly into the liquid which filled the cell. Thus, before entering the drift gap, ionic carriers travelled through a low field region ($\simeq$ 200 V cm^{-1}). Assuming two ionic carriers with differing mobilities, then the pulse of charge would split, and the slower carriers would arrive at the drift gap some time after the faster ions. Thus the majority of the faster ions could have crossed the drift gap before the slower carriers had arrived and two peaks would occur in the current transient. This effect was observed on other occasions when some of the space between the two grids was occupied by n-hexane and to a lesser extent with an air/vapour gap at atmospheric pressure, see Figure 6.15. Introducing very pure argon into the cell above the hexane to atmospheric pressure delayed the appearance of the current by tens of seconds after a normal first transient. The shape of the transients, when they appeared, showed the usual spreading effect, see section 6.7.7. Felici and Sauviat (1972) observed similar delays when negative ions were injected from basic polymers into polar liquids. No satisfactory explanation can be put forward at this time for this delay phenomenon occurring, with photo-injection into argon/hexane vapour. The currents in response to the injection of a pulse of charge containing two carriers of different mobilities

7.2.4

are illustrated in figure 7.2. If both carriers enter the drift field at the same time then the ideal results are as shown in (a) and (b) depending upon the relative contributions of each carrier to the total current. If there is a time-lag between injection and the arrival of the charge in the drift space then the resultant current transient will ideally appear as depicted in (c) or (d).

The 'long-tail' effect

One contributory factor of the 'long-tail' on the trailing edge of a current response to a pulse stimulus could be the simultaneous presence of a number of carriers as suggested by Evison (1975), who also made a comparative study of the results of observations in solid dielectrics, which showed that this phenomenon is not unique in the liquid state. However, it could equally well be caused by movement of charge from a region of space-charge concentration under the influence of the applied field, and since the size of the tail was observed by Evison to change with temperature, either of these explanations would be feasible.

7.2.5 Summary; distortion of current transients

The influence of space-charge, bulk-ionisation and grids in the test cell, combined with the possibility of e.h.d. convection, make the interpretation of current transients a hazardous task. It is very easy to assume that only one of these sources of distortion is the contributory factor, whereas a number or all of them may be responsible. The method of using a computer model of the charge injection process (Evison, 1975) is an attractive way of investigating the effects of these various sources of distortion upon the current transient. By altering the charge distribution to simulate, for example, regions of space-charge concentration, two

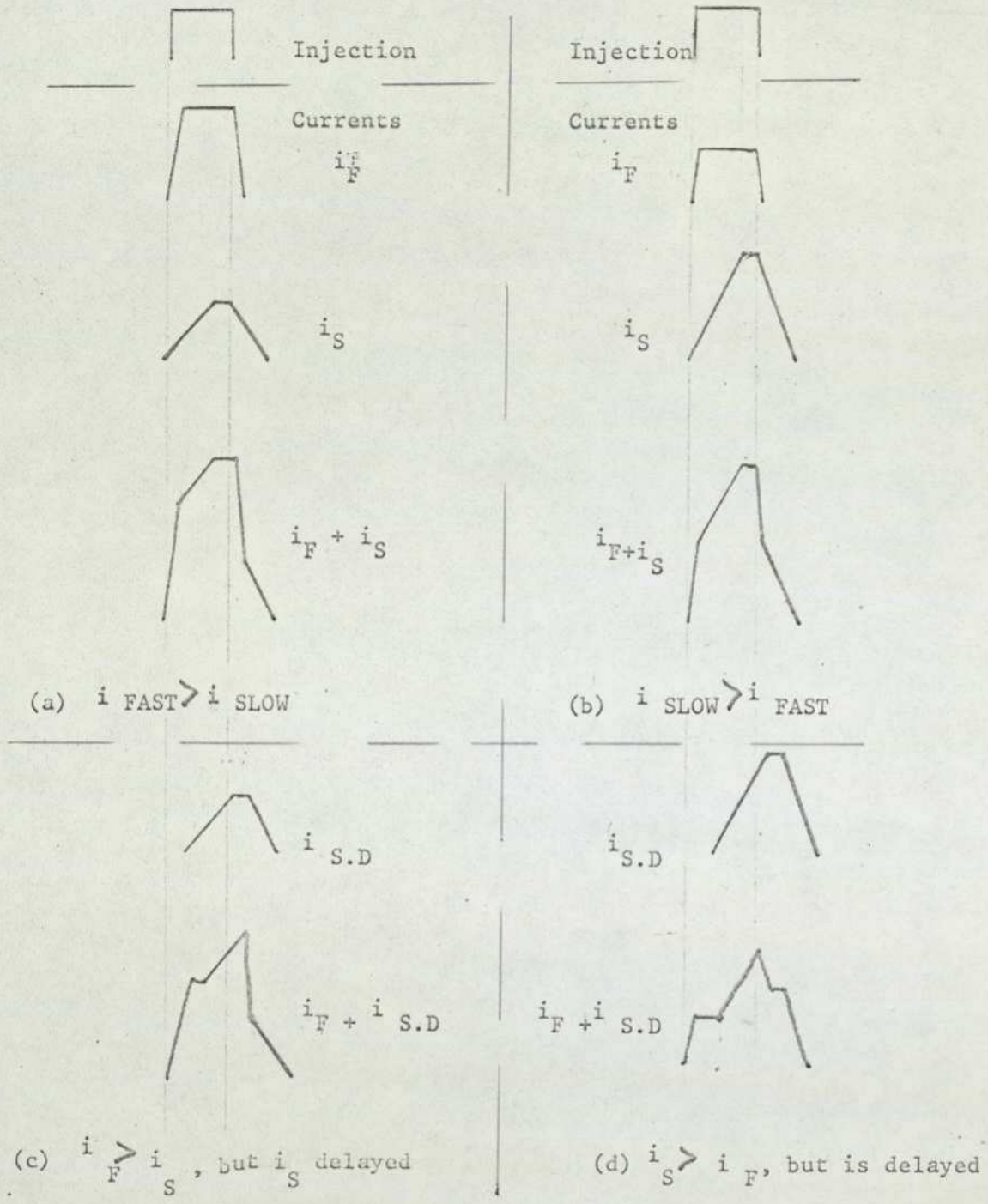


Figure 7.2. The effects on current transients of 2 charge carriers one fast, one slow; (a)&(b) both injected at the same time, (c)&(d) slow carrier injected after fast carrier.

7.2.5

carriers of differing mobilities, or the effects of e.h.d. convection, the current transient could be built up and compared with the measured result. The reverse process, that of adapting the model to fit the measured current transient, is even more attractive, but is not without its problems especially if more than one source of distortion is present. It is unfortunate that Evison (1975) did not give a more comprehensive selection of results from his model. It would be interesting, for example, to have more evidence of the effect of s.c.p. on 'turn-off' transients, which might have thrown more light on the 'long-tail' effect.

7.3 E.h.d. convection

7.3.1 Introduction

The motive force of e.h.d. convection is not dielectrophoretic but the normal electrostatic force acting on a space charge which is being transported by a fluid, thus whenever conduction in a liquid is attended by the formation of space charge, convective motion is likely to occur (Felici, 1971b). Since the fundamental theory of e.h.d. stability following unipolar charge injection was firmly established by Atten and Moreau (1970), attempts have been made to relate experimental results to this theory with varying success. One difficulty, which is fully appreciated by Atten (1974), is that of defining the experimental conditions, which are inevitably full of imperfections. Apart from those associated with the charge-injection mechanism, there is the geometry of the test cell, which in this work is responsible for non-uniform fields as well as local space-charge accumulations. In addition there are approximations inherent in the simple mathematical continuum model for the liquid on which the analysis is based, and the possibility of thermal and other imperfections (Brignell, 1972). Thus it would be remarkable

7.3.1

if a close quantitative agreement existed between experimental and theoretical results from studies of e.h.d. stability. One would expect, however, that there would be a close qualitative agreement i.e. the laws of variation should be accurately predicted by the theory.

7.3.2 Studies of e.h.d. stability

Earlier work in this laboratory on enhanced conduction by photo-injection into n-hexane found an absence of any dependence of the apparent mobility of photo-injected charges on electrical power input (Brignell and Buttle, 1971). The results were interpreted as implying that previous determinations of mobility by this method were unlikely to have been subjected to errors of an electrohydrodynamic origin. In the light of the present work, and that of Minday, Schmidt and Davis (1971) in which they observed convection during their measurements of 'fast-carrier' mobilities, this implication is no longer valid. This illustrates the hazard of making assumptions based on indirect evidence, a danger which even Minday et al have not entirely avoided, since, conversely, they deduce the 'onset of e.h.d. convection' from a sudden change in the gradient of the leading edge of a current pulse. Evison (1975) made the same inference whereas this point of inflexion could have been caused by two ionic carriers, amongst other possibilities, as discussed in section 7.2. The suggestion of Secker and Lewis (1965), see section 2.2.3, that liquid motion was present in their cell and its magnitude and the time taken for it to reach a steady value were related to the power input to the cell is a further example of indirect evidence. A similar criticism can be levelled at the extrapolation methods employed by Essex and Secker (1968) and Gray

7.3.2

and Lewis (1969). The source of charge injection for the work by Essex and Secker was a number of high-field razor-edge emitters, which may be said to inject turbulence into the drift space as well as charge. Under these conditions it is difficult to visualize and probably impossible to model the e.h.d. stability problem, and it appears dubious to extrapolate back to zero current to find the true mobility.

Thus the only method by which the presence of e.h.d. convection can be definitely identified, without introducing impurities into the liquid, is by direct observation with a microscope, or by observing the refraction of a light beam passing through the liquid. This observation using schlieren techniques is normally viewed directly or by cine-film, but in this work a more sensitive method of observing the schlieren disturbances was introduced, i.e. the differential light sensitive amplifier. This has, in addition, the important advantage of providing a signal which can be recorded simultaneously with the current transient, thus enabling correlation to be established between the current and the e.h.d. convection, see figure 2, appendix 10.4. These waveforms and others have been discussed in some detail in section 6.8, and this method of observation is considered to be an important step in the study of e.h.d. convection. Direct visual observations are tedious as well as being less reliable than photo-electric methods which proved to be more sensitive than the human eye. Also, by carefully positioning the photo-diodes in the optically-enlarged schlieren image of the drift field it is possible to measure the velocity of the disturbance which in this work was small ($\simeq 10^{-3}$ m s^{-1}). A weakness of an alternative method of velocity measurement, the Laser-doppler method

7.3.2

(Taylor, 1972), is that it measures the velocity of particles in the liquid, not the liquid itself, thus it again relies on impurities being present, and presumes them to be constrained to move with the liquid.

7.3.3 Deductions from e.h.d. studies

The signals from the light sensitive amplifier, section 6.8, showed that some movement occurred in the liquid, under transient injection conditions, at currents as low as 1 pA and with applied stress as low as 150 V cm^{-1}. With no injection, however, sudden changes in applied stresses, up to 2 kV cm^{-1}, produced no schlieren disturbance signal. These figures for transient injection are lower than expected from the stability criteria, which agrees with the findings of Filippini, Lacroix and Tabazeon (1970) for polar liquids.

The sensitivity of the stability criteria to the value of mobility has been shown in section 4.6, i.e. $J_{CRIT} \propto \mu^3$ and $V_{CRIT} \propto \mu$. Thus a wrong choice of the value of μ is one factor which might account for the lower critical values. A more disturbing possibility is that the theory of stability is based on macroscopic values of the liquid parameters, whereas there may be microscopic local variations in, for example, the permittivity ε as the packet of charge moves through the liquid.

The time-lag between onset of motion and current transient was found by simultaneous measurements of both signals to vary approximately as E^{-2} which agrees with the findings of Filippini, Gosse, Lacroix and Tobazeon (1970), again in polar liquids.

The peak signal from the light detector is thought to correspond to the turbulent region behind the front of the disturbance

7.3.3

observed by these workers and Hopfinger and Gosse (1971). With a current pulse the intensity of the disturbance diminishes gradually, whereas the schlieren photographs of Hopfinger and Gosse are for step-injection of charge. For a long-pulse, approaching steady-state, the light detector signal persisted and only slowly decreased in amplitude, see figure 6.19, section 6.8.3.

Relatively impure hexane was found to be unstable to very small values of applied stress, particularly after the cell had been left undisturbed with zero applied stress for a period of time, which indicates that this motion is related to the clearing action upon ionic carriers of an applied field (section 6.8.6). This observation is in accordance with the theories put forward by Felici (1972) and Atten (1972) with regard to convection in a conducting liquid.

7.4 General remarks

7.4.1 Photo-injection

Some problems were encountered in this work with deterioration in the photo-emitters. It is felt, in the light of experience, that these can only be overcome satisfactorily by evaporating the metal film onto the substrate, within the measuring system. Pugh (1968) found, as did the author, that the life of the emitters was increased if they were kept under vacuum, but it is impossible to avoid some exposure to air and the subsequent oxidation appears to cause the deterioration. This is accentuated if an air/vapour gap is used as the irradiation then appears to speed up the process of deterioration, see section 6.3. Recently, Martin and Secker (1975) obtained improved injection with gold-palladium photo-emitters, but even these deteriorated after a period of tens of

7.4.1

hours when used in hydrocarbon vapours.

Photo-chemical reactions occur in hexane, especially in the presence of oxygen (Pugh, 1968), when it is subjected to u.v. irradiation, thus even with back-illumination the liquid sample absorbs u.v. radiation after being used for a number of experiments and must be re-purified.

7.4.2 Signal Processing

The digital correlation method of signal identification, which was used to evaluate the impulse response of the system, including the test cell and liquid, presents certain problems. There were the purely practical difficulties of adjusting and maintaining the voltage levels of the stimulus applied to the control grid, see section 6.6, and adequately screening the test cell to eliminate capacitive breakthrough spikes. This latter precaution was very necessary, since to inject sufficient charge when breakthrough spikes dominated the response, the period of the sequence had to be long ($\simeq$ 100 seconds) and even then the response was small, see figures 6.8 and 6.9, section 6.6. Low-frequency drift can introduce severe distortion of the response but it was not a problem in the present work over the period of time necessary to obtain the response samples. Thus there was no need to resort to the various methods of minimizing the effect of this type of disturbance, e.g. Macleod (1968).

The cumulative-average method is more prone to the effects of drift since the period of time required to average, say 100 samples, can be as long as one hour. With a smaller gap and higher applied stress, this time could be reduced, but not in proportion to the transit time, since an adequate rest-period must be allowed between

7.4.2

samples to allow the effects of e.h.d. convection to subside. This method gave more consistent results than the digital correlation method and the facility of viewing the accumulated result after each transient was particularly attractive. The noise reduction achieved by averaging only a few samples was quite significant.

7.4.3 Trapping Model of charge-transit

Le Blanc (1959) introduced the trapping model to explain the charge mobilities ($\simeq 10^{-7}$ m^2 V^{-1} s^{-1}) which he measured in n-hexane with photo-injection enhancement of carriers. He proposed that the trapping hypothesis of Crowe (1956) put forward to explain the low drift mobility in n-hexane, was applicable, see section 4.4.6. Metzmacher and Brignell (1970) pointed out an error in Crowe's interpretation of the statistics of the breakdown phenomena but that, fortuitously, the corrected results fitted the hypothesis. It should be noted that this is based on a crude approximation, that the formative time-lag represents one transit. Minday, Schmidt and Davis (1971) also propose a trapping model for the free carrier mobility, based on the frequency of trapping collisions of the free electron and the mean trapping time. For the ionic carriers, which they found had a constant mobility independent of concentration, they considered two models. The first proposed that ions could be formed close to the cathode by high-energy electrons, but this was rejected as it would result in a higher ion-electron ratio at high fields. The second proposed that electrons in transit via traps could form ions with impurity molecules anywhere in the drift space. The ratio of ionic to total current was found to vary as $E^{-\frac{1}{2}}$. This was in reasonable agreement with the theoretical analysis which also predicts the observed field independance of mobility in the absence

7.4.3

of e.h.d. convection.

With higher impurity concentrations, as in the present work, one could reasonably expect all the electrons to form ions with impurity molecules before travelling far into the vapour or drift space. Lower mobilities could result from attachment of these ions to form molecular clusters. Although the case for more than one charge carrier is not yet proven, the evidence is that slower carriers are present and become apparent at low charge injection densitites. At higher densities the slower carriers form a small proportion of the total. This would help to explain the long-tail effect; although in this work it is felt there is also a contribution from the space charge accumulations in the grids.

7.5 Conclusions

The problems associated with small signal measurement have been considerably reduced by using an on-line digital computer to measure the current transients, calculate the cumulative average or digital correlation, and display the results. Many of the previous restrictions which were imposed on the use of these techniques have been removed by the choice of computer, however, it is still necessary to aim for maximum sensitivity and minimum noise in the basic measuring apparatus, if the full potential of these signal-processing methods is to be realized. In addition, the computer was used to record and process signals emanating from e.h.d. disturbances in the drift space, simultaneously with the current transient and thus establish a correlation between the current transient and e.h.d. convection. Disturbances were present even at very small currents and fields, and no critical values could be established for the onset of instability in purified n-hexane. A possible reason is that with photo-injection into a vapour gap, the charge carriers arriving at the vapour/liquid interface are negative ions, with a greater momentum than electrons, and, therefore, capable of causing more disturbance. However, previous observations of the onset of instability have been subject to the limitations of the human eye, and the use of a more sensitive detector of variations in light intensity, such as that used in this work, might yield different results. Most previous observers have found lower critical values than the present theories indicate and this is thought to be due to the approximations inherent in the theoretical treatment, e.g. their theory assumes macroscopic values of the liquid parameters ε, μ, η, whereas there could be deviations from these values locally in the liquid. An on-line program is available in the

7.5

computer to calculate the critical numbers for the onset of instability (after Atten and Moreau) for any experimental values of current density and applied voltage.

Among the suggestions put forward for inexplicable results using photo-injection enhancement of conduction in non-polar liquids are the presence of bulk ionisation, liquid motion, space-charge and impurities. Bulk ionisation has been obviated in this work by the use of a control grid, and although this has introduced some distortion of the wave-shape, one result has been a fuller understanding of the effects of local concentrations of space charge. The effects of impurities have been studied, but it is clear that for a thorough investigation an ultra-pure liquid system is necessary so that controlled concentrations of impurities can be introduced.

Finally, this work has indicated that local concentrations of space charge are the major cause of distortions in the current transients from unipolar-charge injection into liquid insulants. For e.h.d. convection to occur, it is not necessary for the liquid to be of poor resistivity, but there must be space-charge concentration, as can occur with grids.

7.6 Suggestions for further work

The simultaneous recording of current transients and the disturbance signal from the differential light sensitive amplifier has considerable potential as a method of studying e.h.d. convection and stability, and it would be instructive to apply it to polar liquids to examine further the critical conditions of e.h.d. stability.

In a future test cell the electrode system should be capable of withstanding higher electric stress and the whole of the drift gap should be visible for schlieren observation. For the study of ionic charge carriers a fast optical shutter would appear to be preferable to the grid method of controlling injection.

To study the effect of impurities upon conduction more pure liquid is necessary and this would mean adopting the methods of Minday, Schmidt and Davis (1970). In this event the deterioration problems of the photo-emitters would be reduced and larger currents could be photo-injected.

The delay of the current response observed in argon requires further investigation.

The adaptive modelling of the charge-transit under varying conditions of injection, space charge and e.h.d. convection presents an interesting line of future research.

8.0 Acknowledgements

The award of a contract (B/SR 75920) by the Science Research Council to assist with the purchase of the FM1600 B computer used in this work is gratefully acknowledged.

The author is also grateful to Professor A.J. Ellison and his predecessor Professor P.F. Soper for the provision of research facilities and support.

It is with pleasure that I thank my colleague [redacted] for his continual encouragement and many helpful discussions throughout this project.

My thanks also go to [redacted], especially for his assistance with liquid preparation and drawings, also to [redacted] for his glass blowing and to [redacted] and his workshop staff for work on the test cell.

I must also extend thanks to other colleagues including [redacted] for their assistance at various times.

I also thank [redacted] for her care and skill in the typing of this thesis.

In conclusion, I thank my wife [redacted] for her constant devotion and selfless support, particularly at this time.

[redacted]

Chapter 9

References

9. REFERENCES

Abbis J.B., Chubb T.W., Pike E.R., 1974, Optical and Laser Technology, 249.

Adamczewski I., 1969, 'Ionization, Conductivity and Breakdown in dielectric liquids', Taylor and Francis, London.

Atten P., 1972, Proc. 4th Int. Conf. on Conduction and Breakdown in Dielectric Liquids, Dublin, 85.

Atten P., 1974, Phys. Fluids, 17, 1822.

Atten P., and Moreau R., 1969, C.R. Acad. Sci., Paris, A269, 469.

Atten P., and Moreau R., 1970, C.R. Acad. Sci., Paris, A270, 415.

Atten P., and Moreau R., 1972, J. Mecanique, 11, 471.

Beck M.S., 1968, El. Letters, 4, 64.

Beddow A.J., 1968, Ph.D. Thesis, University of London.

Belmont M.R., 1973, Ph.D. Thesis, University of Wales.

Bloor A.S., 1970, Ph.D. Thesis, University of Durham.

Bracewell R.N., 1965, 'The Fourier Transform and its applications', McGraw-Hill, New York.

Briere G. and Gosse J.P., 1968, J. Chim. Phys., 65, 725.

Bright A.W., King J., Lame D.R., Makin B., 1970, IEE Conf. on Dielectric Materials, Measurement and Applications, Lancaster, No. 67, 138.

Brignell J.E., 1964, Ph.D. Thesis, University of London.

Brignell J.E., 1972, Rapporteur's Report, Proc. 4th Int. Conf. on Conduction and Breakdown in Dielectric Liquids, Dublin.

Brignell J.E., and Buttle A., 1971, J. Phys. D: Appl. Phys., 4, 1560.

*Brignell J.E., Hewish T.R., and Rhodes G.M., 1973, IEE Conf. Publ. 'The use of digital computers in measurement', York, No. 103, 168.

Brignell J.E., and Rhodes G.M., 1975, 'Laboratory on-line computing' Intertext, London.

Brown D.R., Nature, 1964, 202, 868

Buffam C.J., and Brignell J.E., 1975, Proc. 5th Int. Conf. on Conduction and Breakdown in Dielectric Liquids. Delft.

Beauchamp K.G., 1973, 'Signal Processing' Geo. Allen and Unwin, London.
Brydson J.A., 1969, 'Plastics Materials', Iliffe, London.

* Appendix 10.3

9.

Buttle A.J., 1969, Ph.D. Thesis, The City University.

Buttle A.J., and Brignell J.E., 1968, Coll. Int. C.R.N.S. No. 179, 'Phenomes de conduction dans les liquides isolants', Grenoble, 219.

Buttle A.J., and Brignell J.E., 1969, El. Letts., 5, 687.

Chong P., and Inuishi Y., 1960, Tech. Report, Osaka Univ., No. 414, 545.

Coe G., Hughes J.F., and Secker P.E., 1966, Brit. J. Appl. Phys., 17, 885.

Conrad E.E., and Silverman J., 1969, J. Chem. Phys., 51, 450.

Crowe R.W., 1956, J. Appl. Phys., 27, 156.

Curie P., 1902, C.R. Acad. Sci., 134, 420.

Davies W.D.T., 1966, Control, 10, 302.

Dey T.H., and Lewis T.J., 1968, Brit. J. Appl. Phys., J. Phys. D: 2, 1 1019.

Essex V., and Secker P.E., 1968, Brit. J. Appl. Phys., J. Phys. D: 2, 1 63.

Evison J., 1975, Ph.D. Thesis, The City University.

Faraday M., 1838, 'Experimental Researches', Dover Publications, 1, 507.

Farazmand B., 1961, Brit. J. Appl. Phys., 12, 251.

Felici N.J., 1971a, Direct Current 2, 90.

Felici N.J., 1971b, Direct Current 2, 147.

Felici N.J., 1972, Proc. 4th Int. Conf. on Conduction and Breakdown in Dielectric Liquids, Dublin, 69.

Felici N.J., and Sauviat M., 1972, Proc. 4th Int. Conf. on Conduction and Breakdown in Dielectric Liquids, Dublin 43.

Filippini J.C., Gosse J.P., Lacroix J.C., and Tobazeon R., 1969, C.R. Acad. Sc. Paris, B269, 167 and 736.

Filippini J.C., Gosse J.P., Lacroix J.C., and Tobazeon R., 1970, IEE Conf. on Dielectric Materials, Measurement and Applications, Lancaster, No. 67, 110.

Filippini J.C., Lacroix J.C., and Tobazeon R., 1970, IEE Conf. on Dielectric Materials, Measurement and Applications, Lancaster, No. 67, 121.

Forster E.O., 1964, J. Chem. Phys. 40, 91.

Forster E.O., 1967, IEEE Trans. on Electrical Insulation EI-2, 1, 10.

Gazda E., 1963, Acta. Phys. Pol., 24, 209.

Gray E., 1967, Ph.D. Thesis, University of London.

Gray E., and Lewis T.J., 1965, Brit. J. Appl. Phys., 16, 1049.

Gray E., and Lewis T.J., 1969, Brit. J. Appl. Phys. [2], 2, 93.

Gzowski O., 1962, Nature, 194, 173.

Hartmann G.C., and Lipari N.O., 1973, J. Appl. Phys., 44, 1676.

Helm H.A., 1959, Bell Syst. Tech. J., 3, 177.

Hewish T.R., and Brignell J.E.,* 1972, Proc. 4th Int. Conf. on Conduction and Breakdown in Dielectric Liquids, Dublin, 5.

Hewish T.R., and Brignell J.E.,** 1972, J. Phys. D: Appl. Phys., 5, 747.

Hewish T.R., and Brignell J.E.,*** 1975, Proc. 5th Int. Conf. on Conduction and Breakdown in Dielectric Liquids, Delft.

Holder D.W., and North R.J., 1963, 'Notes on App. Sci. No. 31, Schlieren methods', H.M.S.O., London.

Hopfinger E.J., and Gosse J.P., 1971, Phys. Fluids, 14, 1671.

Hopfinger E.J., Gosse J.P., and Atten P., 1970, IEE Conf. on Dielectric materials and measurement and applications, Lancaster, No. 67, 125.

Hummell A., and Schmidt W.F., 1974, Radiation Res. Reviews, 5, 199.

Kahan E., 1964, Ph.D. Thesis, University of Durham.

Kahan E., and Morant M.J., 1965, Br. J. Appl. Phys., 16, 943.

Lacroix J.C., and Tobazeon R., 1972, Proc. 4th Int. Conf. on Conduction and Breakdown in Dielectric Liquids, Dublin, 93.

Le Blanc Jnr. O.H., 1959, J. Chem. Phys., 30, 1443.

Macleod C.J., 1968, El. Letts., 4, 11, 220.

Many A., and Rakavy E., 1962, Phys. Rev., 126, 1980.

Martin K., and Secker P.E., 1974, J. Phys. E: Sci. Instr., 7, 432.

Mattieu J., Blanc D., Patau J.P., 1968, Coll. Int. C.N.R.S. No. 179, Phenomes de conduction dans les liquides isolants, Grenoble, 57.

Metzmacher K.D., 1969, Ph.D. Thesis, The City University.

N.B. The publications by the author and J.E. Brignell form appendices 10.1*, 10.2** and 10.4*** of this thesis.

Metzmacher K.D., and Brignell J.E., 1970, J. Phys. D: Appl. Phys., 3, L5.

Miller L.S., Howe S., and Spear W.E., 1968, Phys. Rev. 166, 876.

Minday R.M., Schmidt L.D., and Davis H.T., 1969, J. Chem. Phys., 50, 1473.

Minday R.M., Schmidt L.D., and Davis H.T., 1971, J. Chem. Phys., 54, 3112.

Morant M.J., 1960, Nature, 187, 48.

Mort J., and Scher H., 1971, J. Appl. Phys., 42, 3939.

Ostroumov G., 1954, Zh. Tekh. Fiz., 24, 1915.

Ostroumov G., 1956, Soviet Phys., JETP, 3, 259.

Papadakis A.C., 1967, J. Phys. Chem. Solid, 28, 641.

Papoulis A., 1965, 'Probability, Random Variables and Stochastic Processes', McGraw-Hill, New York.

Pinckard D., 1972, B.Sc. Project Report (Internal) No. 647, The City University).

Pollard A.F., 1971, Ph.D.. Thesis, The City University.

Praglin J., and Nichols W.A., 1960, Proc. I.R.E., 48, 771.

Presley S.R., 1966, Rev. of Sci. Insts., 37, 5, 643.

Pugh D.R., 1968, Ph.D. Thesis, University of Durham.

Rahman J., 1970, Ph.D. Thesis, University of Durham.

Reich H.J., 1944, 'Theory and applications of electron tubes', McGraw-Hill, New York.

Rhodes G.M., 1971, Ph.D. Thesis, The City University.

Schmidt W.F., and Allen A.O., 1969, J. Chem. Phys., 50, 5037.

Schmidt W.F., and Allen A.O., 1970, J. Chem. Phys., 52, 4788.

Schneider J.M., and Watson P.K., 1969, Proc. E.H.D. conf., M.I.T., (Cambridge, Mass: M.I.T.), 74.

Schneider J.M., and Watson P.K., 1970, Phys. Fluids, 13, 1948.

Secker P.E., 1965, Brit. J. Appl. Phys., 16, 1527.

Secker P.E., and Lewis T.J., 1969, Brit. J. Appl. Phys., 16, 1659.

Sharbaugh A.H., and Watson P.K., 1962, Progress in Dielectrics, 4, 199.

Silver M., Onn D.G., Smejtek P., Masoda K., 1967, Phys. Rev. Letts, 19, 11, 626.

Silver M., Choi S.I., Smejtek P., 1968, Coll. Int., C.N.R.S., No. 179, 'Phenomes de conduction dans les liquides isolants, Grenoble', 399.

Smith C.W., and Calderwood J.H., 1968, Coll. Int., C.N.R.S., No. 179, 'Phenomes de conduction dans les liquides isolants, Grenoble', 161.

Spangenberg K.R., 1948, 'Vacuum Tubes', McGraw-Hill, New York.

Swan D.W., 1961, Nature, 190, 204.

Taylor R.J., 1972, Ph.D. Thesis, The City University.

Taylor, R.J., 1972, J. Phys., 5, 1855.

Taylor R.J., and House H., 1971, El. Letts., 7, 14, 404.

Terlecki J., 1962, Nature, 194, 172.

Thomas W.R.L., 1972, Proc. 4th Int. Conf. on Conduction and Breakdown in Dielectric Liquids, Dublin, 73.

Thompson J.J., 1897, Nature, 55, 606.

Watson P.K., 1965, Annual Report Conf. on Elec. Ins., NAS-NRC Publ. No. 1356, 53.

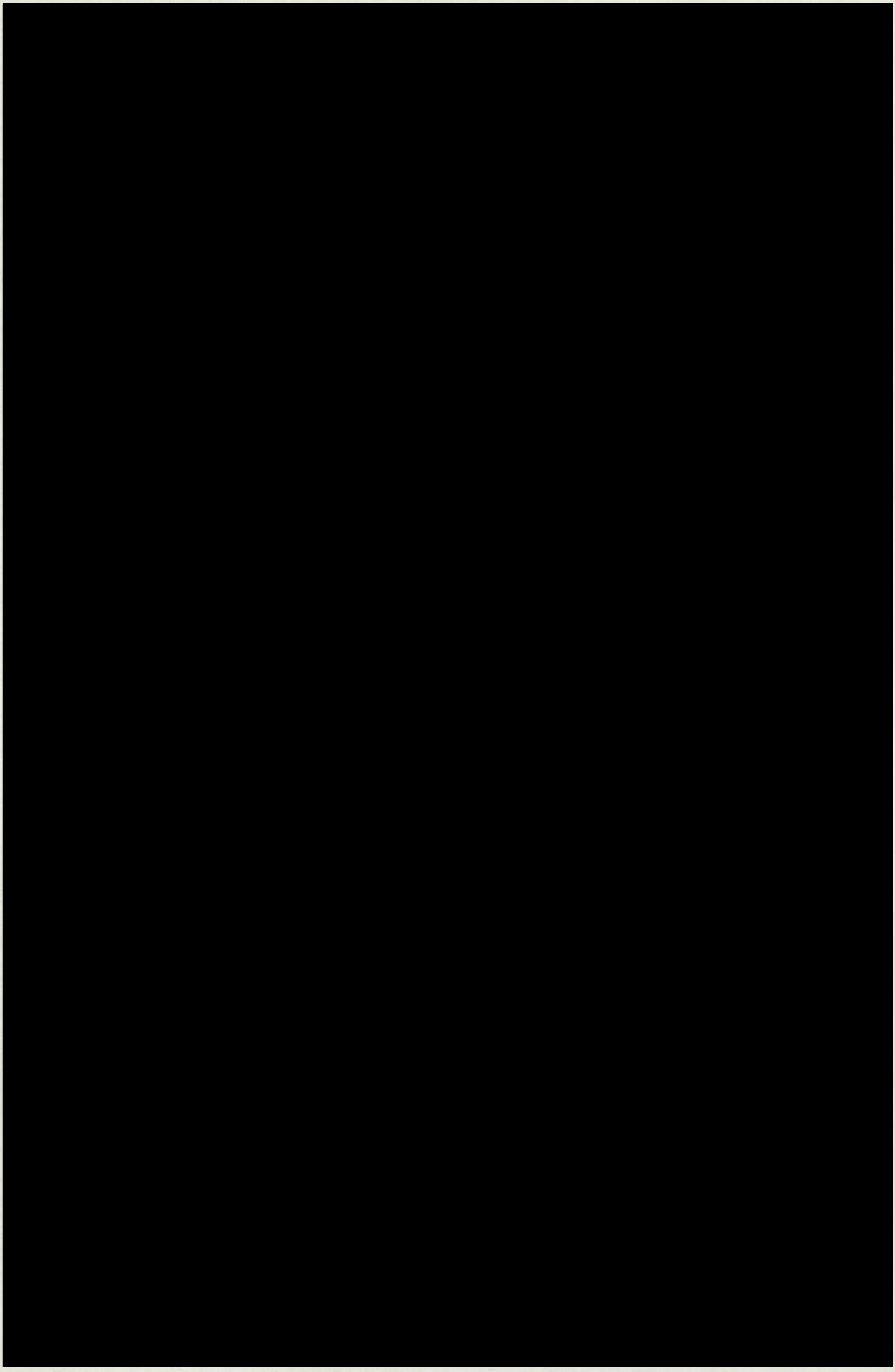
Watson P.K., and Clancy T.M., 1965, Rev. Sci. Insts., 36, 2, 217.

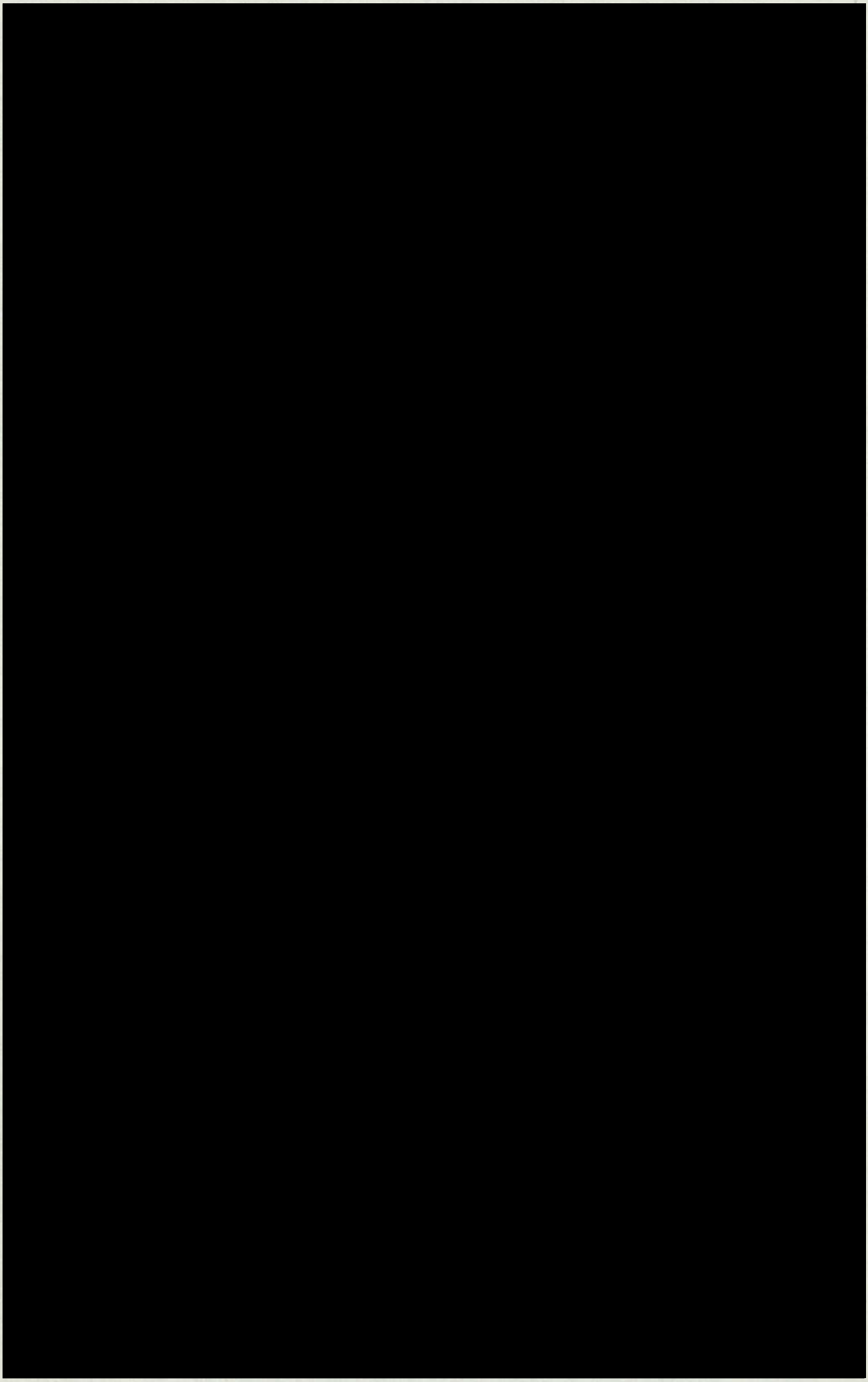
Watson P.K., Schneider J.M., and Till H.R., 1970, Phys. Fluids, 13, 1955.

Chapter 10

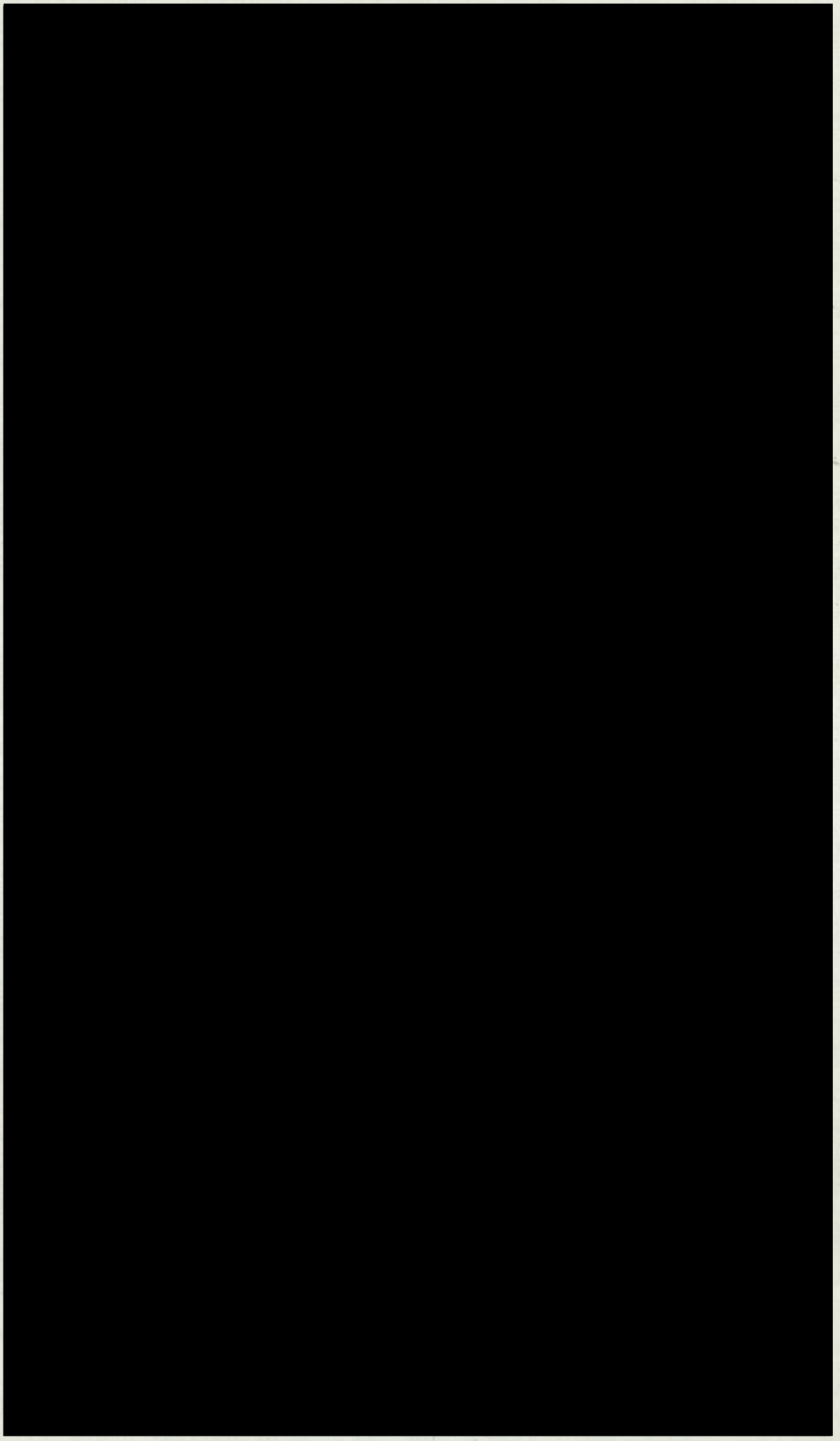
Appendices

Appendix 10.1

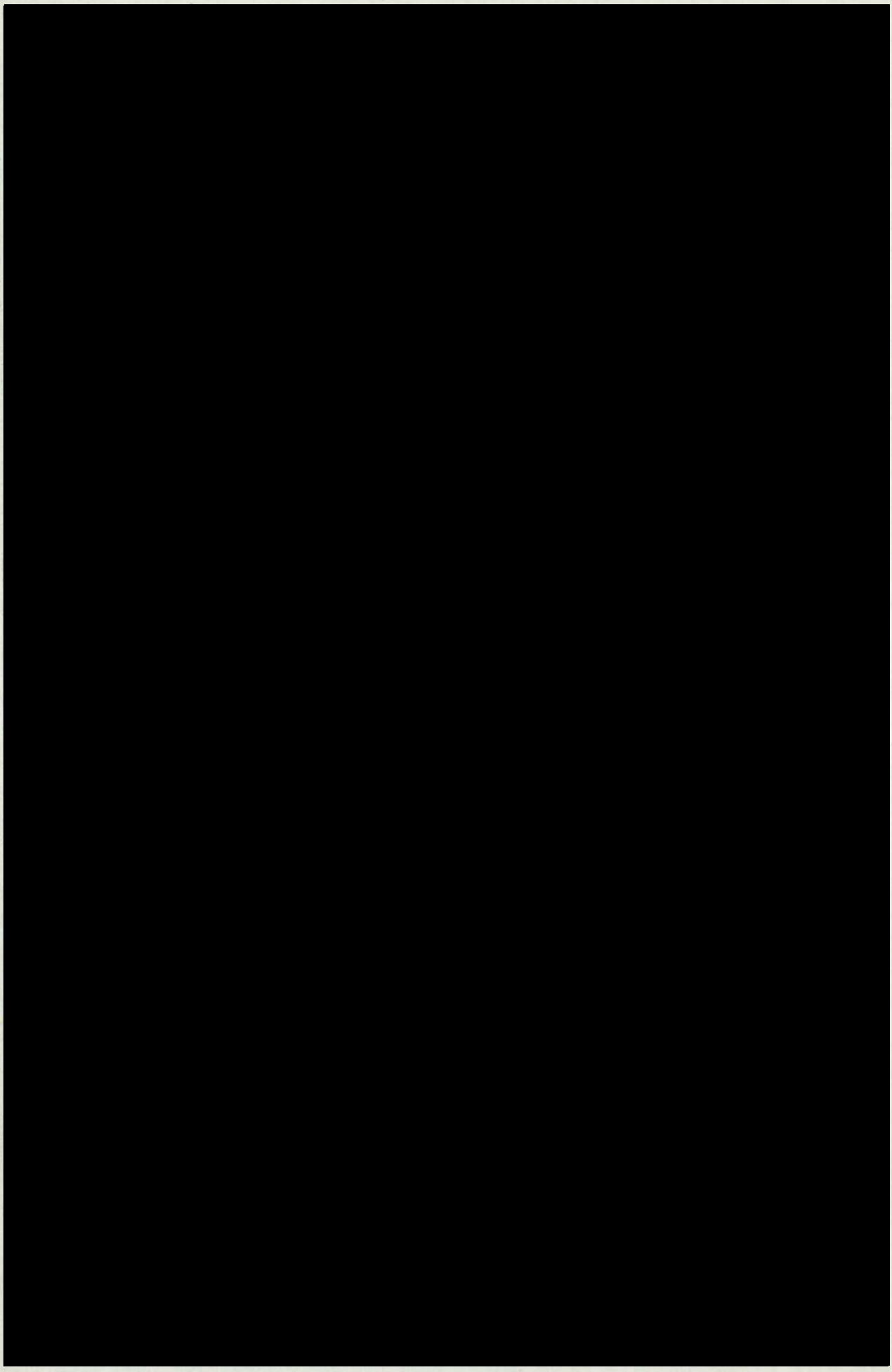


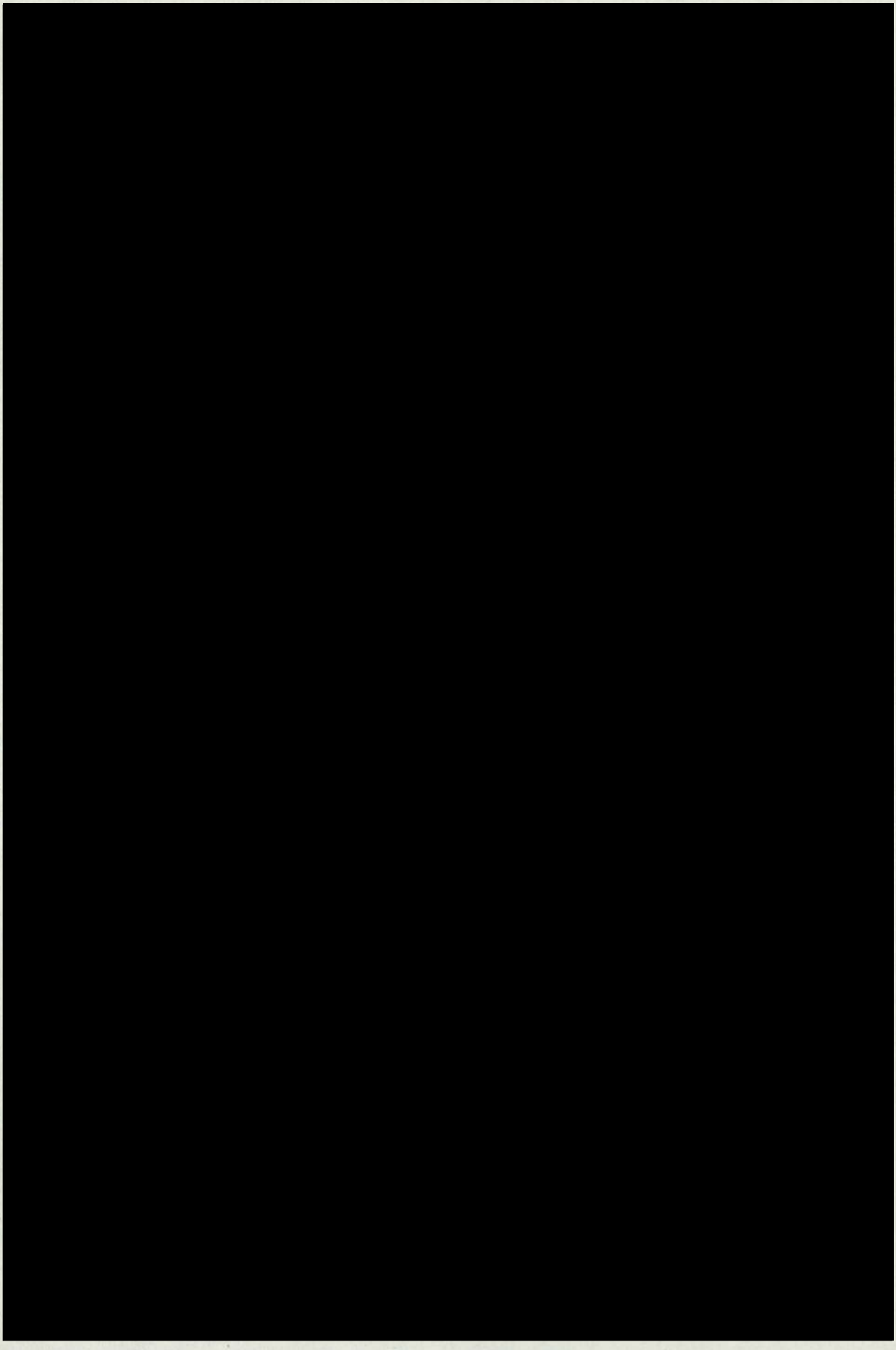


10.1



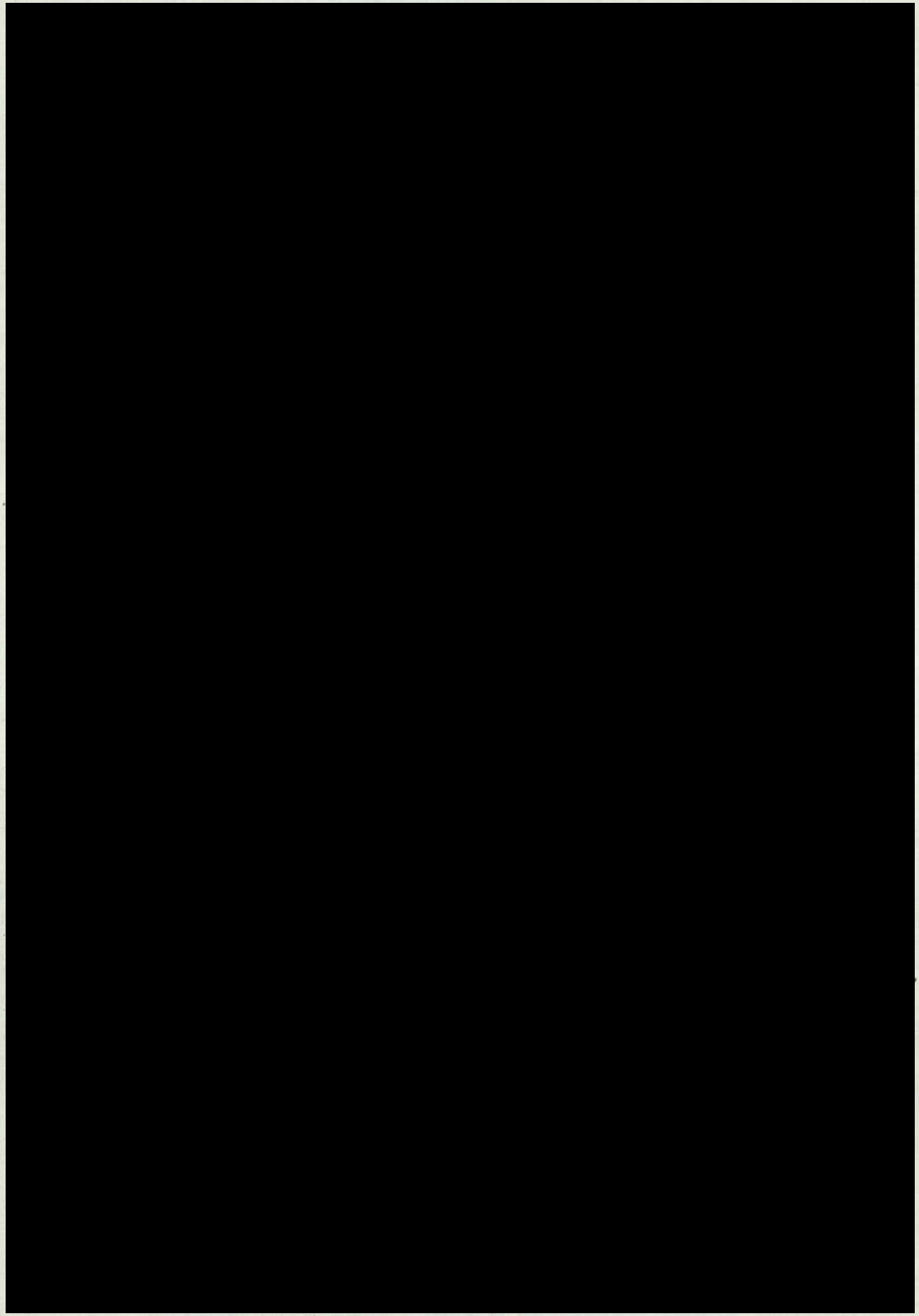
10.1



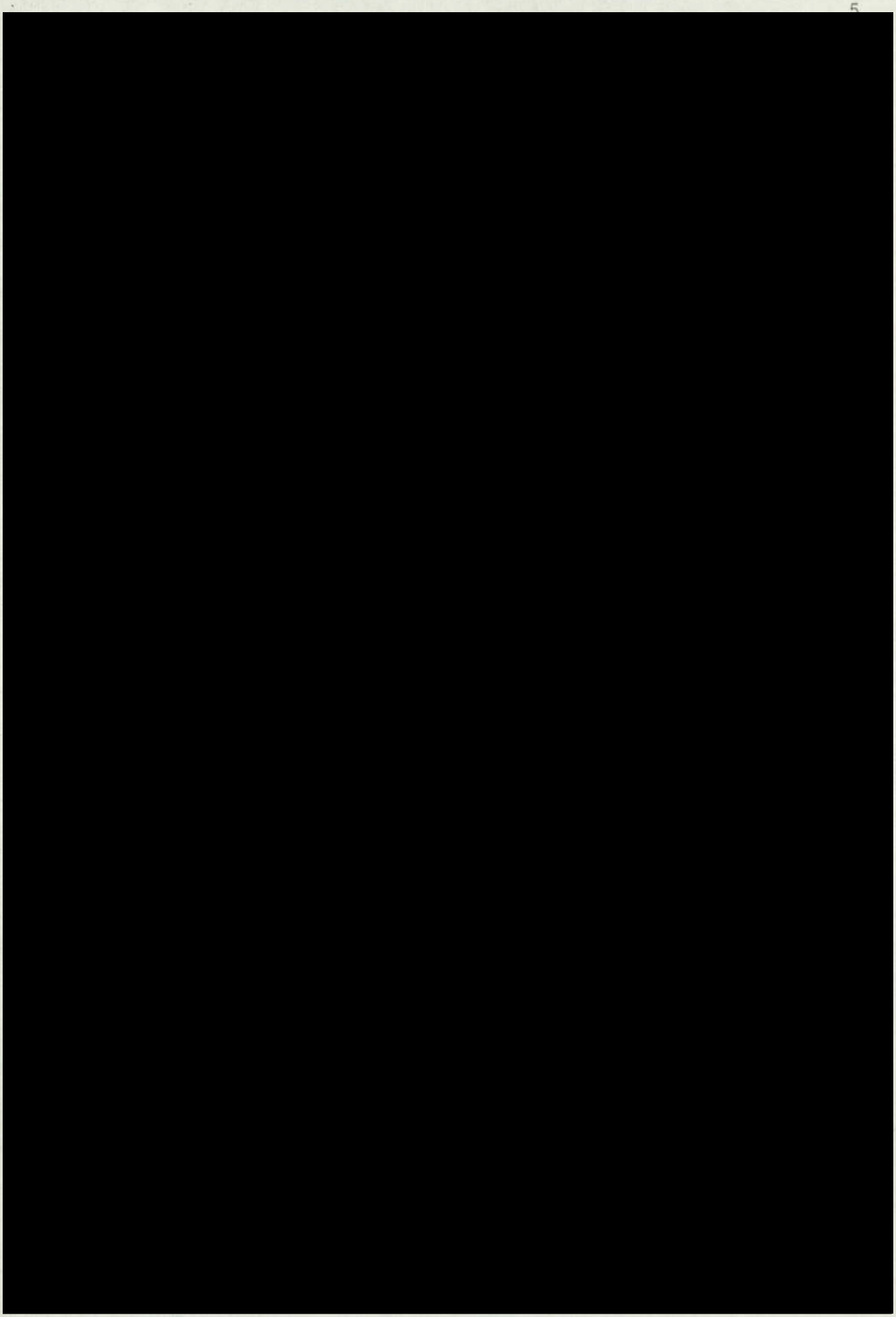


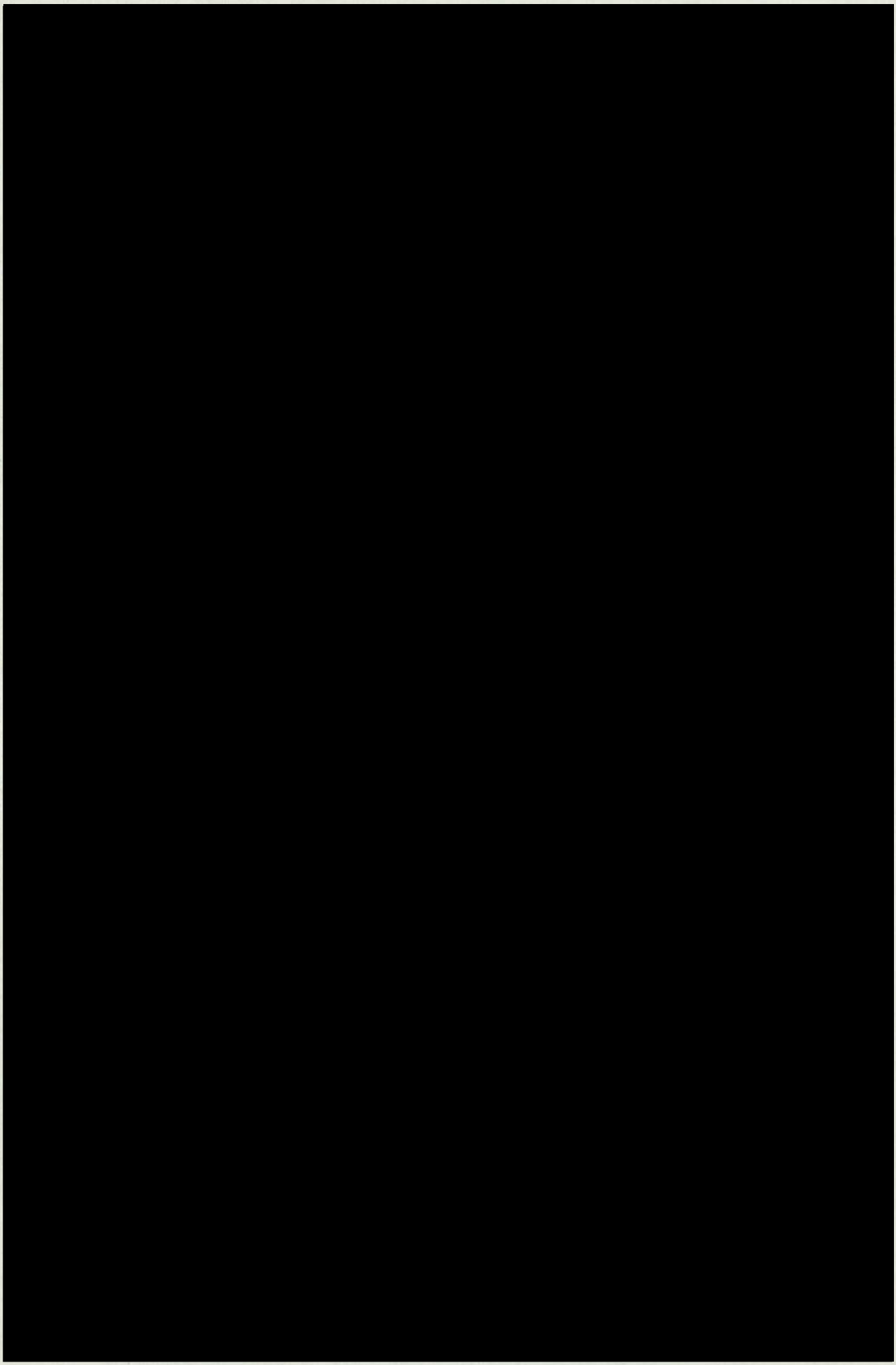


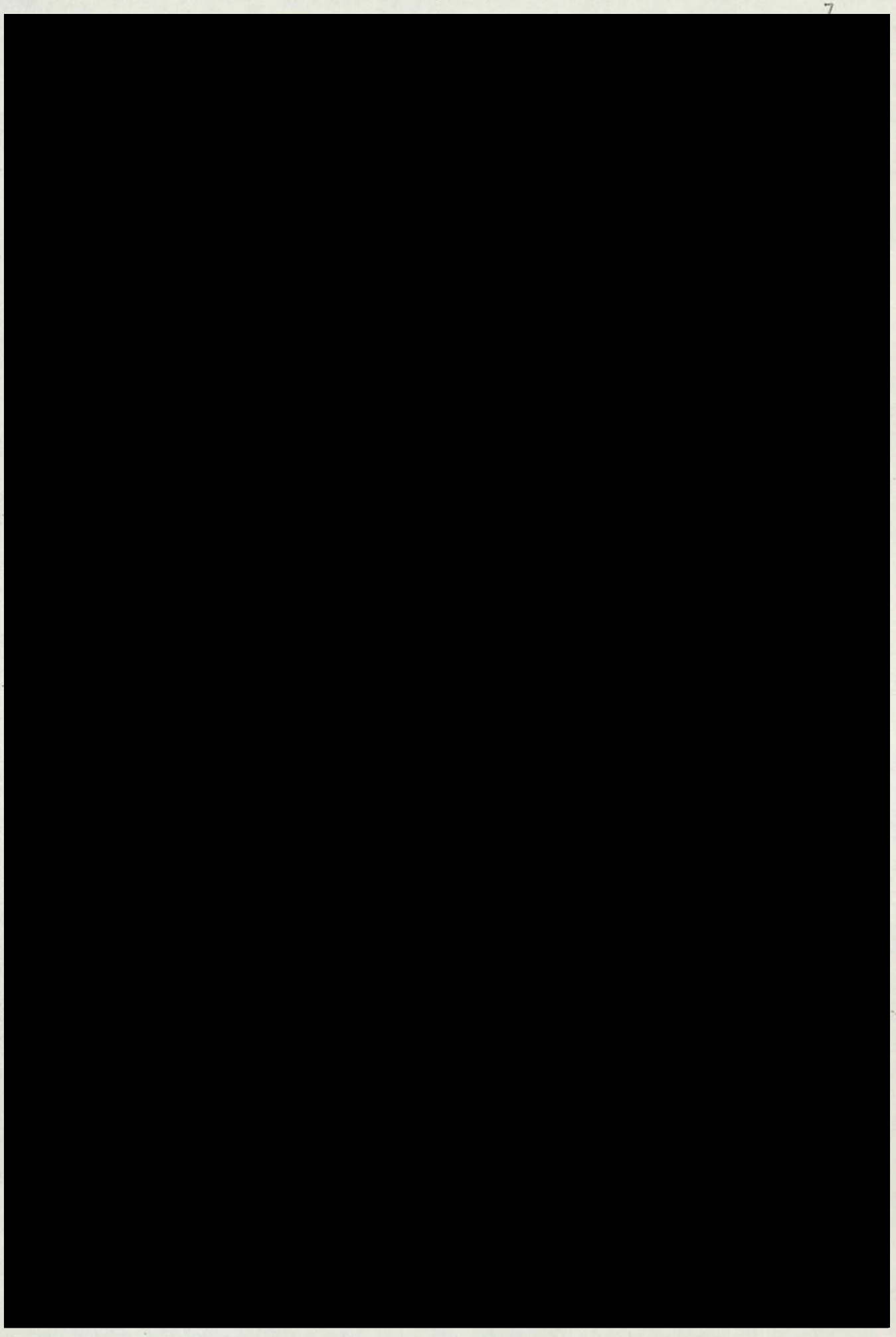
Appendix 10.2



10.2





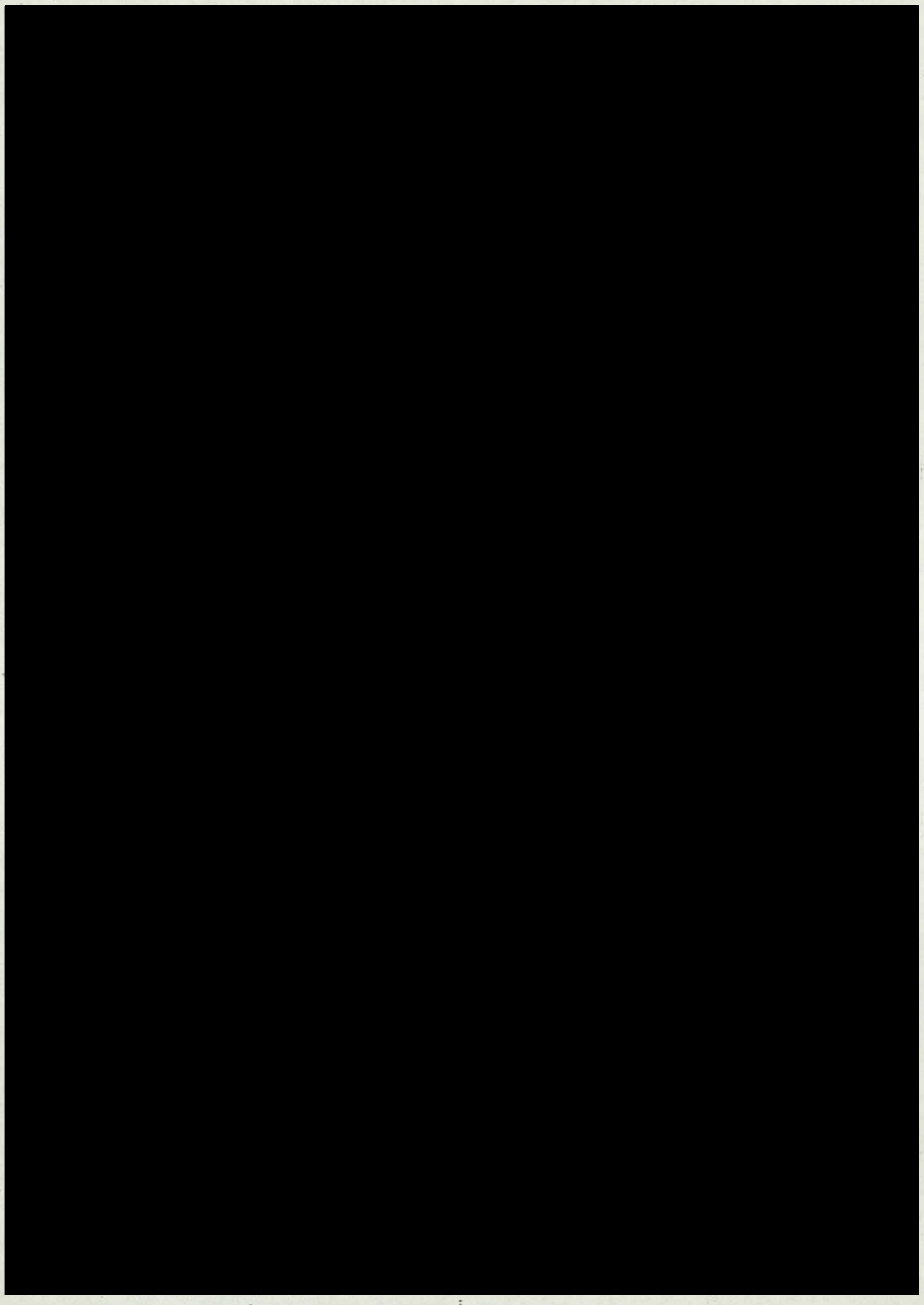


10.2

8

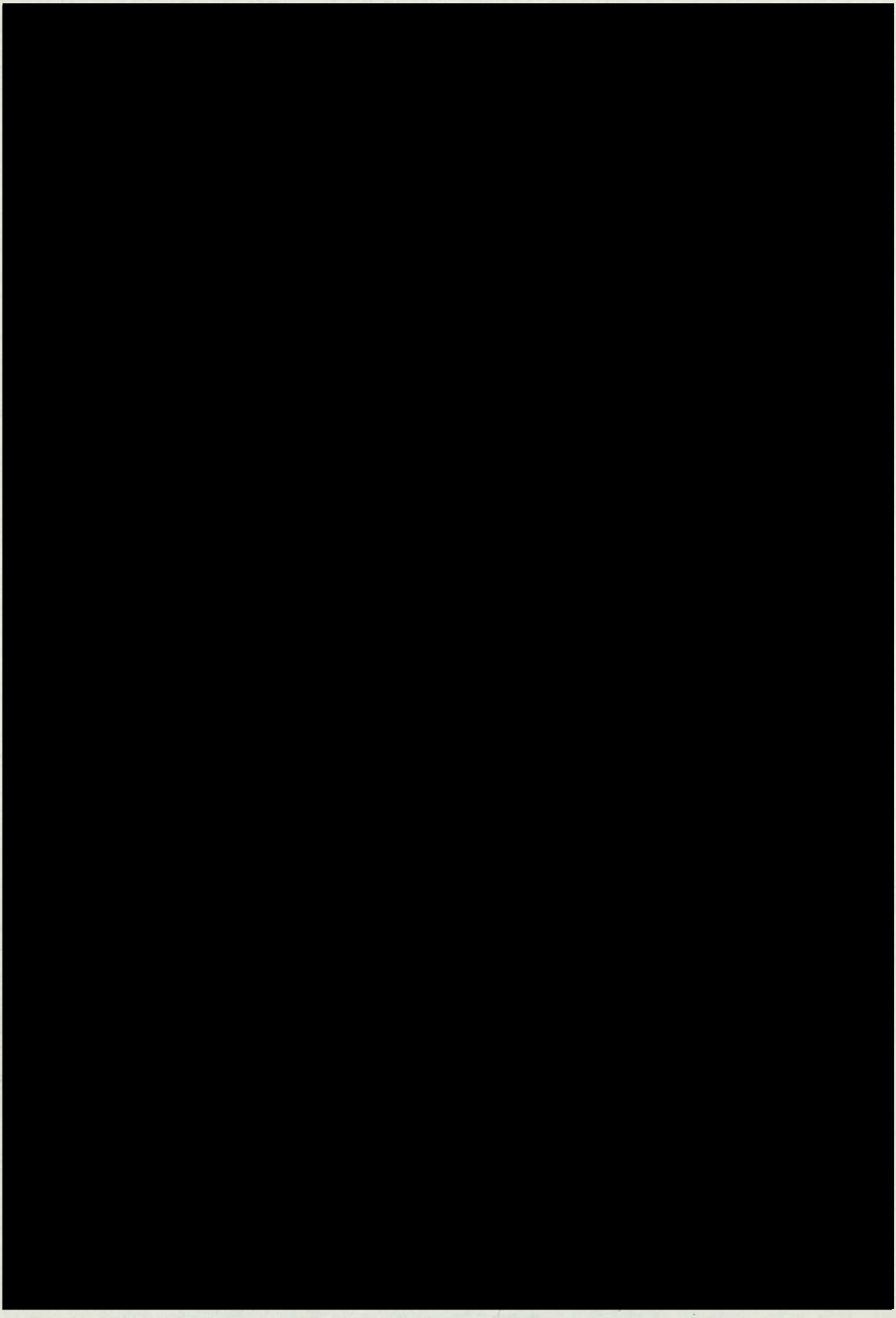


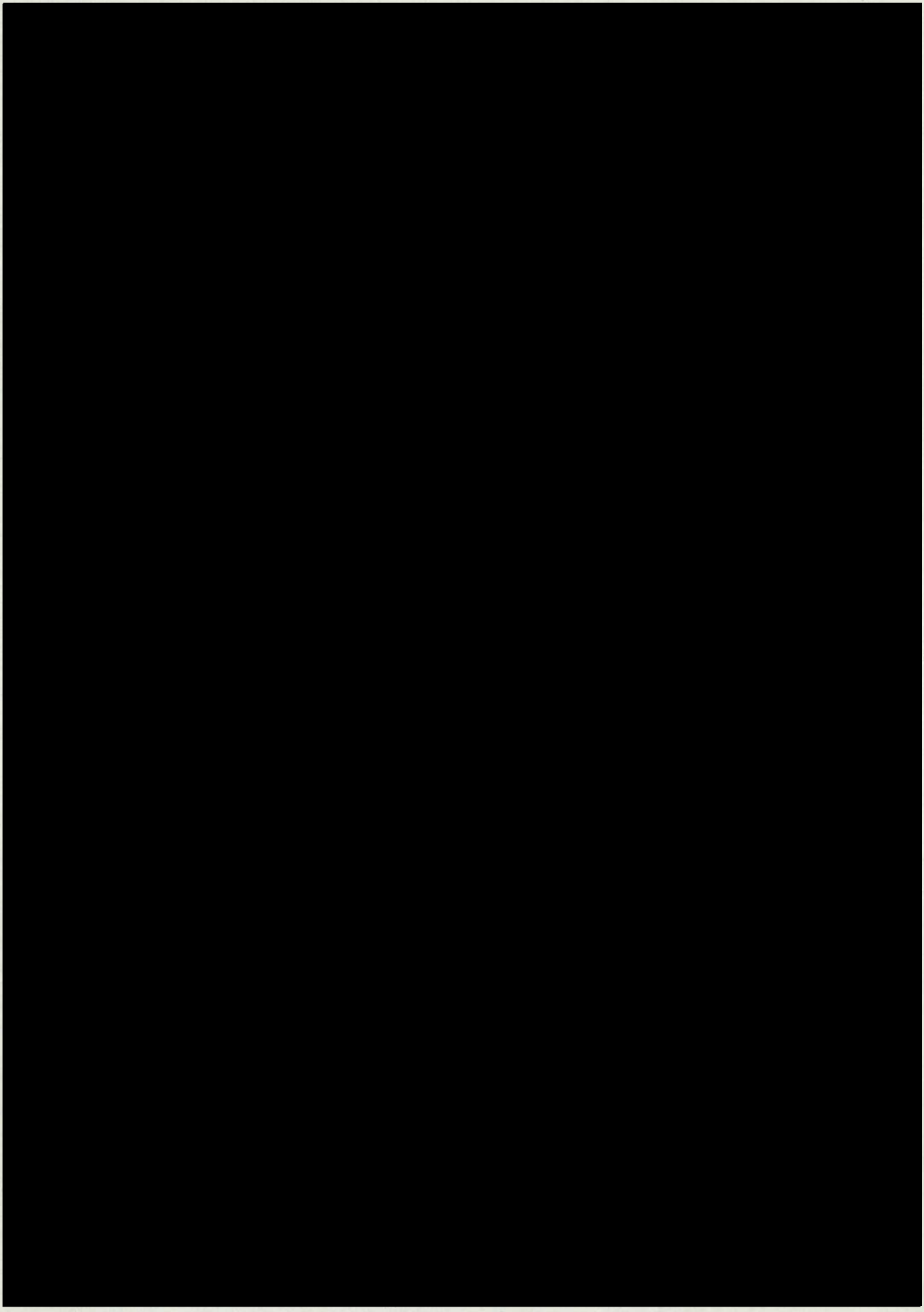
Appendix 10.3

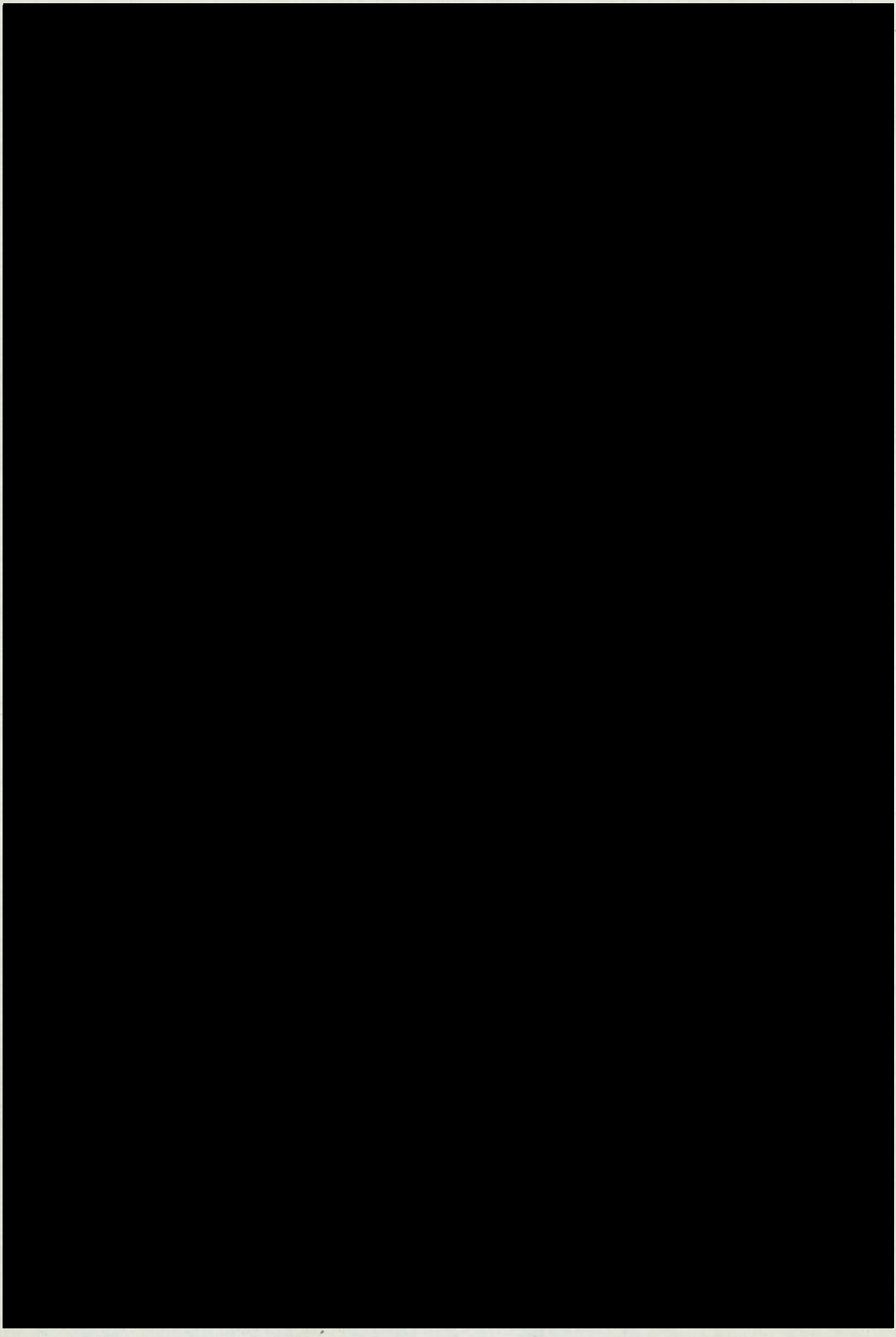


10.3

168

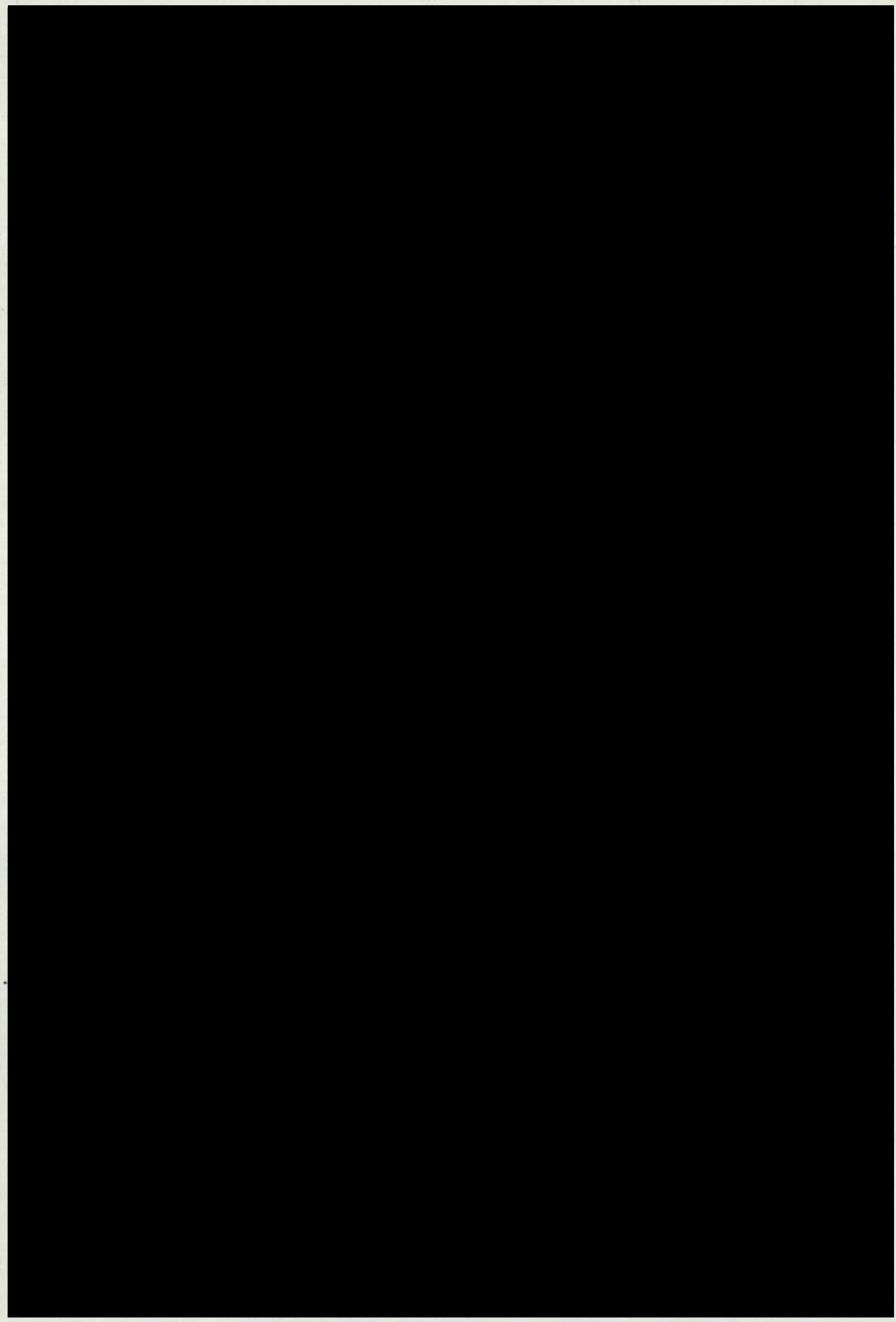






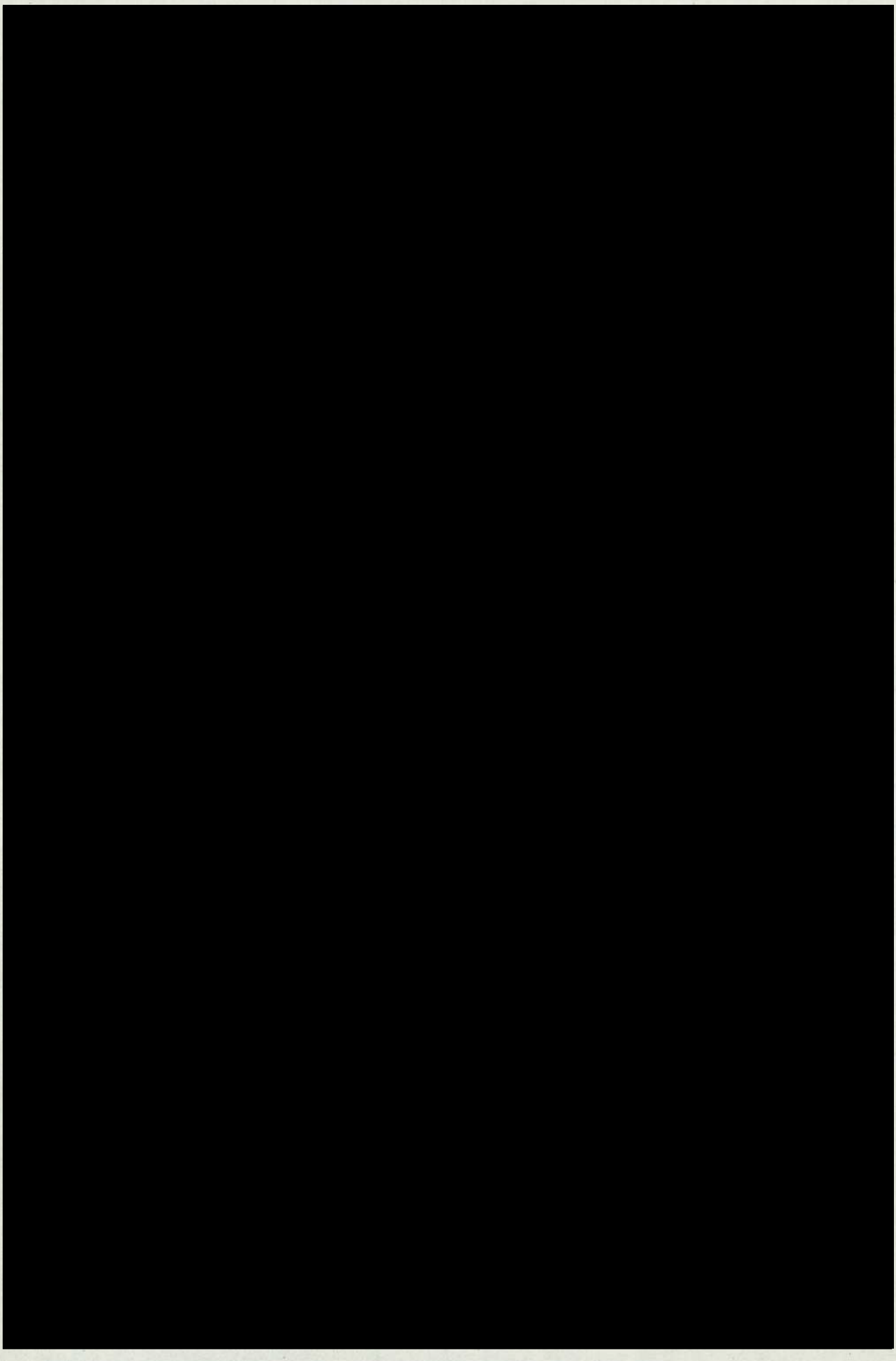
10.3

171



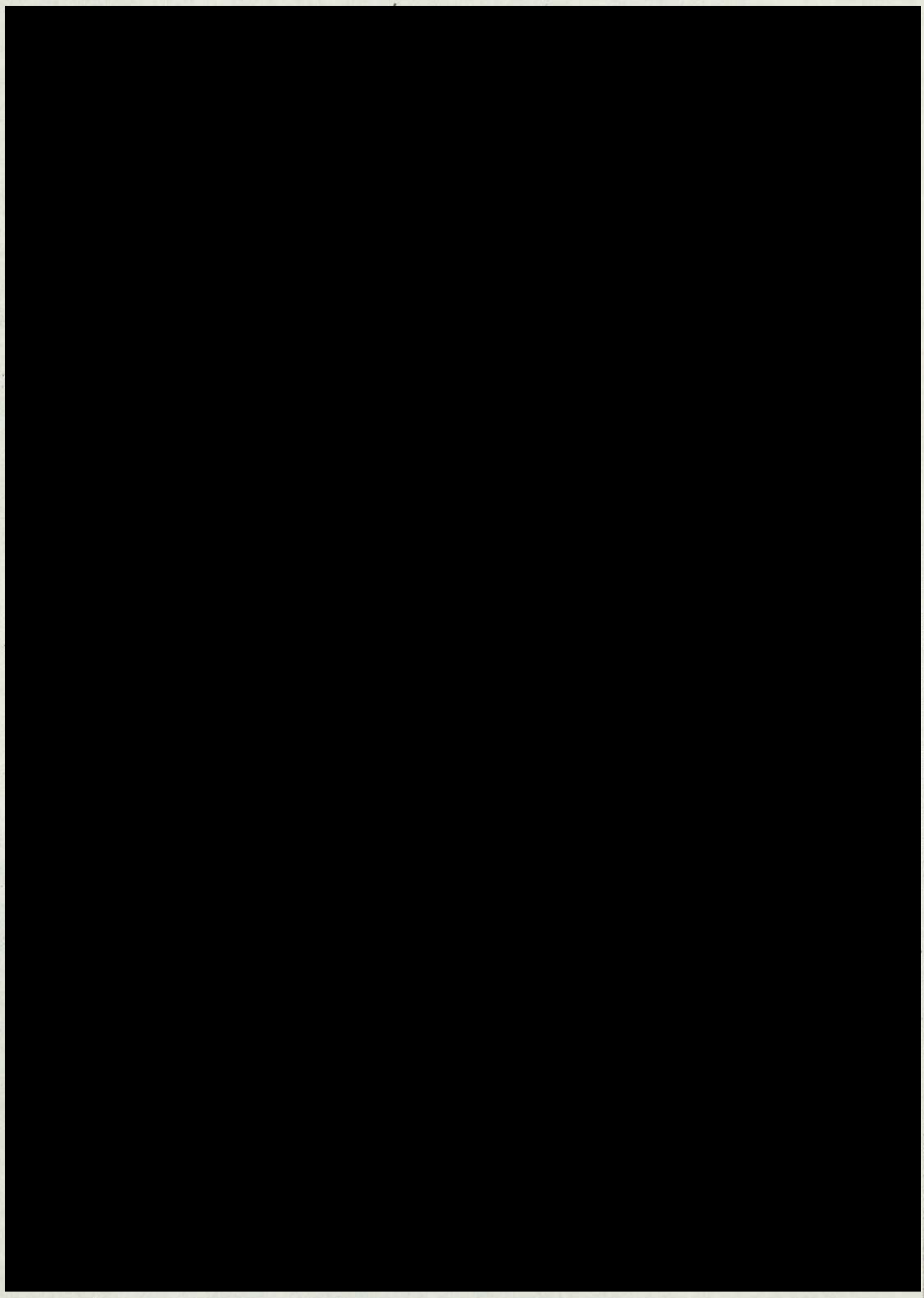
10.3

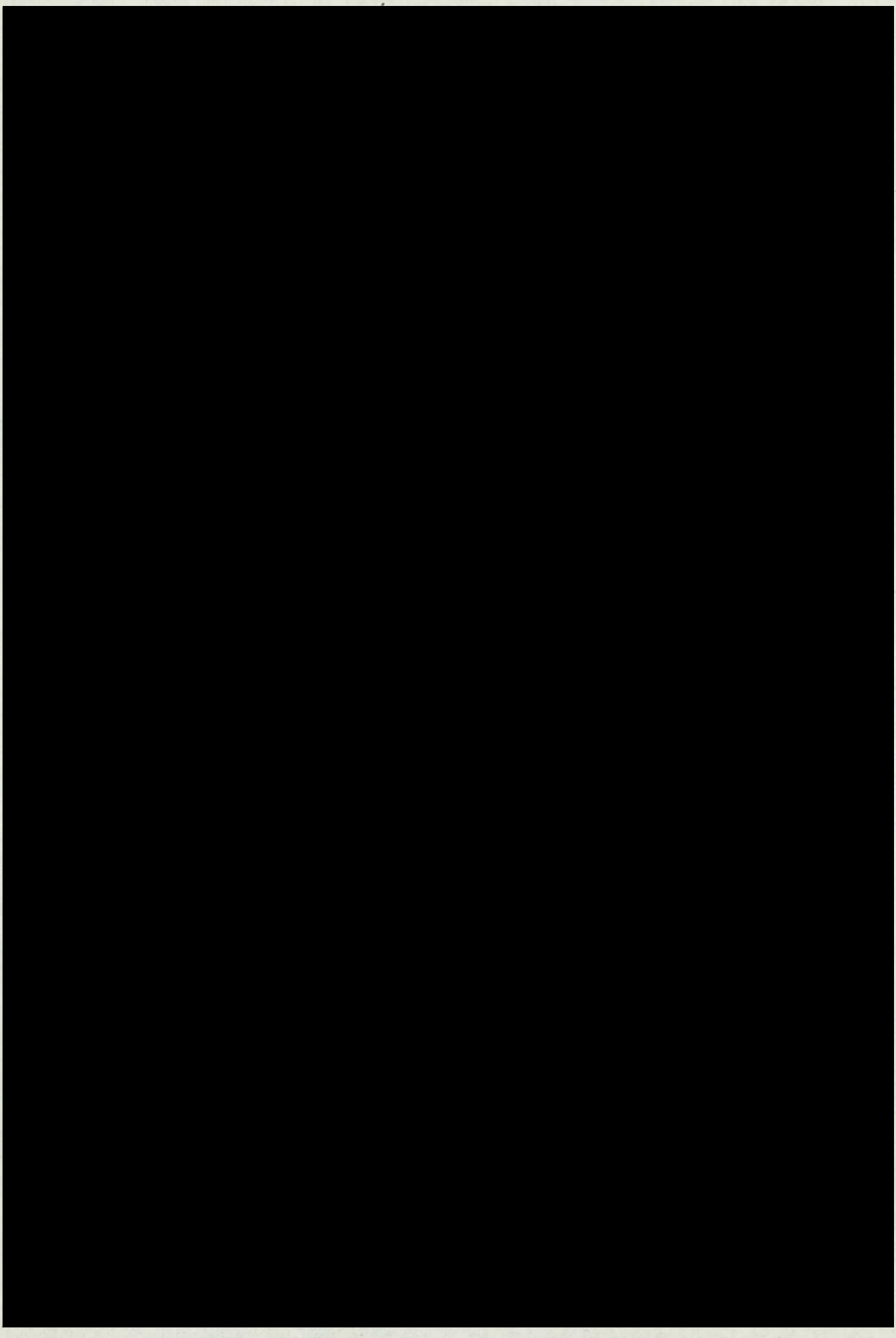
172



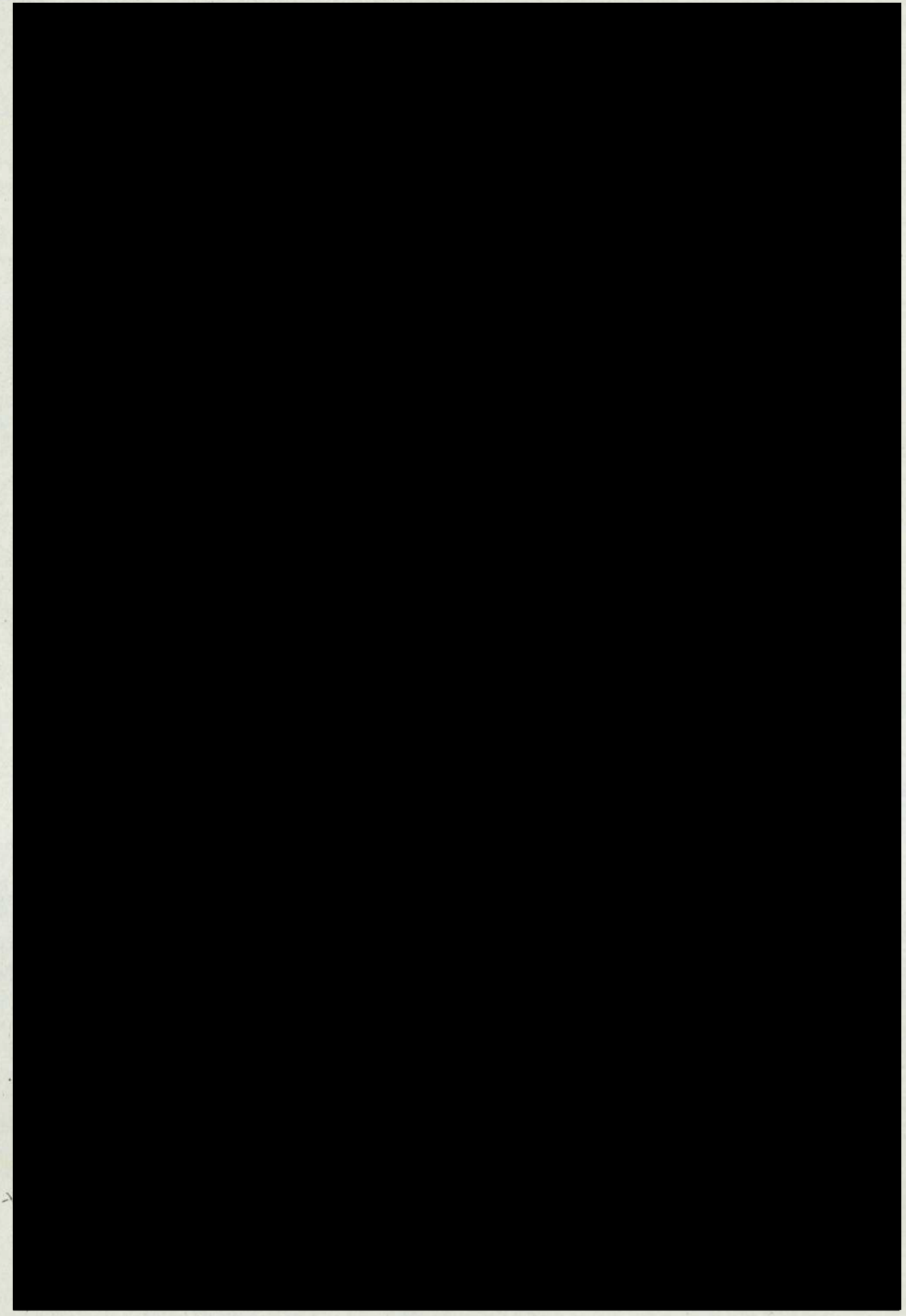
Appendix 10.4 Paper to be presented at Delft conference







10.4



10.4

